IMMOBILIZATION OF ORGANOSILANES ON SUPPORT MATERIALS AND THEIR APPLICATIONS IN CO_2 CAPTURE AND HETEROGENEOUS C–H FUNCTIONALIZATION CATALYSIS

A Dissertation
Presented to
The Academic Faculty

by

Chunjae Yoo

In Partial Fulfillment
of the Requirements for the Degree
Doctor of Philosophy in the
School of Chemical & Biomolecular Engineering

Georgia Institute of Technology
December 2018

IMMOBILIZATION OF ORGANOSILANES ON SUPPORT MATERIALS AND THEIR APPLICATIONS IN CO_2 CAPTURE AND HETEROGENEOUS C–H FUNCTIONALIZATION CATALYSIS

Approved by:

Dr. Christopher W. Jones, Advisor
School of Chemical & Biomolecular Engineering
Georgia Institute of Technology

Dr. Fani Boukouvala
School of Chemical & Biomolecular Engineering
Georgia Institute of Technology

Dr. Carsten Sievers
School of Chemical & Biomolecular Engineering
Georgia Institute of Technology

Dr. Stefan France
School of Chemistry and Biochemistry
Georgia Institute of Technology

Dr. Ryan P. Lively
School of Chemical & Biomolecular Engineering
Georgia Institute of Technology

Date Approved: October 25, 2018

ACKNOWLEDGEMENTS

First, I would like to thank my adviser, Dr. Jones, for supporting my research. His enthusiastic encouragement and valuable critiques on my research let me keep pursuing an academic passion. He always encourages me to have confidence in what I am having and seeking. Whenever I encountered barriers, he did not force me to follow his directions. He just provided possible options and their possibilities of success, which made me understand the situation correctly and escape from the barriers or problems in a short time. Under his patient guidance, I could successfully finish my Ph.D. I truly appreciate his time and advice he gave me.

I also would like to express my very great appreciation to Dr. Davies for his valuable and constructive support and suggestion during the collaboration work. His kindness to take care of me as another his group member has been very much appreciated.

The advice given by my committee members has been a great help to understand my research project from multiple points of view. Their insightful comments and suggestion as well as hard questions during the proposal and predoctoral review gave me a positive motivation for my research.

My sincere thanks also go to my past and present Emory collaborator Dr. Rackl and Wenbin who gave me an enormous synthetic organic chemistry knowledge, which is the biggest asset I have received from our collaboration. Furthermore, without their precious help, it would not be possible to keep maintaining our active collaboration work.

I also would like to thank my group members. Even though Jones group consists of various and distinct personalities, they are acting like one team with dedicated and

cooperative attitude. This atmosphere helps me adapt myself to the new circumstance and develop my research based on the inter-subgroup collaborations.

Lastly, I would like to thank my family and friends for encouraging me to go forward.

TABLE OF CONTENTS

LIST OF TABLES

LIST OF FIGURES

SUMMARY

In chapter 1, the general structure of organosilanes and their chemical properties for the immobilization on the surface were briefly introduced. Since the organosilanes can be strongly binding on the (in)organic surface via covalent bond, and functional groups on the silanes are vastly tunable, they are widely utilized in the surface modification (e.g. hydrophobic/hydrophilic coating) as well as adhesive filler agents between two different polymers or linker agents for immobilization of enzyme or catalyst. In this context, the organosilanes can be used for CO_2 adsorbent or linker agent for the immobilization of expensive precious metal catalyst on a support material. In this dissertation, various organosilanes having various amine moieties are synthesized and utilized to understand the molecular mechanism for CO_2 adsorption (fundamental aim), and immobilization method of dirhodium catalysts on silica support are explored to demonstrate C-H functionalization in flow reactor system (an applied goal).

In chapter 2, an array of aminosilanes is synthesized and grafted onto a mesoporous silica support to evaluate the effect of aminosilane structure on CO_2 adsorption and oxidative stability. Both linear ($NH_2(CH_2)_nNH(CH_2)_3Si(OEt)_3$, L-ethyl for n=2, L-propyl for n=3) and branched ($((NH_2(CH_2)_{2or3})_2N(CH)_3Si(OEt)_3$, B-ethyl for n=2, B-propyl for n=3) aminosilanes containing multiple amine moieties (primary and secondary or primary and tertiary amines) with ethyl or propyl spacers between the amine moieties are prepared. The CO_2 uptakes of the adsorbents are measured using a 400 ppm CO_2 stream, representing the concentration of CO_2 in ambient air. The adsorbents containing with branched silanes show higher CO_2 uptakes than the adsorbents with linear silanes per silane molecule due

to the presence of more effective amine moieties (primary amines > secondary amines) for CO_2 sorption. The thermal and oxidative stability of the adsorbents is evaluated with multiple cycles of CO_2 adsorption and desorption using inert helium or oxidizing air. While all the prepared adsorbents show good thermal stability, the L-propyl adsorbent shows the highest oxidative stability, followed by a stability trend of B-propyl > B-ethyl> L-ethyl materials. The nature of the oxidized species on the adsorbents is monitored by in-situ IR spectroscopy, where amide and imide species are observed. Depending on the oxidative stability of the adsorbents, the order of the normalized H/(C+N) ratios for the oxidized adsorbents varied, showing qualitative good agreement with the order of the normalized CO_2 capacities of the oxidized adsorbents.

In chapter 3, dirhodium complex catalyst for enantioselective C-H functionalization was immobilized on the silica support, whereby optimum conditions for the immobilization were explored to obtain the similar catalytic activities in terms of yield and enantioselectivity compared with the homogeneous catalyst. For the supported dirhodium catalyst, one of the chiral ligands for the Rh_2(S-p-BrTPCP)$_4$ was modified to have alkyne terminal group, and silica support was functionalized with the azido group. The azido group from the silica support and alkyne group from the dirhodium catalyst reacted to form a triazole structure via Cu catalyzed cycloaddition reaction (click reaction). The immobilized dirhodium catalyst prepared by this pathway showed a similar yield and e.e. with homogeneously catalyzed cyclopropanation reaction. The linker structure between dirhodium catalyst and Si atom did show the significant effect on the catalytic activity. When the immobilized catalyst was recycled after filtration and drying process, decreasing e.e. for the cyclopropanation was observed in the batch reactor. However, when the catalyst

was kept in the packed bed reactor without separation and drying, the product was continuously generated in the flow without a significant drop in e. e. The pore structure of the immobilized Rh2 catalyst showed different reaction kinetics for cyclopropanation. The immobilized Rh2 catalyst (Rh-propyl-SBA15PLT) with short pore length and large diameter showed faster kinetics than another immobilized catalyst (Rh-propyl-SBA15) with long pore length and narrow diameter.

In chapter 4, a tandem reaction system has been developed for the preparation of donor-/acceptor-substituted diazo compounds in continuous flow coupled with dirhodium-catalyzed reactions, either C–H functionalization or cyclopropanation. Hydrazone compounds containing trichloroethyl esters were oxidized in flow by solid supported N-iodo p-toluenesulfonamide potassium salt (PS-SO_2NIK) to generate the diazo compounds. Conditions were developed to enable subsequent cyclopropanations and challenging C–H functionalization reactions to be conducted. Overall, comparable yields and enantioselectivities were observed for Rh_2(S-p-BrTPCP)$_4$ and Rh_2(R-3,5-di(p-*t*BuPh)TPCP)$_4$-catalyzed reactions using diazo compounds either generated in flow or by conventional batch reactions.

In chapter 5, a scalable flow reactor is demonstrated for enantioselective and regioselective rhodium carbene reactions (cyclopropanation and C-H functionalization) by developing cascade reaction methods employing a microfluidic flow reactor system containing immobilized dirhodium catalysts in conjunction with the flow synthesis of diazo compounds. This allows the utilization of the energetic diazo compounds in a safe manner and the recycling of the dirhodium catalysts multiple times. This approach is amenable to application in a bulk-scale synthesis employing asymmetric C-H functionalization by

stacking multiple fibers in one reactor module. The products from this sequential flow–flow reactors are compared with a conventional batch reactor or flow–batch reactor in terms of yield, regioselectivity, and enantioselectivity

CHAPTER 1. INTRODUCTION

1.1 Organosilane structure

Organosilanes are versatile organic compounds commonly used for modification of surfaces due to their ability to incorporate four tunable functional groups. In general, organosilanes employed in surface modification have two types of functional groups ($R_{(4-n)}$-Si-$(R'X)_n$ n=1, 2), where R is Cl or an alkoxy group for grafting on the surface, R' is an organic bridge (e.g., alkyl or phenyl spacer) connecting the Si atom, and the targeted organofunctional group X, as shown in figure 1.1. The most commonly used organosilane type used for surface modification of (in)organic supports is a trialkoxysilane. This structure allows the silane to strongly bind to different (in)organic support materials having surface hydroxyl groups. Depending on the application of the silane, the organofunctional group, X, can be amino, mercapto, glycidoxy, vinyl, or methacryloxy groups, among others (figure 1.1).[1]

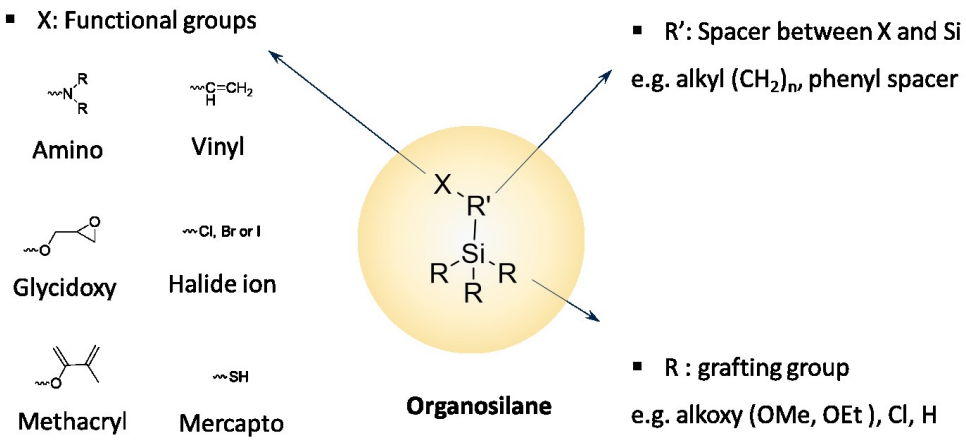

Figure 1.1. Various structures of organosilanes and functional end groups

1.2 Surface modification procedures using organoalkoxysilanes

As noted above, organoalkoxysilanes have been widely used for surface modification of (in)organic support materials that have hydroxyl functional groups on the surface. The degrees of surface modification using organoalkoxysilanes can be controlled by altering the modification conditions such as the solvent, water content, pH, temperature, time, and other factors. In general, the hydroxyl groups of the support material are functionalized by the organosilanes under anhydrous or water induced conditions (Figure 1.2).[2] In the first case, alkoxy and silanol moieties are directly reacted, and alcohol is produced as a byproduct under the initially anhydrous conditions. For this method, anhydrous toluene is most often used as the high-boiling solvent. In the case of the water induced process, the surface functional groups (-OH) are modified by the organoalkoxysilane via two steps, organosilane hydrolysis, and condensation. The rate of hydrolysis and condensation are significantly affected by the pH of the organosilane - solvent mixture. For example, when the pH is neutral (pH = 7), the slowest hydrolysis rate is observed, but the condensation rate is very fast so that as soon as the silanes are hydrolyzed, they are directly condensed.

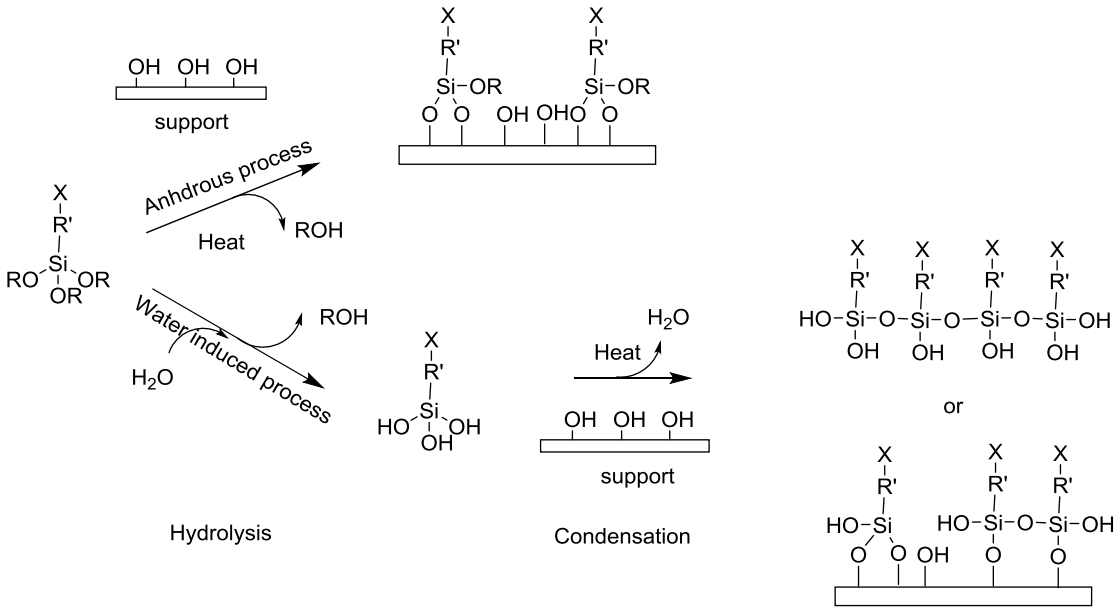

Figure 1.2. Surface modification procedure with organoalkoxysilane under anhydrous and water induced conditions.

The alkoxy groups of the silane also affect the rate of hydrolysis. Under the same hydrolysis conditions, methoxysilanes are more rapidly hydrolyzed than ethoxysilanes.[3] Besides, the length of alkyl chain between the functional end group, X, and the Si atom influences the hydrolysis rate of the silanes. According to Wacker Chemical, the methyl linker silane (α-methacryloxymethyltrimethoxy silane) hydrolyzes 20 times faster than the propyl linker silane (γ-methacryloxypropyltrimethoxy silane) in a water/acetone mixture at pH 4.[4]

Our group has extensively used organosilanes containing stable, target functional groups as well as reactive groups for surface grafting to modify silica and alumina surfaces while imparting specific functionalities. Two major thrusts have been (i) incorporation of molecularly well-defined active sites for heterogeneous catalysis[5–7] and (ii) grafting of adsorption sites for gas separation applications.[7–10] Based on the above synthesis

techniques, I have immobilized organosilanes on support materials to create (a) adsorbents for CO_2 capture to better understand the molecular mechanism for CO_2 adsorption (a fundamental aim) and (ii) heterogeneous C-H functionalization catalysts in conjunction with the development of a flow reactor system (an applied goal).

1.3 CO_2 adsorption with amine functionalized solid sorbents

Amine functionalized porous solids have attracted attention as useful materials for CO_2 adsorption.[11,12] A wide array of amine-containing molecules and macromolecules containing various types of amines (primary, secondary, tertiary and combinations thereof) have been investigated for CO_2 adsorption in combination with numerous solid supports. Previously, we and others have categorized these adsorbents into three classes in accordance with their physical and chemical features (Figure 3).[13,14] In general, class 1 materials are classified as adsorbents containing amine molecules physically impregnated into the pores of the solid support. An array of amines, including those with short alkyl chains (e.g., diethylenetriamine (DETA)[15] and tetraethylenepentamine (TEPA)[16]) and branched polymers (e.g., poly(ethylenimine) (PEI)[17]) have been impregnated into porous support materials. Class 2 materials are based on the amine-containing molecules that can be chemically grafted onto the support materials or are otherwise bound to the adsorbent via covalent bonds. Most commonly, amine-containing alkoxysilanes (e.g., aminopropyltrialkoxysilane (MONO),[18] 3-(2-aminoethylamino)propyltrimethoxy silane (DI)[19] and 3-[2-(2-aminoethylamino)ethylamino]propyltrimethoxysilane (TRI)[20] are grafted to pre-synthesized oxide supports or are co-condensed[21] with silica forming molecules such as tetraethylorthosilicate. Class 3 materials are synthesized by in-situ

polymerization reactions of amine monomers (e.g., aziridine,[22] melamine,[23] L-lysine N-carboxyanhydride[24]) in the pores of the support materials. Considering the potential industrial application of supported amine materials for CO_2 capture from air[25] or flue gas,[11] amine containing solid adsorbents have been proposed as promising materials.

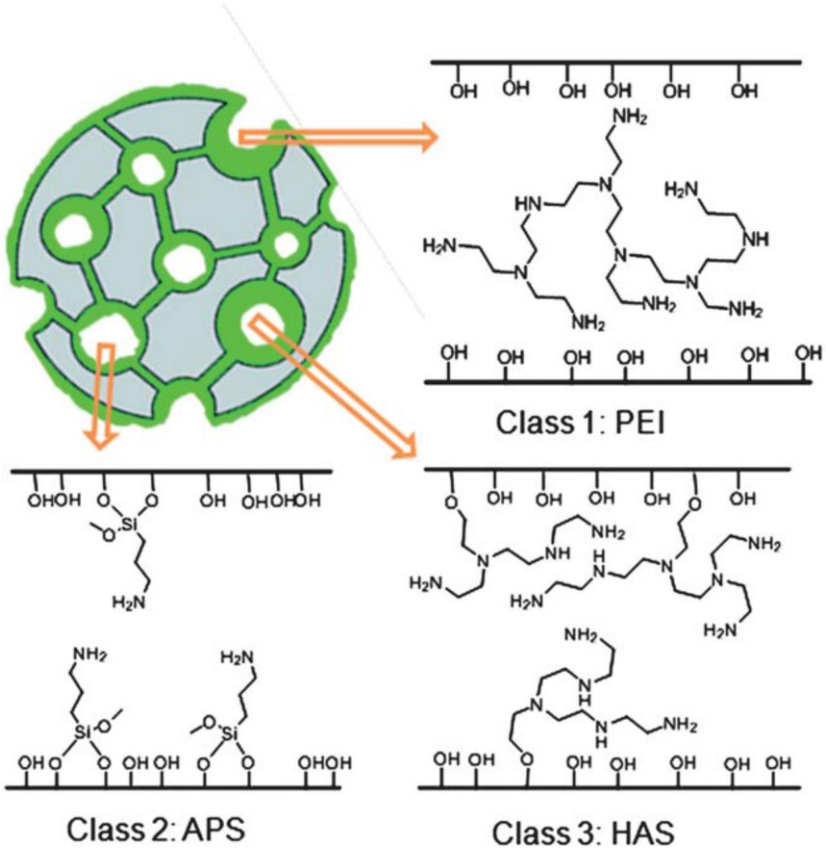

Figure 1.3. Categories of amine containing solid adsorbents. Reproduced with permission from ref 13. Copyright 2011 Royal Society of Chemistry.

1.3.1 Cooperative amine interactions for CO_2 capture

Based primarily on a range of *in-situ* FTIR studies of adsorbents contacted with CO_2,[26–29] the primary adsorbed species on supported amines have been identified as alkyl carbamic acid and alkylammonium carbamate species under both dry and humid conditions. Caplow[30] suggested the mechanism of formation of these species based on

solution studies, involving a zwitterionic mechanism, which requires free bases such as hydroxyl groups, water or another amine (1→2b, below).

$$RNH_2 + CO_2 \rightarrow RNH_2^+COO^- \quad (1)$$

$$RNH_2^+COO^- \rightarrow RNHCOOH \quad (2a)$$

$$RNH_2{}^+COO^- \text{ or } (RNHCOOH) + B \rightarrow RNHCOO^- + BH^+ \quad (2b)$$

where B and R is base and alkyl group, respectively. However, studies utilizing *in-situ* IR spectroscopy and NMR spectroscopy have also identified carbamic acid species on the surface.[31] These may result from the pathway 1 to 2a shown above, with carbamic acid being a metastable species or an intermediate on the way to alkyl ammonium carbamates (1→2a→2b). Some prior reports have suggested that carbamic acid species may be stabilized by free silanols on the silica surface.[32,33] Given these proposed sorption pathways, under dry conditions in the absence of water or hydroxide, two amines are required to adsorb one CO_2 molecule as an alkylammonium carbamate via amine-amine interactions, or one amine may capture one CO_2 molecule as a presumably less stable carbamic acid species. In my master thesis work, I prepared a range of organosilanes containing different amine groups, and I utilized them to study intramolecular vs. intermolecular CO_2 adsorption at the amine sites. For the intramolecular CO_2 adsorption, ultralow loadings of the organosilane molecules were grafted on the mesoporous silica SBA-15 support so that CO_2 could be adsorbed by primarily or only intramolecular amine interactions. As the organosilane loading on the surface increases, CO_2 can be adsorbed by intermolecular interactions, with adjacent amines from another organosilane. The possible chemical species resulting from CO_2 chemisorption via intramolecular and intermolecular

ammine interactions on organosilane (TRI) grafted silica adsorbents are shown in Figure 1.4.

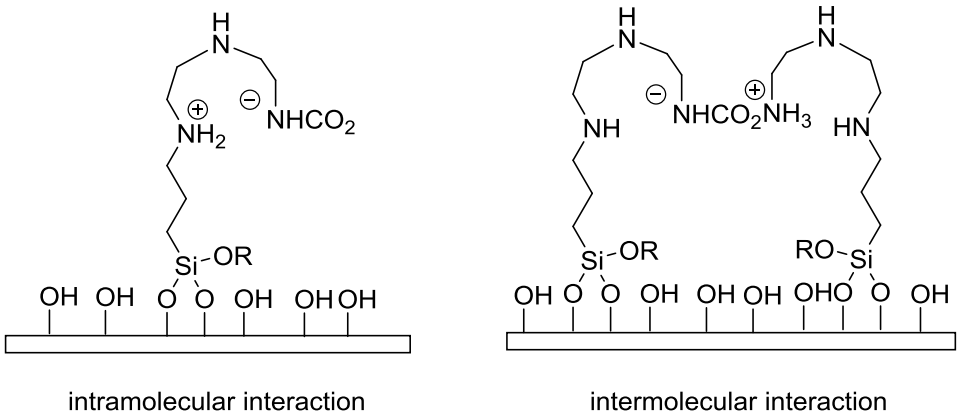

Figure 1.4. Intramolecular vs intermolecular amine interactions for CO_2 adsorption under dry conditions.

1.4 C-H functionalization

C-H functionalization is a rapidly expanding research theme for organic chemists because, historically, the abundant C-H bonds of organic compounds are not easily activated, but modern advances now make this possible. Using the prior, historical paradigm, target molecules needed to be synthesized through complex routes via specific reactions (oxidation/reduction, aromatic substitution, and nucleophilic/electrophilic attack) on limited functional groups rather than via direct activation of the C-H bond (Figure 1.5). As a result, targeted organic compounds have usually been synthesized through multiple reaction and separation steps. This necessitates the utilization of many reaction and separation steps in the synthesis of complex organic molecules, which reduces the overall yield. On the other hand, the abundant C-H bonds in the same molecules, which are relatively stable compared with the sites denoted by the pink arrows, have not historically

been used as reactive sites in the reactions. However, intensive research during the last decade on catalytic C-H functionalization has brought significant innovation in direct C–H activation catalysts and procedures.[34] These advances enable the synthesis of numerous organic compounds within a few steps.

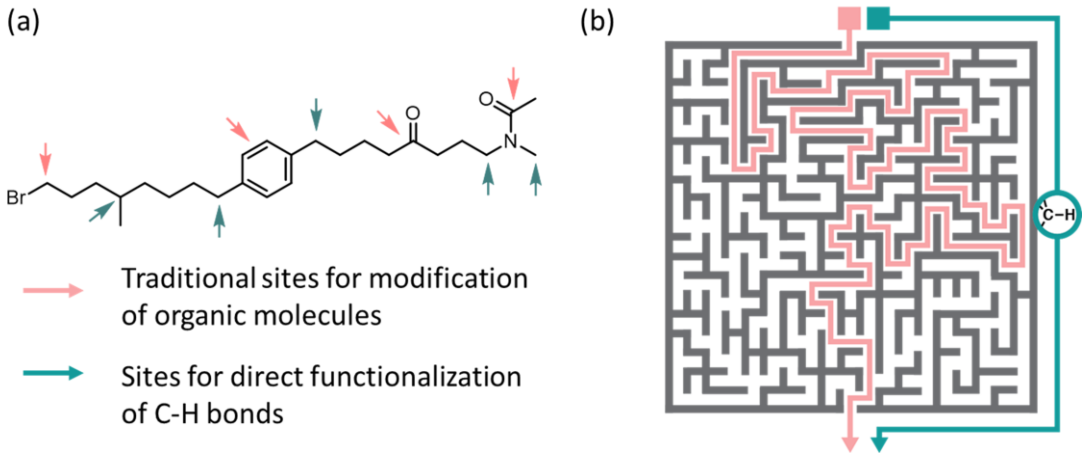

Figure 1.5. (a) The traditional site for organic compound synthesis (pink) and challenging C-H bond for direct functionalization (green)[34], (b) Synthetic route for target material with the conventional method (pink) and C-H functionalization (green).[35] Reproduced with permission from ref 34. Copyright 2008 Nature.

In recent years, dirhodium catalyzed C-H functionalization via dirhodium-carbene intermediates has shown a wide range of intermolecular C-H functionalization pathways, where the site selectivity and stereoselectivity are dominated by catalyst control.[36–43] The dirhodium catalyst consists of two rhodium atoms and two or four identical chiral ligands. The ligands are symmetrically coordinated around the dirhodium core to form the "paddlewheel" structure as shown in Figure 1.6. Depending on the ligand structure, the catalyst shows various symmetries such as D_2, C_2 or C_4 symmetry, among others.

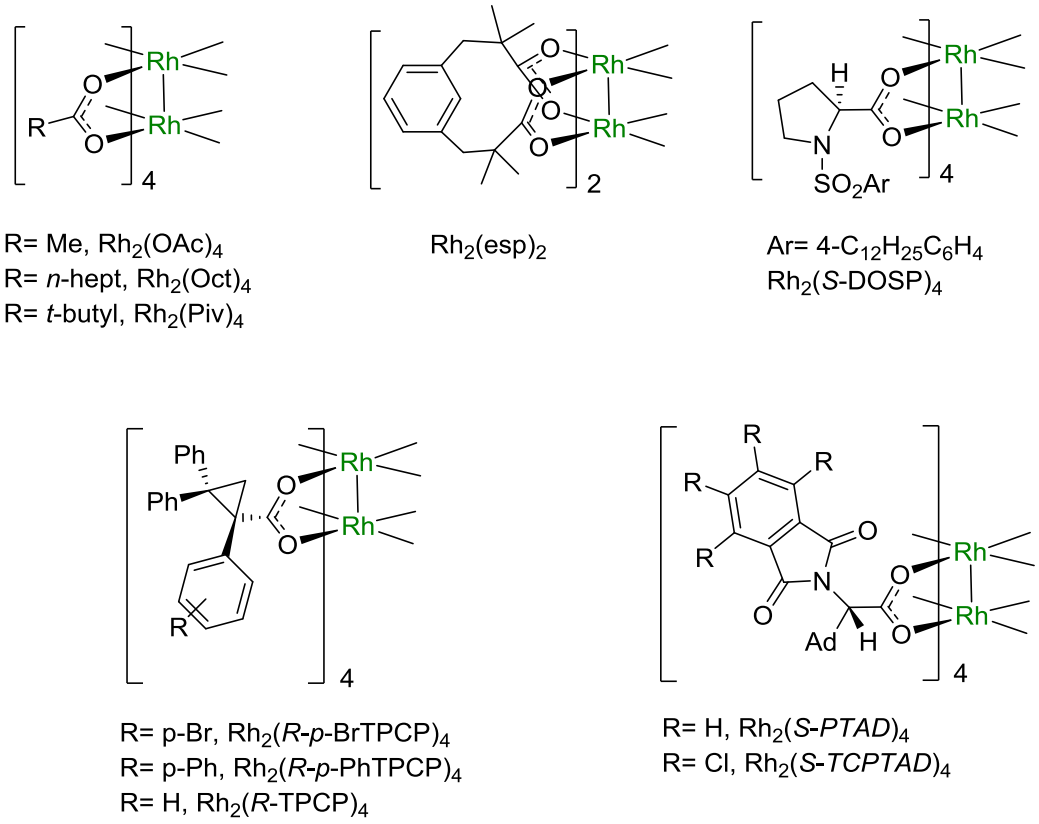

Figure 1.6. Dirhodium catalysts with various ligands[36–43]

The mechanism of the dirhodium catalyzed enantioselective C-H functionalization is shown in Figure 1.7. To form the dirhodium-carbene intermediate, a diazo compound binds on the active site of the dirhodium catalyst, after which dinitrogen (N_2) is detached, and the active dirhodium-carbene species is formed. The ligands of the catalyst act as a directing agent that controls the binding angle of the diazo compound on the dirhodium catalyst and C-H bond of the substrate that can approach the carbene species, allowing for substrate-carbon interaction from a specific direction, leading to stereoselective and/or regioselective C-H functionalization.

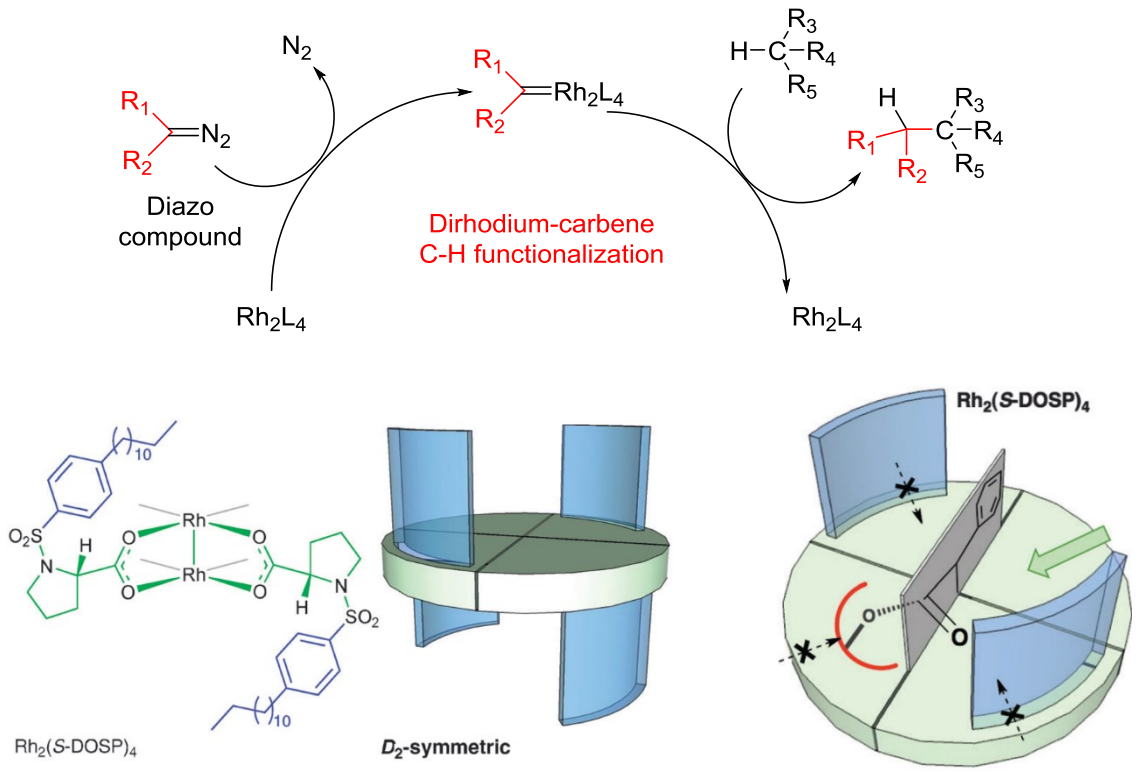

Figure 1.7. (a) Mechanism of dirhodium-carbene intermediated C–H functionalization[34] (b) Schematic structure of dirhodium catalyst (rhodium: green disk, chiral ligand: blue shield)[34]. Reproduced with permission from ref 34. Copyright 2008 Nature.

The dirhodium catalyzed C-H functionalization via dirhodium-carbene intermediates has been applied for the synthesis of pharmaceutical products including Ritalin,[44] Zoloft,[45] Effexor[46] and a drug for cocaine addiction.[47] In addition, the dirhodium based carbene chemistry has also been applied as an innovative methodology for total synthesis. Generally, natural product derivatives are synthesized through multiple synthesis steps due to their complex structures, typically including several chiral centers. However, new methodologies driven by dirhodium catalysts allow for significant improvement in the total synthesis of numerous complex organic molecules regarding yield

and enantioselectivity.[48–50] These pharmaceutical applications of dirhodium catalysts are shown in Figure 1.8.

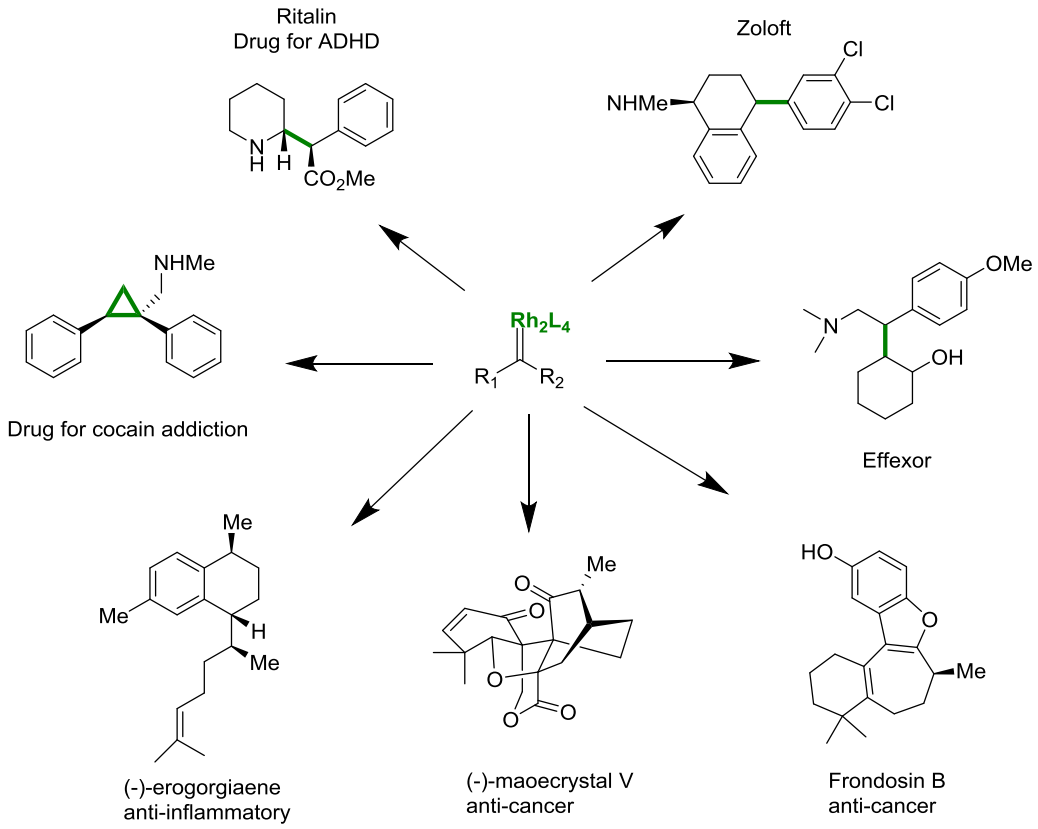

Figure 1.8. The pharmaceutical applications of dirhodium catalysts

Most of the research using dirhodium carbene catalysts have been conducted primarily with soluble molecular catalysts in batch reactors, which has some limitations for scaling up to industrial synthesis scales. As stated earlier, to generate dirhodium-carbene intermediates, utilization of diazo compounds is necessary. Diazo compounds are known as highly energetic and toxic chemicals, such that local storage in bulk is not favorable. Moreover, the expense of the rhodium metal and chiral ligands present another barrier for the application of carbene chemistry in the pharmaceutical industry. To this end,

in this thesis, I will develop new strategies to achieve scalable and sustainable C–H functionalization systems by engineering materials, primarily supported catalysts using organosilane functionalization, and deploying them in flow reactors.

1.5 References

(1) Xie, Y.; Hill, C. a. S. S.; Xiao, Z.; Militz, H.; Mai, C. Silane Coupling Agents Used for Natural Fiber/Polymer Composites: A Review. *Compos. Part A Appl. Sci. Manuf.* **2010**, *41* (7), 806–819.

(2) Brinker, C. J. Hydrolysis and Condensation of Silicates: Effects on Structure. *J. Non. Cryst. Solids* **1988**, *100* (1–3), 31–50.

(3) Kang, H.-J.; Meesiri, W.; Blum, F. D. Nuclear Magnetic Resonance Studies of the Hydrolysis and Molecular Motion of Aminopropylsilane. *Mater. Sci. Eng. A* **1990**, *126* (1–2), 265–270.

(4) Wacker Chemical AG publication. *Organofunctional Silanes from Wacker*; Wacker Chemical AG publication.

(5) Collier, V. E.; Ellebracht, N. C.; Lindy, G. I.; Moschetta, E. G.; Jones, C. W. Kinetic and Mechanistic Examination of Acid-Base Bifunctional Aminosilica Catalysts in Aldol and Nitroaldol Condensations. *ACS Catal.* **2016**, *6* (1), 460–468.

(6) Brunelli, N. A.; Jones, C. W. Tuning Acid-Base Cooperativity to Create next Generation Silica-Supported Organocatalysts. *J. Catal.* **2013**, *308*, 60–72.

(7) Brunelli, N. A.; Didas, S. A.; Venkatasubbaiah, K.; Jones, C. W. Tuning Cooperativity by Controlling the Linker Length of Silica-Supported Amines in Catalysis and CO_2 Capture. *J. Am. Chem. Soc.* **2012**, *134* (34), 13950–13953.

(8) Didas, S. A.; Sakwa-Novak, M. A.; Foo, G. S.; Sievers, C.; Jones, C. W. Effect of Amine Surface Coverage on the Co-Adsorption of CO_2 and Water: Spectral Deconvolution of Adsorbed Species. *J. Phys. Chem. Lett.* **2014**, *5* (5), 4194−4200.

(9) Alkhabbaz, M. A.; Bollini, P.; Foo, G. S.; Sievers, C.; Jones, C. W. Important Roles of Enthalpic and Entropic Contributions to CO_2 Capture from Simulated Flue Gas and Ambient Air Using Mesoporous Silica Grafted Amines. *J. Am. Chem. Soc.* **2014**, *136* (38), 13170–13173.

(10) Bali, S.; Leisen, J.; Foo, G. S.; Sievers, C.; Jones, C. W. Aminosilanes Grafted to Basic Alumina as CO_2 Adsorbents-Role of Grafting Conditions on CO_2 Adsorption Properties. *ChemSusChem* **2014**, *7* (11), 3145–3156.

(11) Choi, S.; Drese, J. H.; Jones, C. W. Adsorbent Materials for Carbon Dioxide Capture from Large Anthropogenic Point Sources. *ChemSusChem* **2009**, *2* (9), 796–854.

(12) Serna-Guerrero, R.; Da'na, E.; Sayari, A. New Insights into the Interactions of CO_2 with Amine-Functionalized Silica. *Ind. Eng. Chem. Res.* **2008**, *47* (23), 9406–9412.

(13) Bollini, P.; Didas, S. A.; Jones, C. W. Amine-Oxide Hybrid Materials for Acid Gas Separations. *J. Mater. Chem.* **2011**, *21* (39), 15100–15120.

(14) Goeppert, A.; Czaun, M.; Surya Prakash, G. K.; Olah, G. A. Air as the Renewable Carbon Source of the Future: An Overview of CO_2 Capture from the Atmosphere. *Energy Environ. Sci.* **2012**, *5* (7), 7833–7853.

(15) Wei, J.; Liao, L.; Xiao, Y.; Zhang, P.; Shi, Y. Capture of Carbon Dioxide by Amine-Impregnated as-Synthesized MCM-41. *J. Environ. Sci.* **2010**, *22* (10), 1558–1563.

(16) Yue, M. B.; Chun, Y.; Cao, Y.; Dong, X.; Zhu, J. H. CO2 Capture by As-Prepared SBA-15 with an Occluded Organic Template. *Adv. Funct. Mater.* **2006**, *16* (13),

1717–1722.

(17) Xu, X.; Song, C.; Andresen, J. M.; Miller, B. G.; Scaroni, A. W. Novel Polyethylenimine-Modified Mesoporous Molecular Sieve of MCM-41 Type as High-Capacity Adsorbent for CO_2 Capture. *Energy and Fuels* **2002**, *16* (6), 1463–1469.

(18) Leal, O.; Bolivar, C.; Sepulveda, G.; Molleja, G.; Martinez, G.; Esparragoza, L. Carbon Dioxide Adsorbent and Method for Producing the Adsorbent. U.S. Patent 5,087,597A, 1992.

(19) Zheng, F.; Tran, D. N.; Busche, B. J.; Fryxell, G. E.; Addleman, R. S.; Zemanian, T. S.; Aardahl, C. L. Ethylenediamine-Modified SBA-15 as Regenerable CO_2 Sorbent. *Ind. Eng. Chem. Res.* **2005**, *44* (9), 3099–3105.

(20) Harlick, P. J. E.; Sayari, A. Applications of Pore-Expanded Mesoporous Silicas. 3. Triamine Silane Grafting for Enhanced CO_2 Adsorption. *Ind. Eng. Chem. Res.* **2006**, *45* (9), 3248–3255.

(21) Huh, S.; Wiench, J. W.; Yoo, J.-C.; Pruski, M.; Lin, V. S.-Y. Organic Functionalization and Morphology Control of Mesoporous Silicas via a Co-Condensation Synthesis Method. *Chem. Mater.* **2003**, *15* (22), 4247–4256.

(22) Hicks, J. C.; Drese, J. H.; Fauth, D. J.; Gray, M. L.; Qi, G.; Jones, C. W. Designing Adsorbents for CO_2 Capture from Flue Gas-Hyperbranched Aminosilicas Capable of Capturing CO_2 Reversibly. *J. Am. Chem. Soc.* **2008**, *130* (10), 2902–2903.

(23) Liang, Z.; Fadhel, B.; Schneider, C. J.; Chaffee, A. L. Stepwise Growth of Melamine-Based Dendrimers into Mesopores and Their CO_2 Adsorption Properties. *Microporous Mesoporous Mater.* **2008**, *111* (1–3), 536–543.

(24) Chaikittisilp, W.; Lunn, J. D.; Shantz, D. F.; Jones, C. W. Poly(L-Lysine) Brush-Mesoporous Silica Hybrid Material as a Biomolecule-Based Adsorbent for CO $_2$ Capture from Simulated Flue Gas and Air. *Chem. - A Eur. J.* **2011**, *17* (38), 10556–10561.

(25) Sanz-Perez, E. S.; Murdock, C. R.; Didas, S. A.; Jones, C. W. Direct Capture of CO_2 from Ambient Air. *Chem. Rev.* **2016**, *116* (19), 11840–11876.

(26) Danon, A.; Stair, P. C.; Weitz, E. FTIR Study of CO_2 Adsorption on Amine-Grafted SBA-15: Elucidation of Adsorbed Species. *J. Phys. Chem. C* **2011**, *115* (23), 11540–11549.

(27) Bacsik, Z.; Atluri, R.; Garcia-Bennett, A. E.; Hedin, N. Temperature-Induced Uptake of CO_2 and Formation of Carbamates in Mesocaged Silica Modified with n-Propylamines. *Langmuir* **2010**, *26* (12), 10013–10024.

(28) Wang, X.; Schwartz, V.; Clark, J. C.; Ma, X.; Overbury, S. H.; Xu, X.; Song, C. Infrared Study of CO_2 Sorption over "Molecular Basket" Sorbent Consisting of Polyethylenimine-Modified Mesoporous Molecular Sieve. *J. Phys. Chem. C* **2009**, *113* (17), 7260–7268.

(29) Hiyoshi, N.; Yogo, K.; Yashima, T. Adsorption Characteristics of Carbon Dioxide on Organically Functionalized SBA-15. *Microporous Mesoporous Mater.* **2005**, *84* (1–3), 357–365.

(30) Caplow, M. Carbamate Formation and Breakdown - Kinetics and Mechanism. **1968**, No. 8, 6795–6803.

(31) Pinto, M. L.; Mafra, L.; Guil, J. M.; Pires, J.; Rocha, J. Adsorption and Activation of CO_2 by Amine-Modified Nanoporous Materials Studied by Solid-State NMR and

$^{13}CO_2$ Adsorption. *Chem. Mater.* **2011**, *23* (6), 1387–1395.

(32) Aziz, B.; Hedin, N.; Bacsik, Z. Quantification of Chemisorption and Physisorption of Carbon Dioxide on Porous Silica Modified by Propylamines: Effect of Amine Density. *Microporous Mesoporous Mater.* **2012**, *159*, 42–49.

(33) Bacsik, Z.; Ahlsten, N.; Ziadi, A.; Zhao, G.; Garcia-Bennett, A. E.; Martín-Matute, B.; Hedin, N. Mechanisms and Kinetics for Sorption of CO_2 on Bicontinuous Mesoporous Silica Modified with N-Propylamine. *Langmuir* **2011**, *27* (17), 11118–11128.

(34) Davies, H. M. L.; Manning, J. R. Catalytic C-H Functionalization by Metal Carbenoid and Nitrenoid Insertion. *Nature* **2008**, *451* (7177), 417–424.

(35) http://www.nsf-cchf.com/.

(36) Qin, C.; Boyarskikh, V.; Hansen, J. H.; Hardcastle, K. I.; Musaev, D. G.; Davies, H. M. L. D_2-Symmetric Dirhodium Catalyst Derived from a 1,2,2-Triarylcyclo-Propanecarboxylate Ligand: Design, Synthesis and Application. *J. Am. Chem. Soc.* **2011**, *133*, 19198–19204.

(37) Guptill, D. M.; Davies, H. M. L. 2,2,2-Trichloroethyl Aryldiazoacetates as Robust Reagents for the Enantioselective C–H Functionalization of Methyl Ethers. *J. Am. Chem. Soc.* **2014**, *136* (51), 17718–17721.

(38) Fu, L.; Wang, H.; Davies, H. M. L. Role of Ortho-Substituents on Rhodium-Catalyzed Asymmetric Synthesis of Beta-Lactones by Intramolecular C-H Insertions of Aryldiazoacetates. *Org. Lett.* **2014**, *16* (11), 3036–3039.

(39) Liao, K.; Negretti, S.; Musaev, D. G.; Bacsa, J.; Davies, H. M. L. Site-Selective and Stereoselective Functionalization of Unactivated C–H Bonds. *Nature* **2016**, *533*

(7602), 230–234.

(40) Liao, K.; Liu, W.; Niemeyer, Z. L.; Ren, Z.; Bacsa, J.; Musaev, D. G.; Sigman, M. S.; Davies, H. M. L. Site-Selective Carbene-Induced C–H Functionalization Catalyzed by Dirhodium Tetrakis(Triarylcyclopropanecarboxylate) Complexes. *ACS Catal.* **2018**, *8* (1), 678–682.

(41) Liao, K.; Pickel, T. C.; Boyarskikh, V.; Bacsa, J.; Musaev, D. G.; Davies, H. M. L. Site-Selective and Stereoselective Functionalization of Non-Activated Tertiary C-H Bonds. *Nature* **2017**, *551* (7682), 609–613.

(42) Goto, T.; Natori, Y.; Takeda, K.; Nambu, H.; Hashimoto, S. Catalytic Enantioselective C–H Functionalization of Indoles with α-Diazopropionates Using Chiral Dirhodium(II) Carboxylates: Asymmetric Synthesis of the (+)-α-Methyl-3-Indolylacetic Acid Fragment of Acremoauxin A. *Tetrahedron: Asymmetry* **2011**, *22* (8), 907–915.

(43) DeAngelis, A.; Shurtleff, V. W.; Dmitrenko, O.; Fox, J. M. Rhodium(II)-Catalyzed Enantioselective C−H Functionalization of Indoles. *J. Am. Chem. Soc.* **2011**, *133* (6), 1650–1653.

(44) Davies, H. M. L.; Hopper, D. W.; Hansen, T.; Liu, Q.; Childers, S. R. Synthesis of Methylphenidate Analogues and Their Binding Affinities at Dopamine and Serotonin Transport Sites. *Bioorganic Med. Chem. Lett.* **2004**, *14* (7), 1799–1802.

(45) Davies, H. M. L.; Stafford, D. G.; Hansen, T. Catalytic Asymmetric Synthesis of Diarylacetates and 4,4-Diarylbutanoates. A Formal Asymmetric Synthesis of (+)-Sertraline. *Org. Lett.* **1999**, *1* (2), 233–236.

(46) Davies, H. M. L.; Ni, A. Enantioselective Synthesis of β-Amino Esters and Its

Application to the Synthesis of the Enantiomers of the Antidepressant Venlafaxine. *Chem. Commun.* **2006**, No. 29, 3110–3112.

(47) Chepiga, K. M.; Qin, C.; Alford, J. S.; Chennamadhavuni, S.; Gregg, T. M.; Olson, J. P.; Davies, H. M. L. Guide to Enantioselective Dirhodium(II)-Catalyzed Cyclopropanation with Aryldiazoacetates Dedicated to Professor Melanie Sanford in Recognition of Her Receipt of the Tetrahedron Young Investigator Award. *Tetrahedron* **2013**, *69* (27–28), 5765–5771.

(48) Olson, J. P.; Davies, H. M. L. Asymmetric [4+3] Cycloadditions between Benzofuranyldiazoacetates and Dienes: Formal Synthesis of (+)-Frondosin B. *Org. Lett.* **2008**, *10* (4), 573–576.

(49) Lu, P.; Mailyan, A.; Gu, Z.; Guptill, D. M.; Wang, H.; Davies, H. M. L.; Zakarian, A. Enantioselective Synthesis of (-)-Maoecrystal v by Enantiodetermining C-H Functionalization. *J. Am. Chem. Soc.* **2014**, *136* (51), 17738–17749.

(50) Davies, H. M. L.; Lian, Y. The Combined C-H Functionalization/Cope Rearrangement: Discovery and Applications in Organic Synthesis. *Acc. Chem. Res.* **2012**, *45* (6), 923–935.

CHAPTER 2. CO_2 ADSORPTION AND OXIDATIVE DEGRADATION OF SILICA-SUPPORTED BRANCHED AND LINEAR AMINOSILANES

2.1 Introduction

Amine groups are known as active moieties for CO_2 adsorption via chemisorption at low temperature (< 100 °C), which allows supported-amine adsorbents to become promising materials for CO_2 capture from dilute (point source flue gas) and ultra-dilute (CO_2 in the ambient air, or direct air capture) gas streams. In this context, a wide array of amine containing molecules and macromolecules containing various types of amines (primary, secondary, and tertiary and combinations thereof) have been investigated for CO_2 adsorption. Numerous research groups have evaluated which amine moieties provide the highest amine efficiencies under controlled conditions, typically using dry gases. For example, several organosilanes containing amine groups such as well-defined primary (3-aminopropylsilyl (APS)), secondary (*n*-methylaminopropylsilyl, MAPS), or tertiary (*n,n*-dimethylaminopropylsilyl DMAPS) amine groups have been grafted on various supports and their CO_2 sorption capacities and amine efficiencies (adsorbed CO_2 mol / N mol) were measured.[1–3] Under dry conditions, the theoretical maximum amine efficiency for chemisorption using primary or secondary amines is 0.5, which means two amines adsorb one CO_2 molecule in the form of ammonium carbamates.[4–6] Under these conditions, because tertiary amines cannot form carbamates, their CO_2 uptake is zero. Generally, APS yields higher amine efficiencies than MAPS, and DMAPS does not adsorb CO_2 via chemisorption. In addition to organosilanes that contain a single amine, researchers have

also studied molecular that contain multiple amine moieties. A popular aminosilane containing primary and secondary amines ([3-(2-Aminoethylamino)propyl]trimethoxysilane, DI), gives an amine efficiency lower than APS because the secondary amine of DI does not effectively adsorb CO_2 molecules as well as the primary amine of APS or DI. While CO_2 chemisorption does not occur with tertiary amines under dry conditions, humidity allows access to adsorption via formation of bicarbonate structures.[5,7] Formation of bicarbonates is also possible with primary and secondary amines, though they form in lower amounts and are challenging to observe spectroscopically, under typical circumstances.[8–10]

During practical application of supported amine adsorbents for CO_2 capture, oxidative degradation of the amine molecule is an important mode of sorbent deactivation, affecting the cyclability and practical lifetime of the adsorbent. The oxidation of amine molecules can transform the amines into less basic and therefore less CO_2-sorbing functional groups, like imines and amides.[11–17] For lab scale CO_2 adsorption studies, oxygen exposure to the amine adsorbents is often limited because ultra-high purity (UHP) gas cylinders are routinely used. However, CO_2 capture processing under oxygen-free UHP gas streams deviates substantially from the conditions of potential industrial application, and under practical conditions the amine may be oxidized by oxygen in the gas streams during adsorption (often a few percents for flue gas, or 21% in air) or more importantly, during desorption, when elevated temperatures are often used. For a robust practical application, oxidation must be avoided or at least minimized.

Several studies have investigated the oxidation of amine molecules in both the liquid and solid phases. For example, in some liquid phase studies,[18–21] various amine

molecules were dissolved in the water and exposed to air at 140 ºC, with the generated species analyzed by GC and NMR methods. In the case of primary amines (e.g., ethanolamine, 2-amino-2-methylpropane-1-ol), dealkylation, dimerization, and piperazinone formation were the main reactions observed, and for secondary and tertiary amines (e.g., N,N,N′,N′-Tetramethylethylenediamine, N,N′-Dimethylethylenediamine), demethylation, methylation, dealkylation, addition, ring closure and replacement of the hydroxyl chain by a methyl group were the main degradation reactions, in which several new species were synthesized by water induced oxidative reactions. It is known from the absorption literature that metal leached from process equipment into aqueous solution can cause amine oxidation during thermal cycling.[22–26] This knowledge was applied to solid phase studies by Choi et al., who reported that the addition of metal chelating agents to silica/amine adsorbents could help stabilize the materials towards oxidative degradation.[27] Our group[14] and others[11,12] previously reported that secondary amine containing aminosilanes were more readily oxidized than aminosilanes containing primary or tertiary amines under the same oxidation conditions (>110 ºC exposure to O_2 for 24 h). From these results, we inferred that the secondary amines make aminosilanes containing various amines (e.g., DI) susceptible to oxidation at high temperatures (>110 ºC). However, in more recent work from our group, an array of different amine molecules containing primary and tertiary amine groups were also shown to oxidize under some conditions, and reduced CO_2 capacities were observed compared to the fresh samples after oxidation.[28] In that paper, the CO_2 uptake of small (< MW 300 g/mol) dendritic and linear amine molecules was measured before and after oxidation of the amine molecules at 110 ºC. Each amine molecule contained either ethyl or propyl carbon linkers between adjacent amine

moieties. A key finding was that propyl linked amine molecules of both the dendritic and linear structures showed higher oxidation resistance compared to the ethyl linked amine molecules.

Thus, the stability of amine adsorbents towards oxidation cannot be categorized solely based on their amine types. Most likely, the stability of various amines depends on the energetics of the conversion of the C-H bond alpha to the amine, which is affected by the molecular structure of the amine moiety. While previous liquid phase studies reported the possible structures of the oxidized species from the various amine molecules, because the structure of the amine molecules used in typical solid sorbents are not same as the amine molecules studied in solution, a clear correlation of the expected oxidation pathways for differently supported amine adsorbents is not available. Additionally, many of the suggested oxidation mechanisms[18,19] for certain species require water for the reactions. Moreover, according to the liquid phase studies, amine molecules can be decomposed into fragments during the oxidation (e.g., dealkylation), which has not been explicitly studied in solid adsorbents containing amine molecules. This is due to the highly volatile nature of these fragmented compounds, which can be challenging to collect and characterize in vapor/gas phase studies. From prior solid phase studies, it is known that the oxidized functional groups observed spectroscopically are amide (–C(=O)NH–) and imine (–CH=N–) groups, but more detailed reaction pathways and product structures for different amines remain unclear.

In this study, we tried to clarify the impact of the structure and nature of the amine moieties on their CO_2 adsorption and oxidative degradation properties. Thus, new branched and linear aminosilanes were designed to contain primary, secondary or tertiary amines

with ethyl or propyl spacers between the adjacent two amines. The synthesized aminosilanes were grafted onto prototypical SBA-15 supports, and their CO_2 capacities and oxidative degradation characteristics were explored.

2.2 Experimental section

2.2.1 Materials

All chemicals (higher than Reagent Grade purity) were used without further purification. Poly(ethylene glycol)-block-poly(propylene glycol)-block-poly(ethylene glycol) (Pluronic P123, Mn ~5800), tetraethylorthosilicate (TEOS), bis(2-chloroethyl)amine hydrochloride, sodium azide, 3-aminopropanol, 3-chloropropanol, anhydrous toluene, potassium carbonate (K_2CO3), were purchased from Sigma-Aldrich. Methanol, hexane, ethyl acetate and chloroform were purchased from EMD. 3-aminopropyl trimethoxysilane, 3-(2-Aminoethylamino)propyltrimethoxysilane, 3-[2-(2-aminoethylamino)ethylamino]propyltri methoxysilane and 3-chloropropyltriethoxysilane were purchased from Gelest.

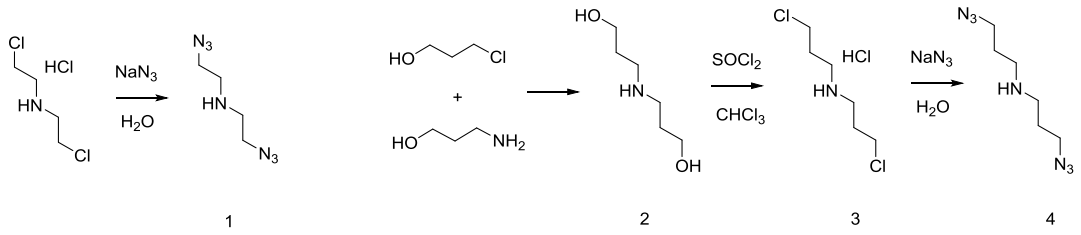

Scheme 2.1. Preparation of diazidoamines with ethyl and propyl spacer.

2.2.2 Preparation of compounds

Preparation of bis(2-azidoethyl)amine **1**[29]

The bis(2-azidoethyl)amine was prepared by reported procedure[29] with minor modification (Caution: Sodium azide is possible explosive material, so evaporation of the solvent (DI water) containing unreacted sodium azide at elevated temperature would be dangerous. For the preparation of **1**, the unreacted sodium azide and generated sodium chloride were separated by phase separation before the evaporation of the solvent (DI water) with rotary evaporator). A mixture of bis(2-chloroethyl)amine hydrochloride (3 g, 21.1 mmol) and sodium azide (6.6 g, 102 mmol) in DI water (100 mL) was heated at 80 °C for 24 hr. Aqueous sodium hydroxide solution was added to the mixture until pH 14, and then the solution was extracted with diethyl ether multiple times. The organic phase was dried with magnesium sulfate and then filtered and evaporated under reduced pressure. The crude product was diluted with 50/50 ethyl acetate/ether and purified with silica gel chromatography. The product fractions were collected, and the solvent was evaporated to yield the final product. The analyzed ^{1}H NMR spectrum for the target compound was similar to that presented in previous literature.[29] **^{1}H NMR** ($CDCl_3$): 3.44 (t, 4H), 2.83 (t, 4H).

Preparation of dipropanolamine **2**[30]

A mixture of 3-aminopropanol (14.5 mL, 190 mmol) and 3-chloropropanol (8 mL, 95.7mmol) in DI water (45mL) was refluxed over 24 h. Then, an excess amount of potassium hydroxide (380 mmol) was added to the mixture. The solvent was evaporated to yield viscous oil and large quantities of potassium chloride, which were filtered and washed with acetone. The organic phase was dried over magnesium sulfate and filtered and evaporated to yield a dark brown oil. The desired product was obtained by distillation of

the oil as a light yellow oil (first fraction: 110 ºC 0.45 mbar, main product: 160 ºC, 0.45 mbar) (Scheme 1). The analyzed ^{1}H NMR spectrum for the target compound was similar to that presented in previous literature.[30] **^{1}H NMR** ($CDCl_3$): 3.76 (t, 4H), 2.82 (t, 4H), 1.71 (m, 4H).

Preparation of bis(3-chloropropyl)amine hydrochloride **3**[28]

To a solution of dipropanolamine (6 mL) in chloroform (45 mL), thionyl chloride (18 mL) diluted in chloroform (15 mL) was added dropwise under vigorous stirring at 0 °C. The mixture was stirred at room temperature for 8 h. As soon as the thionyl chloride was added, a brown solid was formed, which was slowly dissolved after stirring at room temperature. Then the solution was heated to 55 °C for 2 h (precipitant was generated) then cooled down to room temperature and stirred overnight. The precipitant was filtered and washed with ether and acetone several times until the powder became white. The powder was dried at 60 ºC under vacuum overnight. The analyzed ^{1}H NMR spectrum for the target compound was similar to that presented in previous literature.[28] **^{1}H NMR** ($CDCl_3$): 3.72 (t, 4H), 3.17(t, 4H), 2.43(m, 4H).

Preparation of bis(3-azidopropyl)amine **4**[28]

Bis(3-azidopropyl)amine was synthesized by using a similar preparation method as for 1 (Scheme 1). The analyzed ^{1}H NMR spectrum for the target compound was similar to that presented in previous literature.[28] **^{1}H NMR** ($CDCl_3$): 3.38 (t, 4H), 2.71 (t, 4H), 1.77 (m, 4H).

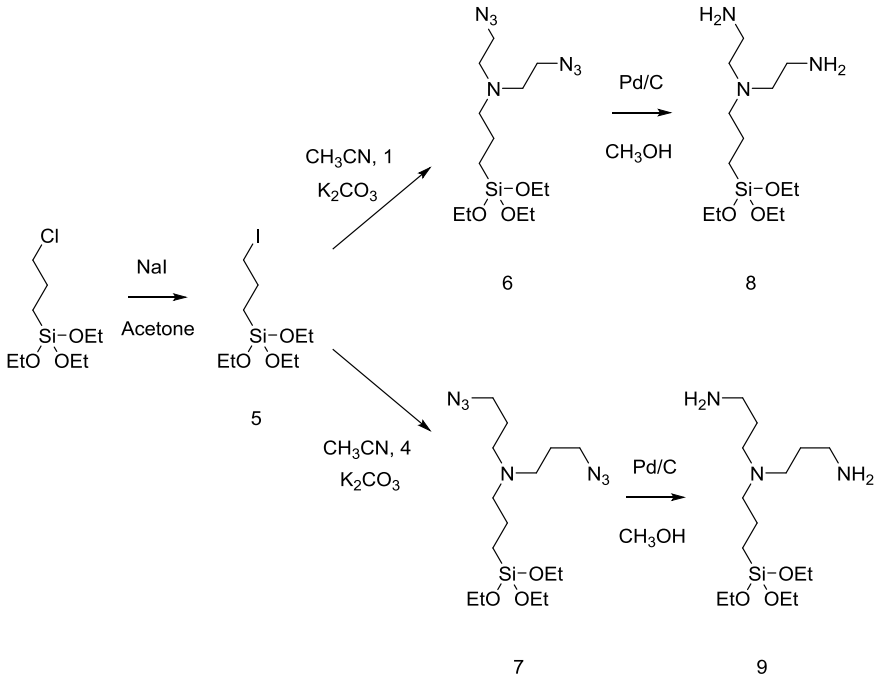

Scheme 2.2. Preparation of branched aminosilane with ethyl and propyl spacer

Preparation of 3-iodopropyltriethoxysiane **5**

A mixture of 3-chloropropyltriethosiane (1 eq) and sodium iodine (3 eq) in anhydrous acetone was refluxed overnight. The solvent was evaporated with reduced pressure. Excess sodium iodide was filtered and washed several times with diethyl ether. The solvent was evaporated with reduced pressure (Scheme 2). The analyzed ^{1}H NMR spectrum for the target compound was similar to that presented in previous literature.[31] **^{1}H NMR** ($CDCl_3$, 400 MHz): 3.86-3.80 (q, 6H), 3.25-3.21 (t, 2H), 1.98-1.90 (m, 2H), 1.25-1.22 (t, 9H), 0.76-0.72 (m, 2H)

Preparation N,N-bis(2-azidoethyl)-3-(triethoxysilyl)propan-1-amine **6** and N,N-bis(3-azidoproyl)-3-(triethoxysilyl)propan-1-amine **7**

Diazidoamine (**1** or **4**, 10 mmol), iodopropyltriethoxysialne (**5**, 10 mmol), potassium carbonate (30 mmol) were dispersed in anhydrous acetonitrile (100 mL). The mixture was heated at 90 °C for 2 days, then filtered and washed with anhydrous acetonitrile several times. The solution was evaporated by a rotary evaporator. The viscous oil was mixed with hexanes and the mixture was filtered by 0.2μm nylon syringe filter. The solvent was evaporated by rotary evaporator to yield the product. **6**: **^{1}H NMR** ($CDCl_3$, 400 MHz): 3.85-3.80 (q, 6H), 3.32-3.29 (t, 4H), 2.74-2.71 (t, 4H), 2.56-2.52 (t, 2H), 1.60-1.54 (m, 2H), 1.25-1.21 (t, 9H), 0.63-0.60 (m, 2H); **7**: **^{1}H NMR** ($CDCl_3$, 400 MHz): 3.85-3.79 (q, 6H), 2.49-2.45 (t, 4H), 2.41-2.37 (t, 2H), 1.73-1.68 (m, 4H), 1.56-1.53 (m, 2H), 1.25-1.21 (t, 9H), 0.60-0.56 (m, 2H)

Preparation of N^1-(2-aminoethyl)-N^1-(3-(triethoxysilyl)propyl)ethane-1,2-diamine **8** and N^1-(3-aminopropyl)-N^1-(3-(triethoxysilyl)propyl)propane-1,3-diamine **9**

To a solution of diazidopropyltriethyoxysialne (**6** or **7**, 4 mmol) in 50 mL of anhydrous ethanol, 5 wt.% Pd/C (0.8 g) was added to the solution under a nitrogen atmosphere. Then the mixture was bubbled by hydrogen for 15 min and stirred for 2 h under hydrogen atmosphere (double layered rubber balloon with H_2). The catalyst, Pd/C, was removed by filtration and the filtrated solution was evaporated by a rotary evaporator. The viscous oil was mixed with hexanes and the mixture was filtered by a 0.2 μm nylon syringe filter. The solvent was evaporated again by a rotary evaporator. **8**: **^{1}H NMR** ($CDCl_3$, 400 MHz): 3.84-3.80 (q, 6H), 2.77-2.75 (t, 4H), 2.53-2.51 (t, 4H), 2.47-2.43 (t, 2H), 1.57-1.50 (m, 2H), 1.24-1.20 (t, 9H), 0.59-0.56 (m, 2H); **^{13}C NMR** ($CDCl_3$, 100 MHz): 58.2, 57.4, 52.3, 39.9, 20.3, 18.2, 7.82; **HRMS** (ESI) calculated $[C_{13}H_{34}N_3O_3Si]^+$

for 308.2364, found 308.2363; **9**: **^{1}H NMR** ($CDCl_3$, 400 MHz): 3.86-3.81 (q, 6H), 2.75-2.45 (t, 4H), 2.43-2.39 (t, 2H), 1.63-1.53 (m, 6H), 1.26-1.22 (t, 9H), 0.62-0.58 (m, 2H); **^{13}C NMR** ($CDCl_3$, 100 MHz): 58.2, 57.1, 51.7, 40.7, 31.0, 20.1, 18.3, 7.9; **HRMS** (ESI) calculated $[C_{15}H_{38}N_3O_3Si]^+$ for 336.2604 found 336.2674.

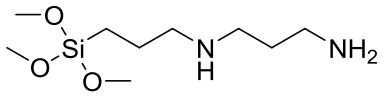

10

Preparation of *N*-(3-(trimethoxysirlyl)propyl)propan-1,3-diamine, **10**[31]

First, 3-chloropropyltrimethoxysialne (20 mmol, 1 eq) and propane-1,3-diamine (100 mmol, 5 eq) were stirred under nitrogen atmosphere at 90 °C for 5 min. The mixture was then added to hexanes, and the precipitate was filtered and washed with hexanes. The filtrate was concentrated to yield the crude compound, which was purified by distillation under reduced pressure (300 mtorr) at 70 °C to yield a colorless liquid. The analyzed ^{1}H NMR spectrum for the target compound was similar to that presented in previous literature.[31] **^{1}H NMR** ($CDCl_3$): 3.58 (s, 9H), 2.78-2.75 (t, 2H), 2.69-2.66 (t, 2H), 2.62-2.60 (t, 2H), 1.65-1.56 (m, 4H), 0.69-0.64 (m, 2H)

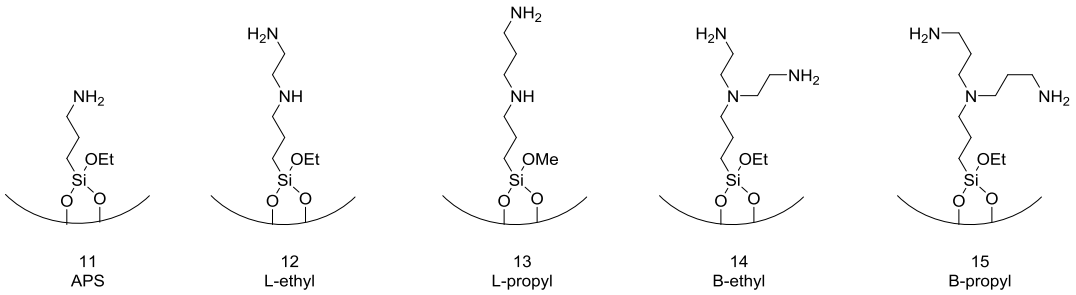

Figure 2.1. The silica supported adsorbents with various aminosilanes.

Preparation of **11, 12, 13, 14, 15**

SBA-15 dried at 100 ºC under vacuum (~20 mTorr) overnight was dispersed in anhydrous toluene for 3 hr. Then, a given amount of branched or linear aminosilane was added dropwise to the mixture, which was heated at 80 °C for 24 h under argon atmosphere. The functionalized SBA-15 was filtered and washed with toluene, hexane, and methanol. The collected adsorbents (**11-15**) were dried at 60 °C under vacuum (~20 mTorr) overnight (Figure 2.1).

2.2.3 Characterization

The surface areas and pore volumes of the adsorbents were calculated or measured from nitrogen physisorption isotherms obtained at 77 K (Tristar II 3020, Micrometrics). Before each analysis, the samples were degassed under 30 mTorr of vacuum at 110 °C for 12 h. The surface areas of the adsorbents were calculated by the BET method. Elemental compositions of the adsorbents were measured at Atlantic Microlab (Norcross, GA). C and N analyses were performed by combustion using an automatic analyzer. CO_2 uptakes for adsorbents were measured by TGA (T500, TA Instruments). First, 15-20 mg of sample was placed on a platinum pan, then heated under helium atmosphere at 110 °C for 3 h. After being equilibrated at 25 ºC, the sample was exposed to 400 ppm CO_2 for 10 h. For the thermal stability tests (adsorption/desorption), the sample was degassed at 110 °C for 3 h, then exposed to CO_2 gas stream at 25 °C for 3 h, which was iterated multiple times. For the oxidation stability test, the degassing process was conducted under 20% O_2/N_2 atmosphere instead of using a He atmosphere. The chemical structures of the synthesized molecules were verified by NMR (solution state ^{1}H NMR, ^{13}C NMR Bruker DMX 400 and

solid state ^{13}C NMR, Bruker DSX 400). For in situ IR measurements, each sample (ca. 15 mg) was pressed into a circular self-supported pellet (2 cm in diameter), which was loaded in the in-situ flow cell. The pellet was activated at 110 °C for 3 h under He flow with 50 mL/min (desorption process), and the gas stream was changed to 20% O_2/N_2 flow with 50 mL/min for 150 min (oxidation process). The IR signal was recorded every 15 mins during the oxidation process with 64 scans at a resolution of 4 cm^{-1}.

2.3 Results and discussion

2.3.1 Preparation of aminosilanes grafted SBA-15

The surface areas and pore volumes of the bare SBA-15 and the aminosilane functionalized adsorbents are shown in Figure 2.2. The synthesized bare SBA-15 had a surface area of 830 m^2/g and a pore volume of 1.02 cm^3/g with 8.3 nm average pore diameter. On this support, various loadings (0.3 – 2.2 mmol Si/g) of linear silanes 3-aminopropyltrimethoxysilane (APS), 3-(2-aminoethylamino)propyltrimethoxysilane (L-ethyl), 3-(2-aminopropylamino)propyl trimethoxysilane (L-propyl), and branched silanes **8** (B-ethyl) or **9** (B-propyl) were grafted (Figure 2.1). As the aminosilane loadings increase, the surface areas and pore volumes of the adsorbents decrease, as the aminosilanes occupy the pore space in the support. While the surface areas and pore volumes of the APS, L-ethyl, L-propyl and B-ethyl samples at a fixed silane loading are similar, the pore spaces of the B-propyl samples (**14**) are further occupied at the similar aminosilane loadings, leaving lower residual porosity.

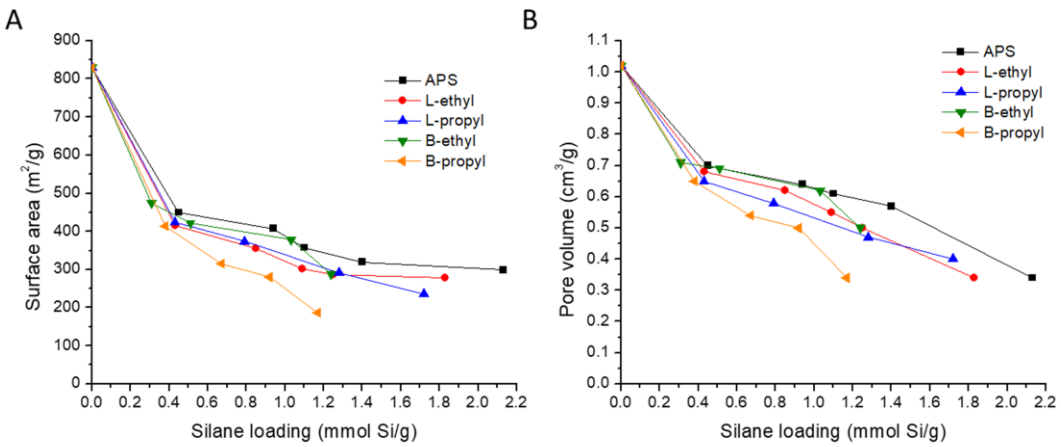

Figure 2.2. (a) Surface areas and (b) pore volumes of bare SBA-15 and an array of aminosilane grafted adsorbents along with their silane loadings.

The grafting yields of the array of aminosilanes on the SBA-15 under the same grafting conditions (80 °C for 24 h) are shown in Figure 2.3. When the added amount of the aminosilane was low (< 0.5 mmol Si/g_{SiO2}), most of the aminosilanes added were grafted on the support (grafting yield > 95%). However, as the added amount of aminosilane increases, the grafting yields for the aminosilanes decrease. It can be inferred that aminosilane is easily grafted on a silanol-rich surface, but as the aminosilane coverage on the surface increases, the free-silanols available for grafting reduce and steric constraints are higher, resulting in a decrease in grafting yield. Since the grafting in this study has been conducted under anhydrous conditions, grafting via self- condensation of aminosilanes (polymerization with water) would not be favored. The grafting yields of the APS and linear aminosilanes (L-ethyl, L-propyl) decrease to 60-70% for ~2 mmol Si/g of aminosilane loadings on the adsorbents. Interestingly, the grafting yield of the branched silanes (B-ethyl, B-propyl) were relatively lower (~ 40%) than the linear silanes, which indicates that the branched structure of the aminosilanes might sterically hinder a dense

grafting on the surface, even though significant surface area and pore volume in the adsorbents remained for additional grafting.

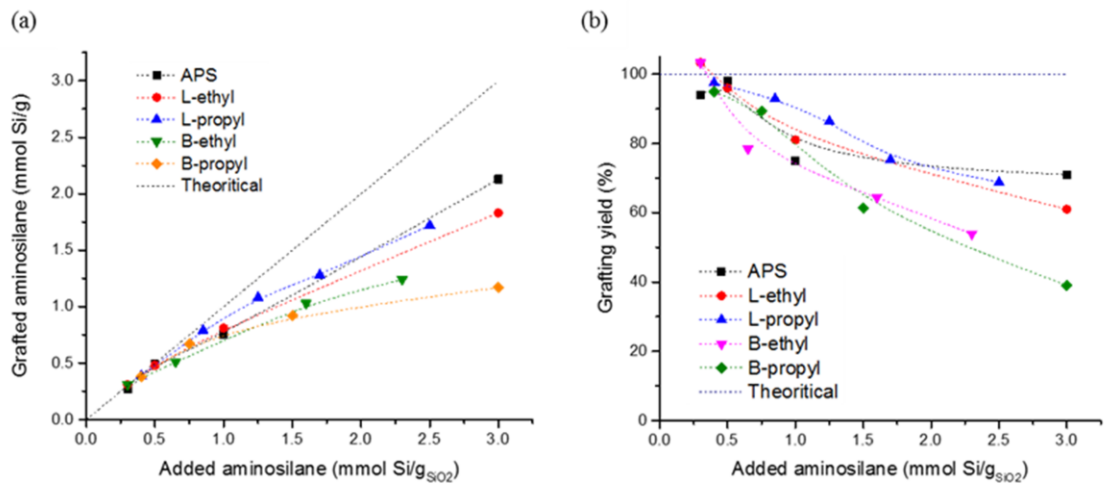

Figure 2.3. (a) Grafted aminosilane and (b) grafting yield of aminosilane on SBA-15 along with the added aminosilane

2.3.2 CO_2 uptake of aminosilane grafted adsorbents

Figure 2.4a shows CO_2 uptakes of the various aminosilane grafted adsorbents along as a function of silane loading. Overall, CO_2 uptakes increased as the silane loadings increased because the increased amine density on the surface allows the adsorption of more CO_2 molecules via ammonium carbamate species. The CO_2 uptakes of all the prepared adsorbents are similar at low silane loadings (0.02-0.04 mmol CO_2/g at 0.31-0.45 mmol Si/g), but the CO_2 uptake trends of each adsorbent are noticeably different as the silane loadings increase. For APS (**11**) adsorbents, CO_2 uptakes do not significantly increase by a silane loading of 1.2 mmol Si/g. However, linear (**12, 13**) and branched (**14, 15**) silane grafted adsorbents start to steeply exceed the CO_2 uptake of APS by silane loadings of 0.8

and 0.6 mmol Si/g, respectively. These threshold silane loadings of adsorbents are related to the length of the alkyl chain and the number of amines in a single silane. The aminosilane grafted adsorbent with longer alkyl chains has a higher propensity to form ammonium carbamate species via intermolecular interaction at lower silane loadings compared with the adsorbents with short alkyl chains (carbamates require two amines per CO_2 under dry conditions, vide infra).[32] Moreover, the number of amines in a single silane is different across the series (APS: one 1° amine; L-ethyl, -propyl: one 1° amine + one 2° amine; B-ethyl, -propyl: two 1° amine + one 3° amine) so that the higher CO_2 uptakes at similar silane loadings can be observed for the adsorbents with branched silanes

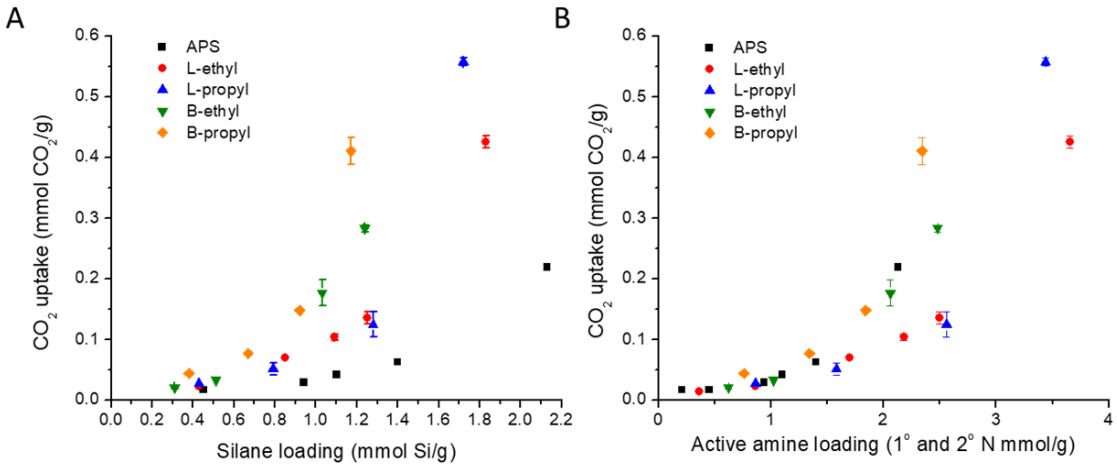

Figure 2.4. CO_2 uptake as a function of amine loadings (a) and active amine loading (b) using the prepared adsorbents.

However, considering the tertiary amine in the branched silanes cannot adsorb CO_2 under dry conditions,[3] adsorbents with linear and branch silanes need to be evaluated based on the number of active amines in a single silane. Figure 2.4b shows the CO_2 uptakes of

the adsorbents along with the active amine loading (primary and secondary amines). APS and branched silane grafted adsorbents (B-ethyl, B-propyl) showed similar CO_2 uptakes at similar active amine loadings. However, the linear silane grafted adsorbents (L-ethyl, -propyl) showed lower CO_2 uptakes at the same active amine loadings. The higher CO_2 uptakes for branched silane grafted adsorbents might be explained by the different chemical nature of the amines. Even though the branched and linear silanes contain the same number of active amines, branched silanes contain two primary amines and linear silanes contain one primary amine and one secondary amine. It is known that the efficiency of binding CO_2 with a primary amine is higher than for secondary amine,[3,33] due to entropic factors, thus the branched silane grafted adsorbents with two primary amines can adsorb more CO_2 than the linear silane grafted adsorbent with primary and secondary amines.

2.3.3 Thermal stability and oxidation resistance

For the thermal stability of the adsorbents, each sample (aminosilane loadings: 1.1-1.3 mmol Si/g) was preheated under helium (UHP level) atmosphere at 110 °C for 3 h (desorption step) and then exposed to 400 ppm CO_2/He balance gas flow at 25 °C for 3 h (adsorption step). These steps were repeated to evaluate the CO_2 capacities of the adsorbents over four cycles, which are shown in Figure 2.5a. All the prepared adsorbents show excellent recyclability regarding CO_2 capacities when they are regenerated under the helium atmosphere at 110 °C. The normalized CO_2 uptakes of all the adsorbents negligibly decreased from 1 to about 0.96 as the number of recycled increased, which means the grafted animosilanes on the surface have excellent thermal stability at the chosen regeneration conditions.

On the other hand, when the prepared adsorbents (aminosilane loadings: 1.1-1.3 mmol Si/g) were exposed to the simulated air (21% O_2/79% N_2) instead of helium (UHP level) at 110 °C (desorption step) for 3 h and 400 ppm CO_2/He balance at 25 °C for 3 h (adsorption) repeatedly, the CO_2 capacities of the prepared adsorbents decreased as the oxidation time increased, as shown in Figure 2.5b. Interestingly, the degree of oxidative degradation of the adsorbents was noticeably different as the oxidation time increased, which suggests that the oxidation resistance of the adsorbents varies depending on the chemical structure of the grafted aminosilanes. For the APS adsorbent, the normalized CO_2 capacity after 12 h of oxidation (0.96) was similar with the normalized CO_2 capacity of the four times helium cycled APS adsorbent (0.95), which shows good agreement with a previous study[14] that suggested that APS was not degraded under such oxidation conditions. On the other hand, the L-ethyl adsorbent shows a significant CO_2 capacity loss after the every 3 h of oxidation treatment at 110 °C (Figure 2.5b), which indicates that the chemical structure of the L-ethyl adsorbent is transformed or degraded during the oxidation to yield a material with lower CO_2 capacity, as the L-ethyl adsorbent showed a stable recyclability when it was regenerated under a helium atmosphere (Figure 2.5a). Interestingly, the linear aminosilane with a propyl spacer between the primary and secondary amine (L-propyl) lost only 10% of its CO_2 capacity after 12 h of oxidation. A similar trend was also observed with the branched aminosilane adsorbents. The normalized CO_2 capacities for the B-propyl adsorbent decreased to 0.85 after 12 h of oxidation, while the B-ethyl adsorbents showed lower normalized CO_2 capacity (0.79). The oxidative degradation of the aminosilanes containing multiple amines (primary secondary or tertiary amines) shows different results relative to previous research on the oxidative degradation

of amine molecules containing only a single amine moiety. Overall, the order of oxidative stability of the prepared aminosilanes is as follows: APS > L-propyl > B-propyl > B-ethyl > L-Ethyl. The strong oxidative resistance of the L-propyl adsorbent suggests that even though the amine molecules contain secondary amines, if the secondary amine and adjacent primary amine are separated with propyl spacer, the amine molecule has a relatively strong resistance against oxidative degradation compared with amine molecules with ethyl spacers.[28] The oxidative degradation of the B-ethyl and B-propyl adsorbents shows that branched amine molecules containing primary and tertiary amines connected by alkyl chains are also oxidized, even though the APS (single primary amine) and DMAPS (single tertiary amine) were not oxidized in previous reports.[14] According to the NMR studies on oxidized aminosilane molecules conducted by Ahmadalinezhad et al., the α carbons near the nitrogen moiety are oxidized to yield amide or imine structures.[12] This is consistent with previous reports detecting such bonds via IR spectroscopy.[11–17] The αC-H bond dissociation energy (BDE) of the amine molecules reported in the literature[34–38] cannot easily explain the observed oxidative degradation trends because the amine molecules in the literature were not the same compounds as in this study. Considering the relative αC-H BDE trend in the literature, however, the relative oxidation reactivity of the αC-H bond near the amine moiety can be estimated. From the literature,[34,35] the αC-H BDE near the primary amine increase as the alkyl chain length increase (e.g. αC-H BDE on propylamine is 389.8 ± 8.4 kJ/mol, αC-H BDE on ethylamine is 377.0 ± 8.4 kJ/mol), which means that the αC-H bond on the propyl linker is stronger than the αC-H bond on the ethyl linker. This supports the hypothesis that the aminosilanes with propyl spacers are more stable than the amine molecules with ethyl spacers due to increased αC-H stability. This would rationalize

the higher oxidative stability of linear amine with propyl spacer (tripropylenetetraamine, TPTA) than ethyl spacer (triethylenetetraamine, TETA) that Pang *et al*. has reported.[28] The αC-H BDEs near the secondary (364-374 kJ/mol) and tertiary amines (372-380 kJ/mol) are relatively lower than the αC-H BDEs near the primary amines.[35–38]. As the alkyl chain length increases near the secondary amine, the αC-H BDEs also slightly increase, as observed for the αC-H BDE near the primary amine. However, αC-H BDE near the tertiary amine shows the opposite trend, where higher αC-H BDEs are obtained on the shorter alkyl chain. This helps rationalize why the L-propyl material has better oxidative stability than the B-propyl (αC-H BDE on secondary amine > αC-H BDE on tertiary amine), while the B-ethyl is more stable than the L-ethyl under the chosen oxidation conditions (αC-H BDE on tertiary amine > αC-H BDE on secondary amine). However, despite these correlating trends, it cannot be explicitly asserted that the oxidation of the aminosilane is caused solely by the αC-H BDE, because the oxidation mechanism is still being explored and the oxidation kinetics of the αC-H groups also need to be considered, in conjunction with the thermodynamic values (αC-H BDEs).

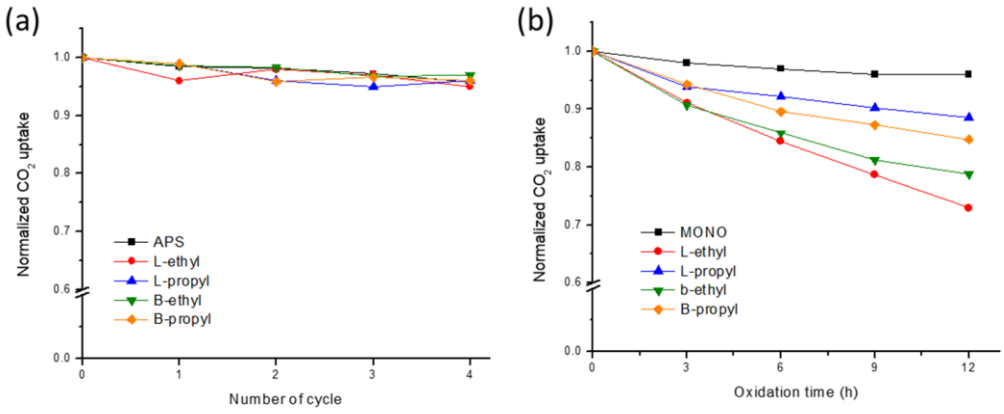

Figure 2.5. Recyclability of the adsorbents after repeated regeneration steps under (a) helium atmosphere at 110 ºC and (b) simulated air atmosphere at 110 ºC

2.3.4 FTIR spectra of CO_2 adsorbents

The FTIR spectra of activated adsorbents after nitrogen purging at 110 °C for 3 h are shown in Figure 2.6. For all of the adsorbents, the peaks at 3361 ($\nu_{asym}NH_2$), 3300 ($\nu_{sym}NH_2$ or νNH) 1598 (δNH_2) and 1470 cm^{-1} (δNH) are assigned to the stretching or scissoring vibrations of primary or secondary amine groups.[39,40] The peaks at 2933 ($\nu_{asym}CH_2$), 2874 ($\nu_{sym}CH_2$), 2813 ($\nu_{sym}CH_2$) and 1460 (δCH_2) cm^{-1} are attributed to the stretching or bending vibrations of methylene groups in the adsorbents.[41,42] The stretching vibration peak at 2813 cm^{-1} is attributed to the specific CH_2 group near secondary or tertiary amine.[43] While two strong peaks (2933 and 2874 cm^{-1}) and a weak shoulder peak (2813 cm^{-1}) are observed from the linear silanes adsorbents, the adsorbents with branched silanes show the three strong peaks at 2933-2813 cm^{-1}. For the adsorbents made with linear silanes, the scissoring methylene peak (δCH_2, 1460 cm^{-1}) and secondary amine peak (δNH, 1470 cm^{-1}) are overlapped. The broad peaks at 1960 and 1850 cm^{-1} are assigned to the vibration of the Si-O overtone, and the peak at 1660 cm^{-1} is attributed to physisorbed water.

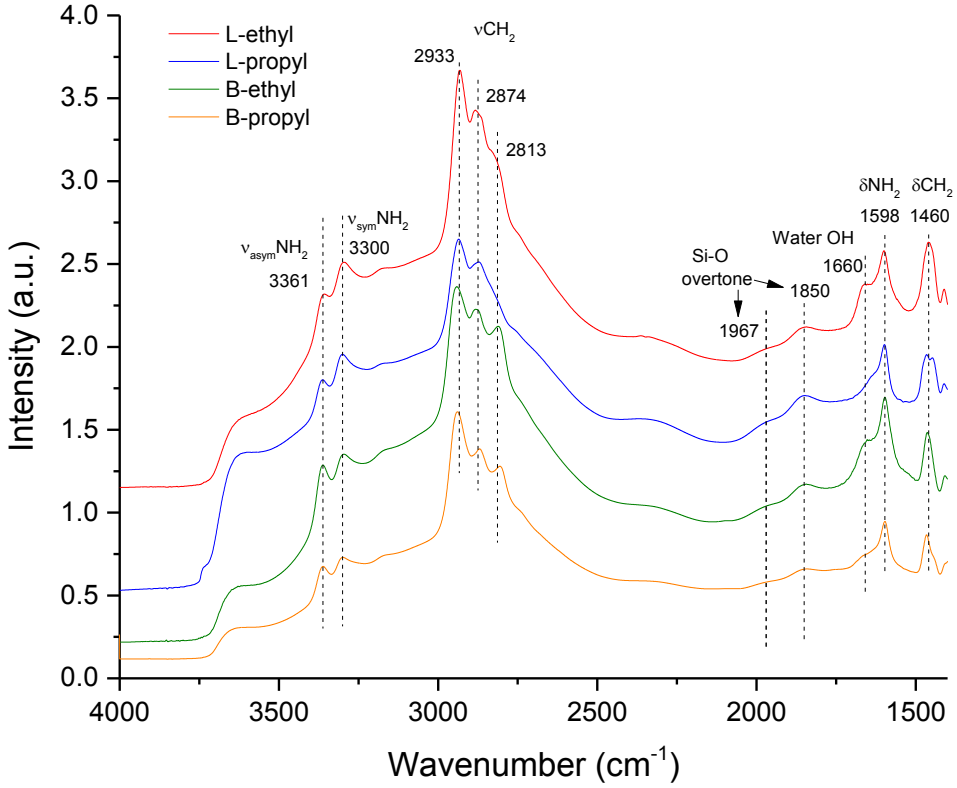

Figure 2.6. FTIR spectra of CO_2 adsorbents activated under nitrogen purging at 110 ˚C for 3 h.

The formation of oxidized species generated on the branched and linear silanes was studied with IR spectroscopy. The observable peaks on the fresh and oxidized adsorbents from ex-situ IR spectroscopy would include overlapped peaks of ammonium carbamate species derived for CO_2 adsorption and oxidized species, making elucidation of the nature of the oxidized species on the prepared silanes challenging. To this end, in situ IR was employed. Before taking a spectrum of the adsorbents under the oxidation conditions (21% O_2/N_2 at 110 ˚C for 150 min), the samples were activated under a He atmosphere at 110 °C for 3 h to remove the adsorbed species (e.g., CO_2 and H_2O). The generation of oxidized

species on the samples was monitored as a function of time, and the spectra are shown in Figure 6. For the adsorbent containing L-ethyl silane (Figure 2.7a), three distinguishable peaks were observed, which are assigned to the stretching vibration of a carbonyl (1633 or 1670 cm^{-1}, C=O), as well as N-H (1600 cm^{-1}) species derived from amide or imine (1633 or 1670 cm^{-1} C=N) species. The possible oxidized species proposed by Ahmadalinezhad et al. are a combination of primary and secondary amide (NH-C=O) or imine groups on the alkyl chain of a linear silane.[12] However, clear assignments for each peak associated with specific species via IR spectroscopy has been challenging due to the similar location of vibrations for amide and imine species. For the adsorbent containing L-propyl groups, as shown in Figure 4b, the oxidation rate of the organic species was slow, such that no noticeable oxidized peak was observed throughout the measurement (Figure 2.7b).

The wavelengths of the oxidized peaks on the branched silanes were slightly different from the linear silanes. While three peaks (1670, 1633, 1601 cm^{-1}) were observed on the adsorbent built with a linear silane (L-ethyl, Figure 6a), only two peaks (1665, 1648 cm^{-1}) appeared on the adsorbent made with branched silanes (Figure 2.7c, 7d). Similar to the above case, the likely oxidized species are a combination of primary and tertiary amide or imine species on the branched silane. Depending on the species generated near the primary, secondary or tertiary amine, the oxidized peak wavelengths should be shifted.

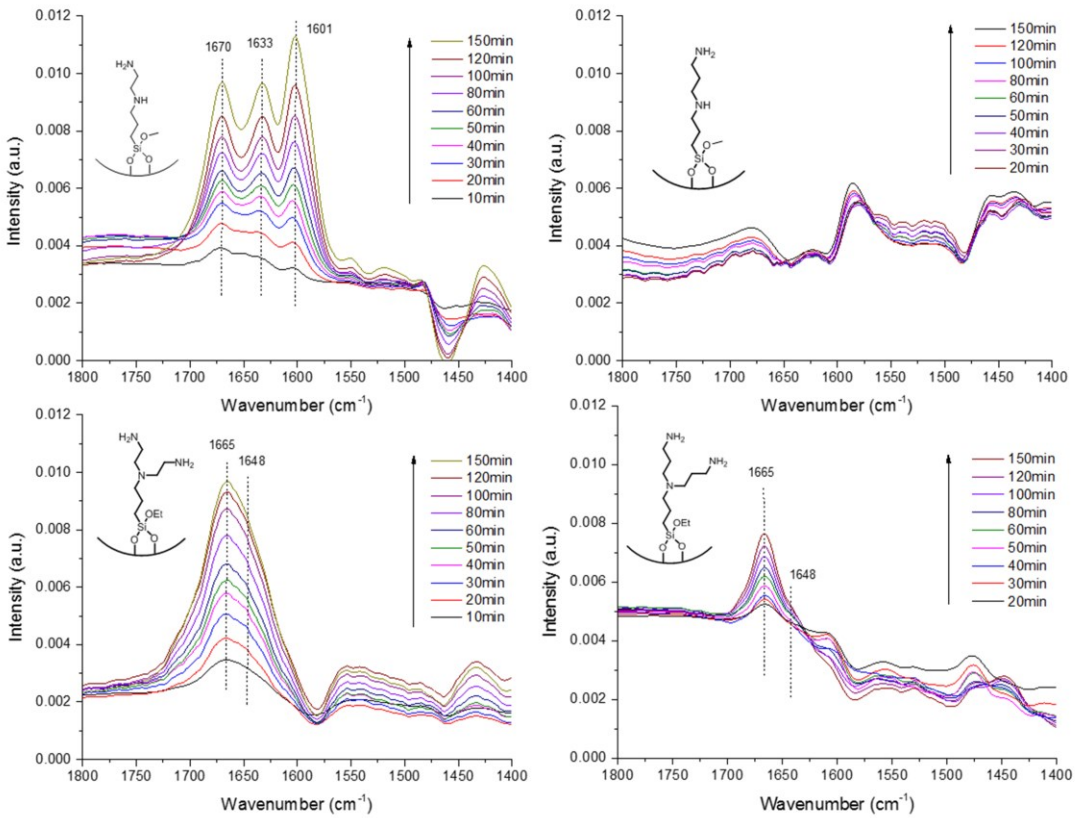

Figure 2.7. In-situ IR spectra for CO_2 adsorbents during the oxidation with 21% O_2/N_2 at 110 ºC for 150 min. (a) L-Ethyl, (b) L-propyl, (c) B-Ethyl, (d) B-propyl.

The elemental analysis of the fresh and oxidized (12 h) adsorbents are shown in Figure 2.8. The mol ratios of the C/N and H/(C+N) were normalized based on the fresh adsorbents. After 12 h of oxidation, the C/N ratios of the adsorbents only slightly changed, in the range of ± 0.05 (0.97 for L-ethyl, 0.95 for L-propyl, 1.03 for B-ethyl and 1.04 for B-propyl). However, the range of the H/(C+N) ratios of the oxidized adsorbents is relatively wider than the C/N ratios, as shown in Figure 7b. The H/(C+N) ratio of the L-propyl adsorbent only decreased to 0.98 after the oxidation, while the ratio for the L-ethyl adsorbent reduced to 0.70. The oxidized adsorbents with branched silanes have 0.80 (B-

ethyl) and 0.92 (B-propyl) H/(C+N) ratios. Since the methylene groups (-CH_2-) near the amine moiety of the aminosilanes are transformed to amide or imine groups during the oxidation, the mol ratio of H/(C+N) of the oxidized adsorbents is expected to decrease compared with the fresh adsorbents. This decreasing trend of the H/(C+N) ratio for the adsorbents is qualitatively similar to the decreasing CO_2 uptake on oxidized adsorbent as shown in Figure 2.5b.

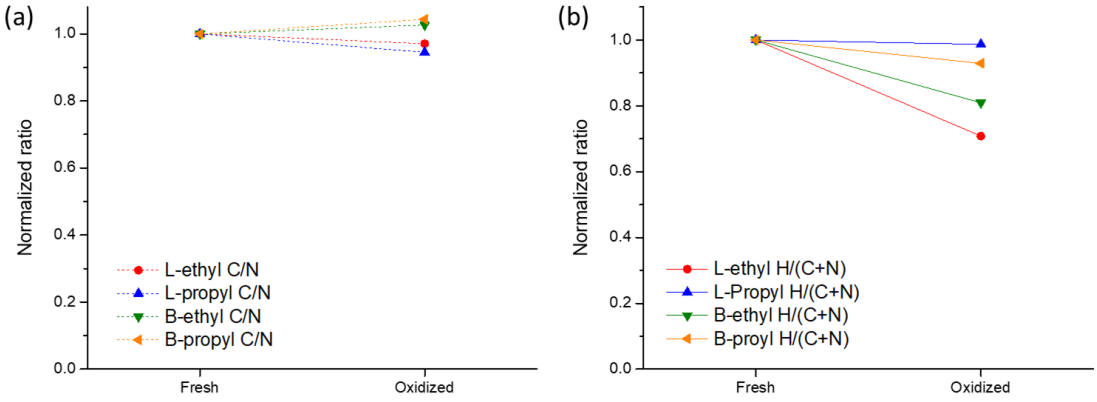

Figure 2.8. The mol ratio of (a) C/N (b) H/(C+N) of fresh and oxidized (12 h) adsorbents

2.4 Conclusions

An array of linear and branched aminosilanes was synthesized and subsequently grafted on a SBA-15 support to yield a series of samples with various silane loading. The adsorbents with branched silanes (B-ethyl, B-propyl) showed a similar amine efficiency (based on active primary and secondary amines) as APS, which were higher than the adsorbents with linear silanes (L-ethyl, L-propyl). This is because the branched silanes have more effective amine moieties for CO_2 adsorption (linear: NH_2+NH vs. branched: NH_2+NH_2). However, the branched structures of B-ethyl and B-propyl prevent the silanes

from being as densely grafted on the surface as the linear silanes. From oxidation studies, the various adsorbents showed a differing degree of oxidative resistance. Among the prepared adsorbents, APS shows the highest oxidative stability, and the order of oxidative stability of the other aminosilanes was shown as L-propyl > B-propyl > B-ethyl > L-Ethyl. The IR peak wavelengths of the oxidized species for the linear aminosilanes were slightly different with those from the branched aminosilanes. The peaks at the wavelengths between 1600-1760cm^{-1} were assigned to amide or imine species. The loss of the H atoms resulting from the oxidation was verified by the normalized mol ratios of H/(C+N) of the fresh and oxidized adsorbents, where the oxidized adsorbents had lower H/(C+N) ratios compared with the fresh adsorbents. The decreasing trend of the H/(C+N) ratio for the adsorbents was similar to the decreasing CO_2 uptake of the oxidized adsorbent. From this array of experiments using adsorbents with linear and branched silanes specifically synthesized to study CO_2 adsorption and chemical resistance to oxidative degradation, evidence has been gathered to clarify the contentious nature of the role of the amine moieties and the spacer length between the adjacent amines toward CO_2 sorption and oxidative degradation. Based on this study, the amine molecules with a linear structure, where the amines are connected via propyl spacer would be promising sorbents that provide a higher CO_2 capacity and oxidative stability.

2.5 References

(1) Hiyoshi, N.; Yogo, K.; Yashima, T. Adsorption Characteristics of Carbon Dioxide on Organically Functionalized SBA-15. *Microporous Mesoporous Mater.* **2005**, *84* (1–3), 357–365.

(2) Watabe, T.; Yogo, K. Isotherms and Isosteric Heats of Adsorption for CO_2 in Amine-Functionalized Mesoporous Silicas. *Sep. Purif. Technol.* **2013**, *120*, 20–23.

(3) Didas, S. A.; Kulkarni, A. R.; Sholl, D. S.; Jones, C. W. Role of Amine Structure on Carbon Dioxide Adsorption from Ultradilute Gas Streams Such as Ambient Air. *ChemSusChem* **2012**, *5* (10), 2058–2064.

(4) Knowles, G. P.; Graham, J. V.; Delaney, S. W.; Chaffee, A. L. Aminopropyl-Functionalized Mesoporous Silicas as CO_2 Adsorbents. *Fuel Process. Technol.* **2005**, *86* (14–15), 1435–1448.

(5) Li, K.; Kress, J. D.; Mebane, D. S. The Mechanism of CO_2 Adsorption under Dry and Humid Conditions in Mesoporous Silica-Supported Amine Sorbents. *J. Phys. Chem. C* **2016**, *120* (41), 23683–23691.

(6) Danon, A.; Stair, P. C.; Weitz, E. FTIR Study of CO_2 Adsorption on Amine-Grafted SBA-15: Elucidation of Adsorbed Species. *J. Phys. Chem. C* **2011**, *115* (23), 11540–11549.

(7) Lee, J. J.; Chen, C.-H.; Shimon, D.; Hayes, S. E.; Sievers, C.; Jones, C. W. Effect of Humidity on the CO_2 Adsorption of Tertiary Amine Grafted SBA-15. *J. Phys. Chem. C* **2017**, *121* (42), 23480–23487.

(8) Didas, S. A.; Sakwa-Novak, M. A.; Foo, G. S.; Sievers, C.; Jones, C. W. Effect of Amine Surface Coverage on the Co-Adsorption of CO_2 and Water: Spectral Deconvolution of Adsorbed Species. *J. Phys. Chem. Lett.* **2014**.

(9) Foo, G. S.; Lee, J. J.; Chen, C.-H.; Hayes, S. E.; Sievers, C.; Jones, C. W. Elucidation of Surface Species through in Situ FTIR Spectroscopy of Carbon Dioxide Adsorption on Amine-Grafted SBA-15. *ChemSusChem* **2016**, *10* (1), 266–276.

(10) Chen, C.-H.; Shimon, D.; Lee, J. J.; Mentink-Vigier, F.; Hung, I.; Sievers, C.; Jones, C. W.; Hayes, S. E. The "Missing" Bicarbonate in CO_2 Chemisorption Reactions on Solid Amine Sorbents. *J. Am. Chem. Soc.* **2018**, *140* (28), 8648–8651.

(11) Heydari-gorji, A.; Belmabkhout, Y.; Sayari, A. Degradation of Amine-Supported CO_2 Adsorbents in the Presence of Oxygen-Containing Gases. *Microporous Mesoporous Mater.* **2011**, *145* (1–3), 146–149.

(12) Ahmadalinezhad, A.; Tailor, R.; Sayari, A. Molecular-Level Insights into the Oxidative Degradation of Grafted Amines. **2013**, 10543–10550.

(13) Ahmadalinezhad, A.; Sayari, A. Oxidative Degradation of Silica-Supported Polyethylenimine for CO_2 adsorption: Insights into the Nature of Deactivated Species. *Phys. Chem. Chem. Phys.* **2014**, *16* (4), 1529–1535.

(14) Bollini, P.; Choi, S.; Drese, J. H.; Jones, C. W. Oxidative Degradation of Aminosilica Adsorbents Relevant to Postcombustion CO_2 Capture. *Energy Fuels* **2011**, *25* (5), 2416–2425.

(15) Srikanth, C. S.; Chuang, S. S. C. Spectroscopic Investigation into Oxidative Degradation of Silica-Supported Amine Sorbents for CO_2 Capture. *ChemSusChem* **2012**, *5* (8), 1435–1442.

(16) Srikanth, C. S.; Chuang, S. S. C. Infrared Study of Strongly and Weakly Adsorbed CO_2 on Fresh and Oxidatively Degraded Amine Sorbents. *J. Phys. Chem. C* **2013**, *117* (18), 9196–9205.

(17) Heydari-gorji, A.; Sayari, A. Thermal , Oxidative , and CO_2 -Induced Degradation of Supported Polyethylenimine Adsorbents. *Ind. Eng. Chem. Res* **2012**, 51 (19), 6887–6894.

(18) Lepaumier, H.; Picq, D.; Carrette, P. New Amines for CO_2 Capture. II. Oxidative Degradation Mechanisms. *Ind. Eng. Chem. Res.* **2009**, 48 (20), 9068–9075**.**

(19) Lepaumier, H.; Martin, S.; Picq, D.; Delfort, B. New Amines for CO_2 Capture. III. Effect of Alkyl Chain Length between Amine Functions on Polyamines Degradation. *Ind. Eng. Chem. Res.* **2010**, 49 (10), 4553–4560.

(20) Vega, F.; Sanna, A.; Navarrete, B.; Maroto-Valer, M. M.; Cortés, V. J. Degradation of Amine-Based Solvents in CO_2 Capture Process by Chemical Absorption. *Greenh. Gases Sci. Technol. 4* (6), 707–733.

(21) Voice, A. K.; Closmann, F.; Rochelle, G. T. Oxidative Degradation of Amines with High-Temperature Cycling. *Energy Procedia* **2013**, *37*, 2118–2132.

(22) Chi, S.; Rochelle, G. T. Oxidative Degradation of Monoethanolamine. *Ind. Eng. Chem. Res.* **2002**, *41* (17), 4178–4186.

(23) Bedell, S. A. Oxidative Degradation Mechanisms for Amines in Flue Gas Capture. *Energy Procedia* **2009**, *1* (1), 771–778.

(24) Sexton, A. J.; Rochelle, G. T. Reaction Products from the Oxidative Degradation of Monoethanolamine. *Ind. Eng. Chem. Res.* **2011**, *50* (2), 667–673.

(25) Bello, A.; Idem, R. O. Comprehensive Study of the Kinetics of the Oxidative Degradation of CO_2 Loaded and Concentrated Aqueous Monoethanolamine (MEA) with and without Sodium Metavanadate during CO_2 Absorption from Flue Gases. *Ind. Eng. Chem. Res.* **2006**, *45* (8), 2569–2579.

(26) Goff, G. S.; Rochelle, G. T. Oxidation Inhibitors for Copper and Iron Catalyzed Degradation of Monoethanolamine in CO_2 Capture Processes. *Ind. Eng. Chem. Res.* **2006**, *45* (8), 2513–2521.

(27) Min, K.; Choi, W.; Kim, C.; Choi, M. Oxidation-Stable Amine-Containing Adsorbents for Carbon Dioxide Capture. *Nat. Commun.* **2018**, *9* (726), 1-7

(28) Pang, S. H.; Lee, L.-C.; Sakwa-Novak, M. A.; Lively, R. P.; Jones, C. W. Design of Aminopolymer Structure to Enhance Performance and Stability of CO_2 Sorbents: Poly(Propylenimine) vs. Poly(Ethylenimine). *J. Am. Chem. Soc.* **2017**, *139*, 3627–3630.

(29) Gao, Y.; Chen, L.; Zhang, Z.; Gu, W.; Li, Y. Linear Cationic Click Polymer for Gene Delivery: Synthesis, Biocompatibility, and in Vitro Transfection. *Biomacromolecules* **2010**, *11* (11), 3102–3111.

(30) Granier, C.; Guilard, R. First Unequivocal Synthesis of 1 or 8-N-Monosubstituted 1,4,8,12-Tetraazacyclopentadecane. *Tetrahedron* **1995**, *51* (4), 1197–1208.

(31) Aoyagi, N.; Endo, T. CO2capture Capacity of Five- and Six-Membered Cyclic Amidines Bearing Silatranyl Group under Dry Conditions. *Tetrahedron* **2017**, *73* (12), 1529–1533.

(32) Yoo, C.-J.; Lee, L.-C.; Jones, C. W. Probing Intramolecular versus Intermolecular CO_2 Adsorption on Amine-Grafted SBA-15. *Langmuir* **2015**, *31* (49), 13350–13360.

(33) Ko, Y. G.; Shin, S. S.; Choi, U. S. Primary, Secondary, and Tertiary Amines for CO2 Capture: Designing for Mesoporous CO_2 Adsorbents. *J. Colloid Interface Sci.* **2011**, *361* (2), 594–602.

(34) Burkey, T. J.; Castelhano, A. L.; Griller, D.; Lossing, F. P. Heats of Formation and Ionization Potentials of Some α-Aminoalkyl Radicals. *J. Am. Chem. Soc.* **1983**, *105* (14), 4701–4703.

(35) Lalevée, J.; Allonas, X.; Fouassier, J. P. N-H and α(C-H) Bond Dissociation Enthalpies of Aliphatic Amines. *J. Am. Chem. Soc.* **2002**, *124* (32), 9613–9621.

(36) Griller, D.; Lossing, F. P. Thermochemistry of .Alpha.-Aminoalkyl Radicals. *J. Am. Chem. Soc.* **1981**, *103* (6), 1586–1587.

(37) Laarhoven, L. J. J.; Mulder, P.; Wayner, D. D. M. Determination of Bond Dissociation Enthalpies in Solution by Photoacoustic Calorimetry. *Acc. Chem. Res.* **1999**, *32* (4), 342–349.

(38) Dombrowski, G. W.; Dinnocenzo, J. P.; Farid, S.; Goodman, J. L.; Gould, I. R. Alpha -C - H Bond Dissociation Energies of Some Tertiary Amines. *J. Org. Chem.* **1999**, *64* (12), 427–431.

(39) Foo, G. S.; Lee, J. J.; Chen, C.-H.; Hayes, S. E.; Sievers, C.; Jones, C. W. Elucidation of Surface Species through in Situ FTIR Spectroscopy of Carbon Dioxide Adsorption on Amine-Grafted SBA-15. *ChemSusChem* **2017**, *10*, 266–276.

(40) Bacsik, Z.; Ahlsten, N.; Ziadi, A.; Zhao, G.; Garcia-Bennett, A. E.; Martín-Matute, B.; Hedin, N. Mechanisms and Kinetics for Sorption of CO_2 on Bicontinuous Mesoporous Silica Modified with N-Propylamine. *Langmuir* **2011**, *27* (17), 11118–11128.

(41) Tian, R.; Seitz, O.; Li, M.; Hu, W.; Chabal, Y. J.; Gao, J. Infrared Characterization of Interfacial Si-O Bond Formation on Silanized Flat SiO_2/Si Surfaces. *Langmuir* **2010**, *26* (7), 4563–4566.

(42) Sayari, A.; Heydari-Gorji, A.; Yang, Y. CO_2-Induced Degradation of Amine-Containing Adsorbents: Reaction Products and Pathways. *J. Am. Chem. Soc.* **2012**, *134* (33), 13834–13842.

(43) Tumuluri, U.; Isenberg, M.; Tan, C. S.; Chuang, S. S. C. In Situ Infrared Study of the Effect of Amine Density on the Nature of Adsorbed CO_2 on Amine-Functionalized Solid Sorbents. *Langmuir* **2014**, *30* (25), 7405–7413.

CHAPTER 3. IMMOBILIZATION OF DIRHODIUM CATALYSTS FOR ENANTIOSELECTIVE C-H FUNCTIONALIZATION IN BATCH AND FLOW REACTORS

This chapter represents a collaboration between the Huw Davies group at Emory University and the Christopher Jones group at Georgia Tech. The main contributor in the Davies group was Dr. Daniel Rackl. He completed designing an analog ligand of the Rh_2(*S*-Br-TPCP)$_4$ catalyst to have alkyne terminal group, which allows the synthesis of Rh_2(S-p-BrTPCP)$_3$(*S*-*p*-AlkyneTPCP) catalyst after the ligand exchange process. My contributions were the preparation of aryldiazoacetate (Me or TCE type), immobilization of the dirhodium catalyst that Dr. Rackl provided on a silica support, running all the cyclopropanations in batch and flow reactors, analysis of the products with NMR, IR, SEM, HPLC, nitrogen physisorption. We worked side by side at Emory University, and I completed some work alone at Georgia Tech.

3.1 Introduction

In recent years, dirhodium catalyzed C-H functionalization via dirhodium-carbene intermediates has facilitated a wide range of intermolecular C-H functionalizations, where the site selectivity and stereoselectivity are dominated by catalyst control.[1–8] Even though the dirhodium catalyst has been shown to be an effective catalyst for direct C-H functionalization, the expensive rhodium component provides a critical drawback for the practical utilization of these catalysts. Considering a limited supply and increasing demand for Rh metal, the price will likely trend higher in the future. In addition, the synthesis of

the chiral ligand also is substantial compared to technologies that deploy commercially available ligands, such as triphenylphosphine.[9] Considering the combined costs of the rhodium and the chiral ligand, developing high turnover number (TON) catalysts is required to allow for widespread, practical application. To improve the TON of the catalyst, several approaches have been suggested, including (i) recycle the catalyst (ii) increasing the intrinsic rate of the catalytic cycle and (iii) designing a more robust catalyst with a longer lifetime.[9]

To achieve a higher TON catalyst, extensive research has focused on the immobilization of homogeneous catalysts on support materials for various organic synthesis reactions such as C-C coupling, metathesis, hydrogenation, and many others.[9] However, very limited cases have been reported for C-H functionalization with immobilized dirhodium catalysts.[10–17] In the early 2000s, the dirhodium tetracarboxylate complex was immobilized by agitation in the presence of a highly crosslinked poly(styrene) resin with a pyridine pendant, as shown in figure 3.1a.[17] This method brought a convenient universal immobilization of various structures of the dirhodium catalysts on poly(styrene) resins. However, reversible coordination of pyridine to the axial site of the dirhodium catalyst caused leaching problems, whereby significant Rh was lost during the reaction. Doyle et al. and Takeda et al. modified one of the ligands of the dirhodium catalysts (Rh_2(*S*-MEPY)$_4$ or Rh_2(*S*-PTTL)$_4$) to have a linker that can be connected to polymer resin (Figure 3.1b). This approach provided a more robust immobilized catalyst than the catalyst immobilized by reversible coordination with a linker in the axial position.

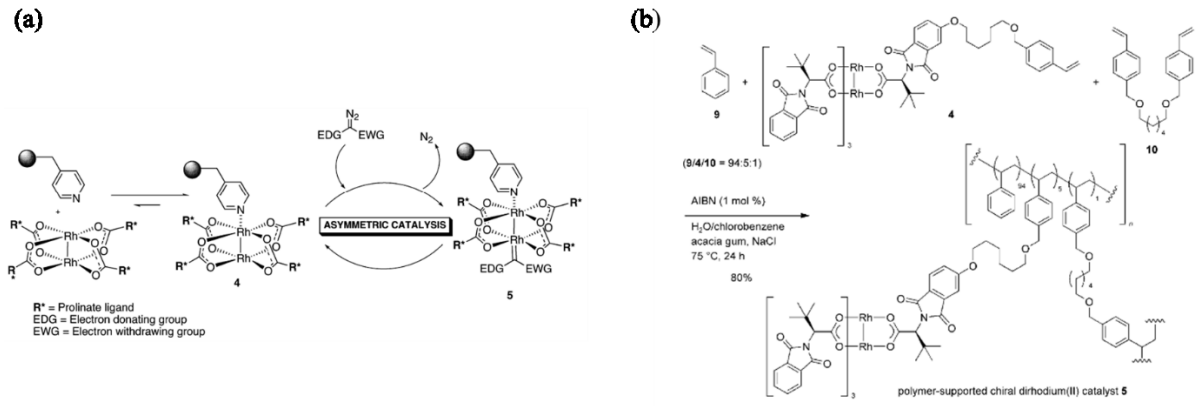

Figure 3.1. (a) Immobilized dirhodium catalyst on polymer resin via pyridine linker[17] (b) preparation of the polymer supported dirhodium catalyst via ligand modification.[12] Reproduced with permission from ref 17. Copyright 2004 ACS publications. Reproduced with permission from ref 12. Copyright 2010 Wiley.

Inspired by these results, the Davies group (Emory University) and the Jones group collaborated to immobilize Rh_2(S-DOSP)$_4$ on a porous silica support, whereby the silica supported catalyst was utilized for various reactions (e.g., cyclopropanation, cyclopropanation, tandem ylide formation/[2,3] sigmatropic rearrangement, and a variety of combined C-H functionalization/Cope rearrangement reactions). The supported catalyst showed stable recyclability in terms of yield (72-78%) and e.e.(77-81%) over five cycles of cyclopropanation.[14] This silica supported of Rh_2(*S*-DOSP)$_4$ derivative catalyst was adapted for use in a microfluidic flow reactor (silica embedded hollow fiber) for C-H functionalization.[13]

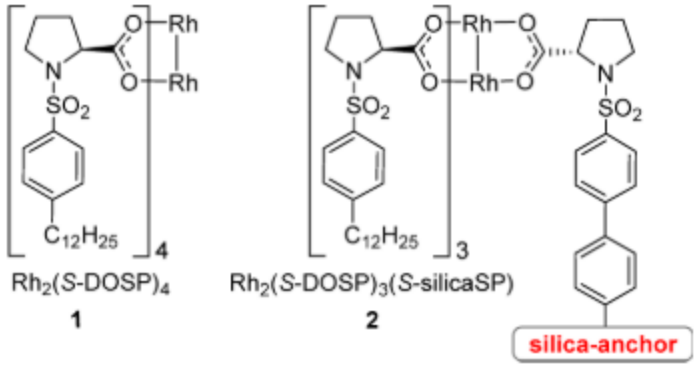

Figure 3.2. Immobilization of Rh_2(s-DOSP)$_4$ catalyst on silica support. Reproduced with permission from ref 14. Copyright 2013 ACS publications.

The previous studies on silica supported dirhodium catalysts focused on the evaluation of the heterogenized dirhodium catalyst in targeted C-H functionalization reactions, along with an assessment of whether the catalyst can be competitive with a homogeneous catalyst with regard to reaction selectivity and product yield. For the development of a higher TON catalyst, however, more comprehensive understanding of the immobilized dirhodium catalyst is required.

In this study, I sought to elucidate the key factors (e.g., immobilization sequence, linker structure, the pore structure of support) that can affect the catalytic performance (yield, stereoselectivity, and kinetics) for a better understanding of the immobilized dirhodium catalyst on silica supports. The insight from this work may be utilized in the design of new heterogenized dirhodium catalysts seeking both ability to recover and recycle the catalyst along with higher turnover numbers.

3.2 Experimental section

3.2.1 Materials

All solvents were purified and dried by a Glass Contour Solvent Purifier System unless otherwise stated. DCM for cyclopropanation and C–H insertion reactions were dried over activated 4 Å MS. All chemicals were obtained from Fluka, Aldrich, Merck, or Acros and used as received.

3.2.2 Conventional SBA-15 synthesis

First, 12 g of Pluronic P123 copolymer was dissolved in 60 mL of HCl and 318 g of DI water in a 1000 mL Erlenmeyer flask. Since the P123 copolymer is highly gluey, it can be easily stick on the upper wall of the Erlenmeyer flask while it is transferred to the flask. In this case, the P123 copolymer on the upper wall of the flask is not easily dissolved in the given volume aqueous HCl solution. To transfer the sticky P123 copolymer to the Erlenmeyer flask without any loss, the P123 was initially charged in 15 mL of plastic syringe, and then the P123 was placed on the bottom of Erlenmeyer flask by squeezing the syringe. The solution was stirred at 40 °C until the polymer was fully dissolved. To this solution, 23.13 g of TEOS was slowly added and stirred at 40 °C for 20 h. Then, the mixture was heated to 100 °C for 24 h without stirring. The reaction mixture was quenched with 200 mL of DI water, and white precipitant was filtered and washed with copious DI water. The white precipitant was dried overnight at 75 °C and dried material was calcined with following procedure: i) ramp to 200 °C at 1.2 °C/min, ii) hold at 200 °C for 1 h, iii) ramp to 550 °C at 1.2 °C/min, iv) hold at 550 °C for 12 h, v) cool to room temperature at 10 °C/min.

3.2.3 Platelet SBA-15 synthesis

SBA-15 with plate-like, 2D particle structures (SBA-15PLT) was synthesized as reported in the literature.[18] In brief, 2.4 g of Pluronic P123 copolymer was dissolved in 84 mL of HCl solution (1.07 M) and stirred at room temperature until the polymer was completely dissolved in the solution. To make 1.07 M of HCl solution, 7.38 mL of stock HCl solution (37 wt.% HCl solution) was slowly added to the 21 mL of DI water. Then additional DI water was added to the mixture to adjust the final volume of the solution to 84 mL. Then, 13.9 g of decane was added to the solution with stirring at room temperature for 1 h. Finally, 0.027 g of NH_4F and 5.1 g of TEOS were added to the mixture, which was stirred at 40 °C for 20 h and then the mixture was transferred to autoclaves (30 mL x 3 ea) for further reaction at 100 °C for 48 h. The white precipitant was filtered and washed with copious DI water. The white precipitant was dried overnight at 75 ^oC, and the dried material was calcined at the same conditions of conventional SBA-15.

3.2.4 Synthesis of Dirhodium tetrakis((S)-1-(4-bromophenyl)-2,2-diphenylcyclopropanecarboxylate)

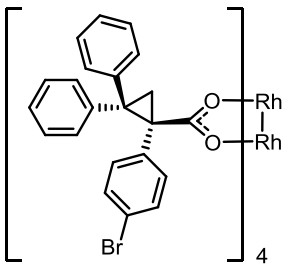

A solution of sodium rhodium carbonate $[Na_4Rh_2(CO_3)_4]\cdot 2.5H_2O$ (557 mg, 1.0 equiv.) and (*S*)-1-(4-bromophenyl)-2,2-diphenylcyclopropanecarboxylic acid (3.0 g, 8.0 equiv.) in 60 mL of DI water was refluxed for 3 days under argon, and then the solution was extracted with dichloromethane (3 x 100 mL). The organic extracts were combined and washed with saturated sodium bicarbonate (3 x 10 mL), 10% sodium hydroxide (3 x 10 mL) and brine (3 x 10 mL). The organic solution was dried over

anhydrous $MgSO_4$, and concentrated by a rotary evaporator. The crude material was purified using flash column chromatography eluting with a 50:1 mixture of toluene and acetonitrile to provide the desired catalyst as a green solid (1.07 g, 63% yield).

mp: 235-237 °C; Rf = 0.25 (toluene/acetonitrile = 50/1); $[\alpha]^{20}_D$ 140.9° (c=0.02, $CHCl_3$); **^{1}H NMR** (400 MHz, $CDCl_3$): δ 7.23−7.15 (m, 7H), 6.90-6.81 (m, 7H), 2.30 (d, 1H, *J* = 5.0 Hz), 2.39 (d, 1H, *J* = 5.0 Hz). **^{13}C NMR** (100 MHz, $CDCl_3$) δ 188.9, 142.4, 140.8, 135.7, 132.8, 130.6, 129.9, 129.2, 128.3, 127.9, 126.6, 126.4, 120.9, 46.9, 42.7, 23.6; **IR** (neat): 1577, 1490, 1447, 1397, 1379, 1277, 1156, 1076, 1010, 991, 906, 823, 777, 733; **HRMS** (ESI) calculated for $C_{88}H_{64}Br_4O_8$ $(M)^+$ 1769.9444 found 1769.94392.

3.2.5 Synthesis of ligand exchanged Rh_2L_3L' catalyst

3.2.6.1. Alkyne-Tagged Dirhodium Catalyst

methyl 2-(4'-bromo-[1,1'-biphenyl]-4-yl)acetate

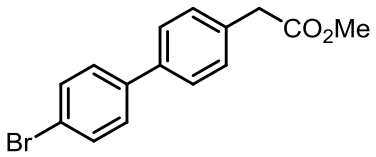

A flame-dried round bottom flask equipped with a pressure-equalizing addition funnel was charged with 2-(4'-bromo-[1,1'-biphenyl]-4-yl)acetic acid (38.3 g, 132 mmol, 1.00 equiv.), methanol (132 mL), and was cooled to 0 °C in an ice/water bath. Acetyl chloride (11.2 mL, 12.4 g, 158 mmol, 1.20 equiv.) was added dropwise via the addition funnel, and the solution was stirred at ambient temperature overnight. The mixture washed with diethyl ether (500 mL) into a separation funnel filled with sat. aq. NH_4Cl (250 mL). The phases were separated, and the aqueous phase was extracted once more with diethyl ether (500 mL). The combined organic phases were washed with sat. aq. $NaHCO_3$ (250 mL), brine (250 mL), and dried over $MgSO_4$. The mixture was filtered and evaporated

under reduced pressure to give the target compound (39.2 g, 129 mmol, 98%) as a slightly yellow oil without further purification.

Rf (hexanes:EtOAc = 6:1) = 0.48; **^{1}H NMR** (600 MHz, $CDCl_3$) δ 7.57 – 7.52 (m, 2H), 7.52 – 7.47 (m, 2H), 7.45 – 7.41 (m, 2H), 7.36 – 7.32 (m, 2H), 3.70 (s, 3H), 3.66 (s, 2H); **^{13}C NMR** (151 MHz, $CDCl_3$) δ 172.0, 139.8, 139.0, 133.6, 132.0, 130.0, 128.8, 127.28, 121.7, 52.3, 41.0; IR (ATR) 3030, 2952, 2843, 1735, 1481, 1435, 1348, 1226, 1166, 1002, 805 cm-1; **HRMS** (NSI) calc. for $[C_{15}H_{14}O_2Br]^+$ 305.0172 found 305.01718.

methyl 2-(4'-bromo-[1,1'-biphenyl]-4-yl)-2-diazoacetate.

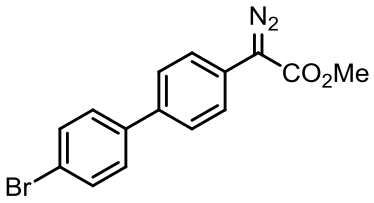

A 500 mL round-bottom flask equipped with a pressure-equalizing addition funnel was charged with methyl 2-(4'-bromo-[1,1'-biphenyl]-4-yl)acetate (36.5 g, 120 mmol, 1.00 equiv.), acetonitrile (120 mL), DCM (120 mL), and 4-acetamidobenzenesulfonyl azide (34.5 g, 144 mmol, 1.20 equiv.). The solution was cooled to 0 °C in an ice/water bath. DBU (36 mL, 0.24 mol, 2.0 equiv.) was added dropwise via the addition funnel. The reaction mixture was stirred at ambient temperature overnight, quenched with sat. aq. NH_4Cl (200 mL), and extracted with diethyl ether (3 x 200 mL). The organic layers were washed with brine, dried over $MgSO_4$, filtered, and evaporated under reduced pressure. The residue was purified by recrystallization in a mixture of 250 mL EtOAc and 250 mL MeOH (55 °C). The vessel was cooled in a freezer overnight and the crystals were collected through filtration with a Buchner funnel, washed with an ice-cold 1:1 mixture of EtOAc and MeOH (2 x 40 mL), and dried in vacuuo to give the target compound (24.2 g, 73.1 mmol, 61%) as orange crystals.

Mp: 108 °C (decom.); Rf (hexanes:EtOAc = 50:1) = 0.31; **^{1}H NMR** (500 MHz, $CDCl_3$) δ 7.63 – 7.53 (m, 6H), 7.50 – 7.44 (m, 2H), 3.91 (s, 3H); **^{13}C NMR** (126 MHz, $CDCl_3$) δ 165.48, 139.20, 137.29, 131.94, 128.42, 127.36, 124.90, 124.29, 121.60, 52.10; **IR** (ATR): 3034, 2953, 2084, 1687, 1604, 1525, 1481, 1433, 1392, 1354, 1278, 1236, 1191, 1155, 1117, 1055, 1019, 1009, 998, 915, 806, 739, 719, 668 cm-1; **HRMS** (NSI) calc. for $[C_{15}H_{12}O_2N_2Br]^+$: 331.00767, found: 331.00822.

methyl (S)-1-(4'-bromo-[1,1'-biphenyl]-4-yl)-2,2-diphenylcyclopropane-1-carboxylate.

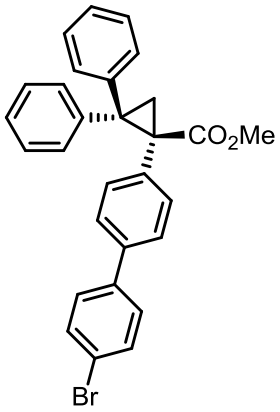

A flame-dried round bottom flask equipped with a pressure-equalizing addition funnel was charged with Rh_2(S-DOSP)$_4$ (7.0 mg, 0.371 mmol, 1.00 mol%), ethene-1,1-diyldibenzene (15 mL, 86 mmol, 2.3 equiv.), and pentane (370 mL). A freshly prepared solution of methyl 2-(4'-bromo-[1,1'-biphenyl]-4-yl)-2-diazoacetate (12.3 g, 37.1 mmol, 1.00 equiv.) in pentane (280 mL) and DCM (180 mL) was added dropwise over 2 h via the addition funnel to the heavily stirred reaction mixture. The mixture was stirred overnight and subsequently evaporated under reduced pressure. Purification was carried out on a Biotage SNAP 340 g SiO_2 column with 2–8% EtOAc in hexanes of 25 column volumes to give the target compound (15.8 g, 32.7 mmol, 88%, 89% ee) as a white solid. The material was further enantioenriched by recrystallization in hot MeOH (300 mL). The vessel was cooled in a freezer, and the crystals were collected through filtration with a Buchner funnel to give the target compound (13.6 g, 28.1 mmol, 76%, 99.6% ee) as white crystals.

Mp: 115 °C; **Rf** (hexanes:EtOAc = 6:1) = 0.45; **^{1}H NMR** (500 MHz, $CDCl_3$) δ 7.54 (dd, J = 8.3, 6.8 Hz, 4H), 7.44 – 7.34 (m, 8H), 7.31 – 7.25 (m, 1H), 7.08 – 7.00 (m, 4H), 7.00 – 6.90 (m, 1H), 3.39 (s, 3H), 2.75 (d, J = 5.6 Hz, 1H), 2.48 (d, J = 5.6 Hz, 1H); **^{13}C NMR** (126 MHz, $CDCl_3$) δ 171.32, 141.94, 139.60, 139.54, 138.36, 135.29, 132.39, 131.75, 129.93, 128.74, 128.58, 128.37, 127.69, 127.01, 126.23, 125.96, 121.41, 52.26, 52.25, 44.65, 42.80, 22.86; **IR** (ATR): 3029, 2991, 2945, 1717, 1600, 1494, 1451, 1434, 1310, 1294, 1218, 1142, 1104, 1074, 1049, 1001, 967, 876, 817, 743, 696 cm-1; **HRMS** (NSI) calc. for $[C_{29}H_{24}O_2Br]^+$: 483.09542, found: 483.09541; **HPLC** (ADH column, 1.0 mL/min, 10% iPrOH in hexanes, λ = 230 nm): tR(major) = 16.3 min, tR(minor) = 7.5 min, 99.6% ee.

methyl (S)-2,2-diphenyl-1-(4'-((triisopropylsilyl)ethynyl)-[1,1'-biphenyl]-4-yl)cyclopropane-1-carboxylate.

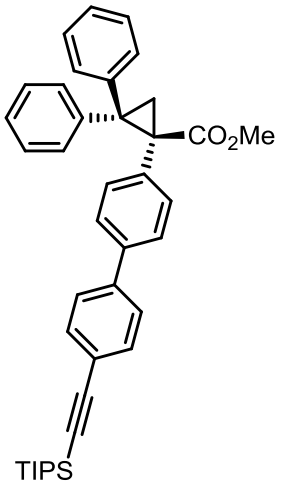

A 25 mL microwave tube was charged with methyl (S)-1-(4'-bromo-[1,1'-biphenyl]-4-yl)-2,2-diphenylcyclopropane-1-carboxylate (3.38 g, 7.00 mmol, 1.00 equiv.), ethynyltriisopropylsilane (1.40 g, 7.70 mmol, 1.10 equiv.), $PdCl_2(PPh_3)2$ (0.25 g, 0.35 mmol, 5.0 mol%), copper(I) iodide (67 mg, 0.35 mmol, 5.0 mol%), triethylamine (7.0 mL, 5.1 g, 50 mmol, 7.2 equiv.) and DMF (3.5 mL) to give a yellow slurry. The reaction mixture was irradiated in a Biotage microwave to 120 °C for 25 min with heavy stirring to give an orange suspension with the white crystalline material. Three such runs were combined, the reaction mixtures were filtered through a plug of Celite 545 in a sintered glass funnel, washed with DCM (100 mL) and the filtrate was evaporated under reduced

pressure. Purification was carried out on a Biotage SNAP 340 g SiO_2 column with 3–6% EtOAc in hexanes of 12 column volumes to give the target compound (9.60 g, 16.4 mmol, 78%) as a white solid.

Mp: 60 °C; Rf (hexanes:EtOAc = 6:1) = 0.67; **^{1}H NMR** (500 MHz, $CDCl_3$) δ 7.61 – 7.52 (m, 4H), 7.51 – 7.48 (m, 2H), 7.46 – 7.36 (m, 6H), 7.33 – 7.26 (m, 1H), 7.10 – 7.02 (m, 4H), 7.01 – 6.96 (m, 1H), 3.41 (s, 3H), 2.77 (d, J = 5.5 Hz, 1H), 2.49 (d, J = 5.6 Hz, 1H), 1.19 (s, 21H); **^{13}C NMR** (126 MHz, $CDCl_3$) δ 171.34, 142.00, 140.53, 139.58, 138.78, 135.27, 132.37, 132.35, 129.97, 128.76, 128.38, 127.71, 127.01, 126.70, 126.25, 126.07, 122.35, 107.03, 91.25, 52.26, 44.67, 42.86, 22.91, 18.73, 11.38; **IR** (ATR) 3030, 2943, 2863, 2151, 1724, 1601, 1493, 1449, 1433, 1302, 1216, 1141, 1074, 1019, 1006, 995, 957, 882, 836, 822, 777, 748, 694, 676, 661 cm^{-1}; **HRMS** (NSI) calc. for $[C_{40}H_{45}O_2Si]^+$: 585.31833, found: 585.31876.

(S)-2,2-diphenyl-1-(4'-((triisopropylsilyl)ethynyl)-[1,1'-biphenyl]-4-yl)cyclo-propane-1-carboxylic acid.

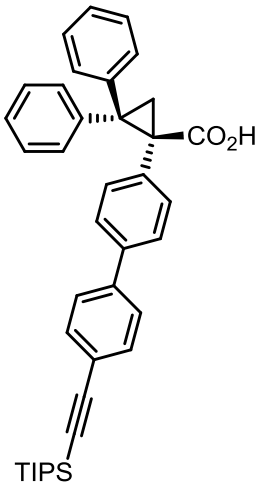

A flame-dried 500 mL round-bottom flask was charged with potassium trimethylsilanolate (7.12 g, 55.5 mmol, 3.00 equiv.), put onto the high vacuum, and heated to 100 °C for 15 min. The flask was cooled to 0 °C, flushed with argon, charged with THF (50 mL) and a solution of methyl (S)-2,2-diphenyl-1-(4'-((triisopropylsilyl)ethynyl)-[1,1'-biphenyl]-4-yl)cyclopropane-1-carboxyl-ate (10.8 g, 18.5 mmol, 1.00 equiv.) in THF (140 mL) was added dropwise to give a colorless solution. The mixture was allowed to reach room

temperature and stirred for 16 h. Another portion of potassium trimethylsilanolate (7.12 g, 55.5 mmol, 3.00 equiv.) was added, and stirring was continued for 24 h until full consumption of starting material was evident as judged by TLC analysis. The mixture was acidified with aq. citric acid (0.5 M, 150 mL), stirred for 30 min, THF was evaporated under reduced pressure, the residue extracted with EtOAc (3 x 100 mL), dried over Na2SO4, filtered, and evaporated under reduced pressure. Purification was carried out on a Silicycle 330 g SiO_2 column with 10–30% EtOAc in hexanes of 10 column volumes to give the target compound (9.10 g, 15.9 mmol, 90%) as a white solid.

Mp: 127 °C; Rf (hexanes:EtOAc = 2:1) = 0.29; **^{1}H NMR** (500 MHz, $CDCl_3$) δ 7.50 – 7.45(m, 4H), 7.45 – 7.43 (m, 2H), 7.36 – 7.35 (m, 6H), 7.35 – 7.33 (m, 1H), 7.01 – 6.99(m, 4H), 2.64 (d, J = 5.5 Hz, 1H), 2.49 (d, J = 5.6 Hz, 1H), 1.13 (s, 21H); **^{13}C NMR** (126 MHz, $CDCl_3$) δ 175.4, 141.7, 140.6, 139.4, 139.1, 135.0, 132.5, 132.45, 130.0, 128.9, 128.6, 127.9, 127.2, 126.8, 126.5, 126.2, 122.5, 107.1, 91.4, 45.9, 42.3, 29.9, 23.6, 18.8, 11.5; IR (ATR) 3030, 2942, 2863, 2151, 1689, 1493, 1449, 1235, 1071, 1005, 991, 836, 820, 758, 744, 724, 676, 659 cm^{-1}; **HRMS** (NSI) calc. for $[C_{39}H_{43}O_2Si]$+: 571.30268, found: 571.30316; **HPLC** (ADH column, 1.0 mL/min, 5% iPrOH in hexanes, λ = 230 nm): tR(major) = 13.7 min, tR(minor) = 7.8 min, 99.3% ee.

Rh_2(S-p-BrTPCP)3(*S*-*p*-AlkyneTPCP).

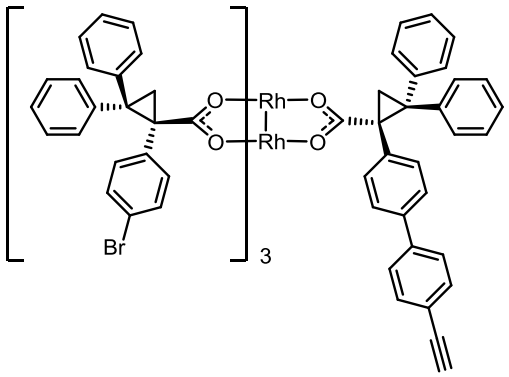

A flame-dried 250 mL 2-neck round-bottom flask was charged with Rh_2(S-p-BrTPCP)$_4$ (2.10 g, 1.18 mmol, 1.00 equiv.) and (S)-2,2-diphenyl-1-(4'-((triisopropylsilyl)ethynyl)-[1,1'-biphenyl]-4-yl)cyclopropane-1-carboxylic acid (743 mg, 1.30 mmol, 1.10 equiv.). The vessel was evacuated and backfilled with argon (3 cycles). Benzene (40 mL) was added to give a green slurry. The reaction mixture was degassed by sparging with argon for 10 min. The reaction vessel was equipped a reflux condenser, and the reaction mixture was stirred under reflux for 16 h. The reaction mixture was evaporated under reduced pressure. Purification was carried out on a Silicycle 120 g SiO_2 column with 10–12% EtOAc in hexanes of 15 column volumes. All fractions containing the mono-exchange product were united and evaporated to give crude Rh_2(S-BTPCP)$_3$(S-p-TIPS-ATPCP) as a green solid (1.30 g, 662 μmol, 56%).

A flame-dried 100 mL round-bottom flask was charged with crude Rh_2(S-p-BrTPCP)$_3$(S-p-TIPS-ATPCP) (1.29 g, 0.661 mmol) and THF (66 mL) to give a green solution. The reaction mixture was cooled to 0 °C in an ice/water bath. A solution of TBAF (Tetra-*n*-butylammonium fluoride) in THF (1.0 M, 2.6 mL, 2.6 mmol, 4.0 equiv.) was added drop-wise via syringe. The reaction mixture was stirred at 0 °C for 30 min until full consumption of starting material was evident as judged by TLC analysis. The reaction mixture was quenched by the addition of H_2O (50 mL). The reaction mixture was evaporated under reduced pressure to remove THF, the aqueous residue extracted with

DCM (3 x 50 mL), the combined organic layers dried over Na_2SO_4, filtered, and evaporated under reduced pressure. Purification was carried out on a Silicycle 120 g SiO_2 column with 13–20% EtOAc in hexanes of 15 column volumes and on a Silicycle 40 g SiO_2 column with 5–20% Et_2O in hexanes of 15 column volumes to give the target compound (506 mg, 282 μmol, 24% over 2 steps) as a green solid. Fractions corresponding to each spot of the TLC plates were collected separately. The fractions corresponding to the mono-exchanged product was selected according to HRMS [Note: compound contains trace amounts of DCM and EtOAc; HRMS was used as the primary analysis tool].

Mp: >225 °C (decomp.); **Rf** (hexanes:EtOAc = 6:1) = 0.42; **^{1}H NMR** (500 MHz, $CDCl_3$) δ 7.62 – 7.48 (m, 4H), 7.47 – 7.28 (m, 23H), 7.24 – 7.10 (m, 8H), 7.07 – 6.84 (m, 22H), 6.83 – 6.71 (m, 3H), 3.60 (s, 1H), 2.47 (brs, 3H), 2.35 (brs, 1H), 2.16 (brs, 2H), 1.84 (brs, 1H), 1.77 (brs, 1H); **^{13}C NMR** (126 MHz, $CDCl_3$) δ 189.18, 188.70, 188.53, 142.71, 142.46, 142.15, 141.09, 140.84, 140.71, 137.86, 136.13, 135.95, 135.65, 133.01, 132.65, 131.47, 130.41, 130.27, 129.90, 129.81, 129.26, 129.13, 128.21, 128.06, 127.75, 127.56, 126.63, 126.54, 126.19, 125.99, 125.59, 120.75, 120.57, 120.49, 84.54, 76.66, 47.39, 47.08, 46.06, 42.97, 42.44, 42.20, 24.16, 22.68; IR (ATR) 3024, 2924, 1686, 1581, 1491, 1381, 908, 732, 702 cm^{-1}; **HRMS** (NSI) calc. for $[C_{96}H_{69}O_8Br_3Rh_2]^+$: 1792.06472, found: 1792.06713.

3.2.6 Immobilization of Rh_2(S-p-Br-TPCP)$_3$(S-p-AkyneTPCP) catalyst on silica embedded in polymeric hollow fibers

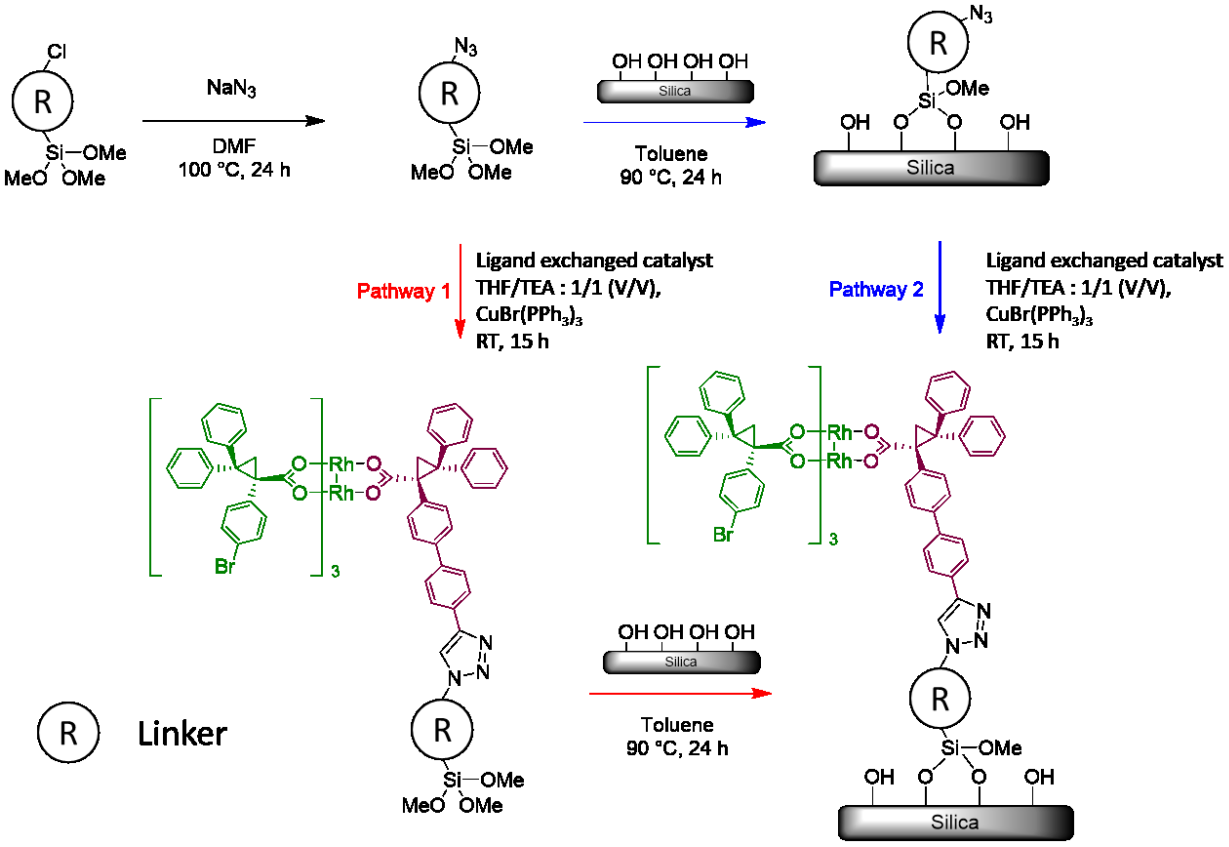

Figure 3.3. The possible synthetic pathways for immobilization of dirhodium catalyst on a silica support

Synthesis of 3-azidopropyltrimethoxysilane

A flame-dried round bottom flask was charged with 3-chloropropyltrimethoxysilane (20 mmol), sodium azide (30 mmol) and 15 mL of anhydrous DMF. The reaction mixture was stirred at 100 °C for 24 h then cooled to room temperature. The mixture was diluted with DI water (30 mL) and diethyl ether (30mL). The organic layer was washed with water three times (30 mL x 3) and saturated aqueous

sodium chloride solution (30 mL x 1). The collected organic layer dried over magnesium sulfite was concentrated to yield 3-azidopropyltriemthosxyilane. The NMR spectra were matched with previous literature.[19] **^{1}H NMR** (400 MHz $CDCl_3$) δ 3.57 (s, 9H), 3.27 (t, 2H), 1.74-1.67 (m, 2H), 0.74-0.67 (m, 2H); **^{13}C NMR** (101 MHz, $CDCl_3$) δ 53.86, 50.72, 22.58, 6.46.

Synthesis of $CuBr(PPh_3)_3$

A 250 mL round bottomed flask equipped with a magnetic stir bar was charged with triphenylphosphine (24.22 g, 92.34 mmol) and methanol (100 mL). The mixture was heated to reflux and copper (II) bromide (5.16 g, 23.09 mmol) was added in 10 portions over 10 min. The reaction mixture was refluxed for 30 min, cooled to room temperature, and filtered through a fritted glass funnel. The white solid was washed with EtOH and Et_2O. The solid was dried in vacuo.

3.2.6.1. Immobilization pathway 1

Dirhodium-silane synthesis

Copper catalyzed alkyne and azide cycloaddition procedure was derived from the work by N. Moitra et al.[20] A flame dried round bottom flask was charged with Rh_2(S-p-Br-TPCP)$_3$(S-p-AkyneTPCP) catalyst (56 μmol, 1 equiv.) and 3-azidopropyltrimethoxysilane (62 μmol, 1.1 equiv.). The solution of $CuBr(PPh_3)_3$ (1 mg, 2 mol %) in anhydrous inhibitor-free THF (0.3 mL) and anhydrous TEA (0.3mL) was added to the round bottom flask. The mixture was stirred at room temperature for 24 h under nitrogen atmosphere. The completion of the reaction was monitored by NMR. As a workup procedure, the solvent was evaporated by a rotary evaporator, and the crude product was washed with anhydrous

methanol to remove TEA (triethylamine) and unreacted 3-azidopropyltrimethoxysilane. The product was dried by vacuum to obtain a purple powder.

Grafting of the dirhodium-silane on silica

A glass vial (4 mL) was charged with 50 mg of silica (syloid, C803), anhydrous toluene (50 mL), and dirhodium-silane (10 mg). The mixture was stirred at 90 °C or room temperature for 48 h. The powder was filtered and washed with DCM multiple times until the color of the powder become blue-green, followed by drying under reduced pressure at room temperature.

3.2.6.2. Immobilization pathway 2

Immobilization of azidosilanes (3-azidopropyltrimethoxysilane, 11-azidopropyl trimethoxysilane, 4-azidomethylphenyltrmethoxysilane) on SiO_2

A flame-dried round bottom glassware (100 mL) was charged with 100 mg of bare silica (SBA-15 or SBA15PLT), anhydrous toluene (15 mL), and azidosilane (0.03 mmol). The mixture was stirred at 80 °C for 24 h. The fiber was washed with toluene, hexanes, and methanol, followed by drying under reduced pressure at 60 °C overnight.

Copper catalyzed alkyne and azide cycloaddition (CuAAC)

A glass vial (4 mL) was charged with azide functionalized silica (20 mg), TEA (0.3 mL), inhibitor-free THF (0.3 mL), Rh_2(S-p-Br-TPCP)$_3$(S-p-AkyneTPCP) catalyst (10 mg) and $CuBr(PPh_3)_3$ (8 mg). The mixture was stirred at room temperature for 2 days. The powder was filtered and washed with DCM multiple times until the color of the powder become blue-green. The catalyst then dried under vacuum at room temperature overnight.

3.3 Results and discussion

3.3.1 Effect of immobilization pathways

The dirhodium catalyst can be immobilized on a silica support via two different pathways, as shown in figure 3.3. Even though the final structures of the immobilized catalyst are, in principle, identical via pathway 1 and pathway 2, the observed catalytic performance was not similar, depending on the immobilization sequence. For pathway 1, first, the 3-azidopropyltrimethoxysilane was reacted with ligand-exchanged dirhodium catalyst (Rh_2(S-p-BrTPCP)$_3$(S-p-AlkyneTPCP)) to yield the Rh-silane via "click chemistry". The Rh-silane was then grafted on the silica support. For pathway 2, the 3-azidopropyltrimethoxysilane was initially grafted on the silica. The ligand-exchanged dirhodium catalyst was then immobilized on the azide functionalized silica surface via click chemistry. The dirhodium loadings on the silica support prepared by the two pathways were 0.22 mmol Rh_2/g (pathway 1) and 0.18 mmol Rh_2/g (pathway 2).

From the Rh_2(S-p-BrTPCP)$_4$ catalyzed cyclopropanation with styrene and *p*-bromodiazoacetate (TCE type), 91% yield and 95% e.e. were observed (Table 3.1, entry 1). The dirhodium-silane catalyzed cyclopropanation showed similar yield (87%) and e.e. (95%) (entry 2) compared with the Rh_2(S-p-BrTPCP)$_4$ catalyzed reaction (entry 1). However, when the dirhodium-silane was grafted on the silica surface (pathway 1), the e.e. of the reaction dropped to 82% (entry 3). On the other hand, when the heterogeneous catalyst was prepared through the pathway 2, the yield (89%) and e.e. (94%) of the reaction (entry 4) were similar with the homogeneous dirhodium catalyzed reaction (entry 1). Clearly, the immobilization method impacts of the reactivity of the catalyst. Considering that the reaction temperature (80 °C) used for ligand exchange of the homogenous

dirhodium catalyst is similar to grafting temperature (90 °C) for silane immobilization, it can be hypothesized that the structure of the dirhodium catalyst might be altered (detachment or rearrangement of the ligands) during the grafting procedure, making the immobilized catalyst unable to finely control the enantioselective cyclopropanation. For this reason, the dirhodium-silane was grafted on the support at room temperature with a trace amount of trimethylamine and DI water (modified pathway 1). Interestingly, the e.e. of the reaction with an immobilized catalyst created by modified pathway 1 improved to 93 %(entry 5), which is consistent with the hypothesis above that high temperature grafting leads to catalyst restructuring or deactivation.

Table 3.1. Cyclopropanation with homogeneous catalysts (entry 1, 2) and heterogeneous catalysts (entry 3-5)

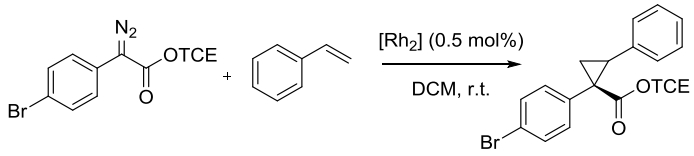

Entry	Catalyst	Yield (%)[a]	e.e. (%)[b]
1	Rh_2(S-p-BrTPCP)$_4$	91	95
2	Dirhodium-silane	87	95
3	Immobilized Rh_2(S-p-BrTPCP)$_3$(S-p-PhTPCP) (pathway 1) Click chemistry (25 °C) → Grafting (90 °C)	86	82
4	Immobilized Rh_2(S-p-BrTPCP)$_3$(S-p-PhTPCP) (pathway 2) Grafting (90 °C) → Click chemistry (25 °C)	89	94
5	Immobilized Rh_2(S-p-BrTPCP)$_3$(S-p-PhTPCP) (modified pathway 1) Click chemistry (25 °C) → Grafting (25 °C)	88	93

[a] isolated yield, [b]enantiomeric excess

3.3.2 Effect of linker structure between the dirhodium catalyst and the support

The silica used in the previous section (effect of immobilization pathways) has a mesoporous structure with a broad pore distribution (20 nm – 1 um). Depending on the immobilization site inside the pores, the interaction of the catalyst with its surroundings will be affected, making a rigorous study on the effect of the linker structure on catalytic activity challenging. Thus, a highly ordered silica support was used in this section, which provides a uniform pore diameter and similar surroundings at any site inside the pores. The immobilized dirhodium catalysts for this study were prepared through the pathway 2.

3.3.2.1. Preparation of conventional SBA-15 and platelet SBA-15

The surface area and pore volume of the SBA-15 and SBA-15PLT support materials are shown in Table 3.2. The SBA-15 is characterized by a surface area of 773 m^2/g and a pore volume of 0.93 cm^3/g. The SBA-15PLT has a lower surface area (560 m^2/g) but higher pore volume (1.35 cm^3/g) compared with the standard SBA-15. Nitrogen adsorption-desorption isotherms for the SBA-15 and SBA-15PLT are shown in figure 3.4a. Both supports have a steep hysteresis loop, which indicates that each support has relatively high pore size uniformity and facile pore connectivity.[21] While the hysteresis loop started from 0.6 of relative pressure for SBA-15, the hysteresis loop started from 0.8 of relative pressure for SBA-15PLT (Figure 3.4a). In general, the relative pressure points at which the hysteresis loops start are related with the pore size of the material. A hysteresis loop at a higher relative pressure point infers that the material has a larger pore size than the material having a hysteresis loop at a lower relative pressure.[22] The pore size distribution of the prepared supports was calculated using the BJH method (adsorption branch), and are

shown in figure 3.4b. SBA-15 and SBA-15PLT both have narrow pore size distributions, as also recognized in steep hysteresis loops in figure 3.4a. The SBA-15 and SBA-15PLT materials have 7 nm and 13 nm pore diameters, respectively, which also shows a good agreement with the relative pressure point at which the hysteresis loops start in figure 3.4a. Figure 3.3 shows the SEM images of the SBA-15 and SBA-15PLT. The inset white scale bar is 5 μm. SBA-15 has a rod shape morphology, where the pore length is approximately longer than 1 μm. On the other hand, SBA-15PLT has a platelet morphology with relatively short pore lengths (< 300 nm).

Table 3.2. The surface areas, pore volumes and silane loadings for bare supports, N_3-supports and Rh_2 immobilized supports with propyl, undecyl and phenyl linkers.

Support	Surface area (m^2/g)	Pore volume (cm^3/g)	Silane loading (mmol Si/g)
SBA-15	773	0.93	n/a
SBA-15PLT	560	1.35	n/a
Propyl-SBA-15	615	0.81	0.20
Rh-propyl-SBA-15	247	0.37	
Undecyl-SBA-15	603	0.81	0.20
Rh-undecyl-SBA-15	201	0.30	
Phenyl-SBA-15	685	0.84	0.17
Rh-phenyl-SBA-15	275	0.47	

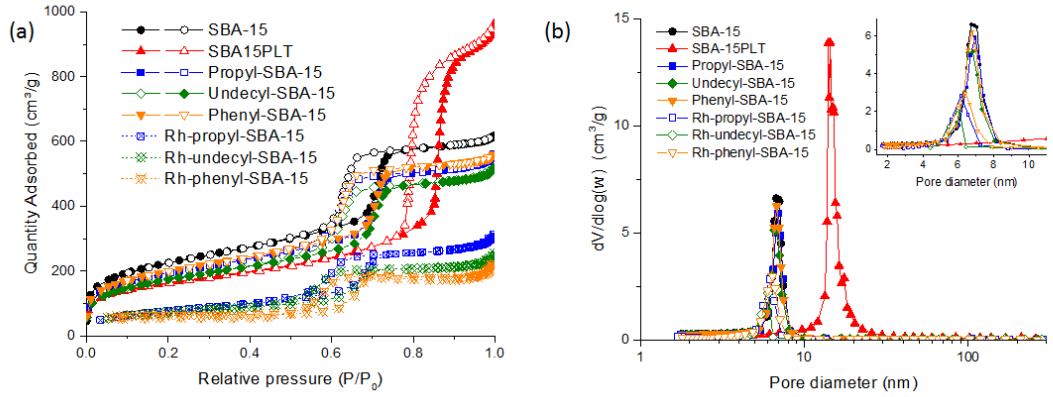

Figure 3.4. (a) Nitrogen adsorption–desorption isotherm and (b) pore diameter distribution of curves of bare supports (SBA-15, SBA-15PLT), N_3-supports (Propyl-SBA-15, Undecyl-SBA-15, Phenyl-SBA-15), Rh_2 immobilized supports (Rh-propyl-SBA-15, Rh-undecyl-SBA-15, Rh-phenyl-SBA-15)

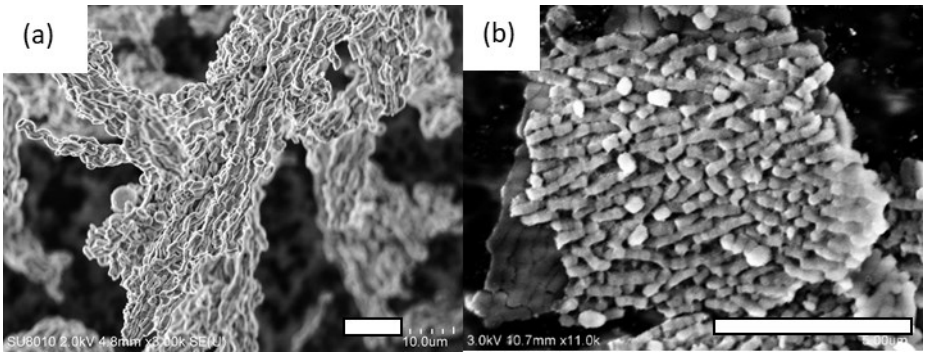

Figure 3.5. SEM images of synthesized (a) conventional SBA-15, (b) platelet SBA-15 (SBA-15PLT). Scale bar is 5µm.

On these SBA-15 supports, three different organosilanes were grafted, as shown in figure 3.4. The propyl (3-azidopropylsilane) and undecyl (11-azidoundecylsilane) linkers are flexible chains, whereas the phenyl linker (4-methylphenylsilane) is expected to be a more rigid chain.

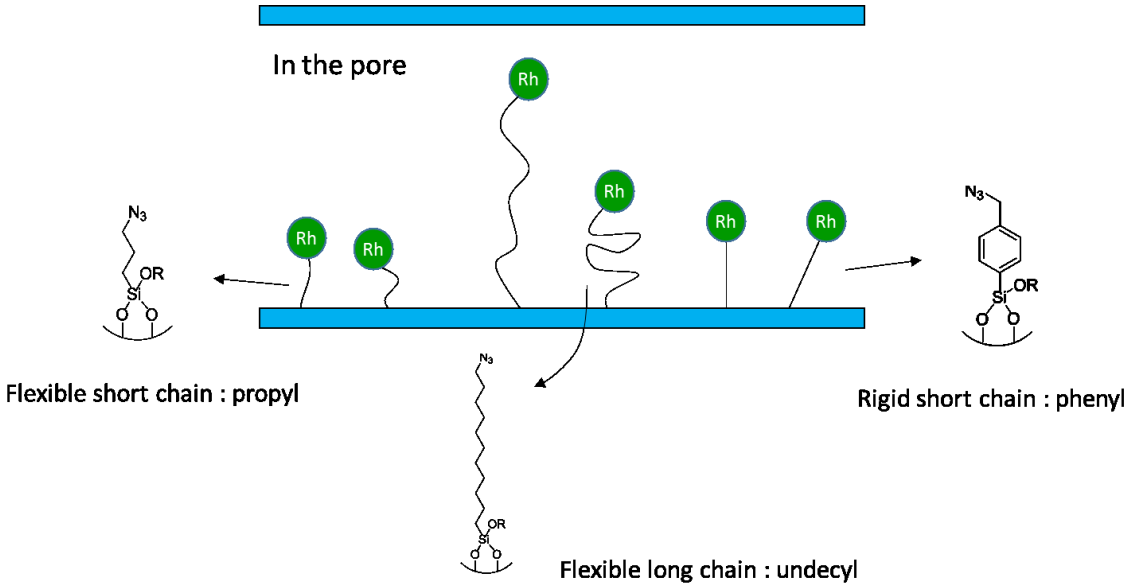

Figure 3.6. Schematic description of immobilized Rh_2 catalysts with various linker structures in the pore of the support.

The surface areas and pore volumes of the azide (N_3) functionalized SBA-15 (N_3-SBA-15), and Rh_2 immobilized catalysts are also summarized in Table 3.2. After the grafting of the three different organosilanes on the bare SBA-15, the prepared N_3-linker-SBA-15 showed slightly decreased surface areas (773→603-685 m^2/g) and pore volumes (0.93→0.81-0.84 cm^3/g) compared with the bare SBA-15. The silane loadings on the N_3-linker-SBA-15 were 0.20, 0.20 and 0.17 mmol Si/g for the propyl, undecyl and phenyl linkers, respectively. Since the silane loadings were low, the average pore diameters of the N_3-SBA-15s were unchanged (7 nm) from the bare SBA-15 (Figure 3.4b, inset figure). In contrast, the surface areas and pore volumes of the N_3 functionalized supports were noticeably reduced (201 - 275 m^2/g and 0.3-0.47 cm^3/g, respectively) after the immobilization of the dirhodium catalyst via click chemistry. The average pore diameters of the catalyst also decreased to 5.7-6 nm.

The FTIR spectra of the azide (N_3) functionalized supports (solid line) and Rh immobilized catalyst (dash line) after immobilization via click chemistry is shown in figure 3.7. For all the samples, the broad peak at 3200 cm^{-1} was assigned to OH stretching vibrations on the silica surface, and the peaks around 2800-2900 cm^{-1} correspond to CH_2 stretching vibrations. Another small, broad peak at 1640 cm^{-1} is attributed to physisorbed water. The peak at 2100 cm^{-1} is only shown in N_3-SBA-15, supporting its assignment to the N_3 stretching vibrational mode. After the click chemistry reaction with terminal alkyne groups on the dirhodium catalyst, the intensity of the N_3 peak (2100 cm^{-1}) for the immobilized Rh_2 catalysts was almost disappeared, which indicates that the most of N_3 functional group were transformed to triazole for successful immobilization of the dirhodium catalyst.

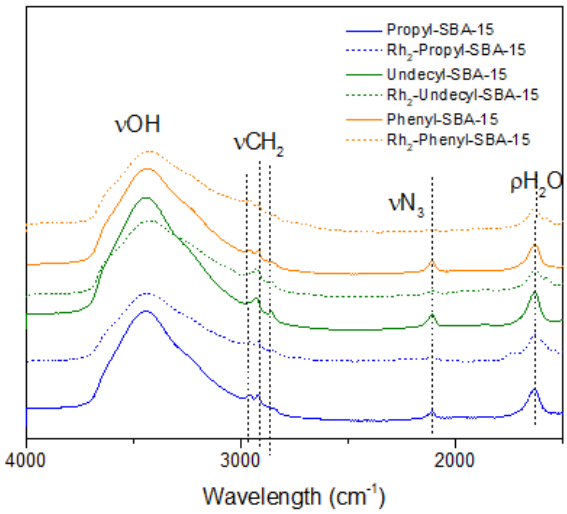

Figure 3.7. FTIR spectra of N_3 functionalized SBA-15 supports (solid line) and silica-immobilized Rh_2 catalysts (dash line)

The catalytic activities of the immobilized catalysts with various linkers were tested for cyclopropanation of styrene (0.5 mmol) using *p*-bromodiazoacetate (0.1 mmol, Me type),

where 1 mol.% of silica immobilized Rh_2 catalyst was used. For the homogeneous catalyst (Rh_2(S-BrTPCP)$_4$), 82% yield and 81% e.e. were obtained (Table 3.3). The immobilized catalyst with the propyl linker (Rh_2-Propyl-SBA-15) shows an identical result (81 % yield, 81% e.e.) with the homogeneously catalyzed reaction. Even though the catalysts with undecyl and phenyl linkers show slightly decreased yield (76% and 80%, respectively) and e.e. (78% and 76%, respectively), significant defects in terms of yield and e.e. were not observed at these low Rh_2 loadings (≈ 0.2 mmol Rh_2/g) across all catalysts studied here.

Table 3.3. Cyclopropanation by homogeneous Rh_2(*S*-BrTPCP)$_4$ catalyst and silica-immobilized catalysts with various linkers.

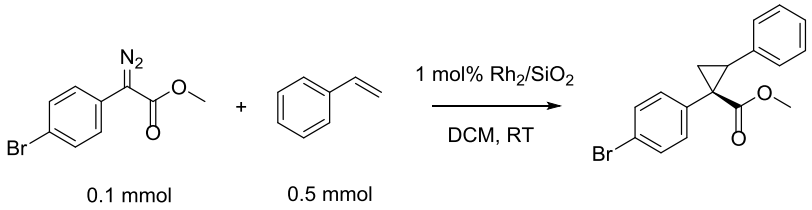

Catalysts	Linker	Yield (%)[a]	e.e. (%)[b]
Rh_2(S-BrTPCP)$_4$	n/a	82	81
Rh_2-Propyl-SBA-15	propylsilane	81	81
Rh_2-undecyl-SBA-15	undecylsilane	76	78
Rh_2-phenyl-SBA-15	phenylsialne	80	76

[a]Isolated yield, [b]enantiomeric excess

Recyclability tests using the prepared catalysts were conducted with the same cyclopropanation reaction in a batch reactor (0.1 mmol of *p*-bromodiazoacetate (Me type) and 0.5 mmol of styrene). For recycle of the catalyst, the used catalyst was recovered by

filtration and washed with DCM multiple times. The filtrate was then concentrated to evaluate the yields and e.e. in subsequent cycles. The washed catalyst was dried under vacuum at room temperature overnight and was reused for the next run. Since all the recycle runs with the catalysts showed similar yield (≈ 78 %), yields are not shown in figure 3.8. When the catalyst with the propyl linker was recycled the first time, the e.e. dropped to 68 %, which dropped further to 62 % with the twice recycled catalyst. Similarly, the catalyst with undecyl and phenyl linkers also showed decreased e.e. upon recycling (78%→ 64% for the undecyl linker, 76% → 56% for the phenyl linker). When scaling up the reaction three times (0.3 mmol of *p*-bromodiazoacetate (Me type) and 1.5 mmol of styrene) with the same amount of propyl linker catalyst (0.34 mol.% silica immobilized Rh_2 catalyst), the e.e. was maintained at 80 %. When the catalyst was recycled and reused for the second run, the e.e dropped to 66%. From this result, it can be inferred that once the catalyst is separated and dried after the reaction, the enantiomeric selectivity properties of the catalyst are changed. However, the specific, molecular level factor leading to decreasing e.e. upon recycle was not experimentally elucidated.

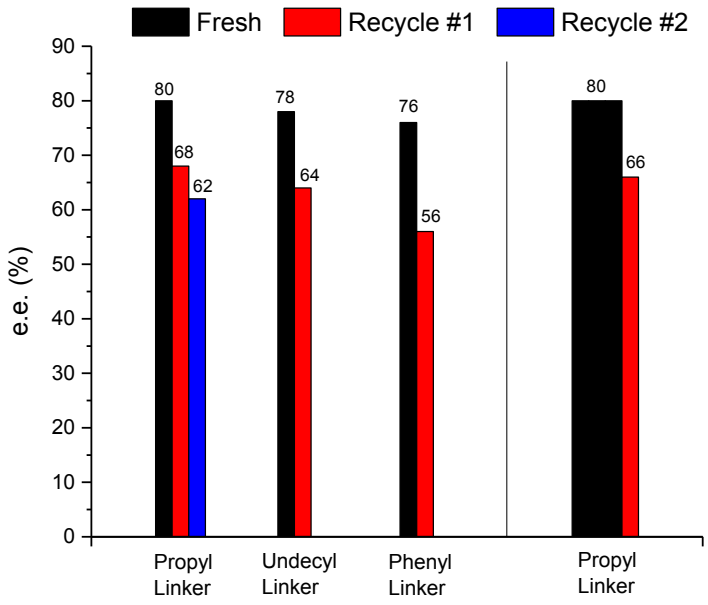

Figure 3.8. The e.e. on the fresh catalyst and recycled, supported catalysts with different linkers. Each run on the left side (propyl, undecyl, phenyl linker) was conducted with 0.1mmol of aryldiazoacetate (thin bar), and the scaled-up reaction on the right side was conducted with 0.3 mmol of aryldiazoacetate (three times thicker bar than a thin bar)

To test the hypothesis that the catalytic activity of the immobilized catalyst may be compromised upon recovery by drying coupled with exposure to the air, a mixture of fresh catalyst (5 mg (1 μmol of Rh_2), silica immobilized Rh_2 catalyst) and bare SiO_2 (15 mg) was charged into a glass column (inner diameter 3 mm x length 10 mm, Omnifit Labware). The overall flow reactor scheme is shown in figure 3.9. The reactants (*p*-bromodiazoacetate (1 mmol, TCE type) and styrene (5 mmol)) in DCM solution (5 mL) were fed into the reactor at a flow rate of 10 μL/min (total volume of 6 mL), and the product was collected in glass vials every 0.6 mL of injection (total ten aliquot).

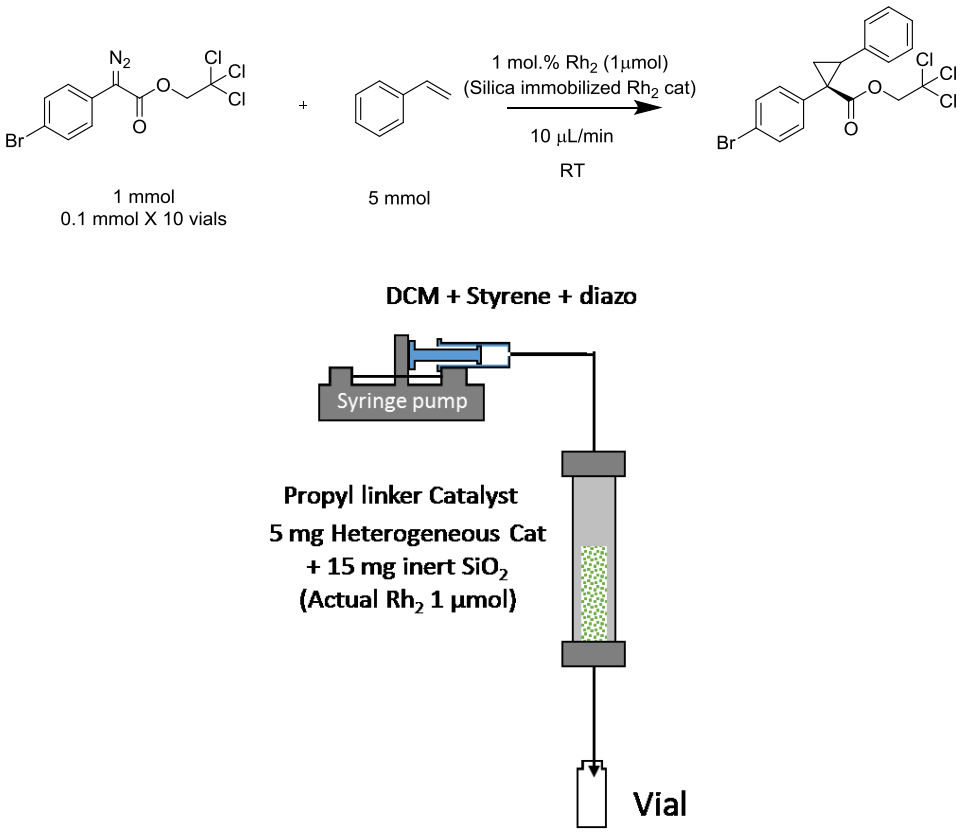

Figure 3.9. The schematic flow packed bed reactor (ID 3 mm x length 10 mm) for the cyclopropanation with *p*-bromodiazoacetate (TCE type) and styrene. The reactants flowed from the top to bottom.

The yield and e.e. of the collected products from the flow reaction were evaluated, and are shown in figure 3.10. The turnover number (TON) was calculated from the yield of each vial, which was accumulated using the same catalyst. Each solid square data point refers to a 0.6 mL of injection. While the 10 vials were collected (total volume 6 mL), the yield and e.e. were well maintained at 80±2% and 92±2%, respectively. Overall, no significant decrease of catalytic performance for the immobilized catalyst in terms of yield or e.e. was observed using the flow reactor setup. Considering the significant decreasing

on e.e. after the filtration and drying of the catalyst, the continuous flow reaction without the additional filtration and drying process, would be a promising reaction platform for C-H functionalization with silica immobilized dirhodium catalyst.

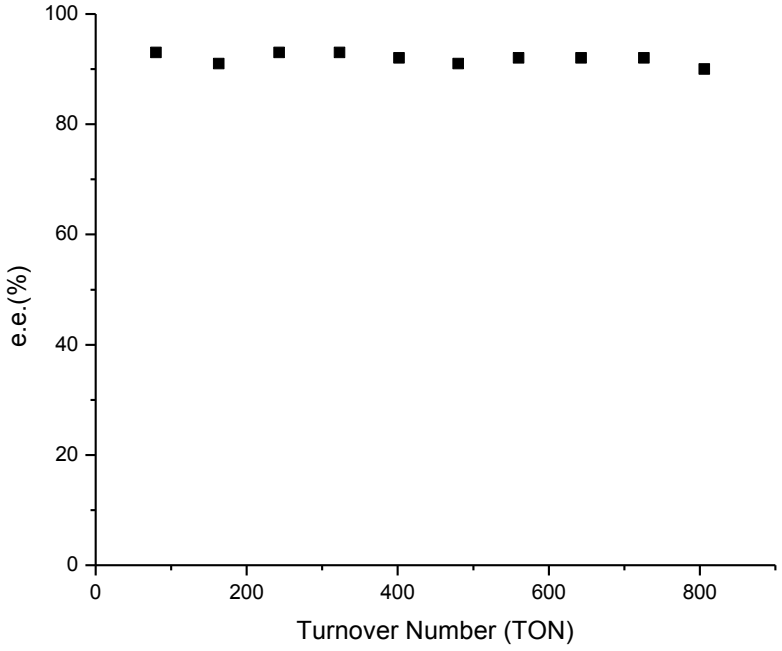

Figure 3.10. The effect of increasing the TON on the e.e. value during the cyclopropanation of *p*-bromodiazoacetate (TCE type) with styrene (figure 3.9). Each solid square data point refers to a 0.6 mL injection of reagents.

In general, reaction kinetics with heterogenized molecular catalysts are slower than with the corresponding homogeneous catalyst system because reactants need to be transported inside the pores of the support to the active sites where the reaction takes place. In the case of the Rh catalyzed C-H functionalization or cyclopropanation with diazo compounds, nitrogen gas is generated during the reaction, as shown in Figure 3.11a. For the homogeneously catalyzed reaction, the nitrogen gas is easily evacuated from the

solvent. However, for the heterogeneously catalyzed reaction, the generated nitrogen gas from the reaction may be trapped in the pores of the support, which may further slow down the mass transfer of the reactants and products into or out of the pores. The cartoon in figure 3.11b provides a schematic of the movement of reactants and nitrogen gas in the pores. The black or red circles refer to the reactant or product, and the green circle indicates the immobilized catalyst in the pore. The yellow color refers to the generated nitrogen gas. Due to the generated nitrogen gas, the product stream was observed to flow discontinuously, even though the reactants were continuously injected without any bubble gap to the catalyst in the packed column (Figure 3.11c).

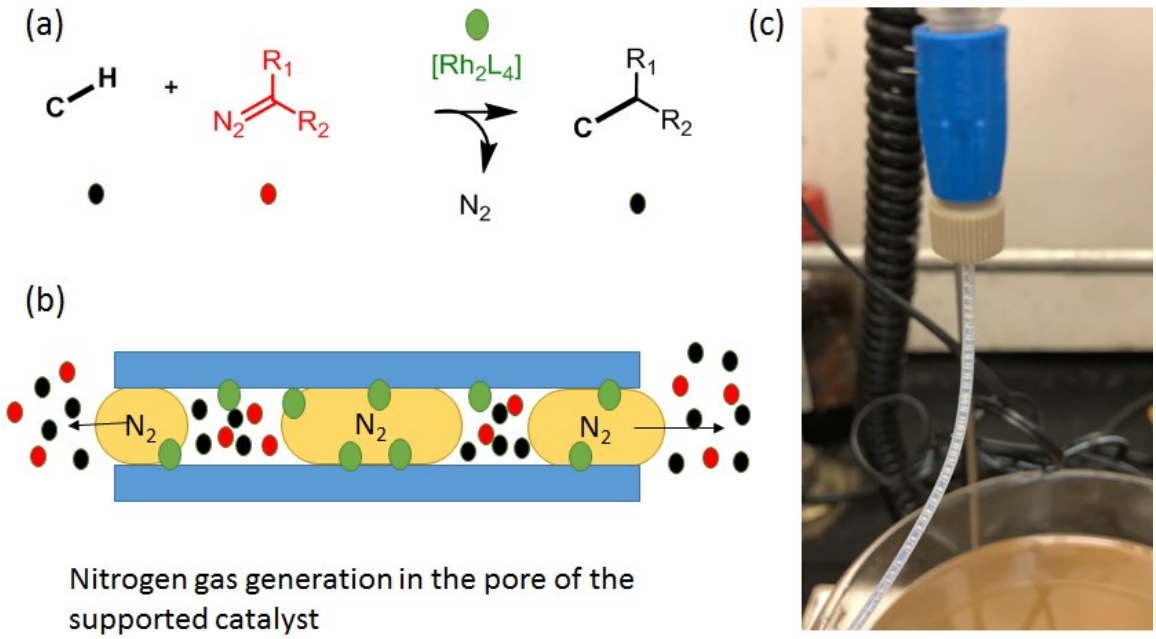

Figure 3.11. (a) Reaction scheme of the Rh_2 catalyzed C-H functionalization where the nitrogen gas is generated as a byproduct, (b) schematic movement of reactants and nitrogen gas in the pore. Reactants (red or black), catalyst (green) and nitrogen gas (yellow), (c) discontinuously flowing product stream from the flow reactor.

Since the generated nitrogen gas from the heterogeneously catalyzed reaction may be trapped in the pores of the support, which may further slow down the mass transfer of the reactants and products into or out of the pores. To explore the effect of the support structure on the reaction kinetics, SBA-15 and SBA-15PLT having different pore lengths and particle sizes were synthesized, as depicted by physical characteristics summarized in figure 3.4 and table 3.2. For these experiments, the propyl silane was grafted on these supports, followed by dirhodium immobilization via click chemistry. The two catalysts made using different supports showed similar dirhodium loadings (Rh-Propyl-SBA-15: 0.29 mmol Rh_2/g, Rh-Propyl-SBA-15PLT: 0.27 mmol Rh_2/g). Each was used in the reaction of *p*-bromodiazoacetate (TCE type) with styrene, and the reaction kinetics were monitored by React-IR, whereby the peak at 2100 cm^{-1}, corresponding to the diazo compound, was selected to track the conversion of the diazo compound to form cyclopropane-based products. The peak at 2100 cm^{-1} did not interfere with any IR signal associated with the products or styrene. For the reaction setup, the IR probe was connected to a flame dried 100 mL three neck round bottom flask. The flask was cooled down under vacuum then backfilled with Ar. Then, 15 mL of distilled DCM was added to the flask, and the IR signal for DCM was recorded after the temperature was stabilized to 25°C (approximately 15 min). Then, a mixture of *p*-bromodiazoacetate (0.4 mmol, TCE type) and styrene (2.0 mmol)) dissolved in 2 mL of DCM was added to the flask via syringe. The saved DCM IR signal was subtracted from the new signal, which could be assigned to the reactants signals. After an additional 15 min with stirring (750 rpm), the silica immobilized Rh_2 catalyst (13.3 mg, 0.04 mmol Rh_2) was added to the flask. The reference peak for the diazo (2100 cm^{-1}) was recorded until the intensity of the peak became zero, indicating

complete reaction (Figure 3.12). The cyclopropanations with the catalysts were completed in 80 min for the Rh-propyl-SBA-15PLT and 120 min for Rh-propyl-SBA15. Even though the TON from this reaction with both catalysts would be the same (89; yield: 89%), the turnover frequency (TOF) for the catalysts were markedly different. Initially, in the 0-20 min period, the Rh-propyl-SBA-15PLT catalyst gave a TOF of 52 h^{-1}, while the Rh-propyl-SBA-15 gave a TOF of only 28 h^{-1}. The reaction kinetics for both catalysts were then accelerated after the induction period to 126 h^{-1} for the Rh-propyl-SBA-15PLT and 82 h^{-1} for the Rh-propyl-SBA-15. From this experiment, it can be suggested that the short pore length allows for the fast mass transfer of the reactants or products, enhancing catalytic productivity, because the generated nitrogen was promptly evacuated from the pore. However, the different pore diameter of the prepared SBA-15 (7 nm) and SBA-15PLT (13nm) might also affect the reaction kinetics. To truly assert that short pore length of the support increases the reaction kinetics, a further study is required with a traditional SBA-15 with the same pore diameter as the platelet sample (SBA-15PLT).

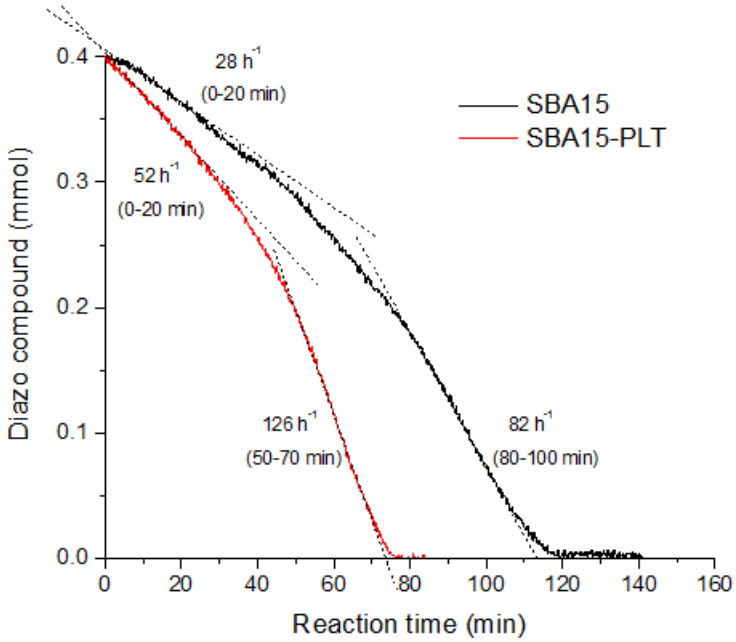

Figure 3.12. The diazo compound consumption along with the reaction time under different catalysts, Rh-propyl-SBA-15 (black) and Rh-propyl-SBA-15PLT (red). The intensity of the IR peak on 2100 cm^{-1} was calibrated to calculate exact mole of the diazo compound in solution.

3.4 Conclusions

In this study, several key factors (e.g., immobilization sequence, linker structure, the pore structure of support) that can affect the catalytic performance (yield, stereoselectivity, and kinetics) of the immobilized dirhodium catalyst on silica supports has been elucidated. The high temperature (>80 °C) treatment on the dirhodium catalyst would lead to the catalyst restructuring or deactivation, which results in low enantioselective cyclopropanation. Thus, the dirhodium catalyst needs to be immobilized on support material at a lower temperature. The linker structure between dirhodium catalyst and Si atom did not significantly affect the catalytic activity. The prepared catalysts with propyl,

undecyl and phenyl linker showed similar catalytic activities. However, the e.e. of the cyclopropanation with the immobilized Rh_2 catalysts were not maintained during the sequential recycle runs via filtration and drying of the catalyst. Surprisingly, the same reaction with packed bed flow reactor provided stable yield and e.e., which suggested that the continuous flow reaction without the additional filtration and drying process, would be a promising reaction platform for C-H functionalization with silica immobilized dirhodium catalyst. The pore structure of the immobilized Rh_2 catalyst showed different reaction kinetics for cyclopropanation, whereby the Rh-propyl-SBA-15PLT catalyst having short pore length with large diameter showed faster kinetics than the Rh-Propyl-SBA-15 catalyst. It can be suggested that the short pore length and wide pore diameter allow for the fast mass transfer of the reactants or products, enhancing catalytic productivity, because the generated nitrogen was promptly evacuated from the pore. This insight from this work may be utilized in the design of new heterogenized dirhodium catalysts seeking higher turnover numbers as well as faster kinetics.

3.5 References

(1) Qin, C.; Boyarskikh, V.; Hansen, J. H.; Hardcastle, K. I.; Musaev, D. G.; Davies, H. M. L. D_2-Symmetric Dirhodium Catalyst Derived from a 1,2,2-Triarylcyclo-Propanecarboxylate Ligand: Design, Synthesis and Application. *J. Am. Chem. Soc.* **2011**, *133* (47), 19198–19204.

(2) Guptill, D. M.; Davies, H. M. L. 2,2,2-Trichloroethyl Aryldiazoacetates as Robust Reagents for the Enantioselective C–H Functionalization of Methyl Ethers. *J. Am. Chem. Soc.* **2014**, *136* (51), 17718–17721.

(3) Fu, L.; Wang, H.; Davies, H. M. L. Role of Ortho-Substituents on Rhodium-Catalyzed Asymmetric Synthesis of Beta-Lactones by Intramolecular C-H Insertions of Aryldiazoacetates. *Org. Lett.* **2014**, *16* (11), 3036–3039.

(4) Liao, K.; Negretti, S.; Musaev, D. G.; Bacsa, J.; Davies, H. M. L. Site-Selective and Stereoselective Functionalization of Unactivated C–H Bonds. *Nature* **2016**, *533* (7602), 230–234.

(5) Liao, K.; Liu, W.; Niemeyer, Z. L.; Ren, Z.; Bacsa, J.; Musaev, D. G.; Sigman, M. S.; Davies, H. M. L. Site-Selective Carbene-Induced C–H Functionalization Catalyzed by Dirhodium Tetrakis(Triarylcyclopropanecarboxylate) Complexes. *ACS Catal.* **2018**, *8* (1), 678–682.

(6) Liao, K.; Pickel, T. C.; Boyarskikh, V.; Bacsa, J.; Musaev, D. G.; Davies, H. M. L. Site-Selective and Stereoselective Functionalization of Non-Activated Tertiary C-H Bonds. *Nature* **2017**, *551* (7682), 609–613.

(7) Goto, T.; Natori, Y.; Takeda, K.; Nambu, H.; Hashimoto, S. Catalytic Enantioselective C–H Functionalization of Indoles with α-Diazopropionates Using Chiral Dirhodium(II) Carboxylates: Asymmetric Synthesis of the (+)-α-Methyl-3-Indolylacetic Acid Fragment of Acremoauxin A. *Tetrahedron: Asymmetry* **2011**, *22* (8), 907–915.

(8) DeAngelis, A.; Shurtleff, V. W.; Dmitrenko, O.; Fox, J. M. Rhodium(II)-Catalyzed Enantioselective C−H Functionalization of Indoles. *J. Am. Chem. Soc.* **2011**, *133* (6), 1650–1653.

(9) Hübner, S.; De Vries, J. G.; Farina, V. Why Does Industry Not Use Immobilized Transition Metal Complexes as Catalysts? *Adv. Synth. Catal.* **2016**, *358* (1), 3–25.

(10) Doyle, M. P.; Timmons, D. J.; Tumonis, J. S.; Gau, H. M.; Blossey, E. C. Preparation and Catalytic Properties of Immobilized Chiral Dirhodium(II) Carboxamidates. *Organometallics* **2002**, *21* (9), 1747–1749.

(11) Takeda, K.; Oohara, T.; Shimada, N.; Nambu, H.; Hashimoto, S. Continuous Flow System with a Polymer-Supported Dirhodium(II) Catalyst: Application to Enantioselective Carbonyl Ylide Cycloaddition Reactions. *Chem. - A Eur. J.* **2011**, *17* (50), 13992–13998.

(12) Takeda, K.; Oohara, T.; Anada, M.; Nambu, H.; Hashimoto, S. A Polymer-Supported Chiral Dirhodium(II) Complex: Highly Durable and Recyclable Catalyst for Asymmetric Intramolecular C-H Insertion Reactions. *Angew. Chem. Int. Ed.* **2010**, *49* (39), 6979–6983.

(13) Moschetta, E. G.; Negretti, S.; Chepiga, K. M.; Brunelli, N. A.; Labreche, Y.; Feng, Y.; Rezaei, F.; Lively, R. P.; Koros, W. J.; Davies, H. M. L.; et al. Composite Polymer/Oxide Hollow Fiber Contactors: Versatile and Scalable Flow Reactors for Heterogeneous Catalytic Reactions in Organic Synthesis. *Angew. Chem. Int. Ed.* **2015**, *54* (22), 6470–6474.

(14) Chepiga, K. M.; Feng, Y.; Brunelli, N. A.; Jones, C. W.; Davies, H. M. L. Silica-Immobilized Chiral Dirhodium(II) Catalyst for Enantioselective Carbenoid Reactions. *Org. Lett.* **2013**, *15* (24), 6136–6139.

(15) Davies, H. M. L.; Walji, A. M. Asymmetric Intermolecular C−H Activation, Using Immobilized Dirhodium Tetrakis((S)-N-(Dodecylbenzenesulfonyl)- Prolinate) as a Recoverable Catalyst. *Org. Lett.* **2003**, *5* (4), 479–482.

(16) Davies, H. M. L.; Walji, A. M. Universal Strategy for the Immobilization of Chiral

Dirhodium Catalysts. *Org. Lett.* **2005**, *7* (14), 2941–2944.

(17) Davies, H. M. L.; Walji, A. M.; Nagashima, T. Simple Strategy for the Immobilization of Dirhodium Tetraprolinate Catalysts Using a Pyridine-Linked Solid Support. *J. Am. Chem. Soc.* **2004**, *126* (13), 4271–4280.

(18) Heydari-Gorji, A.; Yang, Y.; Sayari, A. Effect of the Pore Length on CO_2 Adsorption over Amine-Modified Mesoporous Silicas. *Energy Fuels* **2011**, *25* (9), 4206–4210.

(19) Godula, K.; Rabuka, D.; Nam, K. T.; Bertozzi, C. R. Synthesis and Microcontact Printing of Dual End Functionalized Mucin like Glycopolymers for Microarray Applications. *Angew. Chem. Int. Ed.* **2009**, *48* (27), 4973–4976.

(20) Moitra, N.; Moreau, J. J. E.; Cattoen, X.; Wong Chi Man, M. Convenient Route to Water-Sensitive Sol-Gel Precursors Using Click Chemistry. *Chem. Commun.* **2010**, *46* (44), 8416–8418.

(21) Sing, K. S. W. Reporting Physisorption Data for Gas/Solid Systems with Special Reference to the Determination of Surface Area and Porosity. *Pure Appl. Chem.* **1985**, *57* (4), 603–619.

(22) Groen, J. C.; Peffer, L. A. A.; Pérez-Ramírez, J. Pore Size Determination in Modified Micro- and Mesoporous Materials. Pitfalls and Limitations in Gas Adsorption Data Analysis. *Microporous Mesoporous Mater.* **2003**, *60* (1–3), 1–17.

CHAPTER 4. SYNTHESIS OF DONOR-/ACCEPTOR-SUBSTITUTED DIAZO COMPOUNDS IN FLOW AND THEIR APPLICATIONS IN ENANTIOSELECTIVE DIRHODIUM-CATALYZED CYCLOPROPANATION AND C–H FUNCTIONALIZATION

This chapter represents a collaboration between the Huw Davies group at Emory University and the Christopher Jones group at Georgia Tech. The main contributor in the Davies group was Dr. Daniel Rackl. He prepared donor/acceptor-substituted hydrazones and homogenous Rh_2(*S*-Br-TPCP)$_4$ catalyst and analyzed the products from cyclopropanation and C-H functionalization. He also conducted batch reactions for the effect of anhydrous sodium thiosulfate and iodine addition for benzylic C–H functionalization. My contributions were developing a flow to the batch reactor, preparation of PS-SO_2 NIK resin (oxidant), running all the cyclopropanation and C-H functionalization reactions as well as a screening of drying agent for the flow to the batch reaction. We worked side by side at Emory University, and I completed some work alone at Georgia Tech. As noted in the published article: *Org. Lett*. **2017**, 19, 3055, Dr. Rackl and I contributed equally to the work, and we were co-first-authors on the publication.

4.1 Introduction

C–H functionalization has become an exciting new synthetic strategy, which has brought significant innovation into total synthesis and new methodologies for drug development.[1–10] One particularly useful C–H functionalization procedure has been the C–

H insertion chemistry of transient metal carbenes, typically generated from diazo compounds.[11–16] In recent years, rhodium-stabilized donor/acceptor carbenes have proven to be effective in a wide range of intermolecular C–H functionalization reactions, in which the site selectivity and stereoselectivity is dominated by catalyst control.[17–22] A drawback, however, with the use of diazo compounds as carbene precursors is the issue of safe handling of large quantities of these high energy compounds.[23] Even though there are reports of metal-catalyzed reactions of donor/acceptor diazo compounds conducted on a kilogram or larger scales,[24] the broad utilization of metal carbene chemistry would be greatly facilitated if the diazo compounds were generated under flow conditions and directly used in subsequent reactions.

We have begun applying flow conditions and immobilized catalysts to intermolecular enantioselective C–H functionalization and cyclopropanation reactions of donor/acceptor carbenes.[25,26] We have previously developed an immobilized form of an early generation catalyst, Rh_2(S-DOSP)$_4$ and showed it could be incorporated into fibers and used for cyclopropanation reactions.[26] In this paper we describe the development of suitable flow conditions for the generation of donor-/acceptor-substituted diazo compounds that could be used in batch reactions for Rh_2(*S*-*p*-BrTPCP)$_4$ and Rh_2(R-3,5-di(*p*-*t*BuPh)TPCP)$_4$-catalyzed cyclopropanations and challenging C–H functionalization reactions (Scheme 4.1).[17–22]

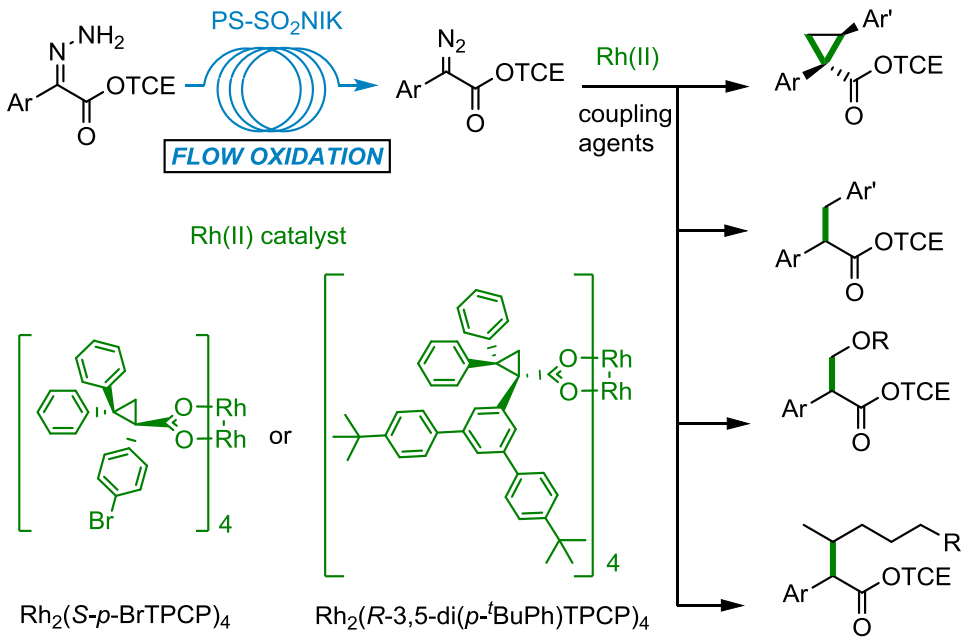

Scheme 4.1. Diazo compound synthesis in flow and its application to cyclopropanation and C–H functionalization.

The preparation of diazo compounds in flow has generated considerable interest in recent years.[27–37] Conventional diazo compound synthesis in the batch system is generally carried out with arylacetate and *p*-acetamidobenzenesulfonyl azide (*p*-ABSA) in the presence of a base (e.g., DBU). Under the base conditions, the arylacetate is protonated to carbanion species, actual reacting reactant, which reacts with *p*-ABSA to yield diazo compound, and the generated acidic *p*-acetamidobenzene sulfonamide is generally separated as a salt bind with the base. Considering the breadth of the chemistry of donor-/acceptor-substituted diazo compounds, several groups have explored methods specifically focused on the synthesis of this type of diazo compound.[27,28,31] The standard diazo transfer reaction using a sulfonyl azide has been employed but has the disadvantage of requiring an in line purification procedure to remove the sulfonamide byproduct.[27] More attractive is

the oxidation of a hydrazone to the diazo compound using either MnO_2[28] or solid supported N-iodo *p*-toluenesulfonamide potassium salt (PS-SO_2NIK)[31] as the oxidant. In all of these reactions, the subsequent reactions were conducted with very reactive trapping agents, such as heteroatoms that would readily form ylide intermediates or styrenes. For these approaches to be effective in our chemistry, it would need to be applied to diazo compounds with trichloroethyl (TCE) esters,[19,20] and further C–H functionalization reactions with much less reactive substrates than anything previously reported would need to be accommodated. On the basis of the prior literature precedence, we concluded that PS-SO_2NIK[31] resin would likely be the most effective because the oxidation reaction is fast under ambient temperature and no interfering by-products would be formed.

The object of this chapter is developing a tandem reaction system for the preparation of donor/acceptor-substituted diazo compounds in a continuous flow from hydrazones which can be coupled to dirhodium catalyzed C−H functionalization or cyclopropanation (flow to the batch reactor).

4.2 Experimental section

4.2.1 General remarks

All solvents were purified and dried by a Glass Contour Solvent Purifier System unless otherwise stated. DCM for cyclopropanation and C–H insertion reactions were dried over activated 4 Å MS. ^{1}H, ^{13}C, and ^{19}F NMR spectra were recorded at either on a Varian Mercury 300 VX spectrometer, a Varian INOVA 500 spectrometer, or on a Varian INOVA 600 spectrometer. NMR spectra were run in solutions of deuterated chloroform ($CDCl_3$) with residual chloroform taken as an internal standard (7.26 ppm for ^{1}H, and 77.16 ppm

for ^{13}C), and were reported in parts per million (ppm). Abbreviations for signal multiplicity are as follows: s = singlet, d = doublet, t = triplet, q = quartet, p = pentet, m = multiplet, etc. Coupling constants (*J* values) were calculated directly from the spectra. IR spectra were collected on a Nicolet iS10 FT-IR spectrometer. Mass spectra were taken on a Thermo Finnigan LTQ-FTMS spectrometer with APCI, ESI or NSI. Thin layer chromatographic analysis was performed with glass-backed silica gel plates, visualizing with UV light and/or staining with ethanolic vanillin stain, Seebach Magic Stain, or aqueous $KMnO_4$ stain. Melting points (Mp) were measured in open capillary tubes with a Mel-Temp Electrothermal melting points apparatus and are thus uncorrected. *In situ* IR monitoring experiments were carried out with a Mettler Toledo ReactIR 45m instrument equipped with a 9.5 mm x 12'' Ag X 1.5 m SiComp probe. Unless otherwise stated, all chemicals were obtained from Fluka, Aldrich, Merck, or Acros and used as received or purified according to standard literature procedures.

4.2.2 *Synthesis of starting materials*

2,2,2-trichloroethyl 2-chloro-2-oxoacetate (1)

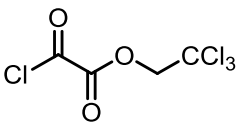

A flame-dried 250 mL round-bottom flask equipped with a pressure-equalizing addition funnel was charged with oxalyl chloride (66 mL, 0.75 mmol, 1.5 equiv.). The reaction mixture was cooled to 0 °C in an ice/water bath. 2,2,2-trichloroethan-1-ol (47.9 mL, 500 mmol, 1.00 equiv.) was added drop-wise via addition funnel over 30 min to give a yellow solution. Afterwards the reaction mixture was stirred at 40 °C for 48 h. Excess oxalyl chloride was removed by vacuum distillation (T,oil = 20 °C, T,vapor <=20 °C, p = 1 mbar) and trapped in a dry-ice/acetone trap. Subsequently, the

target compound (108 g, 450 mmol, 90%) was obtained by vacuum distillation (T,oil = 60 °C, T,vapor = 41 °C, p = 1 mbar) as a colorless oil:

^{1}H NMR (500 MHz, $CDCl_3$) δ 4.97 (s, 2H); **^{13}C NMR** (126 MHz, $CDCl_3$) δ 159.68, 154.12, 93.02, 76.23; **IR** (ATR): 1771, 1445, 1372, 1229, 1082, 1017, 914, 785, 716 cm^{-1}; **HRMS** (NSI) calc. for $[C_4H_3O_4Cl_4]^-$/$[M+OH]^-$: 254.87909, found: 254.87933.

4.2.3 General procedure for the synthesis of 2,2,2-trichloroethyl 2-oxo-2-arylacetates through Friedel–Crafts acylation (GP I)**:**

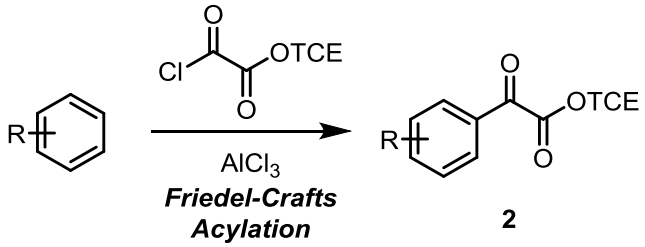

Scheme 4.2. Friedel-Crafts acylation to synthesize trichloroethyl 2-Oxo-2-Arylacetates.

A flame-dried 250 mL 2-necked round-bottom flask equipped with a pressure-equalizing addition funnel was charged with $AlCl_3$ (7.20 g, 54.0 mmol, 1.80 equiv.) and DCM (40 mL). The reaction mixture was cooled to 0 °C in an ice/water bath. 2,2,2-trichloroethyl 2-chloro-2-oxoacetate (6.8 mL, 11 g, 45 mmol, 1.5 equiv.) was added drop-wise via addition funnel over 5 min to give a tan slurry. Arene (30 mmol, 1.0 equiv.) was added drop-wise via addition funnel over 5 min. The reaction mixture was stirred at the indicated parameters till full consumption of starting arene was evident as judged by TLC or LCMS analysis. The reaction mixture was slowly poured into a beaker with ice (150 g) and conc. HCl (50 mL). The mixture was transferred into a separatory funnel and extracted with DCM (3 x 50 mL). The combined organic layers were washed with sat. $NaHCO_3$ (1

x 50 mL) and brine (2 x 50 mL). The organic layer was dried over Na_2SO_4, filtered, and evaporated under reduced pressure to give the crude product as a yellow oil. The crude was purified by automatic flash silica gel chromatography as indicated.

2,2,2-trichloroethyl 2-oxo-2-phenylacetate (2a)

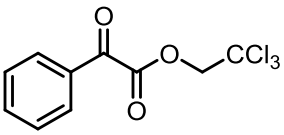

Following GP I (30 mmol scale) resulted in a red slurry after addition of the arene. The mixture stirred at ambient temperature for 16 h followed by refluxing for 30 min. Purification was carried out on a Biotage SNAP 25g SiO_2 column with 0–15% EtOAc in hexanes of 15 column volumes to give the target compound (5.77 g, 20.5 mmol, 68%) as a slightly yellow oil:

R_f (hexanes:EtOAc = 6:1) = 0.57; **^{1}H NMR** (500 MHz, $CDCl_3$) δ 8.08 – 8.01 (m, 2H), 7.73 – 7.64 (m, 1H), 7.58 – 7.50 (m, 2H), 5.04 (s, 2H); **^{13}C NMR** (126 MHz, $CDCl_3$) δ 184.62, 161.85, 135.41, 132.00, 130.11, 129.10, 94.04, 74.48; **IR** (ATR): 1753, 1686, 1595, 1582, 1450, 1321, 1284, 1190, 1167, 1078, 1060, 1029, 1008, 942, 927, 787, 745, 715, 677 cm^{-1}; **HRMS** (NSI) calc. for $[C_{10}H_8O_3Cl_3]^+$: 280.95335, found: 280.95343.

2,2,2-trichloroethyl 2-(4-fluorophenyl)-2-oxoacetate (2b)

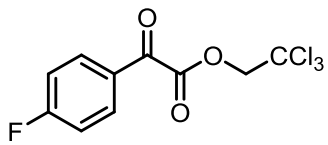

Following GP I (30 mmol scale) resulted in a neon yellow to orange slurry after addition of the arene. The mixture stirred at ambient temperature for 16 h followed by refluxing for 30 min. Purification was carried out on a Biotage SNAP 25g SiO_2 column with 4–8% EtOAc in hexanes of 15 column volumes to give the target compound (6.89 g, 23.0 mmol, 77%) as a yellow oil:

R_f (hexanes:EtOAc = 20:1) = 0.25; **^{1}H NMR** (600 MHz, $CDCl_3$) δ 8.11 – 8.05 (m, 2H), 7.19 (t, *J* = 8.5 Hz, 2H), 5.00 (s, 2H); **^{13}C NMR** (151 MHz, $CDCl_3$) δ 182.75, 167.02 (d, *J* = 259.4 Hz), 161.41, 133.05 (d, *J* = 9.9 Hz), 128.53 (d, *J* = 2.7 Hz), 116.49 (d, *J* = 23.2 Hz), 93.89, 74.50; **^{19}F NMR** (471 MHz, $CDCl_3$) δ -100.00 – -100.09 (m); **IR** (ATR): 1752, 1687, 1596, 1507, 1415, 1372, 1275, 1241, 1177, 1151, 1079, 1009, 931, 852, 812, 795, 714 cm^{-1}; **HRMS** (NSI) calc. for $[C_{10}H_7O_3Cl_3F]^+$: 298.94393, found: 298.94402.

2,2,2-trichloroethyl 2-(4-bromophenyl)-2-oxoacetate (2c)

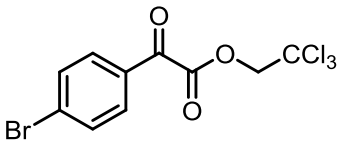

Following GP I (25 mmol scale) resulted in an orange slurry after addition of the arene. The mixture stirred at ambient temperature for 16 h followed by refluxing for 30 min. Purification was carried out on a Silicycle 120 g SiO_2 column with 0–6% EtOAc in hexanes of 15 column volumes to give the target compound (7.70 g, 21.4 mmol, 85%) as a yellow oil:

R_f (hexanes:EtOAc = 6:1) = 0.65; **^{1}H NMR** (400 MHz, $CDCl_3$) δ 7.97 – 7.87 (m, 2H), 7.72 – 7.64 (m, 2H), 5.01 (s, 2H); **^{13}C NMR** (126 MHz, $CDCl_3$) δ 183.60, 161.15, 132.52, 131.59, 131.29, 130.73, 93.92, 74.64; (ATR): 2961, 1751, 1689, 1584, 1485, 1444, 1401, 1371, 1277, 1188, 1163, 1070, 1007, 928, 846, 795, 719 cm^{-1}; **HRMS** (NSI) calc. for $[C_{10}H_7O_3BrCl_3]^+$: 358.86387 found: 358.86452.

2,2,2-trichloroethyl 2-(4-(tert-butyl)phenyl)-2-oxoacetate (2d)

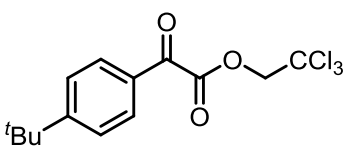

Following GP I (30 mmol scale) resulted in a bordeaux red slurry after addition of the arene. The mixture stirred at

ambient temperature for 1 h followed by refluxing for 30 min. Purification was carried out on a Silicycle 25 g SiO_2 column with 0–10% EtOAc in hexanes of 15 column volumes to give the target compound (9.03 g, 26.7 mmol, 89%) as a slightly yellow solid:

Mp: 25–30 °C; **R_f** (hexanes:EtOAc = 6:1) = 0.57; **^{1}H NMR** (500 MHz, $CDCl_3$) δ 8.08 – 7.98 (m, 2H), 7.60 – 7.55 (m, 2H), 5.05 (s, 2H), 1.37 (s, 9H); **^{13}C NMR** (126 MHz, $CDCl_3$) δ 184.27, 162.10, 159.68, 130.17, 130.17, 129.47, 126.15, 126.14, 94.08, 74.42, 35.49, 30.97; **IR** (ATR): 2965, 2906, 2869, 1748, 1685, 1565, 1429, 1376, 1322, 1284, 1273, 1202, 1170, 1131, 1107, 1078, 1058, 1015, 998, 946, 858, 836, 824, 801, 770, 749, 725, 695 cm^{-1}; **HRMS** (NSI) calc. for $[C_{14}H_{16}O_3Cl_3]^+$: 337.01595, found: 337.01591.

2,2,2-trichloroethyl 2-(4-methoxyphenyl)-2-oxoacetate (*p*-2e)

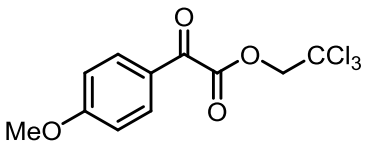

Following GPI (30 mmol scale) resulted in a dark red-brown slurry after addition of the arene. The mixture stirred at ambient temperature for 20 min. Purification was carried out on a Silicycle 330 g SiO_2 column with 4–16% EtOAc in hexanes of 15 column volumes to give 2,2,2-trichloroethyl 2-(4-methoxyphenyl)-2-oxoacetate (5.45 g, 17.5 mmol, 58%) as a slightly yellow solid:

Mp: 41–42 °C; **R_f** (hexanes:EtOAc = 6:1) = 0.46; **^{1}H NMR** (500 MHz, $CDCl_3$) δ 8.07 – 8.03 (m, 2H), 7.04 – 7.00 (m, 2H), 5.03 (s, 2H), 3.93 (s, 3H); **^{13}C NMR** (126 MHz, $CDCl_3$) δ 183.04, 165.42, 162.22, 132.73, 125.05, 114.47, 114.45, 94.09, 74.41, 55.74; **IR** (ATR): 3016, 2970, 2851, 1753, 1672, 1596, 1511, 1466, 1426, 1366, 1318, 1291, 1269, 1226, 1189, 1153, 1124, 1084, 1056, 1023, 1010, 1001, 954, 947, 840, 804, 790, 764, 733, 711, 693 cm^{-1}; **HRMS** (NSI) calc. for $[C_{11}H_{10}O_4Cl_3]^+$: 310.96392, found: 310.96427.

2,2,2-trichloroethyl 2-(2-methoxyphenyl)-2-oxoacetate (*o*-2e)

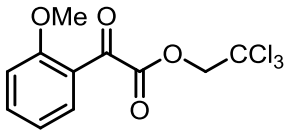

The above mentioned purification also gave 2,2,2-trichloroethyl 2-(2-methoxyphenyl)-2-oxoacetate (2.74 g, 8.80 mmol, 29%) as a slightly yellow oil:

R_f (hexanes:EtOAc = 6:1) = 0.38; **^{1}H NMR** (500 MHz, $CDCl_3$) δ 7.94 (dd, *J* = 7.8, 1.8 Hz, 1H), 7.64 (ddd, *J* = 8.4, 7.3, 1.8 Hz, 1H), 7.12 (ddd, *J* = 8.1, 7.4, 0.9 Hz, 1H), 7.02 (dd, *J* = 8.5, 0.9 Hz, 1H), 4.93 (s, 2H), 3.90 (s, 3H); **^{13}C NMR** (126 MHz, $CDCl_3$) δ 184.56, 163.33, 160.39, 136.89, 130.91, 122.17, 121.46, 111.96, 94.00, 75.00, 56.24; **IR** (ATR): 2949, 1756, 1668, 1598, 1581, 1485, 1467, 1438, 1374, 1307, 1265, 1177, 1159, 1112, 1045, 1018, 956, 807, 777, 753, 716, 668 cm^{-1}; **HRMS** (NSI) calc. for $[C_{11}H_{10}O_4Cl_3]^+$: 310.96392, found: 310.96405.

4.2.4 General procedure for the synthesis of hydrazones (GP II):

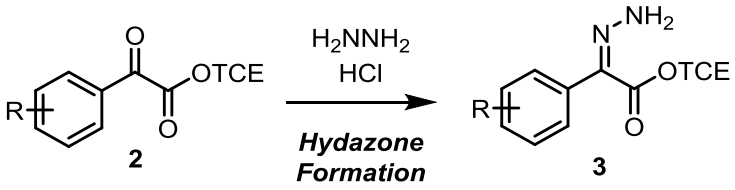

Scheme.4.3. Hydrazones formation from 2,2,2-trichloroethyl 2-Oxo-2-Arylacetates.

A 250 mL round-bottom flask was charged with hydrazine monohydrate (4.85 mL, 5.01 g, 100 mmol, 10.0 equiv.) and MeOH (150 mL). The reaction mixture was cooled to 0 °C in an ice/water bath. HCl (3.0 M, 33 mL, 100 mmol, 100 equiv.) was added slowly. To this solution 2,2,2-trichloroethyl 2-oxo-2-arylacete (10.0 mmol, 1.00 equiv.) in MeOH (10 mL) was added dropwise over about 5 min. The reaction mixture was stirred at 0 °C

until full consumption of starting material was observed by TLC control (unnecessary longer reaction times lead to significantly lower yields). The reaction mixture was quenched by the addition of sat. $NaHCO_3$ (100 mL), MeOH was evaporated under reduced pressure, the residue was transferred into a separatory funnel and extracted with EtOAc (3 x 100 mL). The organic layers were washed with brine (100 mL), filtered, and evaporated under reduced pressure to give the crude products as a yellow solid. The crude was purified by automatic flash silica gel chromatography as indicated.

2,2,2-trichloroethyl (Z)-2-hydrazone-2-phenylacetate (*Z*-3a).

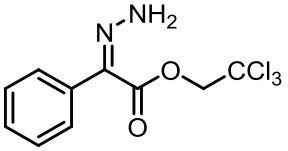

Following GP II (10 mmol scale), the mixture stirred for 18 h. Purification was carried out on a Biotage SNAP 50 g SiO_2 column with 3–45% EtOAc in hexanes of 20 column volumes to give the target compound (1.95 g, 6.59 mmol, 66%) as a slightly yellow solid:

Mp: 50–52 °C; **R_f** (hexanes:EtOAc = 6:1) = 0.29; **^{1}H NMR** (500 MHz, $CDCl_3$) δ 8.71 (s, 2H), 7.69 – 7.60 (m, 2H), 7.45 – 7.32 (m, 3H), 4.93 (s, 2H); **^{13}C NMR** (126 MHz, $CDCl_3$) δ 160.63, 135.88, 128.64, 128.58, 127.91, 127.76, 94.68, 73.75; **IR** (ATR): 3452, 3240, 2958, 1701, 1567, 1515, 1492, 1443, 1365, 1336, 1293, 1260, 1133, 1072, 1062, 1014, 978, 922, 851, 832, 785, 759, 711, 700, 668 cm^{-1}; **HRMS** (NSI) calc. for $[C_{10}H_{10}O_2N_2Cl_3]^+$: 294.98024, found: 294.98019.

2,2,2-trichloroethyl (E)-2-hydrazono-2-phenylacetate (*E*-3a).

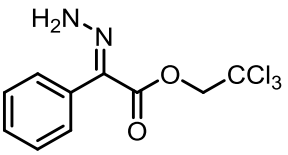

The above mentioned purification also gave 2,2,2-trichloroethyl (E)-2-hydrazono-2-phenylacetate (175 mg, 592 µmol, 5.9%) as a white solid:

Mp: 111–113 °C; **R$_f$** (hexanes:EtOAc = 6:1) = 0.09; **^{1}H NMR** (500 MHz, $CDCl_3$) δ 7.49 (tt, *J* = 6.8, 1.1 Hz, 2H), 7.45 – 7.39 (m, 1H), 7.34 – 7.29 (m, 2H), 6.86 (s, 2H), 4.85 (s, 2H); **^{13}C NMR** (126 MHz, $CDCl_3$) δ 162.82, 134.25, 129.53, 129.27, 128.97, 128.94, 95.11, 74.25; **IR** (ATR): 3401, 3272, 1720, 1551, 1491, 1438, 1375, 1324, 1297, 1275, 1260, 1122, 1076, 1061, 1037, 1021, 976, 818, 790, 775, 718, 706, 691 cm^{-1}; **HRMS** (NSI) calc. for $[C_{10}H_{10}O_2N_2Cl_3]^+$: 294.98024, found: 294.98018.

2,2,2-trichloroethyl (Z)-2-(4-fluorophenyl)-2-hydrazonoacetate (*Z*-3b).

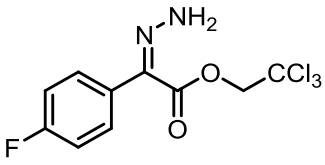

Following GP II (10 mmol scale), the mixture stirred for 20 h. Purification was carried out on a Biotage SNAP 50 g SiO_2 column with 2–70% EtOAc in hexanes of 20 column volumes to give the target compound (1.45 g, 4.62 mmol, 46%) as a white solid:

Mp: 91–93 °C; **R$_f$** (hexanes:EtOAc = 6:1) = 0.39; **^{1}H NMR** (500 MHz, $CDCl_3$) δ 8.71 (s, 2H), 7.61 – 7.56 (m, 2H), 7.10 – 7.03 (m, 3H), 4.91 (s, 2H); **^{13}C NMR** (126 MHz, $CDCl_3$) δ 162.42 (d, *J* = 247.2 Hz), 160.43, 131.94 (d, *J* = 3.3 Hz), 130.34 (d, *J* = 7.4 Hz), 127.64, 114.79 (d, *J* = 21.6 Hz), 94.56, 73.80; **^{19}F NMR** (282 MHz, $CDCl_3$) δ -114.22 – -114.71 (m); **IR** (ATR): 3426, 3288, 1701, 1605, 1561, 1525, 1508, 1431, 1373, 1338, 1293, 1273, 1259, 1234, 1157, 1140, 1073, 1062, 1025, 1016, 984, 833, 814, 784, 752, 713 cm^{-1}; **HRMS** (NSI) calc. for $[C_{10}H_9O_2N_2Cl_3F]^+$: 312.97082, found: 312.97070.

2,2,2-trichloroethyl (E)-2-(4-fluorophenyl)-2-hydrazonoacetate (*E*-3b).

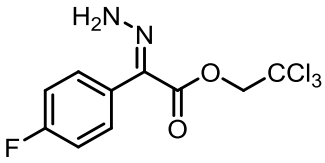

The above mentioned purification also gave 2,2,2-trichloroethyl (E)-2-(4-fluorophenyl)-2-hydrazonoacetate (199 mg, 635 µmol, 6.4%) as a slightly yellow solid:

Mp: 107–108 °C; **R_f** (hexanes:EtOAc = 6:1) = 0.13; **^{1}H NMR** (500 MHz, $CDCl_3$) δ 7.36 – 7.30 (m, 2H), 7.25 – 7.15 (m, 2H), 6.84 (s, 2H), 4.85 (s, 2H); **^{13}C NMR** (126 MHz, $CDCl_3$) δ 163.05 (d, *J* = 249.9 Hz), 162.67, 133.44, 131.14 (d, *J* = 8.4 Hz), 124.76 (d, *J* = 3.5 Hz), 116.50 (d, *J* = 21.6 Hz), 95.01, 74.31; **^{19}F NMR** (282 MHz, $CDCl_3$) δ -110.36 – -110.54 (m); **IR** (ATR): 3406, 3279, 1729, 1603, 1560, 1505, 1437, 1369, 1309, 1295, 1266, 1221, 1155, 1121, 1076, 1035, 1016, 979, 840, 813, 780, 704 cm^{-1}; **HRMS** (NSI) calc. for $[C_{10}H_9O_2N_2Cl_3F]^+$: 312.97082, found: 312.97073.

2,2,2-trichloroethyl (Z)-2-(4-bromophenyl)-2-hydrazonoacetate (*Z*-3c).

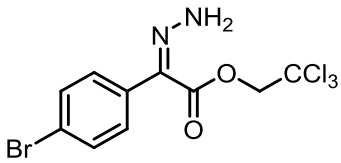

Following GPII (40 mmol scale), the mixture stirred for 22 h. Purification was carried out on a Silicycle 330 g SiO_2 column with 4–17% EtOAc in hexanes of 13 column volumes to give the target compound (8.67 g, 23.2 mmol, 58%) as a white solid:

Mp: 93–95 °C; **R_f** (hexanes:EtOAc = 6:1) = 0.45; **^{1}H NMR** (600 MHz, $CDCl_3$) δ 8.75 (s, 2H), 7.46 (s, 4H), 4.87 (s, 2H); **^{13}C NMR** (126 MHz, $CDCl_3$) δ 160.33, 134.81, 130.99, 130.98, 127.30, 121.85, 94.53, 73.83; **IR** (ATR): 3397, 3244, 3005, 2955, 1698, 1563, 1505, 1488, 1436, 1397, 1362, 1339, 1307, 1285, 1262, 1133, 1103, 1072, 1014, 1006, 981, 957, 842, 824, 794, 707 cm^{-1}; **HRMS** (NSI) calc. for $[C_{10}H_9O_2N_2BrCl_3]^+$: 372.89075, found: 372.89133.

2,2,2-trichloroethyl (E)-2-(4-bromophenyl)-2-hydrazonoacetate (E-3c).

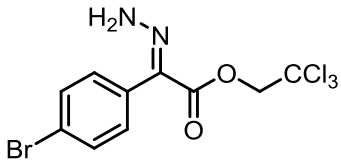

The above mentioned purification also gave 2,2,2-trichloroethyl (E)-2-(4-bromophenyl)-2-hydrazonoacetate (986 mg, 2.63 mmol, 6.6%) as a slightly yellow solid:

Mp: 135–137 °C; **R$_f$** (hexanes:EtOAc = 6:1) = 0.15; **^{1}H NMR** (600 MHz, $CDCl_3$) δ 7.61 (dd, *J* = 8.3, 1.4 Hz, 2H), 7.19 (dd, *J* = 8.3, 1.4 Hz, 2H), 6.74 (s, 2H), 4.83 (s, 2H); **^{13}C NMR** (126 MHz, $CDCl_3$) δ 162.43, 133.39, 132.59, 130.73, 127.67, 123.92, 94.96, 74.33; **IR** (ATR): 3395, 3276, 3067, 2942, 1706, 1590, 1568, 1557, 1487, 1444, 1398, 1377, 1324, 1304, 1230, 1139, 1096, 1070, 1043, 1012, 980, 855, 816, 782, 766, 716 cm^{-1}; **HRMS** (NSI) calc. for $[C_{10}H_9O_2N_2BrCl_3]^+$: 372.89075, found: 372.89100.

2,2,2-trichloroethyl (Z)-2-(4-(tert-butyl)phenyl)-2-hydrazonoacetate (Z-3d).

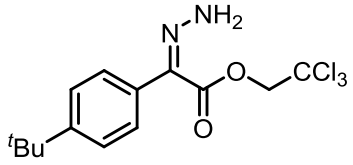

Following GP II (10 mmol scale), the mixture stirred for 16 h. Purification was carried out on a Biotage SNAP 50 g SiO_2 column with 2–50% EtOAc in hexanes of 20 column volumes to give the target compound (2.09 g, 5.94 mmol, 59%) as a slightly yellow solid: **Mp**: 108–110 °C; **R$_f$** (hexanes:EtOAc = 6:1) = 0.45; **^{1}H NMR** (500 MHz, $CDCl_3$) δ 8.69 – 8.55 (m, 2H), 7.63 – 7.52 (m, 2H), 7.43 – 7.39 (m, 2H), 4.94 (s, 2H), 1.35 (s, 9H); **^{13}C NMR** (126 MHz, $CDCl_3$) δ 160.69, 150.71, 132.92, 128.78, 128.07, 124.87, 94.70, 73.63, 34.58, 31.32; **IR** (ATR): 3401, 3269, 2962, 1686, 1562, 1509, 1375, 1267, 1151, 1113, 1091, 1038, 840, 782, 720 cm^{-1}; **HRMS** (NSI) calc. for $[C_{14}H_{18}O_2N_2Cl_3]^+$: 351.04284, found: 351.04276.

2,2,2-trichloroethyl (E)-2-(4-(tert-butyl)phenyl)-2-hydrazonoacetate (E-3d).

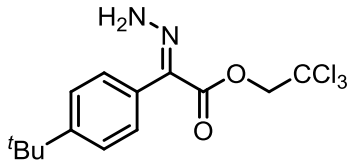

The above mentioned purification also gave 2,2,2-trichloroethyl (E)-2-(4-(tert-butyl)phenyl)-2-

hydrazonoacetate (168 mg, 478 µmol, 4.8%) as a slightly yellow solid:

Mp: 148–150 °C; **R_f** (hexanes:EtOAc = 6:1) = 0.15; **^{1}H NMR** (500 MHz, $CDCl_3$) δ 7.52 (d, *J* = 8.3 Hz, 2H), 7.27 (d, *J* = 8.3 Hz, 1H), 6.81 (s, 2H), 4.88 (s, 2H), 1.35 (s, 9H); **^{13}C NMR** (126 MHz, $CDCl_3$) δ 162.98, 152.55, 134.64, 128.65, 126.16, 125.83, 95.18, 74.23, 34.84, 31.25; **IR** (ATR): 3412, 3282, 2964, 2868, 1714, 1599, 1566, 1508, 1369, 1323, 1270, 1235, 1124, 1107, 1038, 973, 843, 818, 786, 733, 710 cm^{-1}; **HRMS** (NSI) calc. for $[C_{14}H_{18}O_2N_2Cl_3]^+$: 351.04284, found: 351.04260.

2,2,2-trichloroethyl (Z)-2-hydrazono-2-(4-methoxyphenyl)acetate (Z-*p*-3e).

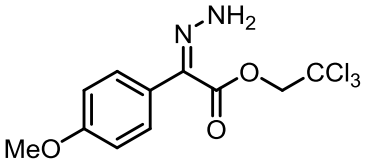

Following GP II (10 mmol scale), the mixture stirred for 6 h. Purification was carried out on a Biotage SNAP 50 g SiO_2 column with 2–50% EtOAc in hexanes of 20 column volumes to give the target compound (1.41 g, 4.33 mmol, 43%) as a slightly yellow solid:

Mp: 94–95 °C; **R_f** (hexanes:EtOAc = 3:1) = 0.47; **^{1}H NMR** (500 MHz, $CDCl_3$) δ 8.60 (s, 2H), 7.61 – 7.51 (m, 2H), 6.94 – 6.89 (m, 2H), 4.92 (s, 2H), 3.84 (s, 3H); **^{13}C NMR** (126 MHz, $CDCl_3$) δ 160.66, 159.25, 129.81, 128.51, 113.32, 94.72, 73.75, 55.29; **IR** (ATR): 3447, 3257, 2958, 2843, 1698, 1603, 1575, 1508, 1465, 1442, 1373, 1331, 1295, 1274, 1237, 1175, 1144, 1113, 1027, 1015, 979, 834, 817, 769, 779, 719 cm^{-1}, **HRMS** (NSI) calc. for $[C_{11}H_{12}O_3N_2Cl_3]^+$: 324.99080, found: 324.99129.

2,2,2-trichloroethyl (E)-2-hydrazono-2-(4-methoxyphenyl)acetate (E-*p*-3e).

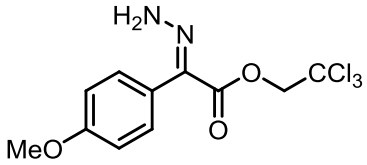

The above mentioned purification also gave 2,2,2-trichloroethyl (E)-2-hydrazono-2-(4-

methoxyphenyl)acetate (157 mg, 482 μmol, 4.8%) as a yellow solid:

Mp: 110–112 °C ; **R_f** (hexanes:EtOAc = 3:1) = 0.16; **^{1}H NMR** (500 MHz, $CDCl_3$) δ 7.33 – 7.25 (m, 2H), 7.05 – 7.01 (m, 2H), 6.60 (s, 2H), 4.89 (s, 2H), 3.86 (s, 3H); **^{13}C NMR** (126 MHz, $CDCl_3$) δ 162.92, 160.26, 135.13, 130.41, 120.74, 114.66, 95.10, 74.29, 55.33; **IR** (ATR): 3447, 3258, 2958, 2843, 1752, 1698, 1604, 1577, 1508, 1465, 1454, 1373, 1332, 1295, 1275, 1237, 1175, 1144, 1114, 1068, 1015, 980, 834, 817, 796, 779, 719 cm^{-1}, **HRMS** (NSI) calc. for $[C_{11}H_{12}O_3N_2Cl_3]^+$: 324.99080, found: 324.99072.

2,2,2-trichloroethyl (Z)-2-hydrazono-2-(2-methoxyphenyl)acetate (Z-*o*-3e).

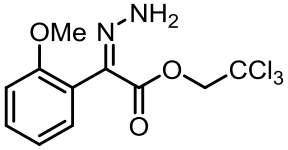

Following GPII (10 mmol scale), the mixture stirred for 6 h. Purification was carried out on a Biotage SNAP 50 g SiO_2 column with 2–50% EtOAc in hexanes of 20 column volumes to give the target compound (672 mg, 2.06 mmol, 21%) as a colorless oil:

R_f (hexanes:EtOAc = 3:1) = 0.36; **^{1}H NMR** (500 MHz, $CDCl_3$) δ 8.45 (s, 2H), 7.36 – 7.31 (m, 2H), 6.99 (td, *J* = 7.4, 1.1 Hz, 1H), 6.88 (dd, *J* = 8.2, 1.0 Hz, 1H), 4.80 (s, 2H), 3.79 (s, 3H); **^{13}C NMR** (126 MHz, $CDCl_3$) δ 160.75, 157.74, 130.38, 129.75, 127.85, 125.47, 120.41, 110.09, 94.75, 73.59, 55.44; **IR** (ATR): 3460, 3298, 2954, 2836, 1701, 1600, 1582, 1526, 1491, 1463, 1435, 1373, 1334, 1257, 1112, 1072, 1049, 1027, 981, 934, 832, 798, 782, 751, 714, 660 cm^{-1}; **HRMS** (NSI) calc. for $[C_{11}H_{12}O_3N_2Cl_3]^+$: 324.99080, found: 324.99081.

4.2.5 General procedure for the flow oxidations of hydrazones (GP III):

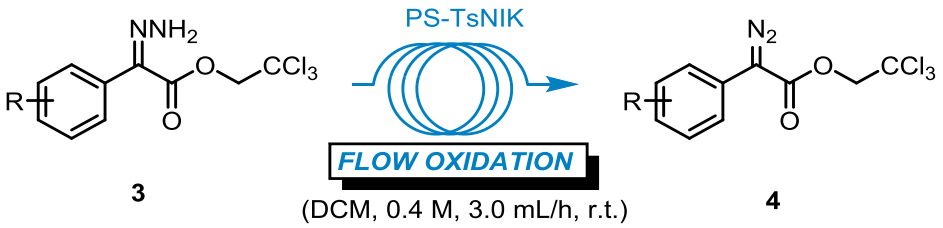

Scheme 4.4. Diazo compounds synthesis from hydrazones in flow

PS-TsNIK resin (1.60 g) was filled into an Omnifit (A = 0.3421 cm²) cartridge. A 25 mL vial was charged with hydrazone (480 µmol, 1.20 equiv.) and DCM (1.20 mL). This solution was injected into a 1.00 mL sample loop (effective starting material: 400 µmol, 1.00 equiv.) of a HPLC valve. The valve was connected to a 10 mL plastic syringe filled with 10 mL dry DCM fitted in a syringe pump. A total volume of 6 mL of DCM at a flowrate of 50 µL/min (3.0 mL/h) was used to push the substrate though the cartridge (stream from bottom to top). The product solution was collected in a weighted 25 mL vial and evaporated under reduced pressure (25 °C water bath temperature) after completion of the run. An exactly weighted aliquot of the product was added to a defined amount of dimethyl fumarate, dissolved in $CDCl_3$, and a ^{1}H-NMR was acquired with a recycle delay (d1) of 30 s to assess the product purity by means of QNMR.

2,2,2-trichloroethyl 2-diazo-2-phenylacetate (4a/Z)

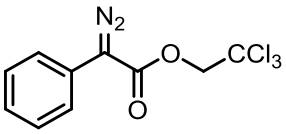

Following GP III (400 µmol scale) using 2,2,2-trichloroethyl (Z)-2-hydrazono-2-phenylacetate no purification was necessary to give the target compound (114 mg, 387 µmol, 97%, 99% purity) as orange solid:

Mp: 71 °C; **R_f** (hexanes:EtOAc = 20:1) = 0.27; **^{1}H NMR** (500 MHz, $CDCl_3$) δ 7.56 – 7.50 (m, 2H), 7.48 – 7.41 (m, 2H), 7.28 – 7.22 (m, 1H), 4.95 (s, 2H); **^{13}C NMR** (126 MHz, $CDCl_3$) δ 163.31, 129.11, 126.33, 124.63, 124.05, 95.08, 73.83; **IR** (ATR) 2993, 2097, 1698, 1595, 1450, 1380, 1233, 1149, 1088, 1030, 946, 837, 779, 713, 686, 667 cm^{-1}; **HRMS** (NSI) calc. for $[C_{10}H_7O_2N_2Cl_3Na]^+$: 314.94653, found: 314.94699.

2,2,2-trichloroethyl 2-diazo-2-(4-fluorophenyl)acetate (4b/Z)

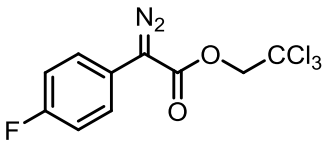

Following GP III (400 µmol scale) using 2,2,2-trichloroethyl (Z)-2-(4-fluorophenyl)-2-hydrazonoacetate no purification was necessary to give the target compound (108 mg, 346 µmol, 86%, 98% purity) as orange oil:

R_f (hexanes:EtOAc = 20:1) = 0.43; **^{1}H NMR** (500 MHz, $CDCl_3$) δ 7.51 – 7.45 (m, 2H), 7.17 – 7.11 (m, 2H), 4.93 (s, 2H); **^{13}C NMR** (126 MHz, $CDCl_3$) δ 161.28 (d, J = 246.9 Hz), 128.45 (d, J = 8.6 Hz), 126.06, 120.41, 116.22 (d, J = 22.0 Hz), 115.59 (d, J = 22.0 Hz), 94.99, 73.87; **^{19}F NMR** (471 MHz, $CDCl_3$) δ -115.35.

2,2,2-trichloroethyl 2-(4-bromophenyl)-2-diazoacetate (4c/Z)

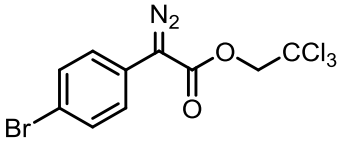

Following GP III (400 µmol scale) using 2,2,2-trichloroethyl (Z)-2-(4-bromophenyl)-2-hydrazonoacetate no purification was necessary to give the target compound (144 mg, 387 µmol, 97%, 98% purity) as orange solid:

R_f (hexanes:EtOAc = 20:1) = 0.47; **^{1}H NMR** (500 MHz, $CDCl_3$) δ 7.57 – 7.52 (m, 2H), 7.42 – 7.38 (m, 2H), 4.93 (s, 2H).

2,2,2-trichloroethyl 2-(4-bromophenyl)-2-diazoacetate (4c/E)

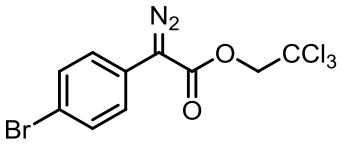

Following GP III (400 µmol scale) using 2,2,2-trichloroethyl (E)-2-(4-bromophenyl)-2-hydrazonoacetate no purification was necessary to give the target compound (137 mg, 368 µmol, 92%, 98% purity) as orange solid:

R_f (hexanes:EtOAc = 20:1) = 0.47; **^{1}H NMR** (500 MHz, $CDCl_3$) δ 7.57 – 7.52 (m, 2H), 7.42 – 7.38 (m, 2H), 4.93 (s, 2H).

2,2,2-trichloroethyl 2-(4-(tert-butyl)phenyl)-2-diazoacetate (4d/Z)

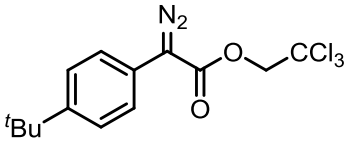

Following GP III (400 µmol scale) using 2,2,2-trichloroethyl (Z)-2-(4-(tert-butyl)phenyl)-2-hydrazonoacetate no purification was necessary to give the target compound (140 mg, 400 µmol, 100%, 97% purity) as orange solid:

R_f (hexanes:EtOAc = 20:1) = 0.60; **^{1}H NMR** (500 MHz, $CDCl_3$) δ 7.49 (d, *J* = 1.2 Hz, 1H), 4.96 (s, 1H), 1.38 (s, 2H).

2,2,2-trichloroethyl 2-diazo-2-(4-methoxyphenyl)acetate (*p*-4e/Z)

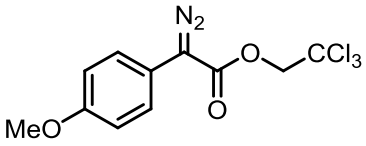

Following GP III (400 µmol scale) using 2,2,2-trichloroethyl (Z)-2-hydrazono-2-(4-methoxyphenyl)acetate no purification was necessary to give the target compound (116 mg, 359 µmol, 90%, 98% purity) as orange solid:

Mp: 53 °C; **R_f** (hexanes:EtOAc = 20:1) = 0.30; **^{1}H NMR** (500 MHz, $CDCl_3$) δ 7.44 – 7.40 (m, 2H), 7.01 – 6.96 (m, 2H), 4.92 (s, 2H), 3.84 (s, 3H); **^{13}C NMR** (126 MHz, $CDCl_3$) δ

158.41, 127.96, 126.12, 115.96, 114.74, 114.04, 95.12, 73.84, 55.38; **IR** (ATR) 3005, 2954, 2936, 2841, 2092, 1689, 1511, 1454, 1380, 1296, 1251, 1234, 1188, 1136, 1086, 1052, 1041, 1030, 934, 924, 833, 813, 795, 728, 710 cm^{-1}; **HRMS** (NSI) calc. for $[C_{11}H_{10}O_3Cl_3]^+$ ($[M-N_2+H]^+$): 294.96900, found: 294.96934.

2,2,2-trichloroethyl 2-diazo-2-(2-methoxyphenyl)acetate (*o*-4e/Z)

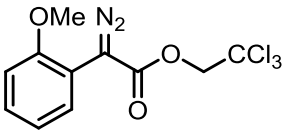

Following GPIII (400 µmol scale) using 2,2,2-trichloroethyl (Z)-2-hydrazono-2-(2-methoxyphenyl)acetate no purification was necessary to give the target compound (117 mg, 362 µmol, 90%, 97% purity)

R_f (hexanes:EtOAc = 20:1) = 0.29; **^{1}H NMR** (500 MHz, $CDCl_3$) δ 7.61 (dd, *J* = 7.8, 1.7 Hz, 1H), 7.32 (ddd, *J* = 8.3, 7.4, 1.7 Hz, 1H), 7.06 (ddd, *J* = 7.5, 1.2 Hz, 1H), 6.94 (dd, *J* = 8.3, 1.2 Hz, 1H), 4.92 (s, 2H), 3.90 (s, 3H); **^{13}C NMR** (126 MHz, $CDCl_3$) δ 155.52, 130.23, 129.09, 121.22, 112.76, 110.92, 95.27, 73.90, 55.59; **IR** (ATR) 2952, 2839, 2101, 1705, 1597, 1580, 1497, 1463, 1436, 1373, 1292, 1248, 1138, 1120, 1051, 1024, 925, 822, 792, 772, 749, 712, 659 cm^{-1}; **HRMS** (NSI) calc. for $[C_{11}H_{10}O_3Cl_3]^+$ ($[M-N_2+H]^+$): 294.96900, found: 294.96934

4.2.6 Cyclopropanation reactions

4.2.6.1. General procedure for the synthesis of cyclopropanes in a batch process (GP IV):

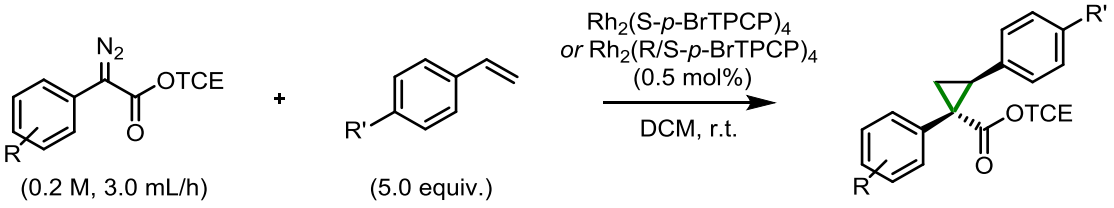

Scheme 4.5. Rh (II) catalyzed cyclopropanations in a batch reactor.

A flame dried 10 mL round bottom flask equipped with a magnetic stir-bar was charged with Rh_2(S-p-BrTPCP)$_4$ or for racemic products Rh_2-R/S-p-BrTPCP)$_4$ (3.6 mg, 2.0 μmol, 0.5 mol%) and silica-plug-filtered styrene (0.23 mL, 0.21 g, 2.0 mmol, 5.0 equiv.), evacuated and backfilled with argon (3x), charged with DCM (2.0 mL), and magnetically stirred (about 600 rpm) at ambient temperature. A flame-dried 10 mL pear-shaped flask was charged with diazo (400 μmol, 1.00 equiv.), evacuated and backfilled with argon (3x), and charged with DCM (2.0 mL). This solution was transferred to a syringe and dropwise added to the reaction vessel at a flowrate of 50 μL/min (3.0 mL/h) via syringe pump. The pear-shaped flask was rinsed with DCM (2 x 0.5 mL) and the solution slowly added to the reaction mixture, which was stirred for 30 min at ambient temperature, and evaporated under reduced pressure. Trichloroethylene (typically 25–50 μL) was added as an internal standard (if needed $CDCl_3$ was added to obtain a fully homogeneous sample), and the crude yield determined by ^{1}H-NMR analysis. The NMR sample was added back to the remaining crude material, the combined sample evaporated under reduced pressure, and purified by automatic flash column chromatography (typically 12 g SiO_2, 1–3% Et_2O in hexanes over 20 CV). The ee of the material was determined by chiral HPLC analysis as indicated.

2,2,2-trichloroethyl (1R,2S)-1-(4-bromophenyl)-2-phenylcyclopropane-1-carboxylate (5c-Batch)[38]

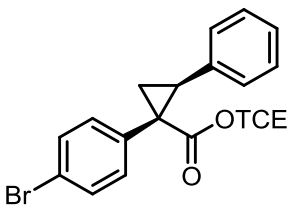

Following GPIV (400 μmol scale) using 2,2,2-trichloroethyl 2-(4-bromophenyl)-2-diazoacetate gave the target compound (163 mg, 363 μmol, 91%) as a white solid:

R_f (hexanes:EtOAc = 6:1) = 0.59; **^{1}H NMR** (500 MHz, $CDCl_3$) δ 7.32 – 7.27 (m, 2H), 7.19 – 7.09 (m, 3H), 7.01 – 6.95 (m, 2H), 6.84 (dd, *J* = 6.8, 2.9 Hz, 2H), 4.87 (d, *J* = 11.9 Hz, 1H), 4.68 (d, *J* = 11.9 Hz, 1H), 3.26 (dd, *J* = 9.4, 7.5 Hz, 1H), 2.32 (dd, *J* = 9.4, 5.2 Hz, 1H), 2.01 (dd, *J* = 7.5, 5.2 Hz, 1H); **HPLC** (OJH column, 1.0 mL/min, 1 % iPrOH in hexanes, λ = 230 nm): t_R(major) = 8.0 min, t_R(minor) = 12.7 min, 95% ee.

2,2,2-trichloroethyl (1R,2S)-1,2-diphenylcyclopropane-1-carboxylate (5a-Racemate)

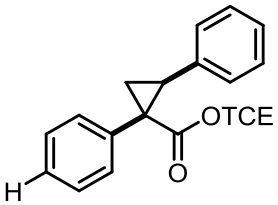

Following GPIV (400 μmol scale) using 2,2,2-trichloroethyl 2-diazo-2-phenylacetate gave the target compound (138 mg, 374 μmol, 94%) as a white solid:

Mp: 61 °C; **R_f** (hexanes:EtOAc = 6:1) = 0.58; **^{1}H NMR** (500 MHz, $CDCl_3$) δ 7.21 – 7.16 (m, 3H), 7.14 – 7.09 (m, 5H), 6.90 – 6.81 (m, 2H), 4.89 (d, *J* = 11.9 Hz, 1H), 4.69 (d, *J* = 11.9 Hz, 1H), 3.27 (dd, *J* = 9.4, 7.4 Hz, 1H), 2.33 (dd, *J* = 9.4, 5.1 Hz, 1H), 2.06 (dd, *J* = 7.4, 5.1 Hz, 1H); **^{13}C NMR** (126 MHz, $CDCl_3$) δ 172.13, 135.75, 133.69, 132.07, 128.15, 127.85, 127.74, 127.34, 126.64, 95.13, 74.38, 37.28, 33.92, 20.35; **IR** (ATR) 3064, 1724, 1603, 1499, 1439, 1359, 1257, 1235, 1212, 1156, 1149, 1096, 1076, 1065, 1054, 1002, 886, 813, 784, 711, 697, 656 cm^{-1}; **HRMS** (NSI) calc. for $[C_{18}H_{16}O_2Cl_3]^+$: 369.02104, found: 369.02251; **HPLC** (OJH column, 1.0 mL/min, 1 % iPrOH in hexanes, λ = 230 nm): t_R = 8.1 min, 13.5 min.

2,2,2-trichloroethyl (1R,2S)-1-(4-methoxyphenyl)-2-phenylcyclopropane-1-carboxylate (5e-Racemate)

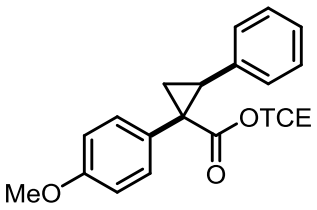

Following GPIV (200 μmol scale) using 2,2,2-trichloroethyl 2-diazo-2-(4-methoxyphenyl)acetate gave the target compound (66.5 mg, 166 μmol, 83%) as a colorless oil:

R_f (hexanes:EtOAc = 6:1) = 0.39; **^{1}H NMR** (500 MHz, $CDCl_3$) δ 7.17 – 7.09 (m, 3H), 7.04 – 6.98 (m, 2H), 6.87 – 6.81 (m, 2H), 6.72 – 6.67 (m, 2H), 4.87 (d, *J* = 11.9 Hz, 1H), 4.68 (d, *J* = 11.9 Hz, 1H), 3.74 (s, 3H), 3.21 (dd, *J* = 9.4, 7.4 Hz, 1H), 2.30 (dd, *J* = 9.4, 5.0 Hz, 1H), 1.98 (dd, *J* = 7.4, 5.0 Hz, 1H);**^{13}C NMR** (126 MHz, $CDCl_3$) δ 172.39, 158.63, 135.86, 133.05, 128.16, 127.83, 126.55, 125.77, 113.16, 95.15, 74.33, 55.12, 36.56, 33.94, 20.54; **IR** (ATR) 2954, 2836, 1731, 1612, 1581, 1515, 1499, 1456, 1378, 1294, 1240, 1177, 1149, 1095, 1052, 1032, 970, 831, 812, 797, 783, 771, 744, 695 cm^{-1}; **HRMS** (NSI) calc. for $[C_{19}H_{17}O_3Cl_3Na]^+$: 421.01335, found: 421.01365; **HPLC** (OJH column, 1.0 mL/min, 1 % iPrOH in hexanes, λ = 230 nm): t_R = 14.6 min, 32.6 min.

2,2,2-trichloroethyl (1R,2S)-1-(2-methoxyphenyl)-2-phenylcyclopropane-1-carboxylate (5f-Racemate)

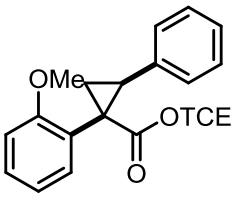

Following GPIV (200 μmol scale) using 2,2,2-trichloroethyl 2-diazo-2-(4-methoxyphenyl)acetate gave the target compound (66.5 mg, 166 μmol, 83%) as a colorless oil:

R_f (hexanes:EtOAc = 6:1) = 0.50; **^{1}H NMR** (500 MHz, $CDCl_3$) δ 7.20 – 7.13 (m, 2H), 7.08 – 7.02 (m, 3H), 6.88 – 6.82 (m, 3H), 4.86 (d, *J* = 11.9 Hz, 1H), 4.64 (d, *J* = 11.9 Hz, 1H), 3.40 (s, 3H), 3.34 (dd, *J* = 9.3, 7.5 Hz, 1H), 2.14 (dd, *J* = 9.3, 5.2 Hz, 1H), 2.00 (dd, *J* =

7.5, 5.2 Hz, 1H); **^{13}C NMR** (126 MHz, $CDCl_3$) δ 172.19, 158.84, 136.23, 131.62, 128.99, 127.79, 127.11, 126.18, 122.80, 119.72, 109.89, 95.16, 74.35, 54.82, 33.92, 33.02, 20.64; **IR** (ATR) 3031, 2953, 2834, 1734, 1604, 1585, 1496, 1463, 1435, 1379, 1304, 1278, 1238, 1208, 1151, 1123, 1109, 1092, 1030, 971, 812, 795, 783, 751, 712, 694 cm^{-1}; **HRMS** (NSI) calc. for $[C_{19}H_{17}O_3Cl_3Na]^+$: 421.01355, found: 421.01343; **HPLC** (SS Whelk column, 1.0 mL/min, 0.1 % iPrOH in hexanes, λ = 230 nm): t_R = 16.0 min, 19.7 min.

4.2.6.2. General procedure for the synthesis of cyclopropanes in a flow-to-batch Process (GPV):

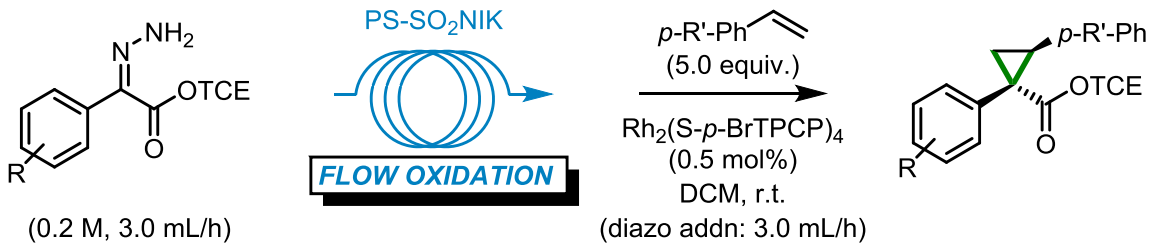

Scheme 4.6. Rh (II) catalyzed cyclopropanations in a flow to batch reactor.

PS-TsNIK resin (1.6 g) was filled into an Omnifit (A = 0.3421 cm^2) cartridge. A second Omnifit (A = 0.3421 cm^2) cartridge was filled with activated drying agent (typically Acros <50µm 4Å MS). The inlet of a manual HPLC valve was connected (with PTFE tubing) to a 10 mL glass syringe filled with 10 mL DCM fitted in a syringe pump. The outlet of the HPLC valve was connected to the vertically-aligned column filled with PS-TsNIK resin (stream from bottom to top) followed by the vertically-aligned column filled with the drying agent (stream from bottom to top). A flame dried 25 mL round bottom flask equipped with a magnetic stir-bar was charged with Rh_2(S-p-BrTPCP)$_4$ (3.6 mg, 2.0 µmol, 0.5 mol%) and silica-plug-filtered styrene derivative (2.0 mmol, 5.0 equiv.), evacuated and

backfilled with argon (3x), charged with DCM (2.0 mL), connected to the outlet of the drying column, and magnetically stirred (about 600 rpm) at ambient temperature. A flame-dried 10 mL pear-shaped flask was charged with hydrazone (440 µmol, 1.10 equiv.), evacuated and backfilled with argon (3x), and charged with DCM (2.20 mL). This solution was injected into a 2.00 mL sample loop (effective starting material: 400 µmol, 1.00 equiv.) of the HPLC valve. A total volume of 8 mL of DCM at a flowrate of 50 µL/min (3.0 mL/h) was used to push the substrate though the flow setup into the reaction vessel. After completion of the addition, the reaction vessel was evaporated under reduced pressure, and trichloroethylene (typically 25–50 µL) was added as an internal standard (if needed $CDCl_3$ was added to obtain a fully homogeneous sample), and the crude yield determined by ^{1}H-NMR analysis. The NMR sample was added back to the remaining crude material, the combined sample evaporated under reduced pressure, and purified by automatic flash column chromatography (typically 12 g SiO_2, 1–5% Et_2O in hexanes over 20 CV). The ee of the material was determined by chiral HPLC analysis as indicated.

2,2,2-trichloroethyl (1R,2S)-1,2-diphenylcyclopropane-1-carboxylate (5a-Flow)

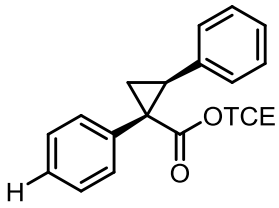

Following GPV (400 µmol scale) using 2,2,2-trichloroethyl (Z)-2-phenyl-2-hydrazonoacetate gave the target compound (119 mg, 307 µmol, 77%) as a white solid:

Mp: 62 °C; **^{1}H NMR** (500 MHz, $CDCl_3$) δ 7.21 – 7.16 (m, 3H), 7.14 – 7.09 (m, 5H), 6.90 – 6.81 (m, 2H), 4.89 (d, *J* = 11.9 Hz, 1H), 4.69 (d, *J* = 11.9 Hz, 1H), 3.27 (dd, *J* = 9.4, 7.4 Hz, 1H), 2.33 (dd, *J* = 9.4, 5.1 Hz, 1H), 2.06 (dd, *J* = 7.4, 5.1 Hz, 1H); **HPLC** (OJH column,

1.0 mL/min, 1 % iPrOH in hexanes, λ = 230 nm): t_R(major) = 8.2 min, t_R(minor) = 14.2 min, 91% ee.

2,2,2-trichloroethyl (1R,2S)-1-(4-fluorophenyl)-2-phenylcyclopropane-1-carboxylate (5b-Flow)[38]

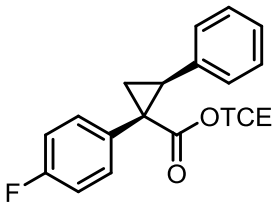

Following GPV (400 μmol scale) using 2,2,2-trichloroethyl (Z)-2-(4-fluorophenyl)-2-hydrazonoacetate gave the target compound (119 mg, 307 μmol, 77%) as a white solid:

^{1}H NMR (500 MHz, $CDCl_3$) δ 7.16 – 7.12 (m, 3H), 7.10 – 7.02 (m, 2H), 6.92 – 6.79 (m, 4H), 4.87 (d, *J* = 11.9 Hz, 1H), 4.69 (d, *J* = 11.9 Hz, 1H), 3.26 (dd, *J* = 9.4, 7.4 Hz, 1H), 2.33 (dd, *J* = 9.4, 5.2 Hz, 1H), 2.02 (dd, *J* = 7.4, 5.2 Hz, 1H); **HPLC** (OJH column, 1.0 mL/min, 1 % iPrOH in hexanes, λ = 230 nm): t_R(major) = 8.0 min, t_R(minor) = 13.1 min, 92% ee.

2,2,2-trichloroethyl (1R,2S)-1-(4-bromophenyl)-2-phenylcyclopropane-1-carboxylate (5c-Flow)[38]

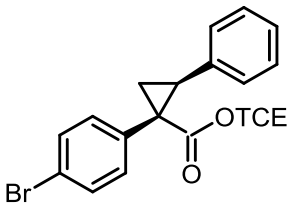

Following GPV (400 μmol scale) using 2,2,2-trichloroethyl (Z)-2-(4-bromophenyl)-2-hydrazonoacetate gave the target compound (160 mg, 357 μmol, 89%) as a white solid:

^{1}H NMR (500 MHz, $CDCl_3$) δ 7.32 – 7.27 (m, 2H), 7.19 – 7.09 (m, 3H), 7.01 – 6.95 (m, 2H), 6.84 (dd, *J* = 6.8, 2.9 Hz, 2H), 4.87 (d, *J* = 11.9 Hz, 1H), 4.68 (d, *J* = 11.9 Hz, 1H), 3.26 (dd, *J* = 9.4, 7.5 Hz, 1H), 2.32 (dd, *J* = 9.4, 5.2 Hz, 1H), 2.01 (dd, *J* = 7.5, 5.2 Hz, 1H);

HPLC (OJH column, 1.0 mL/min, 1 % iPrOH in hexanes, λ = 230 nm): t_R(major) = 8.0 min, t_R(minor) = 12.8 min, 93% ee.

2,2,2-trichloroethyl (1R,2S)-1-(4-(tert-butyl)phenyl)-2-phenylcyclopropane-1-carboxylate. (5d-Flow)[38]

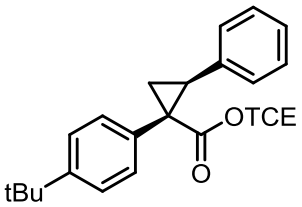

Following GPV (400 μmol scale) using 2,2,2-trichloroethyl (Z)-2-(4-(tert-butyl)phenyl)-2-hydrazonoacetate gave the target compound (140 mg, 328 μmol, 82%) as a white solid:

^{1}H NMR (500 MHz, $CDCl_3$) δ 7.23 – 7.17 (m, 2H), 7.14 – 7.09 (m, 3H), 7.06 – 7.02 (m, 2H), 6.86 – 6.82 (m, 2H), 4.88 (d, *J* = 11.9 Hz, 1H), 4.70 (d, *J* = 11.9 Hz, 1H), 3.24 (dd, *J* = 9.4, 7.4 Hz, 1H), 2.34 (dd, *J* = 9.4, 5.1 Hz, 1H), 2.02 (dd, *J* = 7.4, 5.1 Hz, 1H), 1.28 (s, 9H); **HPLC** (OJH column, 1.0 mL/min, 1 % iPrOH in hexanes, λ = 230 nm): t_R(major) = 5.3 min, t_R(minor) = 3.4 min, 98% ee.

2,2,2-trichloroethyl (1R,2S)-1-(4-methoxyphenyl)-2-phenylcyclopropane-1-carboxylate (5e-Flow)

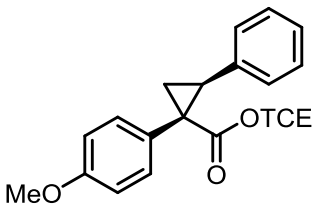

Following GPV (400 μmol scale) using 2,2,2-trichloroethyl (Z)-2-hydrazono-2-(4-methoxyphenyl)acetate gave the target compound (136 mg, 340 μmol, 85%) as a white solid:

^{1}H NMR (500 MHz, $CDCl_3$) δ 7.17 – 7.09 (m, 3H), 7.04 – 6.98 (m, 2H), 6.87 – 6.81 (m, 2H), 6.72 – 6.67 (m, 2H), 4.87 (d, *J* = 11.9 Hz, 1H), 4.68 (d, *J* = 11.9 Hz, 1H), 3.74 (s, 3H), 3.21 (dd, *J* = 9.4, 7.4 Hz, 1H), 2.30 (dd, *J* = 9.4, 5.0 Hz, 1H),

1.98 (dd, *J* = 7.4, 5.0 Hz, 1H); **HPLC** (OJH column, 1.0 mL/min, 1 % iPrOH in hexanes, λ = 230 nm): t_R(major) = 14.9 min, t_R(minor) = 34.4 min, 97% ee.

2,2,2-trichloroethyl (1R,2S)-1-(2-methoxyphenyl)-2-phenylcyclopropane-1-carboxylate (5f-Flow)

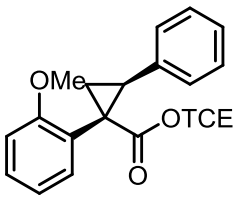

Following GPV (400 μmol scale) using 2,2,2-trichloroethyl 1-(2-methoxyphenyl)-2-phenylcyclopropane-1-carboxylate gave the target compound (122 mg, 305 μmol, 76%) as a white solid:

^{1}H NMR (500 MHz, $CDCl_3$) δ 7.20 – 7.13 (m, 2H), 7.08 – 7.02 (m, 3H), 6.88 – 6.82 (m, 3H), 4.86 (d, *J* = 11.9 Hz, 1H), 4.64 (d, *J* = 11.9 Hz, 1H), 3.40 (s, 3H), 3.34 (dd, *J* = 9.3, 7.5 Hz, 1H), 2.14 (dd, *J* = 9.3, 5.2 Hz, 1H), 2.00 (dd, *J* = 7.5, 5.2 Hz, 1H); **HPLC** (SS Whelk column, 1.0 mL/min, 0.1 % iPrOH in hexanes, λ = 230 nm): t_R(major) = 14.9 min, t_R(minor) = 18.2 min, 67% ee.

2,2,2-trichloroethyl (1R,2S)-1-(4-bromophenyl)-2-(4-methoxyphenyl)cyclopropane-1-carboxylate (5g-Flow)[38]

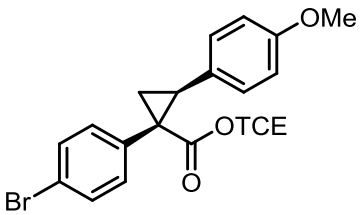

Following GPV (400 μmol scale) using 2,2,2-trichloroethyl (Z)-2-(4-bromophenyl)-2-hydrazonoacetate gave the target compound (168 mg, 350 μmol, 88%) as a white solid:

^{1}H NMR (500 MHz, $CDCl_3$) δ 7.33 – 7.28 (m, 2H), 7.00 – 6.95 (m, 2H), 6.78 – 6.74 (m, 2H), 6.70 – 6.66 (m, 2H), 4.86 (d, *J* = 11.9 Hz, 1H), 4.66 (d, *J* = 11.9 Hz, 1H), 3.74 (s, 3H), 3.21 (dd, *J* = 9.5, 7.5 Hz, 1H), 2.29 (dd, *J* = 9.5, 5.2 Hz, 1H), 1.93 (dd, *J* = 7.5, 5.2 Hz, 1H);

HPLC (SS Whelk column, 1.0 mL/min, 1.0 % iPrOH in hexanes, λ = 230 nm): t_R(major) = 16.2 min, t_R(minor) = 13.5 min, 90% ee.

2,2,2-trichloroethyl (1R,2S)-1-(4-bromophenyl)-2-(4-chlorophenyl)cyclopropane-1-carboxylate (5h-Flow)[38]

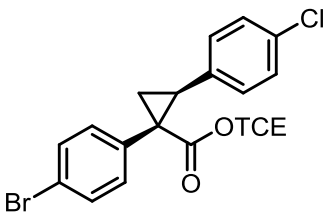

Following GPV (400 µmol scale) using 2,2,2-trichloroethyl (Z)-2-(4-bromophenyl)-2-hydrazonoacetate gave the target compound (169 mg, 350 µmol, 87%) as a white solid:

^{1}H NMR (500 MHz, $CDCl_3$) δ 7.34 – 7.30 (m, 2H), 7.13 – 7.08 (m, 2H), 6.98 – 6.94 (m, 2H), 6.77 – 6.73 (m, 2H), 4.85 (d, *J* = 11.9 Hz, 1H), 4.66 (d, *J* = 11.9 Hz, 1H), 3.20 (dd, *J* = 9.4, 7.4 Hz, 1H), 2.31 (dd, *J* = 9.4, 5.3 Hz, 1H), 1.94 (dd, *J* = 7.4, 5.3 Hz, 1H); **HPLC** (OJH column, 1.0 mL/min, 1.0 % iPrOH in hexanes, λ = 230 nm): t_R(major) = 11.5 min, t_R(minor) = 22.2 min, 91% ee.

4.2.7 *C–H Insertion reactions into benzylic positions*

4.2.7.1. General procedure for the insertion into benzylic C–H bonds in a batch process (GP VI):

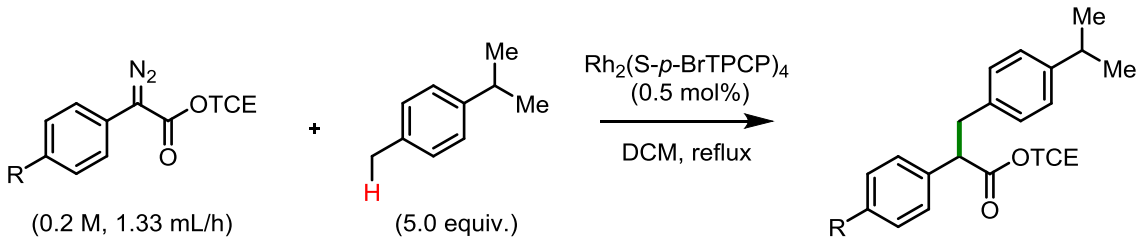

Scheme 4.7. Rh (II) catalyzed benzylic C-H insertions in a batch reactor.

A flame dried 10 mL round bottom flask equipped with a magnetic stir-bar and a reflux condenser was charged with Rh_2(S-p-BrTPCP)$_4$ or for racemic products Rh_2-R/S-p-BrTPCP)$_4$ (3.6 mg, 2.0 μmol, 0.5 mol%) and p-cymene (0.31 mL, 0.27 g, 2.0 mmol, 5.0 equiv.), evacuated and backfilled with argon (3x), charged with DCM (2.0 mL), and magnetically stirred (about 600 rpm) at reflux. A flame-dried 10 mL pear-shaped flask was charged with diazo (400 μmol, 1.00 equiv.), evacuated and backfilled with argon (3x), and charged with DCM (2.0 mL). This solution was transferred to a syringe and dropwise added to the reaction vessel at a flowrate of 22.2 μL/min (1.33 mL/h) via syringe pump. The pear-shaped flask was rinsed with DCM (2 x 0.5 mL) and the solution slowly added to the reaction mixture, which was stirred for another 1.5 h at reflux, and subsequently evaporated under reduced pressure. Trichloroethylene (typically 25–50 μL) was added as an internal standard (if needed $CDCl_3$ was added to obtain a fully homogeneous sample), and the crude yield determined by ^{1}H-NMR analysis. The NMR sample was added back to the remaining crude material, the combined sample evaporated under reduced pressure, and purified by automatic flash column chromatography (typically 12 g SiO_2, 1–3% Et_2O in hexanes over 20 CV). The ee of the material was determined by chiral HPLC analysis as indicated.

2,2,2-trichloroethyl (R)-2-(4-bromophenyl)-3-(4-isopropylphenyl)propanoate (8c-Batch)

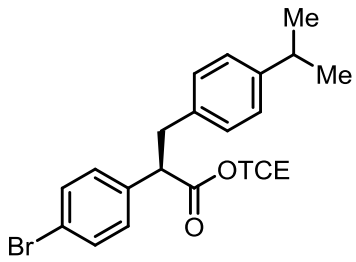

Following GPVI (400 μmol scale) using 2,2,2-trichloroethyl 2-(4-bromophenyl)-2-diazoacetate gave the target compound (162 mg, 339 μmol, 85%) as a white solid:

Mp: 72 °C; **R_f** (hexanes:EtOAc = 20:1) = 0.48; **^{1}H NMR** (500 MHz, $CDCl_3$) δ 7.55 – 7.46 (m, 2H), 7.36 – 7.29 (m, 2H), 7.21 – 7.09 (m, 4H), 4.75

(d, J = 11.9 Hz, 1H), 4.65 (d, J = 12.0 Hz, 1H), 4.03 (dd, J = 9.2, 6.5 Hz, 1H), 3.47 (dd, J = 13.9, 9.1 Hz, 1H), 3.11 (dd, J = 13.9, 6.5 Hz, 1H), 2.91 (hept, J = 6.7 Hz, 1H), 1.27 (d, J = 6.9 Hz, 6H); **^{13}C NMR** (126 MHz, $CDCl_3$) δ 171.36, 147.32, 136.74, 135.35, 131.86, 131.85, 129.92, 128.91, 126.60, 121.78, 94.69, 74.14, 52.97, 39.05, 33.76, 24.09;**IR** (ATR) 2960, 1742, 1509, 1468, 1464, 1438, 1374, 1341, 1169, 1139, 1072, 1020, 1010, 836, 819, 800, 754, 722, 681 cm^{-1}; **HRMS** (NSI) calc. for $[C_{20}H_{19}O_2BrCl_3]^+$: 474.96395, found: 474.96445; **HPLC** (OJ column, 1.0 mL/min, 0 % iPrOH in hexanes, λ = 230 nm): t_R(major) = 46.0 min, t_R(minor) = 25.7 min, 96% ee.

Racemate. 2,2,2-trichloroethyl 3-(4-isopropylphenyl)-2-phenylpropanoate (8a-Racemate)

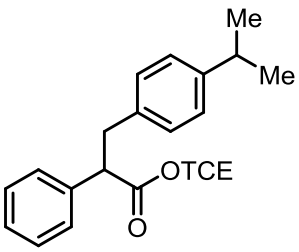

Following GPVI (200 μmol scale) using 2,2,2-trichloroethyl 2-(4-bromophenyl)-2-diazoacetate gave the target compound (73.3 mg, 183 μmol, 92%) as a colorless oil:

R_f (hexanes:EtOAc = 20:1) = 0.41; **^{1}H NMR** (500 MHz, $CDCl_3$) δ 7.48 – 7.43 (m, 2H), 7.40 – 7.36 (m, 2H), 7.35 – 7.31 (m, 1H), 7.17 (s, 4H), 4.75 (d, J = 12.0 Hz, 1H), 4.62 (d, J = 12.0 Hz, 1H), 4.07 (dd, J = 9.7, 5.9 Hz, 1H), 3.50 (dd, J = 13.9, 9.7 Hz, 1H), 3.13 (dd, J = 13.9, 5.9 Hz, 1H), 2.90 (hept, J = 6.9 Hz, 1H), 1.27 (dd, J = 7.0, 0.6 Hz, 6H); **^{13}C NMR** (126 MHz, $CDCl_3$) δ 171.80, 147.16, 137.84, 135.85, 128.90, 128.74, 128.12, 127.72, 126.50, 94.74, 74.06, 53.58, 39.14, 33.74, 24.06; **IR** (ATR) 2958, 1751, 1601, 1512, 1496, 1455, 1373, 1262, 1201, 1131, 1055, 1020, 819, 798, 769, 717, 696 cm^{-1}; **HRMS** (NSI) calc. for $[C_{20}H_{20}O_2Cl_3]^-$: 397.05344, found: 397.05353; **HPLC** (ODH column, 0.25 mL/min, 0 % iPrOH in hexanes, λ = 230 nm): t_R = 58.7, 73.6 min.

Racemate. 2,2,2-trichloroethyl 2-(4-bromophenyl)-3-(4-isopropylphenyl)propanoate (8c-Racemate)

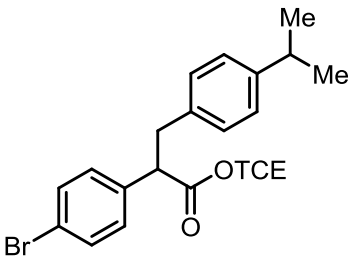

Following GPVI (200 µmol scale) using 2,2,2-trichloroethyl 2-(4-bromophenyl)-2-diazoacetate gave the target compound (90.6 mg, 189 µmol, 95%) as a white solid:

^{1}H NMR (500 MHz, $CDCl_3$) δ 7.55 – 7.46 (m, 2H), 7.36 – 7.29 (m, 2H), 7.21 – 7.09 (m, 4H), 4.75 (d, *J* = 11.9 Hz, 1H), 4.65 (d, *J* = 12.0 Hz, 1H), 4.03 (dd, *J* = 9.2, 6.5 Hz, 1H), 3.47 (dd, *J* = 13.9, 9.1 Hz, 1H), 3.11 (dd, *J* = 13.9, 6.5 Hz, 1H), 2.91 (hept, *J* = 6.7 Hz, 1H), 1.27 (d, *J* = 6.9 Hz, 6H); **HPLC** (OJ column, 1.0 mL/min, 0 % iPrOH in hexanes, λ = 230 nm): t_R = 22.2 min, 39.6 min.

4.2.7.2. General procedure for the insertion into benzylic C–H bonds in a flow-to-batch process (GP VII):

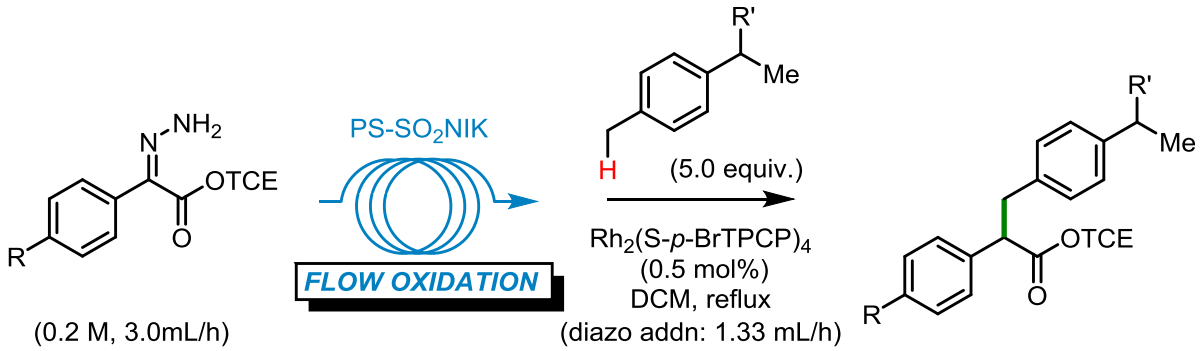

Scheme 4.8. Rh (II) catalyzed benzylic C-H insertions in a flow to batch reactor.

PS-TsNIK resin (1.6 g) was filled into an Omnifit (A = 0.3421 cm²) cartridge. A second Omnifit (A = 0.3421 cm²) cartridge was filled first with anhydrous $Na_2S_2O_3$ (0.2 g) followed by activated drying agent (typically Acros <50µm 4Å MS). The inlet of a manual

HPLC valve was connected (with PTFE tubing) to a 10 mL glass syringe filled with 10 mL DCM fitted in a syringe pump. The outlet of the HPLC valve was connected to the vertically-aligned column filled with PS-TsNIK resin (stream from bottom to top) followed by the vertically-aligned column filled with the drying agent (stream from bottom to top, $Na_2S_2O_3$ layer on the bottom). A flame dried 25 mL round bottom flask equipped with a magnetic stir bar and a reflux condenser was charged with Rh_2(S-p-BrTPCP)$_4$ (3.6 mg, 2.0 μmol, 0.5 mol%) and a ethyl toluene derivative (2.0 mmol, 5.0 equiv.), evacuated and backfilled with argon (3x), charged with DCM (2.0 mL), connected to the outlet of the drying column, and magnetically stirred (about 600 rpm) at reflux. A flame-dried 10 mL pear-shaped flask was charged with hydrazone (440 μmol, 1.10 equiv.), evacuated and backfilled with argon (3x), and charged with DCM (2.20 mL). This solution was injected into a 2.00 mL sample loop (effective starting material: 400 μmol, 1.00 equiv.) of the HPLC valve. 3 mL of DCM at a flow rate of 50 μL/min (3.0 mL/h) was used to push the hydrazone though the oxidizing and drying column. Right before the intensely yellow/orange colored diazo-containing stream entered the reaction vessel the flow rate was reduced to 22.2 μL/min (1.33 mL/h), and 5 mL of DCM was pumped through the setup at this flow rate. After completion of the addition, the reaction vessel was evaporated under reduced pressure, and trichloroethylene (typically 25–50 μL) was added as an internal standard (if needed $CDCl_3$ was added to obtain a fully homogeneous sample), and the crude yield determined by ^{1}H-NMR analysis. The NMR sample was added back to the remaining crude material, the combined sample evaporated under reduced pressure, and purified by automatic flash column chromatography (typically 12 g SiO_2, 1–3% Et_2O in hexanes over 20 CV). The ee of the material was determined by chiral HPLC analysis as indicated.

2,2,2-trichloroethyl (R)-3-(4-isopropylphenyl)-2-phenylpropanoate (8a-Flow)

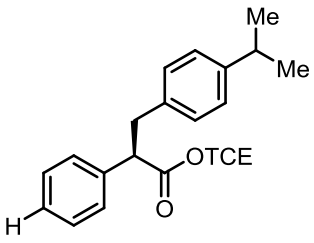

Following GPVII (400 μmol scale) using 2,2,2-trichloroethyl 2-(4-bromophenyl)-2-diazoacetate gave the target compound (146 mg, 364 μmol, 91%) as a white solid: **^{1}H NMR** (500 MHz, $CDCl_3$) δ 7.48 – 7.43 (m, 2H), 7.40 – 7.36 (m, 2H), 7.35 – 7.31 (m, 1H), 7.17 (s, 4H), 4.75 (d, *J* = 12.0 Hz, 1H), 4.62 (d, *J* = 12.0 Hz, 1H), 4.07 (dd, *J* = 9.7, 5.9 Hz, 1H), 3.50 (dd, *J* = 13.9, 9.7 Hz, 1H), 3.13 (dd, *J* = 13.9, 5.9 Hz, 1H), 2.90 (hept, *J* = 6.9 Hz, 1H), 1.27 (dd, *J* = 7.0, 0.6 Hz, 6H); **HPLC** (ODH column, 0.25 mL/min, 0 % iPrOH in hexanes, λ = 230 nm): t_R(major) = 57.0 min, t_R(minor) = 75.2 min, 95% ee.

2,2,2-trichloroethyl (R)-2-(4-bromophenyl)-3-(4-isopropylphenyl)propanoate (8c-Flow)

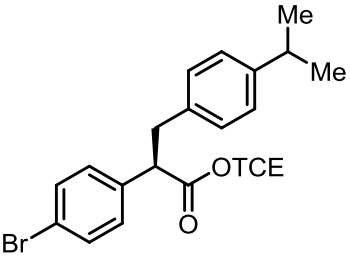

Following GPVII (400 μmol scale) using 2,2,2-trichloroethyl 2-(4-bromophenyl)-2-diazoacetate gave the target compound (162 mg, 339 μmol, 85%) as a white solid: **^{1}H NMR** (500 MHz, $CDCl_3$) δ 7.55 – 7.46 (m, 2H), 7.36 – 7.29 (m, 2H), 7.21 – 7.09 (m, 4H), 4.75 (d, *J* = 11.9 Hz, 1H), 4.65 (d, *J* = 12.0 Hz, 1H), 4.03 (dd, *J* = 9.2, 6.5 Hz, 1H), 3.47 (dd, *J* = 13.9, 9.1 Hz, 1H), 3.11 (dd, *J* = 13.9, 6.5 Hz, 1H), 2.91 (hept, *J* = 6.7 Hz, 1H), 1.27 (d, *J* = 6.9 Hz, 6H); **HPLC** (OJ column, 1.0 mL/min, 0 % iPrOH in hexanes, λ = 230 nm): t_R(major) = 37.2 min, t_R(minor) = 20.6 min, 96% ee.

4.2.8 C–H Insertion reactions into methyl ethers

4.2.8.1. General procedure for the insertion into methyl ether C–H bonds in a batch process (GP VIII):

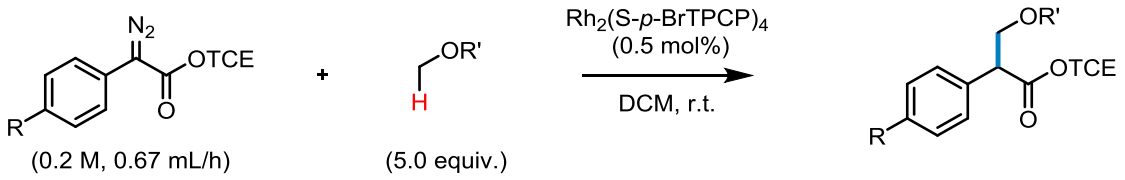

Scheme 4.9. Rh (II) catalyzed ether C-H insertions in a batch reactor.

A flame dried 10 mL round bottom flask equipped with a magnetic stir bar was charged with Rh_2(S-p-BrTPCP)$_4$ (3.6 mg, 2.0 µmol, 0.5 mol%), evacuated and backfilled with argon (3x), charged freshly distilled methyl tert-butylether (0.24 mL, 0.18 g, 2.0 mmol, 5.0 equiv.) and DCM (2.0 mL), and magnetically stirred (about 600 rpm) at ambient temperature. A flame-dried 10 mL pear-shaped flask was charged with diazo (400 µmol, 1.00 equiv.), evacuated and backfilled with argon (3x), and charged with DCM (2.0 mL). This solution was transferred to a syringe and dropwise added to the reaction vessel at a flow rate of 11.2 µL/min (0.67 mL/h) via syringe pump. The pear-shaped flask was rinsed with DCM (2 x 0.5 mL), and the solution slowly added to the reaction mixture, which was stirred for another 1.5 h at ambient temperature, and subsequently evaporated under reduced pressure. Trichloroethylene (typically 25–50 µL) was added as an internal standard (if needed $CDCl_3$ was added to obtain a fully homogeneous sample), and the crude yield determined by ^{1}H-NMR analysis. The NMR sample was added back to the remaining crude material, the combined sample evaporated under reduced pressure, and purified by automatic flash column chromatography (typically 12 g SiO_2, 1–3% Et_2O in hexanes over 20 CV). The ee of the material was determined by chiral HPLC analysis as indicated.

2,2,2-trichloroethyl (S)-2-(4-bromophenyl)-3-(tert-butoxy)propanoate (10-Batch)[39]

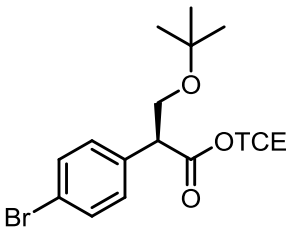

Following GPVIII (400 µmol scale) using 2,2,2-trichloroethyl 2-(4-bromophenyl)-2-diazoacetate gave the target compound (120 mg, 277 µmol, 69%) as a colorless oil:

^{1}H NMR (300 MHz, $CDCl_3$) δ 7.50 – 7.40 (m, 2H), 7.30 – 7.22 (m, 2H), 4.79 (d, *J* = 12.0 Hz, 1H), 4.71 (d, *J* = 12.0 Hz, 1H), 4.03 – 3.84 (m, 2H), 3.58 (dd, *J* = 7.6, 4.2 Hz, 1H), 1.16 (s, 9H). **HPLC** (ASH column, 0.25 mL/min, 0 % iPrOH in hexanes, λ = 230 nm): t_R(major) = 16.8 min, t_R(minor) = 18.9 min, 66% ee.

4.2.8.2. General procedure for the insertion into methyl ether C–H bonds in a batch-to-flow process (GP IX):

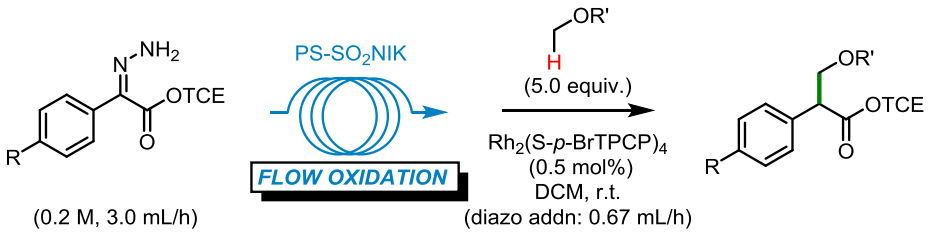

Scheme 4.10. Rh (II) catalyzed ether C-H insertions in a flow to batch reactor.

PS-TsNIK resin (1.6 g) was filled into an Omnifit (A = 0.3421 cm²) cartridge. A second Omnifit (A = 0.3421 cm²) cartridge was filled first with anhydrous $Na_2S_2O_3$ (0.2 g) followed by activated drying agent (typically Acros <50µm 4Å MS). The inlet of a manual HPLC valve was connected (with PTFE tubing) to a 10 mL glass syringe filled with 10 mL DCM fitted in a syringe pump. The outlet of the HPLC valve was connected to the vertically-aligned column filled with PS-TsNIK resin (stream from bottom to top) followed by the vertically-aligned column filled with the drying agent (stream from bottom to top,

$Na_2S_2O_3$ layer on the bottom). A flame dried 25 mL round bottom flask equipped with a magnetic stir bar was charged with Rh_2(S-p-BrTPCP)$_4$ (3.6 mg, 2.0 μmol, 0.5 mol%), evacuated and backfilled with argon (3x), charged with freshly distilled methyl tert-butylether (2.0 mmol, 5.0 equiv.) and DCM (2.0 mL), connected to the outlet of the drying column, and magnetically stirred (about 600 rpm) at ambient temperature. A flame-dried 10 mL pear-shaped flask was charged with hydrazone (440 μmol, 1.10 equiv.), evacuated and backfilled with argon (3x), and charged with DCM (2.20 mL). This solution was injected into a 2.00 mL sample loop (effective starting material: 400 μmol, 1.00 equiv.) of the HPLC valve. 3 mL of DCM at a flow rate of 50 μL/min (3.0 mL/h) was used to push the hydrazone though the oxidizing and drying column. Right before the intensely yellow/orange colored diazo-containing stream entered the reaction vessel the flow rate was reduced to 11 μL/min (0.67 mL/h), and 5 mL of DCM was pumped through the setup at this flow rate. After completion of the addition, the reaction vessel was evaporated under reduced pressure, and trichloroethylene (typically 25–50 μL) was added as an internal standard (if needed $CDCl_3$ was added to obtain a fully homogeneous sample), and the crude yield determined by ^{1}H-NMR analysis. The NMR sample was added back to the remaining crude material, the combined sample evaporated under reduced pressure, and purified by automatic flash column chromatography (typically 12 g SiO_2, 1–3% Et_2O in hexanes over 20 CV). The ee of the material was determined by chiral HPLC analysis as indicated.

2,2,2-trichloroethyl (S)-2-(4-bromophenyl)-3-(tert-butoxy)propanoate (10-Flow)[39]

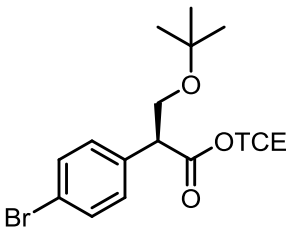

Following GPIX (400 μmol scale) using 2,2,2-trichloroethyl 2-(4-bromophenyl)-2-diazoacetate gave the target compound (120 mg, 278 μmol, 70%) as a colorless oil:

^{1}H NMR (300 MHz, $CDCl_3$) δ 7.50 – 7.40 (m, 2H), 7.30 – 7.22 (m, 2H), 4.79 (d, J = 12.0 Hz, 1H), 4.71 (d, J = 12.0 Hz, 1H), 4.03 – 3.84 (m, 2H), 3.58 (dd, J = 7.6, 4.2 Hz, 1H), 1.16 (s, 9H). **HPLC** (ASH column, 0.25 mL/min, 0 % iPrOH in hexanes, λ = 230 nm): t_R(major) = 16.8 min, t_R(minor) = 19.0 min, 63% ee.

4.2.9 C–H insertion reactions into unactivated Substrates

4.2.9.1. General procedure for the insertion into unactivated C–H bonds in a batch process (GP X):

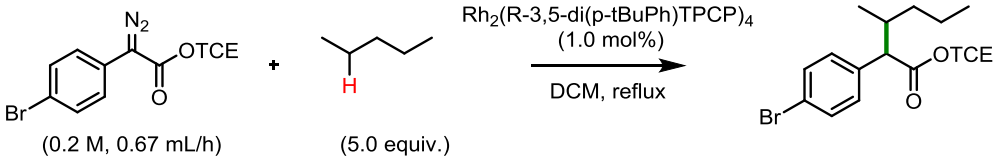

Scheme 4.11. Rh (II) catalyzed pentane C-H insertions in a batch reactor.

A flame dried 10 mL round bottom flask equipped with a magnetic stir bar and a reflux condenser was charged with Rh_2(*R*-3,5-di(*p*-^{t}BuPh)TPCP)$_4$ (10 mg, 4.0 µmol, 1.0 mol%), evacuated and backfilled with argon (3x), charged with pentane (0.23 mL, 0.14 g, 2.0 mmol, 5.0 equiv.) and DCM (2.0 mL), and magnetically stirred (about 600 rpm) at reflux. A flame-dried 10 mL pear-shaped flask was charged with diazo (400 µmol, 1.00 equiv.), evacuated and backfilled with argon (3x), and charged with DCM (2.0 mL). This solution was transferred to a syringe and dropwise added to the reaction vessel at a flow rate of 11 µL/min (0.67 mL/h) via syringe pump. The pear-shaped flask was rinsed with DCM (2 x 0.5 mL), and the solution slowly added to the reaction mixture, which was stirred for another 1.5 h at reflux, and subsequently evaporated under reduced pressure. Trichloroethylene (typically 25–50 µL) was added as an internal standard (if needed $CDCl_3$

was added to obtain a fully homogeneous sample), and the crude yield determined by ^{1}H-NMR analysis. The NMR sample was added back to the remaining crude material, the combined sample evaporated under reduced pressure, and purified by automatic flash column chromatography (typically 12 g SiO_2, 1–3% Et_2O in hexanes over 20 CV). To determine the ee of the material a reduction to the corresponding alcohols was performed: an aliquot was dissolved in DCM (10 mM), cooled to -78 °C, treated with DIBAl-H (1.0 M in DCM, 5 equiv.), allowed to reach room temperature, quenched by the addition of MeOH and water, extracted with DCM, and purified by passage through a silica plug. The ee of the reduced material was then determined by chiral HPLC analysis as indicated.

2,2,2-trichloroethyl (2S,3R)-2-(4-bromophenyl)-3-methylhexanoate (11-Batch) [40]

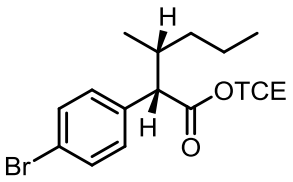

Following GPX (200 μmol scale) using 2,2,2-trichloroethyl 2-(4-bromophenyl)-2-diazoacetate and Rh_2(*R*-3,5-di(*p*-^{t}BuPh)TPCP)$_4$ gave the target compound as an inseparable mixture of regio- and diastereoisomers (r.r = 20:1, d.r. = 8.3:1, 74.7 mg, 179 μmol, 90%) as a colorless oil:

^{1}H NMR (500 MHz, $CDCl_3$, major isomer) δ 7.50 – 7.45 (m, 2H), 7.31 – 7.23 (m, 2H), 4.79 (d, *J* = 12.0 Hz, 1H), 4.65 (d, *J* = 12.0 Hz, 1H), 3.40 (d, *J* = 10.6 Hz, 1H), 2.35 – 2.20 (m, 1H), 1.42 – 1.09 (m, 3H), 1.07 (d, *J* = 6.5 Hz, 3H), 0.98 – 0.86 (m, 1H), 0.79 (t, *J* = 7.2 Hz, 3H); **HPLC** (SS-WHELK column, 0.7 mL/min, 0.5 % iPrOH in hexanes, λ = 210 nm): t_R(major) = 82.3 min, t_R(minor) = 135 min, 93% ee.

4.2.9.2. General procedure for the insertion into unactivated C–H bonds in a flow-to-batch process (GP XI):

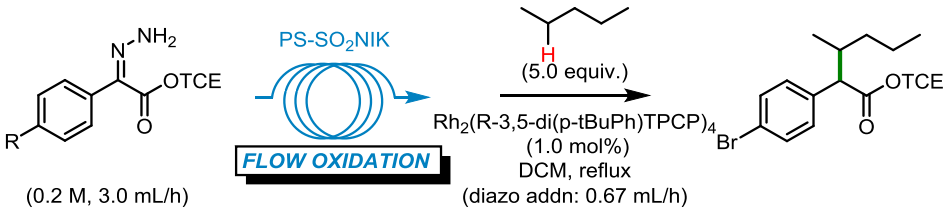

Scheme 4.12. Rh (II) catalyzed pentane C-H insertions in a flow to batch reactor.

PS-TsNIK resin (1.6 g) was filled into an Omnifit (A = 0.3421 cm²) cartridge. A second Omnifit (A = 0.3421 cm²) cartridge was filled first with anhydrous $Na_2S_2O_3$ (0.2 g) followed by activated drying agent (typically Acros <50µm 4Å MS). The inlet of a manual HPLC valve was connected (with PTFE tubing) to a 10 mL glass syringe filled with 10 mL DCM fitted in a syringe pump. The outlet of the HPLC valve was connected to the vertically-aligned column filled with PS-TsNIK resin (stream from bottom to top) followed by the vertically-aligned column filled with the drying agent (stream from bottom to top, $Na_2S_2O_3$ layer on the bottom). A flame dried 25 mL round bottom flask equipped with a magnetic stir bar and a reflux condenser was charged with Rh_2(*R*-3,5-di(*p*-^{t}BuPh)TPCP)$_4$ (10 mg, 4.0 µmol, 1.0 mol%), evacuated and backfilled with argon (3x), charged with pentane (0.23 mL, 0.14 g, 2.0 mmol, 5.0 equiv.) and DCM (2.0 mL), connected to the outlet of the drying column, and magnetically stirred (about 600 rpm) at reflux. A flame-dried 10 mL pear-shaped flask was charged with hydrazone (440 µmol, 1.10 equiv.), evacuated and backfilled with argon (3x), and charged with DCM (2.20 mL). This solution was injected into a 2.00 mL sample loop (effective starting material: 400 µmol, 1.00 equiv.) of the HPLC valve. 3 mL of DCM at a flow rate of 50 µL/min (3.0 mL/h) was used to push the hydrazone

though the oxidizing and drying column. Right before the intensely yellow/orange colored diazo-containing stream entered the reaction vessel the flow rate was reduced to 11 µL/min (0.67 mL/h), and 5 mL of DCM was pumped through the setup at this flow rate. After completion of the addition, the reaction vessel was evaporated under reduced pressure, and trichloroethylene (typically 25–50 µL) was added as an internal standard (if needed $CDCl_3$ was added to obtain a fully homogeneous sample), and the crude yield determined by ^{1}H-NMR analysis. The NMR sample was added back to the remaining crude material, the combined sample evaporated under reduced pressure, and purified by automatic flash column chromatography (typically 12 g SiO_2, 1–3% Et_2O in hexanes over 20 CV). To determine the ee of the material a reduction to the corresponding alcohols was performed: an aliquot was dissolved in DCM (10 mM), cooled to -78 °C, treated with DIBAl-H (1.0 M in DCM, 5 equiv.), allowed to reach room temperature, quenched by the addition of MeOH and water, extracted with DCM, and purified by passage through a silica plug. The ee of the reduced material was then determined by chiral HPLC analysis as indicated.

2,2,2-trichloroethyl (2S,3R)-2-(4-bromophenyl)-3-methylhexanoate (11-Flow). [40]

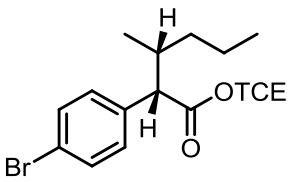

Following GPXI (400 µmol scale) using 2,2,2-trichloroethyl (Z)-2-(4-bromophenyl)-2-hydrazonoacetate and Rh_2(*R*-3,5-di(*p*-^{t}BuPh)TPCP)$_4$ gave the target compound as an inseparable mixture of regio- and diastereoisomers (r.r = 22:1, d.r. = 9.2:1, 149 mg, 357 µmol, 89%) as a colorless oil:

^{1}H NMR (500 MHz, $CDCl_3$) δ 7.50 – 7.43 (m, 2H), 7.31 – 7.24 (m, 2H), 4.79 (d, *J* = 12.0 Hz, 1H), 4.65 (d, *J* = 12.0 Hz, 1H), 3.40 (d, *J* = 10.6 Hz, 1H), 2.28 (d, *J* = 12.7, 10.7, 6.4,

3.0 Hz, 1H), 1.43 – 1.10 (m, 3H), 1.07 (d, *J* = 6.6 Hz, 3H), 0.98 – 0.85 (m, 1H), 0.79 (t, *J* = 7.2 Hz, 3H); **HPLC** (SS-WHELK column, 0.7 mL/min, 0.5 % iPrOH in hexanes, λ = 210 nm): t_R(major) = 82.3 min, t_R(minor) = 135 min, 95% ee.

4.2.10 *PS-SO_2NIK resin synthesis*

The PS-SO_2NIK resin was prepared by the previously reported method.[5]

4.3 Results and discussion

The first stage of the project was to develop an effective protocol for the synthesis of the 2,2,2-trichloroethyl aryldiazoacetates. The required hydrazones were generated in two steps: first, the 2-oxo-2-arylacetates were synthesized through Friedel–Crafts acylation to form **2**. A subsequent condensation with hydrazine monohydrate gave chromatographically separable mixtures of Z and E hydrazones **3**. (Table 4.1). Both isomers of the hydrazones were cleanly oxidized by the PS-SO2NIK resin[31] to the aryldiazoacetates **4** in high yield and purity (Table 4.1). An excess PS-SO2NIK resin[31] (5 equiv) was used to ensure full conversion of the hydrazones to the corresponding diazo compound because any unreacted hydrazone in the product stream would likely poison the dirhodium catalyst in the downstream reaction.

Table 4.1. Aryldiazoacetate synthesis in flow from pre-synthesized hydrazones

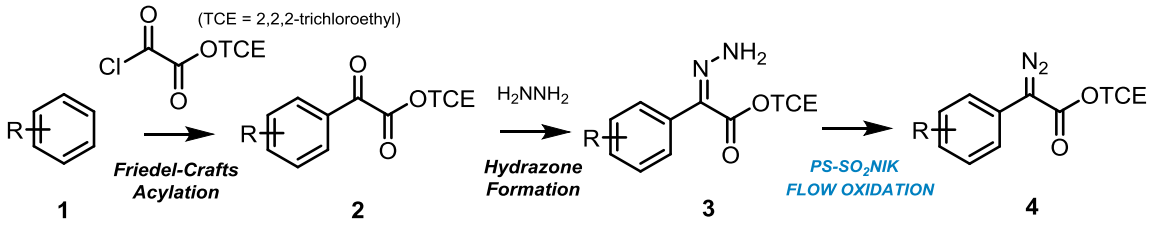

a: R = H , **b**: R = F, **c**: R = Br, **d**: R = tBu, **e**: R=OMe

Cmpd	R	**2** yield, %	**3** yield, %	**4** yield, %[a]	**4** purity, %[b]
a	H	68	66 (Z), 6 (E)	97	99
b	F	77	46 (Z), 6 (E)	87	97
c	Br	85	58 (Z), 7 (E)	97	98
d	tBu	89	59 (Z), 5 (E)	100	97
e	OMe	58 (p) +29 (o)	43 (p/Z), 21 (o/Z)	90 (p), 90 (o)	98 (p), 97 (o)

[a]From Z-hydrazone. [b]Determined by Q-NMR.

The initial studies to directly utilize the as-generated stream of donor/acceptor-substituted diazo species for subsequent dirhodium-catalyzed reactions were not very successful. When attempting Rh_2(S-p-BrTPCP)$_4$-catalyzed cyclopropanation with **4c** and styrene to form **5**, the alcohol **6**, derived from O–H insertion into the water, was a significant byproduct (Table 4.2, entry 1). Prolonged drying of the PS-SO_2NIK resin (and all other materials) in vacuo over potassium hydroxide did not improve the situation. To remove trace water from the diazo product stream, we therefore examined various drying agents such as sulfate salts and silica for their drying capability under the conditions employed, but none were very effective (Table 4.2, entries 2-4). Better results were

obtained using molecular sieves (Table 4.2, entries 5-7), with fine powdered 4Å molecular sieves giving the best recovery and drying capacity (Table 4.2, entry 7).

Table 4.2. Effect of drying agents for cyclopropanations

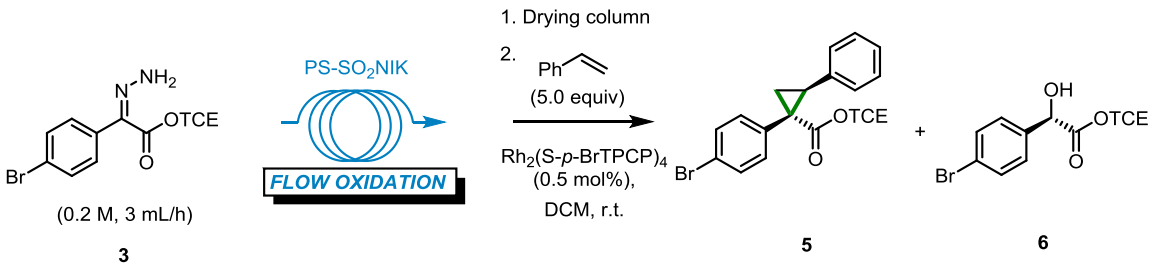

Entry	Drying Column	**5c** yield, %	**6c** yield, %	Combined yield, %
1	None	72	24	96
2	Na_2SO_4	69	13	82
3	$MgSO_4$	77	12	89
4	flash silica gel	70	11	81
5	<50 µM 3 Å MS[a]	75	10	85
6	120–320 µm 4 Å MS	73	8	81
7	<50 µM 4 Å MS[a]	89	5	93

[a]MS: molecular sieve

The optimized flow synthesis and drying conditions were then applied to the enantioselective synthesis of a series of cyclopropanes **5a-h** (Figure 4.1).[38] The in-flow synthesized aryldiazoacetates **4** were directly consumed downstream by reacting them with appropriate coupling agents in the presence of dirhodium catalysts. The advantage of this system is that additional separation steps after the aryldiazoacetate synthesis are not

required. The cyclopropanes **5a-e** were synthesized in good yields (77-88%) and high levels of enantioselectivity (91-99% ee). However, cyclopropane 5f, stemming from o-methoxyphenyldiazoacetate afforded only moderate enantioselectivity (67% ee). The 4-chloro and 4-methoxy substituted styrenes afforded cyclopropanes 5g and 5h in similar yield (88%, 87%, respectively) and enantioselectivity (90% ee, 91% ee, respectively). For a direct comparison in terms of the operating reaction conditions, the concentration (0.2 M) and flow rate (3 mL/min) of the aryldiazoacetates in DCM were matched with the conventional batch reaction conditions. The Rh_2(*S*-*p*-BrTPCP)$_4$ catalyzed synthesis of cyclopropane 5c through flow synthesis showed very similar yield (89% vs. 91% in batch) and levels of enantioselectivity (93% vs. 95% ee in batch) to the conventional batch reaction.

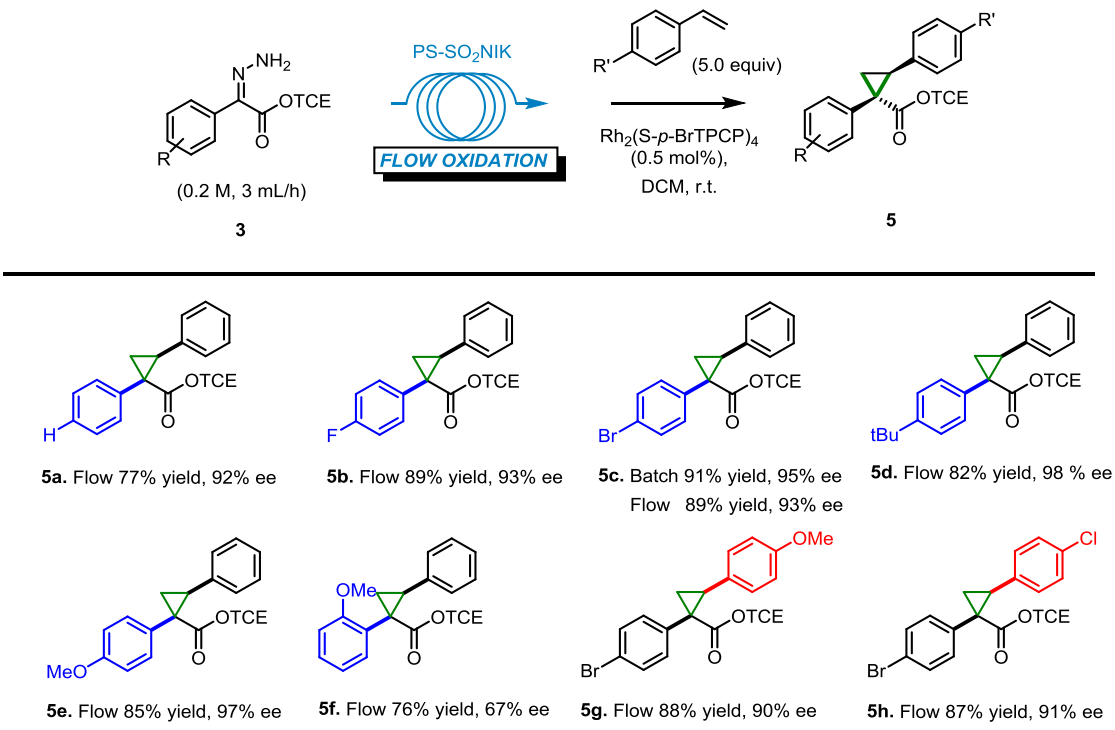

Figure 4.1. Cyclopropanations with aryldiazoacetates synthesis in flow.

While the optimized process for drying the diazo stream was effective for cyclopropanation reactions, the application of the same protocol to the more challenging C–H functionalization reactions was unsuccessful. The dichloromethane wash of the PS-SO_2NIK resin had a faint violet color, suggesting that iodine was leaching from the resin. Control studies were conducted to determine the influence of iodine and the reducing agent sodium thiosulfate. The iodine color dissipated on exposure to solid sodium thiosulfate and the diazo compound was stable in the presence of sodium thiosulfate as shown in Figure 4.2. (vial #1: DCM solvent that flow through the PS-NIK resin column (slightly pink); vial #2: Discoloration of PS-NIK washing DCM solvent after adding $Na_2S_2O_3$; vial #3: Diazo compound dissolved in pure DCM; vial #4: Diazo compound dissolved in pure DCM + $Na_2S_2O_3$; vial#5: Rh_2 catalyst dissolved in pure DCM; vial #6: Rh_2 catalyst dissolved in PS-NIK washing DCM; vial#7: Rh_2 catalyst dissolved in $Na_2S_2O_3$ pretreated PS-NIK washing DCM; vial #8: Rh_2 catalyst dissolved in pure DCM +$Na_2S_2O_3$)

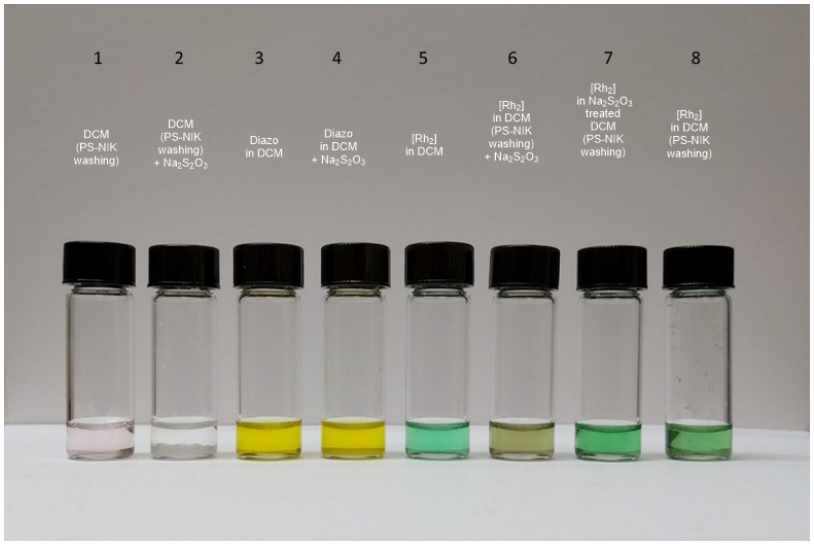

Figure 4.2. Effect of $Na_2S_2O_3$ on the reagent color in pure or PS-NIK washing DCM solution

In batch reactions between aryldiazoacetate **4c** and p-cymene **7**, the standard reaction proceeded in high yield and enantioselectivity, but when 5 mol% of iodine was added, carbene dimer became the dominant product, and virtually none of the C-H insertion product 8c was observed. Carbene dimerization was blocked when 20 mol% of the commercial pentahydrate form of sodium thiosulfate was added, but O-H insertion into the water was the major product. A large amount of O-H insertion was obtained with sodium thiosulfate pentahydrate in the absence of iodine, but the efficiency of the reaction was fully recovered when 20 mol% of anhydrous sodium thiosulfate was used instead (Table 4.3, entry 5).

Table 4.3. The effect of anhydrous sodium thiosulfate and iodine addition for benzylic C–H functionalization

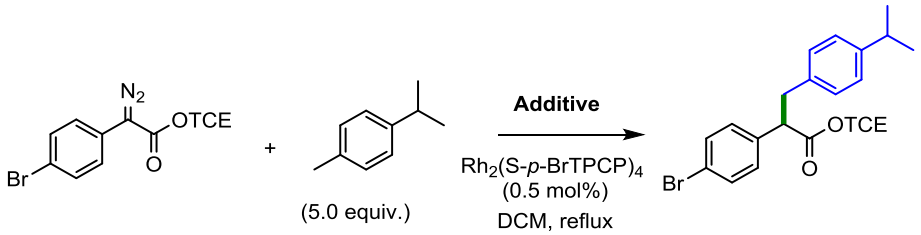

Entry	Additives	Yield (%)[a]	ee (%)
1	none	85	96
2	I_2 (5 mol%)	1b	n.d.
3	I_2 (5 mol%) + $Na_2S_2O_3 \cdot 5H_2O$ (20 mol%)	25c	n.d.
4	$Na_2S_2O_3 \cdot 5H_2O$ (20 mol%)	19c	n.d.
5	$Na2S_2O_3$ (20 mol%)	88	96

[a]Isolated yields. [b]Major amounts of dimerization product. [c]No dimerization, major amounts of O–H insertion products.

On the basis of these control experiments, the diazo drying protocol was modified to include the addition of anhydrous sodium thiosulfate to the bottom of the molecular sieves cartridge. With this adjustment, benzylic C–H functionalization was successfully conducted using aryldiazoacetates generated in flow. When *p*-bromodiazoacetate **4c** reacted with p-cymene **7** as a C–H insertion partner in a batch reaction (Scheme 4.13)[19], compound **8c** was obtained in good yield (85%), regioselectivity (>20:1) and enantioselectivity (96% ee). This matched the result of the standard reaction of the preformed diazo compound generated in a batch reaction (Table 4.3, entry 1). Similarly, the Rh_2(*S*-*p*-BrTPCP)$_4$-catalyzed reaction of the unsubstituted aryldiazoacetate **4a** generated in flow gave the C-H functionalization product **8a**, again in high yield (91%), regioselectivity (>20:1) and enatioselectivity (95% ee).

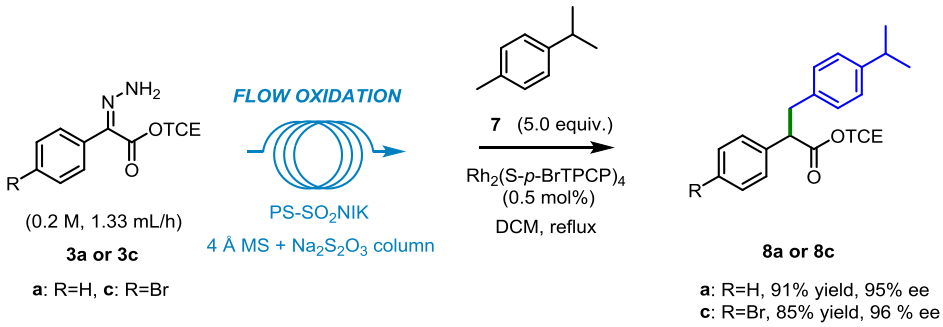

Scheme 4.13. Benzylic C–H insertions with aryldiazoacetates synthesis in flow

The applicability of the developed tandem protocol was further exemplified through the Rh_2(*S*-*p*-BrTPCP)$_4$ catalyzed C–H insertion with *p*-bromophenyldiazoacetate **3c** and methyl tert butyl ether **9** (Scheme 4.14). From the batch reaction, compound **10** was obtained in 69% yield and 66% enantioselectivity. A similar yield (70%) and enantioselectivity (63%) of compound **10** were again achieved through flow synthesis.

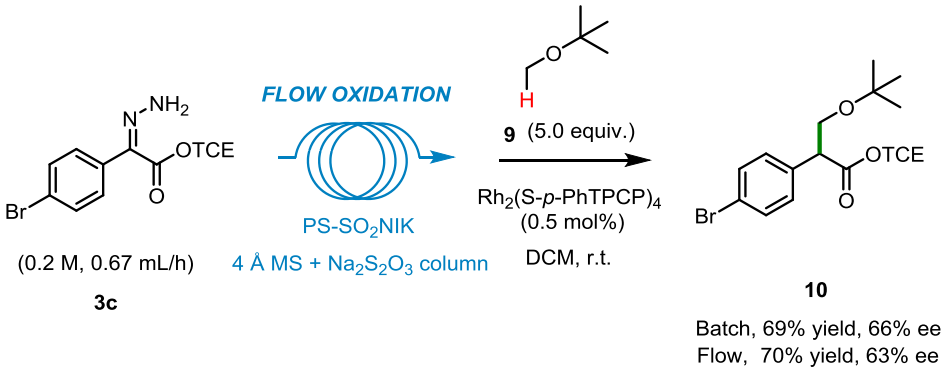

Scheme 4.14. Methyl ether C–H insertions with aryldiazoacetates synthesis in flow

To challenge the effectiveness of the in-line purification of the diazo compound, we studied the C–H functionalization of a completely unfunctionalized and thus highly challenging substrate, pentane. Recently, the Davies group reported a new rhodium catalyst, Rh_2(*R*-3,5-di(*p*-tBuPh)TPCP)$_4$, that showed highly site-selective, diastereoselective and enatioselective C–H functionalization of n-alkanes.[20] Comparison of pentane reactivity under batch and flow reaction conditions with this catalyst (**11**, Batch and Flow) showed that very similar results were obtained in each case (regioisomeric ratio (rr), 20:1 vs 22:1; diastereomeric ratio (dr), 8.3:1 vs 9.2:1; yield, 90% vs 89%; e.e., 93% vs 95%), showcasing that for even a very challenging reaction, the flow-generated diazo compound was equally effective.

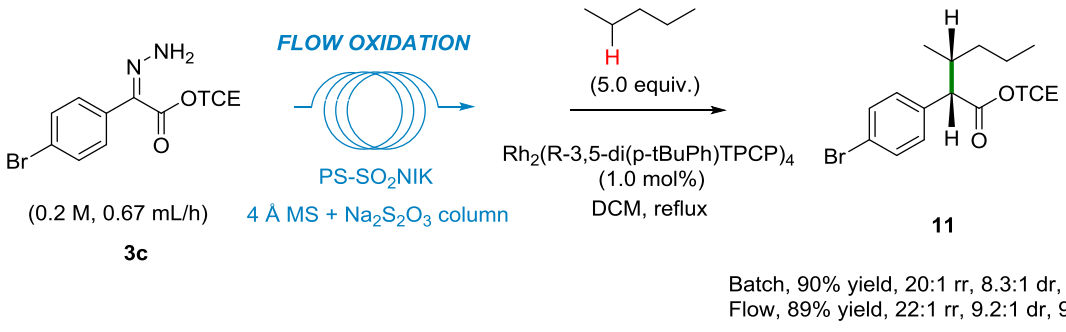

Scheme 4.15. Pentane C–H insertion with aryldiazoacetate synthesis in flow

4.4 Conclusions

Based on the active collaboration work with the Davies group, we have developed a tandem reaction system for rhodium-catalyzed cyclopropanation and C–H functionalization, in which the aryldiazoacetates are generated in flow and used immediately in the subsequent carbenoid transformation. Dr. Rackl from the Davies group made organic synthesis contribution to this chapter as well as analysis of the products. For a critical requirement for ensuring an effective carbene transformation with relatively unreactive substrates is in-flow drying and oxidation of any iodine impurities. When these precautions were made, the aryldiazoacetates generated in flow performed equally well to material generated under standard batch conditions. This process eliminates the need to pre-synthesize and store potentially hazardous diazo compounds and expands the range of carbene reactions of flow-generated diazo compounds to enantioselective cyclopropanation and C-H functionalization. The approach offers a safer way to carry out rhodium-catalyzed reactions of diazo compounds, especially in the context of large scale and industrial applications.

4.5 References

(1) Gutekunst, W. R.; Baran, P. S. Recent Developments in Natural Product Synthesis Using Metal-Catalysed C–H Bond Functionalisation. *Chem. Soc. Rev.* **2011**, *40* (4), 1885–1898.

(2) McMurray, L.; O'Hara, F.; Gaunt, M. J. Recent Developments in Natural Product Synthesis Using Metal-Catalysed C-H Bond Functionalisation. *Chem. Soc. Rev.* **2011**, *40* (4), 1885–1898.

(3) Noisier, A. F. M.; Brimble, M. A. C–H Functionalization in the Synthesis of Amino Acids and Peptides. *Chem. Rev.* **2014**, *114* (18), 8775–8806.

(4) Segawa, Y.; Maekawa, T.; Itami, K. Synthesis of Extended Π-Systems through C–H Activation. *Angew. Chem. Int. Ed.* **2015,** *54* (1), 66–81.

(5) Wencel-Delord, J.; Glorius, F. C-H Bond Activation Enables the Rapid Construction and Late-Stage Diversification of Functional Molecules. *Nat. Chem.* **2013**, *5* (5), 369–375.

(6) Denard, C. A.; Huang, H.; Bartlett, M. J.; Lu, L.; Tan, Y.; Zhao, H.; Hartwig, J. F. Cooperative Tandem Catalysis by an Organometallic Complex and a Metalloenzyme. *Angew. Chem. Int. Ed.* **2014**, *53* (2), 465–469.

(7) Cheng, C.; Hartwig, J. F. Catalytic Silylation of Unactivated C-H Bonds. *Chem. Rev.* **2015**, *115* (17), 8946–8975.

(8) Yamaguchi, J.; Yamaguchi, A. D.; Itami, K. C-H Bond Functionalization: Emerging Synthetic Tools for Natural Products and Pharmaceuticals. *Angew. Chem. Int. Ed.* **2012**, *51* (36), 8960–9009.

(9) Hartwig, J. F. Evolution of C-H Bond Functionalization from Methane to Methodology. *J. Am. Chem. Soc.* **2016**, *138* (1), 2–24.

(10) Davies, H. M. L.; Morton, D. Collective Approach to Advancing C-H Functionalization. *ACS Cent. Sci.* **2017**, *3* (9), 936–943.

(11) Doyle, M. P.; McKervey, M. A.; Ye, T. *Modern Catalytic Methods for Organic Synthesis with Diazo Compounds*; Wiley: New York, 1998.

(12) Davies, H. M. L.; Beckwith, R. E. J. Catalytic Enantioselective C-H Activation by Means of Metal-Carbenoid-Induced C-H Insertion. *Chem. Rev.* **2003**, *103* (8), 2861–

2903.

(13) Doyle, M. P.; Duffy, R.; Ratnikov, M.; Zhou, L. Catalytic Carbene Insertion into C - H Bonds. *Chem. Rev.* **2010**, 704–724.

(14) Davies, H. M. L.; Morton, D. Guiding Principles for Site Selective and Stereoselective Intermolecular C-H Functionalization by Donor/Acceptor Rhodium Carbenes. *Chem. Soc. Rev.* **2011**, *40* (4), 1857–1869.

(15) Davies, H. M. L.; Lian, Y. The Combined C-H Functionalization/Cope Rearrangement: Discovery and Applications in Organic Synthesis. *Acc. Chem. Res.* **2012**, *45* (6), 923–935.

(16) Ford, A.; Miel, H.; Ring, A.; Slattery, C. N.; Maguire, A. R.; McKervey, M. A. Modern Organic Synthesis with ??-Diazocarbonyl Compounds. *Chem. Rev.* **2015**, *115* (18), 9981–10080.

(17) Qin, C.; Davies, H. M. L. Role of Sterically Demanding Chiral Dirhodium Catalysts in Site-Selective C-H Functionalization of Activated Primary C-H Bonds. *J. Am. Chem. Soc.* **2014**, *136* (27), 9792–9796.

(18) Qin, C.; Boyarskikh, V.; Hansen, J. H.; Hardcastle, K. I.; Musaev, D. G.; Davies, H. M. L. D_2-Symmetric Dirhodium Catalyst Derived from a 1,2,2-Triarylcyclo-Propanecarboxylate Ligand: Design, Synthesis and Application. *J. Am. Chem. Soc.* **2011**, *133(47)*, 19198–19204.

(19) Guptill, D. M.; Davies, H. M. L. 2,2,2-Trichloroethyl Aryldiazoacetates as Robust Reagents for the Enantioselective C–H Functionalization of Methyl Ethers. *J. Am. Chem. Soc.* **2014**, *136* (51), 17718–17721.

(20) Liao, K.; Negretti, S.; Musaev, D. G.; Bacsa, J.; Davies, H. M. L. Site-Selective and

Stereoselective Functionalization of Unactivated C–H Bonds. *Nature* **2016**, *533* (7602), 230–234.

(21) Liao, K.; Pickel, T. C.; Boyarskikh, V.; Bacsa, J.; Musaev, D. G.; Davies, H. M. L. Site-Selective and Stereoselective Functionalization of Non-Activated Tertiary C-H Bonds. *Nature* **2017**, *551* (7682), 609–613.

(22) Liao, K.; Liu, W.; Niemeyer, Z. L.; Ren, Z.; Bacsa, J.; Musaev, D. G.; Sigman, M. S.; Davies, H. M. L. Site-Selective Carbene-Induced C–H Functionalization Catalyzed by Dirhodium Tetrakis(Triarylcyclopropanecarboxylate) Complexes. *ACS Catal.* **2018**, *8* (1), 678–682.

(23) Clark, J. D.; Shah, A. S.; Peterson, J. C. Understanding the Large-Scale Chemistry of Ethyl Diazoacetate via Reaction Calorimetry. *Thermochim. Acta* **2002**, *392–393*, 177–186.

(24) Parsons, R. L. Discovery and Development of a Scalable Synthesis for the HCV NS5B Inhibitor BMS-791325; 245th ACS National Meeeting: New Orleans, 2013.

(25) Chepiga, K. M.; Feng, Y.; Brunelli, N. A.; Jones, C. W.; Davies, H. M. L. Silica-Immobilized Chiral Dirhodium(II) Catalyst for Enantioselective Carbenoid Reactions. *Org. Lett.* **2013**, *15* (24), 6136–6139.

(26) Moschetta, E. G.; Negretti, S.; Chepiga, K. M.; Brunelli, N. A.; Labreche, Y.; Feng, Y.; Rezaei, F.; Lively, R. P.; Koros, W. J.; Davies, H. M. L.; et al. Composite Polymer/Oxide Hollow Fiber Contactors: Versatile and Scalable Flow Reactors for Heterogeneous Catalytic Reactions in Organic Synthesis. *Angew. Chem. Int. Ed.* **2015**, 54 (22), 6470–6474.

(27) Müller, S. T. R.; Murat, A.; Maillos, D.; Lesimple, P.; Hellier, P.; Wirth, T. Rapid

Generation and Safe Use of Carbenes Enabled by a Novel Flow Protocol with In-Line IR Spectroscopy. *Chem. Eur. J.* **2015**, *21* (19), 7016–7020.

(28) Roda, N. M.; Tran, D. N.; Battilocchio, C.; Labes, R.; Ingham, R. J.; Hawkins, J. M.; Ley, S. V. Cyclopropanation Using Flow-Generated Diazo Compounds. *Org. Biomol. Chem.* **2015**, *13* (9), 2550–2554.

(29) Audubert, C.; Marin, O. J. G.; Lebel, H. Batch and Continuous Flow One-Pot Processes Using Amine Diazotization to Produce Silylated Diazo Reagents. *Angew. Chem. Int. Ed.* **2017**, *56* (22), 6294–6297.

(30) Nicolle, S. M.; Moody, C. J. Potassium N-Iodo p-Toluenesulfonamide (TsNIK, Iodamine-T): A New Reagent for the Oxidation of Hydrazones to Diazo Compounds. *Chem. Eur. J.* **2014**, *20* (15), 4420–4425.

(31) Nicolle, S. M.; Hayes, C. J.; Moody, C. J. Alkyl Halide-Free Heteroatom Alkylation and Epoxidation Facilitated by a Recyclable Polymer-Supported Oxidant for the in-Flow Preparation of Diazo Compounds. *Chem. Eur. J.* **2015**, *21* (12), 4576–4579.

(32) Müller, S. T. R.; Wirth, T. Diazo Compounds in Continuous-Flow Technology. *ChemSusChem* **2015**, *8* (2), 245–250.

(33) Poh, J. S.; Tran, D. N.; Battilocchio, C.; Hawkins, J. M.; Ley, S. V. A Versatile Room-Temperature Route to Di- and Trisubstituted Allenes Using Flow-Generated Diazo Compounds. *Angew. Chem. Int. Ed.* **2015**, *54* (27), 7920–7923.

(34) Tran, D. N.; Battilocchio, C.; Lou, S.-B.; Hawkins, J. M.; Ley, S. V. Flow Chemistry as a Discovery Tool to Access SP_2 –SP_3 Cross-Coupling Reactions via Diazo Compounds. *Chem. Sci.* **2015**, *6* (2), 1120–1125.

(35) Lévesque, É.; Laporte, S. T.; Charette, A. B. Continuous Flow Synthesis and

Purification of Aryldiazomethanes through Hydrazone Fragmentation. *Angew. Chem. Int. Ed.* **2017**, *56* (3), 837–841.

(36) Poh, J.-S.; Makai, S.; von Keutz, T.; Tran, D. N.; Battilocchio, C.; Pasau, P.; Ley, S. V. Rapid Asymmetric Synthesis of Disubstituted Allenes by Coupling of Flow-Generated Diazo Compounds and Propargylated Amines. *Angew. Chem. Int. Ed.* **2017**, *56* (7), 1864–1868.

(37) Deadman, B. J.; O'Mahony, R. M.; Lynch, D.; Crowley, D. C.; Collins, S. G.; Maguire, A. R. Taming Tosyl Azide: The Development of a Scalable Continuous Diazo Transfer Process. *Org. Biomol. Chem.* **2016**, *14* (13), 3423–3431.

(38) Negretti, S.; Cohen, C. M.; Chang, J. J.; Guptill, D. M.; Davies, H. M. L. Enantioselective Dirhodium(II)-Catalyzed Cyclopropanations with Trimethylsilylethyl and Trichloroethyl Aryldiazoacetates. *Tetrahedron* **2015**, *71* (39), 7415–7420.

(39) Guptill, D. M.; Davies, H. M. L. 2,2,2-Trichloroethyl Aryldiazoacetates as Robust Reagents for the Enantioselective C-H Functionalization of Methyl Ethers. *J. Am. Chem. Soc.* **2014**, *136* (51), 17718–17721.

(40) Liao, K.; Negretti, S.; Musaev, D. G.; Bacsa, J.; Davies, H. M. L. Site Selective and Stereoselective Functionalization of Unactivated C–H Bonds. *Nature* **2016**, *7602*, 230–234.

CHAPTER 5. DIRHODIUM IMMOBILIZED HOLLOW FIBER FLOW REACTOR FOR SCALABLE AND SUSTAINABLE C-H FUNCTINOALIZATION IN CONTINUOUS FLOW

5.1 Introduction

Intensive research over the last decade on catalytic C–H functionalization with noble metal catalysts has brought significant innovation in new methodologies for drug development and total synthesis.[1–4] These discoveries enable the synthesis of numerous organic compounds within a few steps, while conventional organic synthesis routes require multiple synthetic and separation steps due to the restricted number of functional groups that can be utilized in the reactions. As a result, the pharmaceutical industry is facing a problem of extensive waste generation in chemical production,[5–7] which leads to low overall yield and high operation cost for waste control. Considering this situation, efficient, scalable catalytic C–H functionalization could be a promising solution for mitigating these issues. Specifically, C–H functionalization via metal carbene structures (donor-acceptor) as intermediate species using dirhodium catalysts has shown the capability of outstanding enantioselective and regioselective C–H bond functionalization.[8–16]

However, there are several critical drawbacks for this chemistry that present potential barriers to the application in the pharmaceutical industry on a large scale. First, the metal carbenes are created by using relatively reactive and unstable diazo compounds, which are potentially explosive and highly toxic. Thus, such reactive compounds are ideally not stored in large quantities on site, and just-in-time syntheses are preferred.[17–27] The price of the soluble dirhodium catalysts (Rh_2L_4, L= ligand) is another barrier for

industrial applications. Rhodium is a very expensive noble metal, and the cost for the synthesis of these ligands for the catalysts also cannot be ignored. To recycle the homogenous dirhodium catalysts, additional separation steps are required, and the catalytic activities are often not maintained after recovery and recycle. Thus, new methodologies for maximizing catalyst turnover number (TON) and recovering Rh for reprocessing are needed; one such approach involves immobilizing these catalysts on a support material.

Previously, our group described a cascade reaction protocol for C–H functionalization, where the diazo compounds were synthesized in flow from hydrazone starting materials, then the diazo compounds were added to the batch reactor containing homogenous dirhodium catalyst and substrates (Flow-Batch, Chapter 4).[28] Even though the diazo generation for sequential C–H functionalization potentially resolved the problems of storage of diazo compounds on a bulk scale, recyclability of the soluble dirhodium catalyst was not achieved. Several studies have recently reported expanding the utilization of diazo compounds in flow; however, the subsequent diazo-consuming reactions were conducted in a batch reactor with a homogeneous catalyst.[17,18,20,22,29] Relatively few reports have tried to increase the TON of dirhodium catalysts for C–H functionalization by immobilization of the catalysts.[30–34] These studies have mainly focused on the catalytic performance of the immobilized catalyst with diazo compounds. To the best of our knowledge, no one has resolved all the challenges stated above to date; herein, we introduce a scalable flow process for C–H functionalization with dirhodium catalysts by developing cascade reaction protocols employing microfluidic flow reactor systems.

5.2 Experimental section

5.2.1 General remarks

All solvents were purified and dried by a Glass Contour Solvent Purifier System unless otherwise stated. DCM for cyclopropanation and C–H insertion reactions were dried over activated 4 Å MS. ^{1}H, ^{13}C, and ^{19}F NMR spectra were recorded at either on a Bruker Advance III 400 spectrometer, a Varian INOVA 500 spectrometer, or on a Varian INOVA 600 spectrometer. NMR spectra were run in solutions of deuterated chloroform ($CDCl_3$) with residual chloroform taken as an internal standard (7.26 ppm for ^{1}H, and 77.16 ppm for ^{13}C), and were reported in parts per million (ppm). Abbreviations for signal multiplicity are as follows: s = singlet, d = doublet, t = triplet, q = quartet, p = pentet, m = multiplet, etc. Coupling constants (*J* values) were calculated directly from the spectra. IR spectra were collected on a Nicolet iS10 FT-IR spectrometer. Mass spectra were taken on a Thermo Finnigan LTQ-FTMS spectrometer with APCI, ESI or NSI. Thin layer chromatographic analysis was performed with glass-backed silica gel plates, visualizing with UV light and/or staining with ethanolic vanillin stain, Seebach Magic Stain, or aqueous $KMnO_4$ stain. Melting points (Mp) were measured in open capillary tubes with a Mel-Temp Electrothermal melting points apparatus and are thus uncorrected. Unless otherwise stated, all chemicals were obtained from Fluka, Aldrich, Merck, or Acros and used as received.

5.2.2 Synthesis of silica embedded hollow fiber

The following chemicals were used as received unless otherwise specified. Torlon® 4000T- HV (Solvay), Syloid C 803 silica (Grace Davison),

poly(vinylpyrrolidone) (K30 MW 40,000, TCI), N-Methyl-2-pyrrolidone (ACS grade, VWR), DI H_2O (15 mΩ).

All polymer and silica were dried overnight at 80 °C under vacuum to remove adsorbed water prior to use. Initially, a prime dope consisting of 20% of the total solvent, non-solvent, and polymer was mixed in a sealed glass jar on a roller 24 h prior to synthesis of the full dope. To a solution of 80% of the total solvent/non-solvent mixture, all of the silica was added and mixed via rotating impeller until homogeneous. This dispersion dope was further dispersed 3 times using a sonication horn for 60 s and impeller alternatingly. To this dispersion dope, the prime dope was added and similarly mixed and dispersed. Lastly, the rest of the dry polymer was added to the dope and mixed using the impeller for several hours until homogeneous at 60 °C while covered to prevent evaporation. The dope was then loaded into a syringe pump and degassed overnight at 50 °C prior to spinning. Fibers were extruded through a coaxial spinneret using a dry-jet wet-quench method into a water bath, then onto a take-up drum in a secondary water bath (scheme 5.1). The spinning conditions and dope composition are summarized in Table 5.1 and 5.2

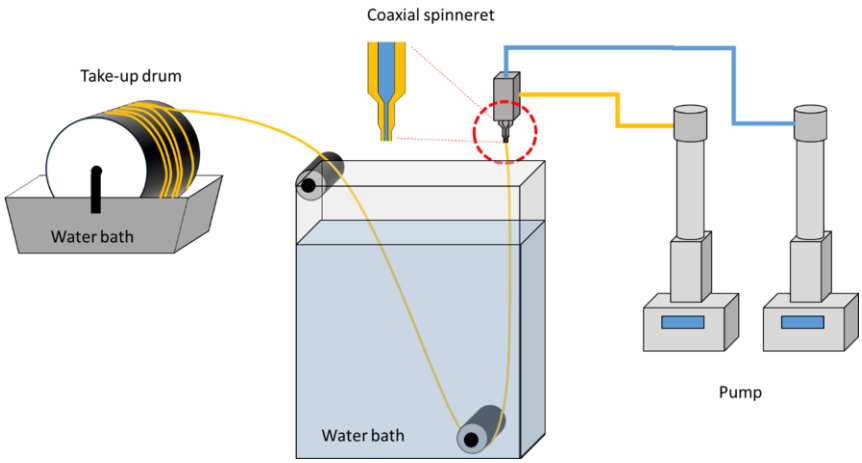

Scheme 5.1. Diagram of the spinning system.

Table 5.1. Spinning Conditions

Polymer Dope	600 ml/h
Bore Fluid (80 wt.% NMP/20 wt.% H_2O)	100 ml/h
Drum Speed	20 m/min
Air Gap	3 cm
Operating Temperature	50 °C
Bath Temperature	60 °C

Table 5.2. Dope Composition (wt.%)

Torlon® 4000T-HV	16%
PVP K30	4%
NMP	60%
H_2O	8%
Silica	12%

5.2.3 Synthesis of ligand exchanged Rh_2L_3L' catalyst

methyl 2-(4'-bromo-[1,1'-biphenyl]-4-yl)acetate

A flame-dried round bottom flask equipped with a pressure-equalizing addition funnel was

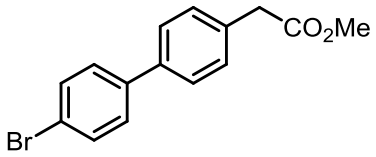

charged with 2-(4'-bromo-[1,1'-biphenyl]-4-yl)acetic acid (38.3 g, 132 mmol, 1.00 equiv.), methanol (132 mL), and was cooled to 0 °C in an ice/water bath. Acetyl chloride (11.2 mL, 12.4 g, 158 mmol, 1.20 equiv.) was added dropwise via the addition funnel, and the solution was stirred at ambient temperature overnight. The mixture washed with diethyl ether (500 mL) into a separation

funnel filled with sat. aq. NH_4Cl (250 mL). The phases were separated, and the aqueous phase was extracted once more with diethyl ether (500 mL). The combined organic phases were washed with sat. aq. $NaHCO_3$ (250 mL), brine (250 mL), and dried over $MgSO_4$. The mixture was filtered and evaporated under reduced pressure to give the target compound (39.2 g, 129 mmol, 98%) as a slightly yellow oil without further purification.

R_f (hexanes:EtOAc = 6:1) = 0.48; **^{1}H NMR** (600 MHz, $CDCl_3$) δ 7.57 – 7.52 (m, 2H), 7.52 – 7.47 (m, 2H), 7.45 – 7.41 (m, 2H), 7.36 – 7.32 (m, 2H), 3.70 (s, 3H), 3.66 (s, 2H); **^{13}C NMR** (151 MHz, $CDCl_3$) δ 172.0, 139.8, 139.0, 133.6, 132.0, 130.0, 128.8, 127.28, 121.7, 52.3, 41.0; **IR** (ATR) 3030, 2952, 2843, 1735, 1481, 1435, 1348, 1226, 1166, 1002, 805 cm^{-1}; **HRMS** (NSI) calc. for $[C_{15}H_{14}O_2Br]^+$ 305.0172 found 305.01718.

methyl 2-(4'-bromo-[1,1'-biphenyl]-4-yl)-2-diazoacetate

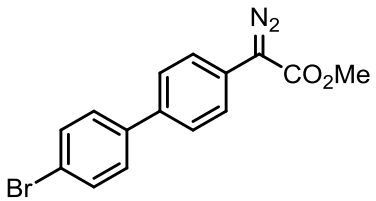

A 500 mL round-bottom flask equipped with a pressure-equalizing addition funnel was charged with methyl 2-(4'-bromo-[1,1'-biphenyl]-4-yl)acetate (36.5 g, 120 mmol, 1.00 equiv.), acetonitrile (120 mL), DCM (120 mL), and 4-acetamidobenzenesulfonyl azide (34.5 g, 144 mmol, 1.20 equiv.). The solution was cooled to 0 °C in an ice/water bath. DBU (36 mL, 0.24 mol, 2.0 equiv.) was added dropwise via the addition funnel. The reaction mixture was stirred at ambient temperature overnight, quenched with sat. aq. NH_4Cl (200 mL), and extracted with diethyl ether (3 x 200 mL). The organic layers were washed with brine, dried over $MgSO_4$, filtered, and evaporated under reduced pressure. The residue was purified by recrystallization in a mixture of 250 mL EtOAc and 250 mL MeOH (55 °C). The vessel was cooled in a freezer overnight and the crystals were collected

through filtration with a Buchner Funnel, washed with an ice-cold 1:1 mixture of EtOAc and MeOH (2 x 40 mL), and dried in vacuum to give the target compound (24.2 g, 73.1 mmol, 61%) as orange crystals.

Mp: 108 °C (decom.); **R_f** (hexanes:EtOAc = 50:1) = 0.31; **^{1}H NMR** (500 MHz, $CDCl_3$) δ 7.63 – 7.53 (m, 6H), 7.50 – 7.44 (m, 2H), 3.91 (s, 3H); **^{13}C NMR** (126 MHz, $CDCl_3$) δ 165.48, 139.20, 137.29, 131.94, 128.42, 127.36, 124.90, 124.29, 121.60, 52.10; **IR** (ATR): 3034, 2953, 2084, 1687, 1604, 1525, 1481, 1433, 1392, 1354, 1278, 1236, 1191, 1155, 1117, 1055, 1019, 1009, 998, 915, 806, 739, 719, 668 cm^{-1}; **HRMS** (NSI) calc. for $[C_{15}H_{12}O_2N_2Br]^+$: 331.00767, found: 331.00822.

methyl(S)-1-(4'-bromo-[1,1'-biphenyl]-4-yl)-2,2-diphenylcyclopropane-1-carboxylate

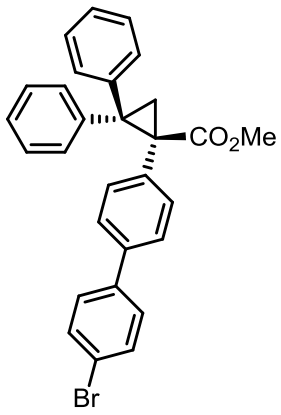

A flame-dried round bottom flask equipped with a pressure-equalizing addition funnel was charged with Rh_2(S-DOSP)$_4$ (7.0 mg, 0.371 mmol, 1.00 mol%), ethene-1,1-diyldibenzene (15 mL, 86 mmol, 2.3 equiv.), and pentane (370 mL). A freshly prepared solution of methyl 2-(4'-bromo-[1,1'-biphenyl]-4-yl)-2-diazoacetate (12.3 g, 37.1 mmol, 1.00 equiv.) in pentane (280 mL) and DCM (180 mL) was added dropwise over 2 h via the addition funnel to the heavily stirred reaction mixture. The mixture was stirred overnight and subsequently evaporated under reduced pressure. Purification was carried out on a Biotage SNAP 340 g SiO_2 column with 2–8% EtOAc in hexanes of 25 column volumes to give the target compound (15.8 g, 32.7 mmol, 88%, 89% ee) as a white solid. The material was further enantioenriched by recrystallization in hot MeOH (300 mL). The vessel was cooled in a freezer and the crystals

were collected through filtration with a Buchner funnel to give the target compound (13.6 g, 28.1 mmol, 76%, 99.6% ee) as white crystals.

Mp: 115 °C; **R_f** (hexanes:EtOAc = 6:1) = 0.45; **^{1}H NMR** (500 MHz, $CDCl_3$) δ 7.54 (dd, *J* = 8.3, 6.8 Hz, 4H), 7.44 – 7.34 (m, 8H), 7.31 – 7.25 (m, 1H), 7.08 – 7.00 (m, 4H), 7.00 – 6.90 (m, 1H), 3.39 (s, 3H), 2.75 (d, *J* = 5.6 Hz, 1H), 2.48 (d, *J* = 5.6 Hz, 1H); **^{13}C NMR** (126 MHz, $CDCl_3$) δ 171.32, 141.94, 139.60, 139.54, 138.36, 135.29, 132.39, 131.75, 129.93, 128.74, 128.58, 128.37, 127.69, 127.01, 126.23, 125.96, 121.41, 52.26, 52.25, 44.65, 42.80, 22.86; **IR** (ATR): 3029, 2991, 2945, 1717, 1600, 1494, 1451, 1434, 1310, 1294, 1218, 1142, 1104, 1074, 1049, 1001, 967, 876, 817, 743, 696 cm^{-1}; **HRMS** (NSI) calc. for $[C_{29}H_{24}O_2Br]^+$: 483.09542, found: 483.09541; **HPLC** (ADH column, 1.0 mL/min, 10% iPrOH in hexanes, λ = 230 nm): t_R(major) = 16.3 min, t_R(minor) = 7.5 min, 99.6% ee.

methyl (S)-2,2-diphenyl-1-(4'-((triisopropylsilyl)ethynyl)-[1,1'-biphenyl]-4-yl)cyclo propane-1-carboxylate

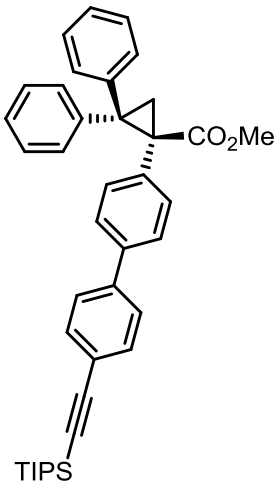

A 25 mL microwave tube was charged with methyl (S)-1-(4'-bromo-[1,1'-biphenyl]-4-yl)-2,2-diphenylcyclopropane-1-carboxylate (3.38 g, 7.00 mmol, 1.00 equiv.), ethynyltriisopropylsilane (1.40 g, 7.70 mmol, 1.10 equiv.), $PdCl_2(PPh_3)_2$ (0.25 g, 0.35 mmol, 5.0 mol%), copper(I) iodide (67 mg, 0.35 mmol, 5.0 mol%), triethylamine (7.0 mL, 5.1 g, 50 mmol, 7.2 equiv.) and DMF (3.5 mL) to give a yellow slurry. The reaction mixture was irradiated in a Biotage microwave to 120 °C for 25 min with heavy stirring to give an orange suspension with white crystalline material. Three such runs were combined,

the reaction mixtures were filtered through a plug of Celite 545 in a sintered glass funnel, washed with DCM (100 mL) and the filtrate was evaporated under reduced pressure. Purification was carried out on a Biotage SNAP 340 g SiO_2 column with 3–6% EtOAc in hexanes of 12 column volumes to give the target compound (9.60 g, 16.4 mmol, 78%) as a white solid.

Mp: 60 °C; **R_f** (hexanes:EtOAc = 6:1) = 0.67; **^{1}H NMR** (500 MHz, $CDCl_3$) δ 7.61 – 7.52 (m, 4H), 7.51 – 7.48 (m, 2H), 7.46 – 7.36 (m, 6H), 7.33 – 7.26 (m, 1H), 7.10 – 7.02 (m, 4H), 7.01 – 6.96 (m, 1H), 3.41 (s, 3H), 2.77 (d, J = 5.5 Hz, 1H), 2.49 (d, J = 5.6 Hz, 1H), 1.19 (s, 21H); **^{13}C NMR** (126 MHz, $CDCl_3$) δ 171.34, 142.00, 140.53, 139.58, 138.78, 135.27, 132.37, 132.35, 129.97, 128.76, 128.38, 127.71, 127.01, 126.70, 126.25, 126.07, 122.35, 107.03, 91.25, 52.26, 44.67, 42.86, 22.91, 18.73, 11.38; **IR** (ATR) 3030, 2943, 2863, 2151, 1724, 1601, 1493, 1449, 1433, 1302, 1216, 1141, 1074, 1019, 1006, 995, 957, 882, 836, 822, 777, 748, 694, 676, 661 cm^{-1}; **HRMS** (NSI) calc. for $[C_{40}H_{45}O_2Si]^+$: 585.31833, found: 585.31876.

(S)-2,2-diphenyl-1-(4'-((triisopropylsilyl)ethynyl)-[1,1'-biphenyl]-4-yl)cyclo-propane-1-carboxylic acid

A flame-dried 500 mL round-bottom flask was charged with potassium trimethylsilanolate (7.12 g, 55.5 mmol, 3.00 equiv.), put onto the high vacuum, and heated to 100 °C for 15 min. The flask was cooled to 0 °C, flushed with Argon, charged with THF (50 mL) and a solution of methyl (S)-2,2-diphenyl-1-(4'-((triisopropylsilyl)ethynyl)-[1,1'-biphenyl]-4-yl)cyclopropane-1-carboxyl-ate (10.8 g, 18.5 mmol, 1.00 equiv.) in THF (140 mL) was added dropwise to give a colorless solution. The mixture was allowed to reach

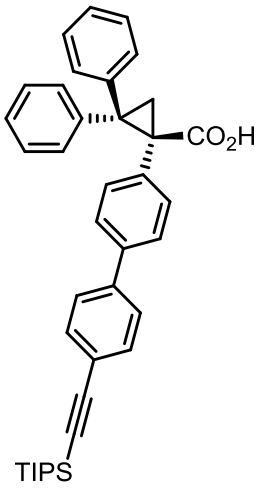

room temperature and stirred for 16 h. Another portion of potassium trimethylsilanolate (7.12 g, 55.5 mmol, 3.00 equiv.) was added and stirring was continued for 24 h until full consumption of starting material was evident as judged by TLC analysis. The mixture was acidified with aq. citric acid (0.5 M, 150 mL), stirred for 30 min, THF was evaporated under reduced pressure, the residue extracted with EtOAc (3 x 100 mL), dried over Na_2SO_4, filtered, and evaporated under reduced pressure. Purification was carried out on a Silicycle 330 g SiO_2 column with 10–30% EtOAc in hexanes of 10 column volumes to give the target compound (9.10 g, 15.9 mmol, 90%) as a white solid.

Mp: 127 °C; **R_f** (hexanes:EtOAc = 2:1) = 0.29; **^{1}H NMR** (500 MHz, $CDCl_3$) δ 7.50 – 7.45(m, 4H), 7.45 – 7.43 (m, 2H), 7.36 – 7.35 (m, 6H), 7.35 – 7.33 (m, 1H), 7.01 – 6.99(m, 4H), 2.64 (d, *J* = 5.5 Hz, 1H), 2.49 (d, *J* = 5.6 Hz, 1H), 1.13 (s, 21H); **^{13}C NMR** (126 MHz, $CDCl_3$) δ 175.4, 141.7, 140.6, 139.4, 139.1, 135.0, 132.5, 132.45, 130.0, 128.9, 128.6, 127.9, 127.2, 126.8, 126.5, 126.2, 122.5, 107.1, 91.4, 45.9, 42.3, 29.9, 23.6, 18.8, 11.5; **IR** (ATR) 3030, 2942, 2863, 2151, 1689, 1493, 1449, 1235, 1071, 1005, 991, 836, 820, 758, 744, 724, 676, 659 cm^{-1}; **HRMS** (NSI) calc. for $[C_{39}H_{43}O_2Si]^+$: 571.30268, found: 571.30316; **HPLC** (ADH column, 1.0 mL/min, 5% iPrOH in hexanes, λ = 230 nm): t_R(major) = 13.7 min, t_R(minor) = 7.8 min, 99.3% ee.

Rh_2(S-*p*-BrTPCP)$_3$(S-*p*-AlkyneTPCP)

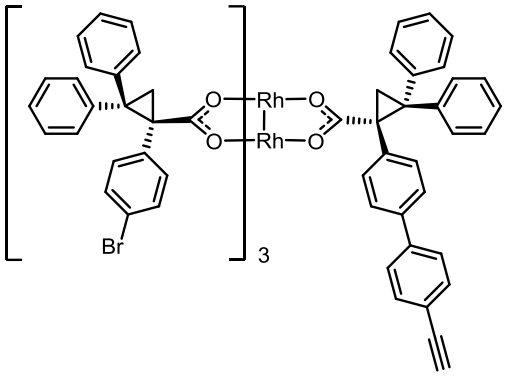

A flame-dried 250 mL 2-neck round-bottom flask was charged with Rh_2(S-*p*-BrTPCP)$_4$ (2.10 g, 1.18 mmol, 1.00 equiv.) and (S)-2,2-diphenyl-1-(4'-((triisopropylsilyl)ethynyl)-[1,1'-biphenyl]-4-yl)cyclopropane-1-carboxylic acid (743 mg, 1.30 mmol, 1.10 equiv.). The vessel was evacuated and backfilled with argon (3 cycles). Benzene (40 mL) was added to give a green slurry. The reaction mixture was degassed by sparging with argon for 10 min. The reaction vessel was equipped a reflux condenser, and the reaction mixture was stirred under reflux for 16 h. The reaction mixture was evaporated under reduced pressure. Purification was carried out on a Silicycle 120 g SiO_2 column with 10–12% EtOAc in hexanes of 15 column volumes. All fractions containing the mono-exchange product were united and evaporated to give crude Rh_2(S-BTPCP)$_3$(S-p-TIPS-ATPCP) as a green solid (1.30 g, 662 μmol, 56%).

A flame-dried 100 mL round-bottom flask was charged with crude Rh_2(S-*p*-BrTPCP)$_3$(S-*p*-TIPS-ATPCP) (1.29 g, 0.661 mmol) and THF (66 mL) to give a green solution. The reaction mixture was cooled to 0 °C in an ice/water bath. A solution of TBAF (Tetra-*n*-butylammonium fluoride) in THF (1.0 M, 2.6 mL, 2.6 mmol, 4.0 equiv.) was added drop-wise via syringe. The reaction mixture was stirred at 0 °C for 30 min until full consumption of starting material was evident as judged by TLC analysis. The reaction mixture was quenched by the addition of H_2O (50 mL). The reaction mixture was evaporated under reduced pressure to remove THF, the aqueous residue extracted with DCM (3 x 50 mL),

the combined organic layers dried over Na_2SO_4, filtered, and evaporated under reduced pressure. Purification was carried out on a Silicycle 120 g SiO_2 column with 13–20% EtOAc in hexanes of 15 column volumes and on a Silicycle 40 g SiO_2 column with 5–20% Et_2O in hexanes of 15 column volumes to give the target compound (506 mg, 282 μmol, 24% over 2 steps) as a green solid. Fractions corresponding to each spot of the TLC plates were collected separately. The fractions corresponding to the mono-exchanged product was selected according to HRMS [Note: compound contains trace amounts of DCM and EtOAc; HRMS was used as a primary analysis tool].

Mp: >225 °C (decomp.); **R_f** (hexanes:EtOAc = 6:1) = 0.42; **^{1}H NMR** (500 MHz, $CDCl_3$) δ 7.62 – 7.48 (m, 4H), 7.47 – 7.28 (m, 23H), 7.24 – 7.10 (m, 8H), 7.07 – 6.84 (m, 22H), 6.83 – 6.71 (m, 3H), 3.60 (s, 1H), 2.47 (brs, 3H), 2.35 (brs, 1H), 2.16 (brs, 2H), 1.84 (brs, 1H), 1.77 (brs, 1H); **^{13}C NMR** (126 MHz, $CDCl_3$) δ 189.18, 188.70, 188.53, 142.71, 142.46, 142.15, 141.09, 140.84, 140.71, 137.86, 136.13, 135.95, 135.65, 133.01, 132.65, 131.47, 130.41, 130.27, 129.90, 129.81, 129.26, 129.13, 128.21, 128.06, 127.75, 127.56, 126.63, 126.54, 126.19, 125.99, 125.59, 120.75, 120.57, 120.49, 84.54, 76.66, 47.39, 47.08, 46.06, 42.97, 42.44, 42.20, 24.16, 22.68; **IR** (ATR) 3024, 2924, 1686, 1581, 1491, 1381, 908, 732, 702 cm^{-1}; **HRMS** (NSI) calc. for $[C_{96}H_{69}O_8Br_3Rh_2]^+$: 1792.06472, found: 1792.06713.

Rh_2(S-*p*-PhTPCP)$_3$(S-*p*-AlkyneTPCP).

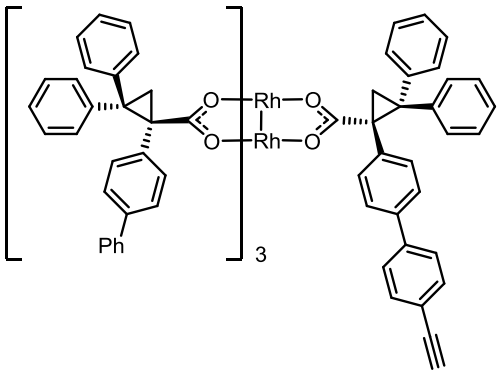

A flame-dried 250 mL 2-neck round-bottom flask was charged with Rh_2(S-*p*-PhTPCP)$_4$ (440 mg, 0.25 mmol, 1.00 equiv.) and (S)-2,2-diphenyl-1-(4'-((triisopropylsilyl)ethynyl)-[1,1'-biphenyl]-4-yl)cyclopropane-1-carboxylic acid (157 mg, 0.27 mmol, 1.10 equiv.). The vessel was evacuated and backfilled with argon (3 cycles). Benzene (25 mL) was added to give a green slurry. The reaction mixture was degassed by sparging with argon for 10 min. The reaction vessel was equipped a reflux condenser, and the reaction mixture was stirred under reflux for 16 h. The reaction mixture was evaporated under reduced pressure. Purification was carried out on a Silicycle 120 g SiO_2 column with 10–12% EtOAc in hexanes of 15 column volumes. All fractions containing the mono-exchange product were united and evaporated to give crude Rh_2(S-p-PhTPCP)$_3$(S-p-TIPS-ATPCP) as a green solid (291 mg, 0.15 mmol, 60%).

A flame-dried 100 mL round-bottom flask was charged with crude Rh_2(S-*p*-BrTPCP)$_3$(S-*p*-TIPS-ATPCP) (290 mg, 0.15 mmol) and THF (15 mL) to give a green solution. The reaction mixture was cooled to 0 °C in an ice/water bath. A solution of TBAF (Tetra-*n*-butylammonium fluoride) in THF (1.0 M, 0.3 mL, 0.30 mmol, 2.0 equiv.) was added drop-wise via syringe. The reaction mixture was stirred at 0 °C for 30 min until full consumption of starting material was evident as judged by TLC analysis. The reaction mixture was quenched by the addition of H_2O (15 mL). The reaction mixture was evaporated under reduced pressure to remove THF, the aqueous residue extracted with DCM (3 x 20 mL),

the combined organic layers dried over Na_2SO_4, filtered, and evaporated under reduced pressure. Purification was carried out on a Silicycle 80 g SiO_2 column with 13–20% EtOAc in hexanes of 15 column volumes and on a Silicycle 40 g SiO_2 column with 5–20% Et_2O in hexanes of 15 column volumes to give the target compound (144 mg, 80 μmol, 32% over 2 steps) as a green solid. Fractions corresponding to each spot of the TLC plates were collected separately. The fractions corresponding to the mono-exchanged product was selected according to HRMS. [Note: compound contains trace amounts EtOAc; HRMS was used as primary analysis tool].

Mp: >225 °C (decomp.); **R_f** (hexanes:EtOAc = 6:1) = 0.40; **^{1}H NMR** (500 MHz, $CDCl_3$) δ 7.37 – 7.36 (m, 2H), 7.32 – 7.28 (m, 23H), 7.26 – 7.23 (m, 14H), 7.19 – 7.08 (m, 14H), 6.93 – 6.85 (m, 18H), 6.81 – 6.79 (m, 4H), 3.15 (s, 1H), 2.46 (d, 2H), 2.42 (d, 2H), 2.01 (d, 2H), 1.87 (d, 2H); **^{13}C NMR** (126 MHz, $CDCl_3$) δ 189.18, 189.06, 188.99, 142.82, 142.76, 142.67, 141.24, 141.16, 141.03, 140.63, 138.84, 138.70, 137.67, 136.23, 135.73, 135.59, 132.59, 131.56, 130.12, 130.08, 129.32, 129.28, 128.85, 128.76, 128.48, 128.25, 128.22, 127.57, 127.54, 127.00, 126.90, 126.88, 126.66, 126.47, 126.33, 125.95, 125.90, 125.82, 120.65, 83.91, 46.97, 46.92, 46.45, 43.13, 23.81, 23.18; **IR** (ATR) 3028, 2246, 1577, 1489, 1447, 1382, 905, 762, 694 cm^{-1}; **HRMS** (NSI) calc. for $[C_{114}H_{85}O_8Rh_2]^+$: 1787.43492, found: 1787.43295

5.2.4 Immobilization of Rh_2(S-p-Br/Ph-TPCP)$_3$(S-p-AkyneTPCP) catalyst on silica embedded hollow fiber

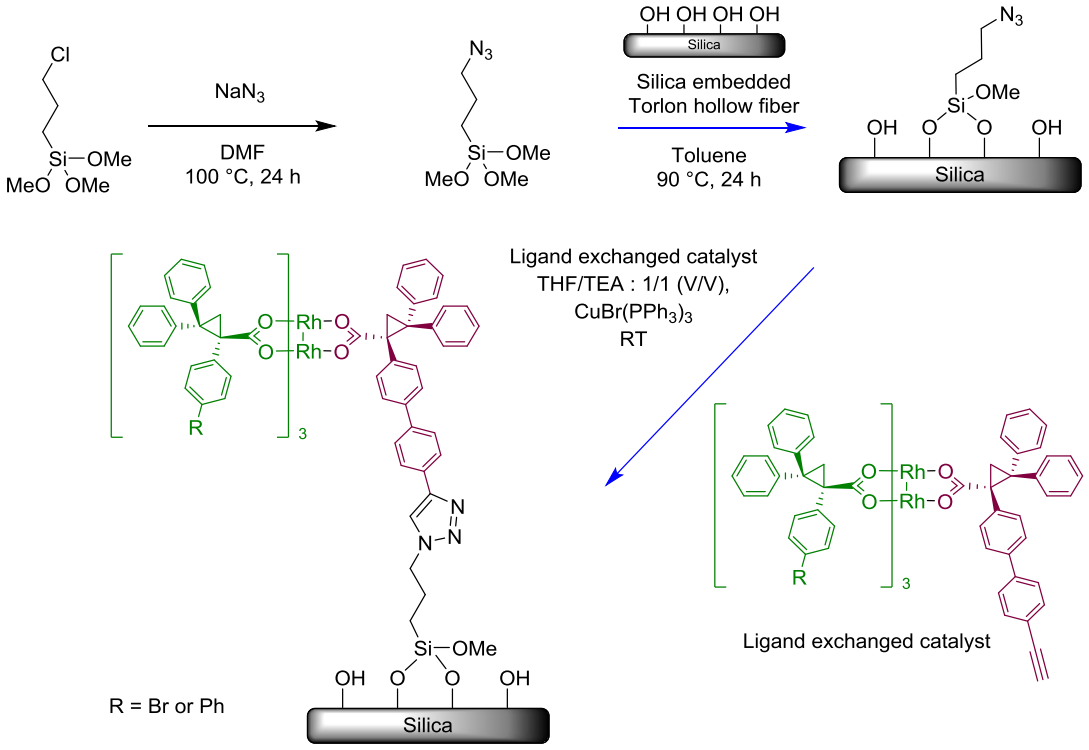

Scheme 5.2. Schematic procedure of dirhodium immobilization on silica embedded hollow fiber.

3-azidopropyltrimethoxysilane

A flame-dried round bottom flask was charged with 3-chloropropyltrimethoxysilane (20 mmol), sodium azide (30 mmol) and 15 mL of anhydrous DMF. The reaction mixture was stirred at 100 °C for 24 h then cooled to room temperature. The mixture was diluted with DI water (30 mL) and diethyl ether (30 mL). The organic layer was washed with water three times (30 mL x 3) and saturated aqueous sodium chloride solution (30mL x 1). The collected organic layer dried over magnesium sulfite was concentrated to yield 3-azidopropyltriemthosxyilane. The NMR spectra matched the previous literature.[35] **^{1}H**

NMR (400 MHz $CDCl_3$) δ 3.57 (s, 9H), 3.27 (t, 2H), 1.74-1.67 (m, 2H), 0.74-0.67 (m, 2H); **^{13}C NMR** (101 MHz, $CDCl_3$) δ 53.86, 50.72, 22.58, 6.46.

Synthesis of $CuBr(PPh_3)_3$ catalyst for click chemistry

A 250 mL round bottomed flask equipped with a magnetic stir bar was charged with triphenylphosphine (24.22 g, 92.34 mmol) and methanol (100 mL). The mixture was heated to reflux and copper (II) bromide (5.16 g, 23.09 mmol) was added in 10 portions over 10 min. The reaction mixture was refluxed for 30 min, cooled to room temperature, and filtered through a fritted glass funnel. The white solid was washed with EtOH and Et_2O. The solid was dried in vacuo.

Immobilization of 3-azidopropyltrimethoxysilane on silica embedded hollow fiber

A flame-dried round bottom glassware (60 mL) was charged with silica embedded hollow fibers (3 m, 5 cm x 60 ea), anhydrous toluene (50 mL), 3-azidopropyltrimethoxysilane (1.2 mL) and TEA (150 μL). The mixture was stirred at 90 °C for 24 h. The fiber was washed with toluene (50 mL x 3 times) and hexanes (50 mL x 3 times), followed by drying under reduced pressure at 60 °C overnight.

Copper catalyzed alkyne and azide cycloaddition (CuAAC)

A glass tube (20 mL) was charged with azide functionalized hollow fiber (3 m, 5 cm x 60 ea), TEA (5 mL), inhibitor-free THF (5 mL), Rh_2(S-*p*-Br/Ph-TPCP)$_3$(S-p-AkyneTPCP) catalyst (60 mg) and $CuBr(PPh_3)_3$ (2 mg). The mixture was stirred with a vortex mixer (500 RPM) at room temperature for 3 days. The fibers transferred to round

bottom glassware were washed with DCM (50 mL x 3 times) and hexanes (50 mL x 3 times), followed by drying under reduced pressure at 60 °C overnight.

5.2.5 General procedure for the synthesis of hydrazones (GP I):

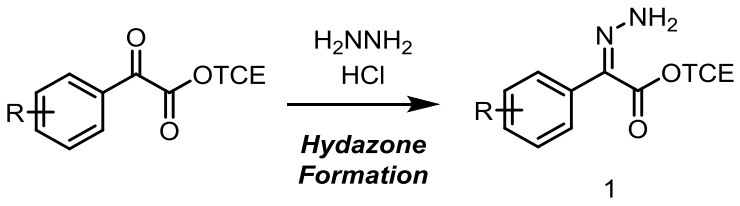

Scheme 5.3. Synthesis of hydrazones from arylketones

A 250 mL round-bottom flask was charged with hydrazine monohydrate (4.85 mL, 5.01 g, 100 mmol, 10.0 equiv.) and MeOH (150 mL). The reaction mixture was cooled to 0 °C in an ice/water bath. HCl (3.0 M, 33 mL, 100 mmol, 100 equiv.) was added slowly. To this solution 2,2,2-trichloroethyl 2-oxo-2-arylacete (10.0 mmol, 1.00 equiv.) in MeOH (10 mL) was added dropwise over 5 min. The reaction mixture was stirred at 0 °C until full consumption of starting material was observed by TLC control (unnecessary longer reaction times lead to significantly lower yields). The reaction mixture was quenched by the addition of sat. $NaHCO_3$ (100 mL), MeOH was evaporated under reduced pressure, the residue was transferred into a separatory funnel and extracted with EtOAc (3 x 100 mL). The organic layers were washed with brine (100 mL), filtered, and evaporated under reduced pressure to give the crude products as a yellow solid. The crude was purified by automatic flash silica gel chromatography as indicated.

5.2.6 General procedure for flow oxidations of hydrazones (GP II)

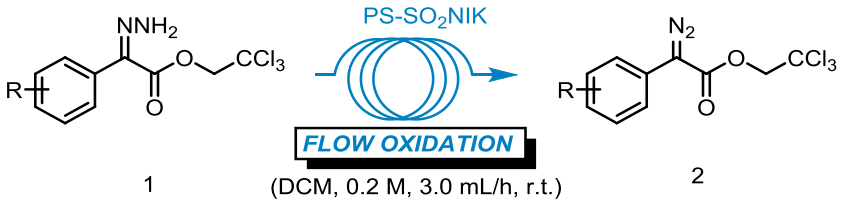

Scheme 5.4. synthesis of the diazo compound from hydrazone compound

PS-TsNIK resin (1.60 g) was filled into an Omnifit (A = 0.3421 cm²) cartridge. A 25 mL vial was charged with hydrazone (240 µmol, 1.20 equiv.) and DCM (1.20 mL). This solution was injected into a 1.00 mL sample loop (effective starting material: 200 µmol, 1.00 equiv.) of a HPLC valve. The valve was connected to a 10 mL glass syringe filled with 10 mL dry DCM fitted in a syringe pump. A total volume of 6 mL of DCM at a flow rate of 3.0 mL/h was used to push the substrate through the cartridge (stream from bottom to top). The product solution was collected in a weighted 25 mL vial and evaporated under reduced pressure (25 °C water bath temperature) after completion of the run. An exactly weighted aliquot of the product was added to a defined amount of dimethyl fumarate, dissolved in $CDCl_3$, and a ^{1}H-NMR was acquired with a recycle delay (d1) of 30 s to assess the product purity by means of QNMR.

5.2.7 Cascade flow reactor setup

The overall flow reactor setup is shown in scheme 5.5. First column (Omnifit glass column, ID= 10 mm, L =10 cm) was filled with PS-SO_2NIK resin and a second column (Omnifit glass column, ID= 10 mm, L =10 cm) was filled first with anhydrous $Na_2S_2O_3$ (0.3 g) followed by activated drying agent (typically Acros <50 µm 4 Å MS). All parts

were connected with PTFE tubing (OD: 1.5 mm) and HPLC fitting. The Rh immobilized fiber (15-30 cm) was loaded in PTFE tubing, which was immersed in a temperature-controlled water bath for constant temperature during the reaction time. The inlet of a manual HPLC 6 port valve (Valco) was connected to a 10 mL gas tight glass syringe (SGE, 10MDR-LL-GT) fitted in a syringe pump (KD scientific, KDS 210). The volume of the sampling loop was 1 mL. The outlet of the HPLC valve was connected to the vertically-aligned column filled with PS-SO_2NIK resin (stream flow from bottom to top), followed by a t-connector where the mixture of substrate and DCM was injected. The two streams (generated diazo from first column and substrate from syringe pump) were mixed and dried in a second column. The mixture then flowed to dirhodium immobilized hollow flow reactor. The back pressure regulator (40 psi) was installed at the end of the flow reactor, and the crude product was collected in a round bottom flask.

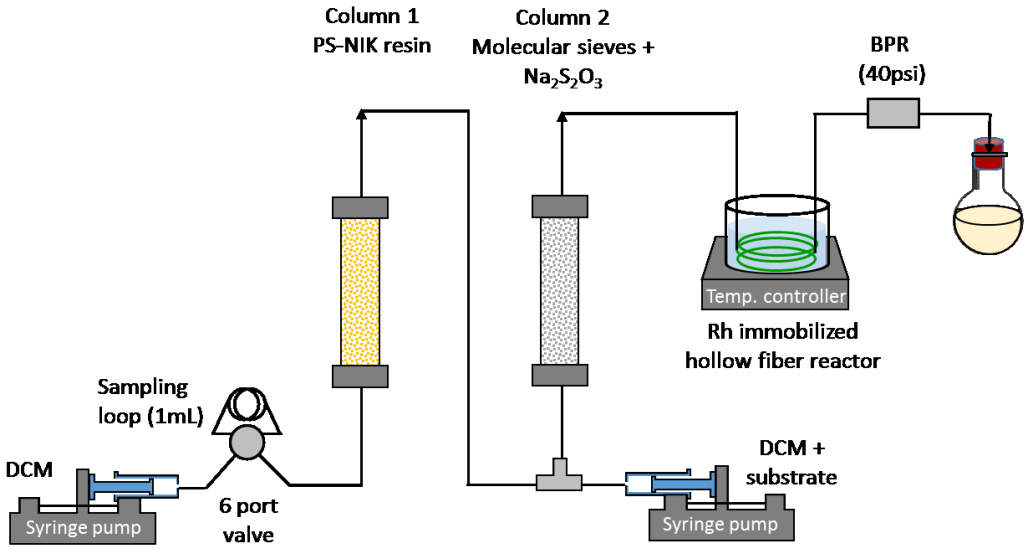

Scheme 5.5. Overall schematic cascade flow reactor for C–H functionalization

5.2.8 PS-SO_2NIK resin synthesis

The PS-SO2NIK resin was prepared by a previously reported method.[20]

5.2.9 General procedure for the synthesis of cyclopropanes in a flow-to-flow process (GP III):

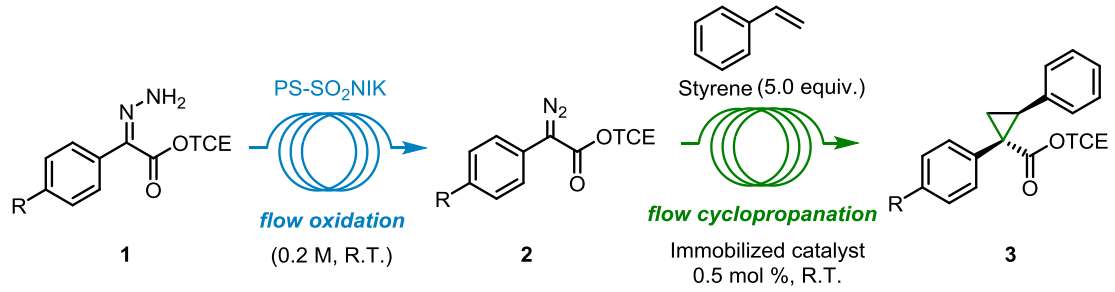

a: R= Br, **b**: R= H, **c**: R= F, **d**: R=^{t}Bu

Scheme 5.6. Synthesis of cyclopropanes in sequential flow-flow reactors

The first column was charged with PS-NIK resin (1.6 g) and the second column was filled first with anhydrous $Na_2S_2O_3$ (0.3 g) followed by activated drying agent (typically Acros <50 µm 4 Å MS). The Rh immobilized hollow fiber (15 cm, c.a. 0.5 mol%) was loaded into the PTFE tubing. A flame-dried 10 mL pear-shaped flask was charged with hydrazone (220 µmol, 1.1 equiv.), evacuated and backfilled with argon (3x), and charged with DCM (1.1 mL). This solution was injected into a 1.0 mL sample loop (effective starting material: 200 µmol, 1 equiv. 0.2 M) of the HPLC valve. 3 mL of DCM at a flowrate of 2.4 mL/h was used to push the hydrazone though the oxidizing and drying column. Another syringe pump was charged with silica-plug-filtered styrene in DCM (1 M, 5 mL). Before the intensely yellow/orange colored diazo-containing stream reached the t-connector (before the second column), the styrene solution was simultaneously fed together

at a flow rate of 2.4 mL/h (overall flow 4.8 mL/h). When the mixture exited from the second column, the flow rates of two syringe pumps were reduced to 1.0 mL/h, each (overall flow rate: 2.0 mL/h). After completion of the addition, the reaction vessel was evaporated under reduced pressure, and trichloroethylene (typically 25–50 µL) was added as an internal standard (if needed $CDCl_3$ was added to obtain a fully homogeneous sample), and the crude yield determined by ^{1}H-NMR analysis. The NMR sample was added back to the remaining crude material, the combined sample evaporated under reduced pressure, and purified by automatic flash column chromatography (typically 12 g SiO_2, 1–3% Et_2O in hexanes over 20 CV). The ee of the material was determined by chiral HPLC analysis as indicated.

2,2,2-trichloroethyl (1R,2S)-1-(4-bromophenyl)-2-phenylcyclopropane-1-carboxylate (3a Flow-Flow)[28]

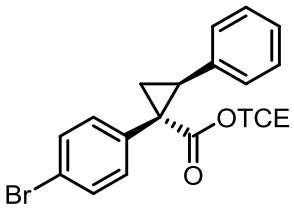

Following GP III (200 µmol scale) using 2,2,2-trichloroethyl (Z)-2-(4-bromophenyl)-2-hydrazonoacetate (**1a**) gave the target compound (84 mg, 186 µmol, 93%) as a white solid: **^{1}H NMR** (500 MHz, $CDCl_3$) δ 7.32 – 7.27 (m, 2H), 7.19 – 7.09 (m, 3H), 7.01 – 6.95 (m, 2H), 6.84 (dd, *J* = 6.8, 2.9 Hz, 2H), 4.87 (d, *J* = 11.9 Hz, 1H), 4.68 (d, *J* = 11.9 Hz, 1H), 3.26 (dd, *J* = 9.4, 7.5 Hz, 1H), 2.32 (dd, *J* = 9.4, 5.2 Hz, 1H), 2.01 (dd, *J* = 7.5, 5.2 Hz, 1H); **^{13}C NMR** (126 MHz, $CDCl_3$) δ 171.60. 135.20, 133.65, 132.92, 130.92, 128.08, 128.04, 126.88, 121.52, 94.96, 74.39, 36.60, 33.96, 20.19; **HPLC** (OJH column, 1.0 mL/min, 1% iPrOH in hexanes, λ = 230 nm): t_R(major) = 10.2 min, t_R(minor) = 17.5 min, 93% ee.

2,2,2-trichloroethyl (1R,2S)-1,2-diphenylcyclopropane-1-carboxylate (3b Flow-Flow)[28]

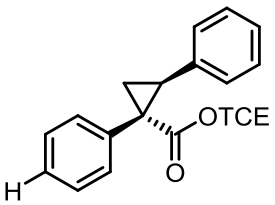

Following GP III (200 µmol scale) using 2,2,2-trichloroethyl (Z)-2-phenyl-2-hydrazonoacetate (**1b**) gave the target compound (68 mg, 182 µmol, 91%) as a white solid:

Mp: 62 °C; **^{1}H NMR** (500 MHz, $CDCl_3$) δ 7.21 – 7.16 (m, 3H), 7.14 – 7.09 (m, 5H), 6.90 – 6.81 (m, 2H), 4.89 (d, *J* = 11.9 Hz, 1H), 4.69 (d, *J* = 11.9 Hz, 1H), 3.27 (dd, *J* = 9.4, 7.4 Hz, 1H), 2.33 (dd, *J* = 9.4, 5.1 Hz, 1H), 2.06 (dd, *J* = 7.4, 5.1 Hz, 1H); **^{13}C NMR** (126 MHz, $CDCl_3$) δ 172.13, 135.73, 133.66, 132.03, 128.12, 127.81, 127.70, 127.30, 126.60, 95.07, 74.36, 37.24, 33.87, 20.30; **HPLC** (OJH column, 1.0 mL/min, 1% iPrOH in hexanes, λ = 230 nm): t_R(major) = 9.3 min, t_R(minor) = 17.3 min, 92% ee.

2,2,2-trichloroethyl (1R,2S)-1-(4-fluorophenyl)-2-phenylcyclopropane-1-carboxylate (3c Flow-Flow) [28]

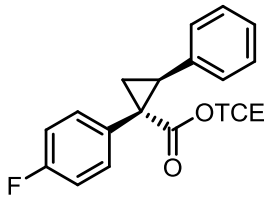

Following GP III (200 µmol scale) using 2,2,2-trichloroethyl (Z)-2-(4-fluorophenyl)-2-hydrazonoacetate (**1c**) gave the target compound (71 mg, 184 µmol, 92%) as a white solid:

^{1}H NMR (600 MHz, $CDCl_3$) δ 7.16 – 7.12 (m, 3H), 7.10 – 7.02 (m, 2H), 6.92 – 6.79 (m, 4H), 4.87 (d, *J* = 11.9 Hz, 1H), 4.69 (d, *J* = 11.9 Hz, 1H), 3.26 (dd, *J* = 9.4, 7.4 Hz, 1H), 2.33 (dd, *J* = 9.4, 5.2 Hz, 1H), 2.02 (dd, *J* = 7.4, 5.2 Hz, 1H); **^{13}C NMR** (150 MHz, $CDCl_3$) δ 172.0, 161.8 (d, J = 246.2 Hz), 135.3, 133.4 (d, J = 8.3 Hz), 129.6 (d, J = 3.4 Hz), 128.1, 127.9, 126.8, 114.7 (d, J = 21.4), 95.0, 74.4, 36.4, 34.0, 20.4; **HPLC** (OJH column, 1.0 mL/min, 1% iPrOH in hexanes, λ = 230 nm): t_R(major) = 9.2 min, t_R(minor) = 16.5 min, 92% ee.

2,2,2-trichloroethyl (1R,2S)-1-(4-(tert-butyl)phenyl)-2-phenylcyclopropane-1-carboxylate. (3d Flow-Flow)[28]

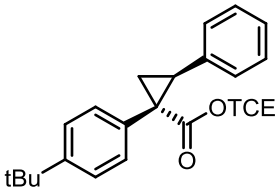

Following GP III (200 µmol scale) using 2,2,2-trichloroethyl (Z)-2-(4-(tert-butyl)phenyl)-2-hydrazonoacetate (**1d**) gave the target compound (77 mg, 180 µmol, 90%) as a white solid: **^{1}H NMR** (500 MHz, $CDCl_3$) δ 7.23 – 7.17 (m, 2H), 7.14 – 7.09 (m, 3H), 7.06 – 7.02 (m, 2H), 6.86 – 6.82 (m, 2H), 4.88 (d, *J* = 11.9 Hz, 1H), 4.70 (d, *J* = 11.9 Hz, 1H), 3.24 (dd, *J* = 9.4, 7.4 Hz, 1H), 2.34 (dd, *J* = 9.4, 5.1 Hz, 1H), 2.02 (dd, *J* = 7.4, 5.1 Hz, 1H), 1.28 (s, 9H); **^{13}C NMR** (126 MHz, CDCl3) δ 172.2, 150.1, 135.9, 131.6, 130.5, 128.1, 127.7, 126.4, 124.6, 95.2, 74.3, 36.9, 34.4, 33.7, 31.3, 20.4; **HPLC** (OJH column, 1.0 mL/min, 1% iPrOH in hexanes, λ = 230 nm): t_R(major) = 6.7 min, t_R(minor) = 4.9 min, 99% ee.

5.2.10 General procedure for the insertion into benzylic C–H bonds in a batch process (GP IV):

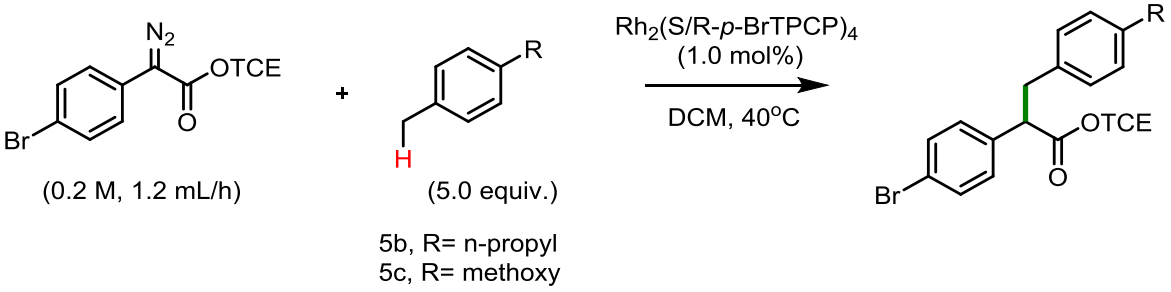

Scheme 5.7. Benzylic C-H insertion in a batch reactor

A flame dried 10 mL round bottom flask equipped with a magnetic stir bar and a reflux condenser was charged with racemic products Rh_2-R/S-p-BrTPCP)$_4$ (3.6 mg, 2.0 µmol, 1.0 mol%) and 4-*n*-propyltoluene (**5b**) (0.16 mL, 1.0 mmol, 5.0 equiv.) or 4-

methoxytoluene (**5c**) (0. 13 mL, 1.0 mmol, 5.0 equiv.), evacuated and backfilled with argon (3x), charged with DCM (2.0 mL), and magnetically stirred (about 600 rpm) at reflux. A flame-dried 10 mL pear-shaped flask was charged with diazo (200 μmol, 1.00 equiv.), evacuated and backfilled with argon (3x), and charged with DCM (2.0 mL). This solution was transferred to a syringe and dropwise added to the reaction vessel at a flow rate of 1.2 mL/h via syringe pump. The pear-shaped flask was rinsed with DCM (2 x 0.5 mL), and the solution slowly added to the reaction mixture, which was stirred for another 1.5 h at reflux, and subsequently evaporated under reduced pressure. Trichloroethylene (typically 25–50 μL) was added as an internal standard (if needed $CDCl_3$ was added to obtain a fully homogeneous sample), and the crude yield determined by ^{1}H-NMR analysis. The NMR sample was added back to the remaining crude material, the combined sample evaporated under reduced pressure, and purified by automatic flash column chromatography (typically 12 g SiO_2, 1–3% Et_2O in hexanes over 20 CV). The ee of the material was determined by chiral HPLC analysis as indicated.

2,2,2-trichloroethyl (R)-2-(4-bromophenyl)-3-(4-propylphenyl)propanoate (4d racemate)

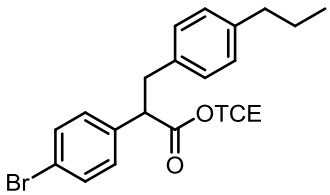

Following GP IV using 2,2,2-trichloroethyl 2-(4-bromophenyl)-2-diazoacetate (**2a**) and 4-n-propyltoluene (**5b**) gave the target compound as a white solid:

^{1}H NMR (400 MHz, $CDCl_3$) δ 7.45 – 7.43 (m, 2H), 7.25 – 7.24 (m, 2H), 7.04 (s, 4H), 4.68 (d, *J* = 12.0 Hz, 1H), 4.62 (d, *J* = 12.0 Hz, 1H), 3.96 (dd, *J* = 9.2, 6.5 Hz, 1H), 3.40 (dd, *J* = 13.9, 9.2 Hz, 1H), 3.03 (dd, *J* = 13.9, 6.5 Hz, 1H), 2.52 (t, 2H), 1.60 (m, 2H) 0.90 (t, 3H); **^{13}C NMR** (101 MHz, $CDCl_3$) δ 171.37, 141.12, 136.64, 135.16, 131.79, 129.88,

128.77, 128.59, 121.71, 94.63, 74.12, 52.95, 38.99, 37.61, 24.54, 13.82; **IR** (ATR) 2957, 2929, 2870, 2159, 2027, 1752, 1488, 1442, 1372, 1266, 1202, 1074, 1101, 806, 754, 720; **HRMS** (NSI) calc. for $[C_{20}H_{21}O_2Cl_3Br]^+$ 476.97850 found 476.97911.; **HPLC** (SSWhelk column, 0.5 mL/min, 0% iPrOH in hexanes, λ = 230 nm): t_R = 28.7 min, t_R = 32.1 min

2,2,2-trichloroethyl 2-(4-bromophenyl)-3-(4-methoxyphenyl)propanoate (4e racemate)

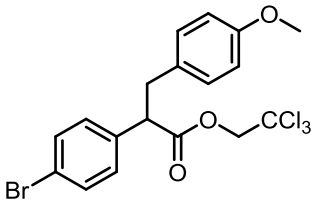

Following GP IV using 2,2,2-trichloroethyl (Z)-2-(4-bromophenyl)-2-hydrazonoacetate (**1a**) and 4-methoxyltoluene (**5c**) gave the target compound as a colorless oil.

Rf = 0.51 (pentane/ethyl ether= 19/1); **^{1}H** NMR (400 MHz, $CDCl_3$) δ 7.44 (d, *J* = 8.5 Hz, 2H), 7.22 (d, *J* = 8.4 Hz, 2H), 7.04 (d, *J* = 8.7 Hz, 2H), 6.77 (d, *J* = 8.7 Hz, 2H), 4.68 (d, *J* = 12.0 Hz, 1H), 4.64 (d, *J* = 12.0 Hz, 1H), 3.92 (dd, *J* = 8.5, 7.1 Hz, 1H), 3.76 (s, 3H), 3.38 (dd, *J* = 13.9, 8.6 Hz, 1H), 3.02 (dd, *J* = 13.9, 7.1 Hz, 1H); **^{13}C NMR** (101 MHz, $CDCl_3$) δ 171.36, 158.37, 136.54, 131.81, 130.02, 129.96, 129.92, 121.73, 113.90, 94.66, 74.14, 55.25, 53.17, 38.54; **IR** (ATR) 2954, 2835, 1749, 1512, 1488, 1246, 1134, 1035, 1011, 823, 719 cm^{-1}; **HRMS** (NSI) calc. for $[C_{18}H_{17}O_3Cl_3Br]$ $]^+$ 464.94212 found 464.92437; **HPLC** (OD column, 0.5 mL/min, 1% iPrOH in hexanes, λ = 230 nm): t_R = 20.1 min, t_R = 22.0 min.

5.2.11 General procedure for the insertion into benzylic C–H bonds in a flow-to-flow process (GP V):

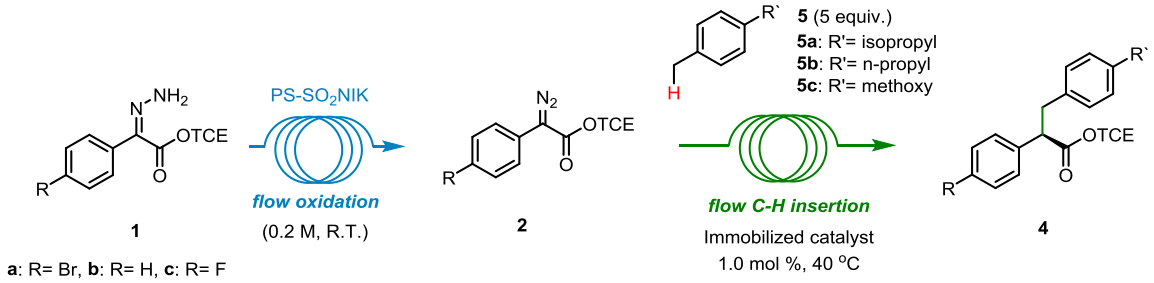

Scheme 5.8. Benzylic C-H insertion in sequential flow-flow reactors

The first column was charged with PS-NIK resin (1.6 g) and the second column was filled first with anhydrous $Na_2S_2O_3$ (0.3 g) followed by activated drying agent (typically Acros <50 µm 4Å MS). Rh immobilized hollow fiber (30 cm, c.a. 1.0 mol%) was loaded into the PTFE tubing. A flame-dried 10 mL pear-shaped flask was charged with hydrazone (220 µmol, 1.1 equiv.), evacuated and backfilled with argon (3x), and charged with DCM (1.1 mL). This solution was injected into a 1.0 mL sample loop (effective starting material: 200 µmol, 1 equiv. 0.2 M) of the HPLC valve. Next, 3 mL of DCM at a flow rate of 2.4 mL/h was used to push the hydrazone though the oxidizing and drying column. Another syringe pump was charged with toluene substrate (**5**) in DCM (1 M, 5 mL). Before the intensely yellow/orange colored diazo-containing stream reached the t-connector (before the second column), the styrene solution was simultaneously fed together at a flow rate of 2.4 mL/h (overall flow 4.8 mL/h). When the mixture exited from the second column, the flow rates of the two syringe pumps were reduced to 0.6 mL/min, each (overall flow rate: 1.2 mL/h). After completion of the addition, the reaction vessel was evaporated under reduced pressure, and trichloroethylene (typically 25–50 µL) was added as an

internal standard (if needed $CDCl_3$ was added to obtain a fully homogeneous sample), and the crude yield determined by ^{1}H-NMR analysis. The NMR sample was added back to the remaining crude material, the combined sample evaporated under reduced pressure, and purified by automatic flash column chromatography (typically 12 g SiO_2, 1–3% Et_2O in hexanes over 20 CV). The ee of the material was determined by chiral HPLC analysis as indicated.

2,2,2-trichloroethyl (R)-2-(4-bromophenyl)-3-(4-isopropylphenyl)propanoate (4a Flow-Flow)[28]

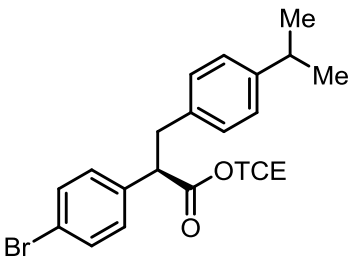

Following GP V (200 µmol scale) using 2,2,2-trichloroethyl (Z)-2-(4-bromophenyl)-2-hydrazonoacetate (**1a**) and 4-isopropyltoluene (**5a**) gave the target compound (79 mg, 166 µmol, 83%) as a white solid:

^{1}H NMR (500 MHz, $CDCl_3$) δ 7.55 – 7.46 (m, 2H), 7.36 – 7.29 (m, 2H), 7.21 – 7.09 (m, 4H), 4.75 (d, *J* = 11.9 Hz, 1H), 4.65 (d, *J* = 12.0 Hz, 1H), 4.03 (dd, *J* = 9.2, 6.5 Hz, 1H), 3.47 (dd, *J* = 13.9, 9.1 Hz, 1H), 3.11 (dd, *J* = 13.9, 6.5 Hz, 1H), 2.91 (hept, *J* = 6.7 Hz, 1H), 1.27 (d, *J* = 6.9 Hz, 6H); **^{13}C NMR** (126 MHz, $CDCl_3$) δ 171.5, 147.4, 136.8, 135.4, 132.0, 130.0, 128.9, 126.7, 121.8, 94.7, 74.2, 53.1, 39.1, 33.8, 24.2; **HPLC** (OJ column, 1.0 mL/min, 0% iPrOH in hexanes, λ = 230 nm): t_R(major) = 46.3 min, t_R(minor) = 23.9 min, 96% ee.

2,2,2-trichloroethyl (R)-3-(4-isopropylphenyl)-2-phenylpropanoate (4b Flow-Flow)[28]

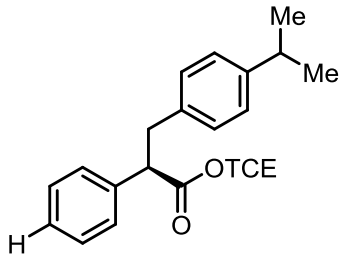

Following GP V (200 μmol scale) using 2,2,2-trichloroethyl (Z)-2-hydrazono-2-phenylacetate (**1b**) and 4-isopropyltoluene (**5a**) gave the target compound (61 mg, 152 μmol, 76%) as a white solid:

^{1}H NMR (600 MHz, $CDCl_3$) δ 7.48 – 7.43 (m, 2H), 7.40 – 7.36 (m, 2H), 7.35 – 7.31 (m, 1H), 7.17 (s, 4H), 4.75 (d, *J* = 12.0 Hz, 1H), 4.62 (d, *J* = 12.0 Hz, 1H), 4.07 (dd, *J* = 9.7, 5.9 Hz, 1H), 3.50 (dd, *J* = 13.9, 9.7 Hz, 1H), 3.13 (dd, *J* = 13.9, 5.9 Hz, 1H), 2.90 (hept, *J* = 6.9 Hz, 1H), 1.27 (dd, *J* = 7.0, 0.6 Hz, 6H); **^{13}C NMR** (126 MHz, $CDCl_3$) δ 171.78, 147.16, 137.83, 135.82, 128.87, 128.70, 128.10, 127.68, 126.47, 94.72, 74.06, 53.54, 39.10, 33.70, 24.00; **HPLC** (ODH column, 0.25 mL/min, 0% iPrOH in hexanes, λ = 230 nm): t_R(major) = 66.9 min, t_R(minor) = 98.7 min, 95% ee.

2,2,2-trichloroethyl (R)-2-(4-fluorophenyl)-3-(4-isopropylphenyl)propanoate (4c Flow-Flow)[36]

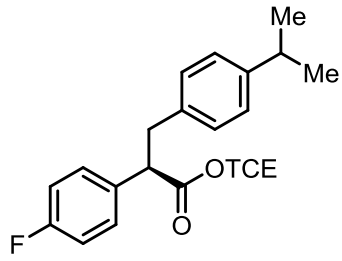

Following GP V (200 μmol scale) using 2,2,2-trichloroethyl (Z)-2-(4-fluorophenyl)-2-hydrazonoacetate (**1c**) and 4-isopropyltoluene (**5a**) gave the target compound (61 mg, 146 μmol, 73%) as a white solid:

^{1}H NMR (600 MHz, $CDCl_3$) δ 7.36 – 7.32 (m, 2H), 7.10 – 7.03 (m, 4H), 7.00 – 6.95 (m, 2H), 4.69 (d, *J* = 12.0 Hz, 1H), 4.61 (d, *J* = 12.0 Hz, 1H), 3.98 (dd, *J* = 9.2, 6.5 Hz, 1H), 3.40 (dd, *J* = 13.9, 9.2 Hz, 1H), 3.03 (dd, *J* = 13.9, 6.5 Hz, 1H), 2.84 (hept, *J* = 6.9 Hz, 1H), 1.21 (dd, *J* = 7.0, 0.6 Hz, 6H); **^{13}C NMR** (151 MHz, $CDCl_3$) δ 171.9, 162.5 (d, J = 246.1

Hz), 147.5, 135.7, 133.7 (d, J = 3.1 Hz), 129.9 (d, J = 8.0 Hz), 129.1, 126.7, 115.8 (d, J = 21.4 Hz), 94.9, 74.3, 52.9, 39.4, 33.9, 24.2; **HPLC** (OJH column, 0.5 mL/min, 0% iPrOH in hexanes, λ = 230 nm): t_R(major) = 53.5 min, t_R(minor) = 42.8 min, 96% ee.

2,2,2-trichloroethyl (R)-2-(4-bromophenyl)-3-(4-propylphenyl)propanoate (4d Flow-Flow)

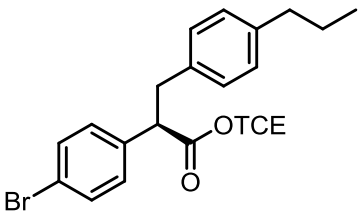

Following GP V (200 µmol scale) using 2,2,2-trichloroethyl (Z)-2-(4-bromophenyl)-2-hydrazonoacetate (**1a**) and 4-n-propyltoluene (**5b**) gave the target compound (69 mg, 144 µmol, 72%):

^{1}H NMR (400 MHz, $CDCl_3$) δ 7.45 – 7.43 (m, 2H), 7.25 – 7.24 (m, 2H), 7.04 (s, 4H), 4.63 (d, *J* = 12.0 Hz, 1H), 4.62 (d, *J* = 12.0 Hz, 1H), 3.96 (dd, *J* = 9.2, 6.5 Hz, 1H), 3.40 (dd, *J* = 13.9, 9.2 Hz, 1H), 3.03 (dd, *J* = 13.9, 6.5 Hz, 1H), 2.52 (t, 2H), 1.6 (m, 2H) 0.9 (t, 3H); **^{13}C NMR** (101 MHz, $CDCl_3$) δ 171.37, 141.12, 136.64, 135.16, 131.79, 129.88, 128.77, 128.59, 121.71, 94.63, 74.12, 52.95, 38.99, 37.61, 24.54, 13.82; **IR** 2957, 2929, 2870, 2159, 2027, 1752, 1488, 1442, 1372, 1266, 1202, 1074, 1101, 806, 754, 720 cm^{-1}; **HRMS** (NSI) calc. for $[C_{20}H_{21}O_2Cl_3Br]^+$ 476.97850 found 476.97911. **HPLC** (SSWhelk column, 0.5 mL/min, 0 % iPrOH in hexanes, λ = 230 nm): t_R(major) = 33.4 min, t_R(minor) = 30.1 min, 97% ee.

2,2,2-trichloroethyl 2-(4-bromophenyl)-3-(4-methoxyphenyl)propanoate (4e Flow-Flow)

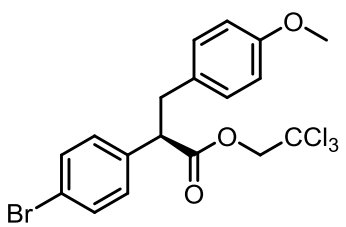

Following GP V (200 µmol scale) using 2,2,2-trichloroethyl (Z)-2-(4-bromophenyl)-2-hydrazonoacetate (**1a**) and 4-n-

propyltoluene (**5b**) gave the target compound (69 mg, 148 µmol, 74%):

Rf = 0.51 (pentane/ethyl ether= 19/1); **[α]$^{20}_{D}$**: -60.6° (c = 1.10, $CHCl_3$); **^{1}H NMR** (600 MHz, $CDCl_3$) **δ** 7.44 (d, *J* = 8.5 Hz, 2H), 7.22 (d, *J* = 8.4 Hz, 2H), 7.04 (d, *J* = 8.7 Hz, 2H), 6.77 (d, *J* = 8.7 Hz, 2H), 4.68 (d, *J* = 12.0 Hz, 1H), 4.64 (d, *J* = 12.0 Hz, 1H), 3.92 (dd, *J* = 8.5, 7.1 Hz, 1H), 3.76 (s, 3H), 3.38 (dd, *J* = 13.9, 8.6 Hz, 1H), 3.02 (dd, *J* = 13.9, 7.1 Hz, 1H); **^{13}C NMR** (151 MHz, $CDCl_3$) δ 171.36, 158.37, 136.54, 131.81, 130.02, 129.96, 129.92, 121.73, 113.90, 94.66, 74.14, 55.25, 53.17, 38.54; **IR** (ATR) 2954, 2835, 1749, 1512, 1488, 1246, 1134, 1035, 1011, 823, 719 cm^{-1}; **HRMS** (NSI) calc. for $[C_{18}H_{17}O_3Cl_3Br]^+$ 464.94212 found 464.92437; **HPLC** (OD column, 0.5 mL/min, 1% iPrOH in hexanes, λ = 230 nm): t_R(major) = 19.9 min, t_R(minor) = 18.4 min, 89% ee.

5.2.12 General procedure for the insertion into methyl ether C–H bonds in a batch process (GP VI):

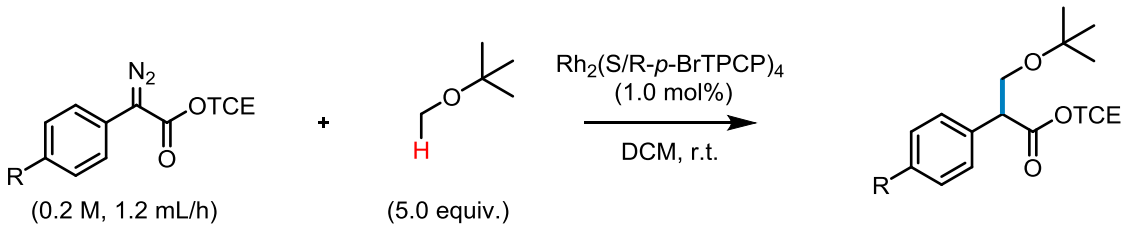

Scheme 5.9. Ether C-H insertion in a batch reactor

A flame dried 10 mL round bottom flask equipped with a magnetic stir bar was charged with Rh_2(S/R-p-BrTPCP)$_4$ (3.6 mg, 2.0 µmol, 1.0 mol %), evacuated and backfilled with argon (3x), charged freshly distilled methyl *tert*-butyl ether (0.11 mL, 0.09 g, 1.0 mmol, 5.0 equiv.) and DCM (2.0 mL), and magnetically stirred (about 600 rpm) at ambient temperature. A flame-dried 10 mL pear-shaped flask was charged with diazo (200

μmol, 1.00 equiv.), evacuated and backfilled with argon (3x), and charged with DCM (2.0 mL). This solution was transferred to a syringe and dropwise added to the reaction vessel at a flow rate of 20 μL/min (1.2 mL/h) via syringe pump. The pear-shaped flask was rinsed with DCM (2 x 0.5 mL), and the solution slowly added to the reaction mixture, which was stirred for another 1.5 h at ambient temperature, and subsequently evaporated under reduced pressure. Trichloroethylene (typically 25–50 μL) was added as an internal standard (if needed $CDCl_3$ was added to obtain a fully homogeneous sample), and the crude yield determined by ^{1}H-NMR analysis. The NMR sample was added back to the remaining crude material, the combined sample evaporated under reduced pressure, and purified by automatic flash column chromatography (typically 12 g SiO_2, 1–3% Et_2O in hexanes over 20 CV). The ee of the material was determined by chiral HPLC analysis as indicated.

2,2,2-trichloroethyl (S)-3-(tert-butoxy)-2-phenylpropanoate (6b Racemate)

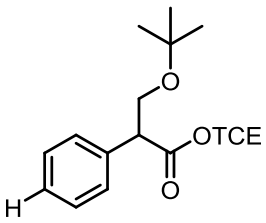

Following GP VI (200 μmol scale) using using 2,2,2-trichloroethyl (Z)-2-hydrazono-2-phenylacetate (**1b**) gave the target compound as a colorless oil:

^{1}H NMR (400 MHz, $CDCl_3$) δ 7.39 – 7.26 (m, 5H), 4.80 (d, J = 9 Hz, 1H), 4.68 (d, J = 9 Hz, 1H), 4.05 – 3.92 (m, 2H), 3.60-3.57 (q, 1H), 1.17 (s, 9H); **^{13}C NMR** (101 MHz, $CDCl_3$) δ 171.19, 135.22, 128.69, 128.33, 127.87, 94.89, 74.10, 73.41, 63.86, 52.84, 27.41; **IR** (ATR) 2974, 2872, 1755, 1498, 1473, 1391, 1363, 1261, 1235, 1194, 1138, 1085, 1046, 1028, 906, 803, 719, 698 cm^{-1}; **HRMS** (NSI) calc. for $[C_{15}H_{20}Cl_3O_3]^+$ 353.03993 found 353.03995; **HPLC** (ASH column, 0.25 mL/min, 0% iPrOH in hexanes, λ = 230 nm): t_R= 14.2 min, t_R= 15.3 min.

5.2.13 .*General procedure for the insertion into methyl ether C–H bonds in a flow-to-flow process (GP VII):*

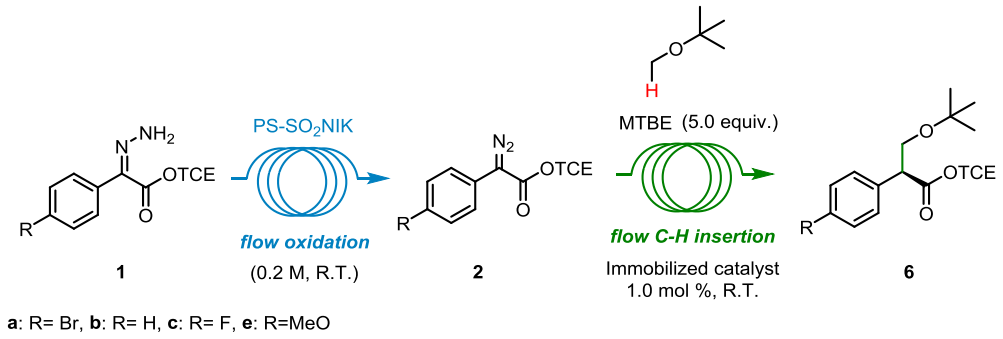

Scheme 5.10. Ether C-H insertion in sequential flow-flow reactors

The first column was charged with PS-NIK resin (1.6 g) and the second column was filled first with anhydrous $Na_2S_2O_3$ (0.3 g) followed by activated drying agent (typically Acros <50 µm 4 Å MS). Rh immobilized hollow fiber (30 cm, c.a. 1.0 mol %) was then loaded into the PTFE tubing. A flame-dried 10 mL pear-shaped flask was charged with hydrazone (220 µmol, 1.1 equiv.), evacuated and backfilled with argon (3x), and charged with DCM (1.1 mL). This solution was injected into a 1.0 mL sample loop (effective starting material: 200 µmol, 1 equiv. 0.2 M) of the HPLC valve. 3 mL of DCM at a flowrate of 2.4 mL/h was used to push the hydrazone though the oxidizing and drying column. Another syringe pump was charged with MTBE in DCM (1 M, 5 mL). Before the intensely yellow/orange colored diazo-containing stream reached the t-connector (before the second column), the styrene solution was simultaneously fed together at a flow rate of 2.4 mL/h (overall flow 4.8 mL/h). When the mixture exited from the second column, the flow rates of two syringe pumps were reduced to 0.6 mL/h, each (overall flow rate: 1.2 mL/h). After completion of the addition, the reaction vessel was evaporated under reduced

pressure, and trichloroethylene (typically 25–50 μL) was added as an internal standard (if needed, $CDCl_3$ was added to obtain a fully homogeneous sample), and the crude yield determined by ^{1}H-NMR analysis. The NMR sample was added back to the remaining crude material, the combined sample evaporated under reduced pressure, and purified by automatic flash column chromatography (typically 12 g SiO_2, 1–3% Et_2O in hexanes over 20 CV). The ee of the material was determined by chiral HPLC analysis as indicated.

2,2,2-trichloroethyl (S)-2-(4-bromophenyl)-3-(tert-butoxy)propanoate (6a Flow-Flow)[10]

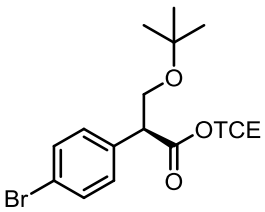

Following GP VII (200 μmol scale) using 2,2,2-trichloroethyl (Z)-2-(4-bromophenyl)-2-hydrazonoacetate (**1a**) gave the target compound (67 mg, 156 μmol, 78%) as a colorless oil:

^{1}H NMR (400 MHz, $CDCl_3$) δ 7.50 – 7.40 (m, 2H), 7.30 – 7.22 (m, 2H), 4.79 (d, *J* = 12.0 Hz, 1H), 4.71 (d, *J* = 12.0 Hz, 1H), 4.03 – 3.84 (m, 2H), 3.58 (dd, *J* = 7.6, 4.2 Hz, 1H), 1.16 (s, 9H); **HPLC** (ASH column, 0.25 mL/min, 0 % iPrOH in hexanes, λ = 230 nm): t_R(major) = 15.1 min, t_R(minor) = 16.0 min, 63% ee with immobilized Rh_2(S-p-BrTPCP)$_4$ derivative catalyst. (ASH column, 0.25 mL/min, 0 % iPrOH in hexanes, λ = 230 nm): t_R(major) = 15.2 min, t_R(minor) = 16.3 min, 91% ee with immobilized Rh_2(S-p-PhTPCP)$_4$ derivative catalyst

2,2,2-trichloroethyl (S)-3-(tert-butoxy)-2-phenylpropanoate (6b Flow-Flow)

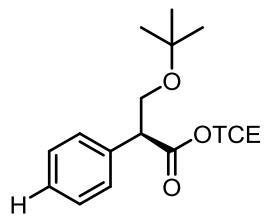

Following GP VII (200 μmol scale) using 2,2,2-trichloroethyl (Z)-2-hydrazono-2-phenylacetate (**1b**) gave the target compound (58 mg, 164 μmol, 82%) as a colorless oil:

^{1}H NMR (400 MHz, $CDCl_3$) δ 7.39–7.26 (m, 5H), 4.80 (d, J = 9 Hz, 1H), 4.68 (d, J = 9 Hz, 1H), 4.05 – 3.92 (m, 2H), 3.60-3.57 (q, 1H), 1.17 (s, 9H); **^{13}C NMR** (101 MHz, $CDCl_3$) δ 171.19, 135.22, 128.69, 128.33, 127.87, 94.89, 74.10, 73.41, 63.86, 52.84, 27.41; **IR** (ATR) 2974, 2872, 1755, 1498, 1473, 1391, 1363, 1261, 1235, 1194, 1138, 1085, 1046, 1028, 906, 803, 719, 698 cm^{-1}; **HRMS** (NSI) calc. for $[C_{15}H_{20}Cl_3O_3]^+$ 353.03993 found 353.03995; **HPLC** (ASH column, 0.25 mL/min, 0% iPrOH in hexanes, λ = 230 nm): t_R(major) = 15.1 min, t_R(minor) = 16.2 min, 42% ee. with immobilized Rh_2(S-p-BrTPCP)$_4$ derivative catalyst. (ASH column, 0.25 mL/min, 0% iPrOH in hexanes, λ = 230 nm): t_R(major) = 14.8 min, t_R(minor) = 16.4 min, 79% ee with immobilized Rh_2(S-p-PhTPCP)$_4$ derivative catalyst.

2,2,2-trichloroethyl (S)-3-(tert-butoxy)-2-(4-fluorophenyl)propanoate (6c Flow-Flow) [10]

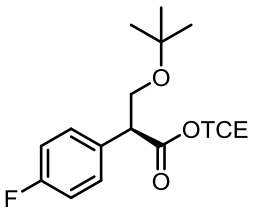

Following GP VII (200 μmol scale) using 2,2,2-trichloroethyl (Z)-2-hydrazono-2-phenylacetate (**1c**) gave the target compound (54 mg, 146 μmol, 73%) as a colorless oil:

^{1}H NMR (400 MHz, $CDCl_3$) δ 7.37–7.33 (m, 2H), 7.04–7.00 (m, 2H) 4.78 (d, J = 9 Hz, 1H), 4.70 (d, J = 9 Hz, 1H), 4.00 – 3.90 (m, 2H), 3.60-3.57 (q, 1H), 1.17 (s, 9H). **^{13}C NMR** (101 MHz, $CDCl_3$) δ 171.10, 163.62, 161.17 131.08, 131.05, 130.04, 129.95, 115.64, 115.43, 94.81, 74.11, 73.46, 63.74, 51.98, 27.37 cm^{-1}; **HPLC** (ASH column, 0.25 mL/min, 0% iPrOH in hexanes, λ = 230 nm): t_R(major) = 14.7 min, t_R(minor) = 15.7 min, 47% ee with immobilized Rh_2(S-p-Br-TPCP)$_4$ derivative catalyst. (ASH column, 0.25 mL/min, 0% iPrOH in hexanes, λ = 230 nm): t_R(major) = 14.9 min, t_R(minor) = 16.0 min, 78% ee with immobilized Rh_2(S-p-PhTPCP)$_4$ derivative catalyst

2,2,2-trichloroethyl (S)-3-(tert-butoxy)-2-(4-(tert-butyl)phenyl)propanoate (6d Flow-Flow)[10]

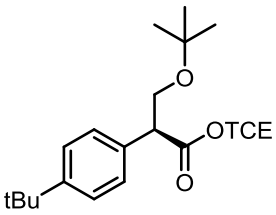

Following GP VII (200 µmol scale) using 2,2,2-trichloroethyl (Z)-2-hydrazono-2-(4-methoxyphenyl)acetate (1e) gave the target compound (55 mg, 144 µmol, 72%) as a colorless oil:

^{1}H NMR (600 MHz; $CDCl_3$) δ 7.34 – 7.31 (m, 2H), 7.31–7.28 (m, 2H), 4.84 (d, J = 12 Hz, 1H), 4.64 (d, J = 12 Hz, 1H), 4.00 (dd, J = 10.3, 8.5 Hz, 1H), 3.92 (dd, J = 10.3, 4.5 Hz, 1H), 3.54 (dd, J = 8.5, 4.5 Hz, 1H), 1.28 (s, 9H), 1.15 (s, 9H); **^{13}C NMR** (150 MHz, $CDCl_3$) δ 171.6, 151, 132.3, 128.1, 125.8, 95.1, 74.3, 73.6, 64.2, 52.6, 34.7, 31.5, 27.6; **IR** (ATR): 2962, 2925, 2869, 1756, 1363 cm^{-1}; **HPLC** (ASH column, 0.25 mL/min, 0% iPrOH in hexanes, λ = 230 nm): t_R(major) = 14.7 min, t_R(minor) = 16.1 min, 68% ee. with immobilized Rh_2(S-p-Br-TPCP)$_4$ derivative catalyst. (ASH column, 0.25 mL/min, 0% iPrOH in hexanes, λ = 230 nm): t_R(major) = 13.5 min, t_R(minor) = 15.6 min, 99% ee. with immobilized Rh_2(S-p-PhTPCP)$_4$ derivative catalyst

5.2.14 General procedure for the insertion into allylic C–H bonds in a batch process (GP VIII):

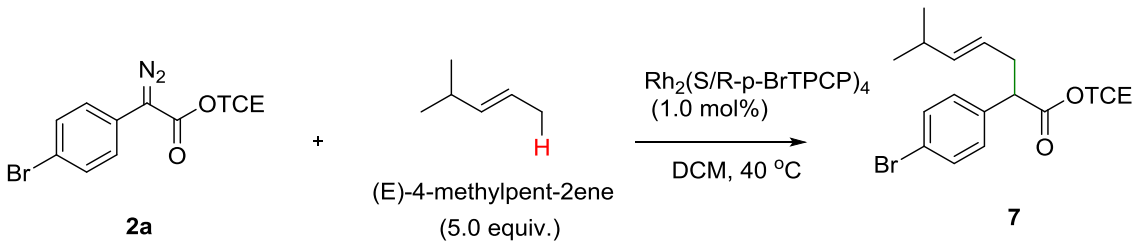

Scheme 5.11. Allylic C-H insertion in a batch reactor

A flame dried 10 mL round bottom flask equipped with a condenser was charged with Rh_2(*S*-*p*-BrTPCP)$_4$ or Rh_2(*S*/*R*-*p*-BrTPCP)$_4$ for racemic (3.6 mg, 2.0 µmol, 1.0 mol%), evacuated and backfilled with argon (3x), charged (E)-4-methylpent-2ene (0. 12 mL, 0.84 g, 1.0 mmol, 5.0 equiv.) and DCM (2.0 mL), and magnetically stirred (about 600 rpm) at 40 °C. A flame-dried 10 mL pear-shaped flask was charged with diazo (200 µmol, 1.00 equiv.), evacuated and backfilled with argon (3x), and charged with DCM (2.0 mL). This solution was transferred to a syringe and dropwise added to the reaction vessel at a flow rate of 20 µL/min (1.2 mL/h) via syringe pump. The pear-shaped flask was rinsed with DCM (2 x 0.5 mL), and the solution slowly added to the reaction mixture, which was stirred for another 1.5 h at 40 °C, and subsequently evaporated under reduced pressure. Trichloroethylene (typically 25–50 µL) was added as an internal standard (if needed, $CDCl_3$ was added to obtain a fully homogeneous sample), and the crude yield determined by ^{1}H-NMR analysis. The NMR sample was added back to the remaining crude material, the combined sample evaporated under reduced pressure, and purified by automatic flash column chromatography (typically 12 g SiO_2, 1–3% Et_2O in hexanes over 20 CV). The ee of the material was determined by chiral HPLC analysis as indicated.

5.2.15 General procedure for the insertion into allylic C–H bonds in a flow-to-flow process Process (GP IX):

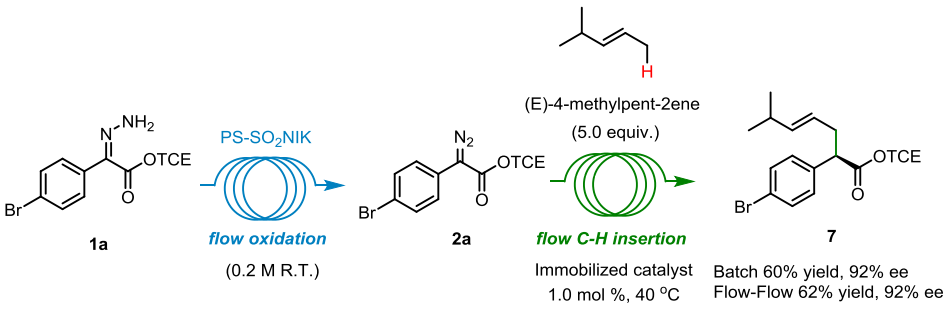

Scheme 5.12. Allylic C-H insertion in sequential flow-flow reactors

The first column was charged with PS-NIK resin (1.6 g) and the second column was filled first with anhydrous $Na_2S_2O_3$ (0.3 g) followed by activated drying agent (typically Acros <50 μm 4 Å MS). Rh immobilized hollow fiber (30 cm, c.a. 1.0 mol %) was loaded into the PTFE tubing. A flame-dried 10 mL pear-shaped flask was charged with hydrazone (220 μmol, 1.1 equiv.), evacuated and backfilled with argon (3x), and charged with DCM (1.1 mL). This solution was injected into a 1.0 mL sample loop (effective starting material: 200 μmol, 1 equiv. 0.2 M) of the HPLC valve. 3 mL of DCM at a flow rate of 2.4 mL/h was used to push the hydrazone though the oxidizing and drying column. Another syringe pump was charged with (E)-4-methylpent-2ene in DCM (1 M, 5 mL). Before the intensely yellow/orange colored diazo-containing stream reached the t-connector (before the second column), the styrene solution was simultaneously fed together at a flow rate of 2.4 mL/h (overall flow 4.8 mL/h When the mixture exited from the second column, the flow rates of two syringe pumps were reduced to 0.6 mL/h, each (overall flow rate: 1.2 mL/h). After completion of the addition, the reaction vessel was evaporated under reduced pressure, and trichloroethylene (typically 25–50 μL) was added as an internal standard (if needed $CDCl_3$ was added to obtain a fully homogeneous sample), and the crude yield determined by ^{1}H-NMR analysis. The NMR sample was added back to the remaining crude material, the combined sample evaporated under reduced pressure, and purified by automatic flash column chromatography (typically 12 g SiO_2, 1–3% Et_2O in hexanes over 20 CV). The ee of the material was determined by chiral HPLC analysis as indicated.

2,2,2-trichloroethyl (E)-2-(4-bromophenyl)-6-methylhept-4-enoate (7 Flow-Flow)

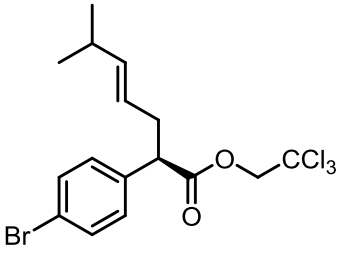

Rf = 0.54 (pentane/ethyl ether= 19/1); **[α]$^{20}_{D}$**: -21.7° (c = 1.05, $CHCl_3$); **^{1}H NMR** (600 MHz, $CDCl_3$) δ 7.45 (d, *J* = 8.5 Hz, 2H), 7.24 – 7.20 (m, 2H), 5.47 (dd, *J* = 15.3, 6.7 Hz, 1H), 5.26 (dtd, *J* = 15.3, 6.9, 1.3 Hz, 1H), 4.74 (d, *J* = 12.0 Hz, 1H), 4.67 (d, *J* = 12.0 Hz, 1H), 3.70 (dd, *J* = 8.5, 6.9 Hz, 1H), 2.83 – 2.74 (m, 1H), 2.51 – 2.43 (m, 1H), 2.22 – 2.14 (m, 1H), 0.90 (t, *J* = 6.6 Hz, 6H); **^{13}C NMR** (151 MHz, $CDCl_3$) δ 171.48, 141.35, 136.70, 131.73, 129.93, 122.45, 121.56, 94.76, 74.15, 51.47, 36.17, 31.02, 22.43, 22.39; **IR** (ATR) 2957, 2868, 1751, 1488, 1130, 1074, 1012, 971, 824, 719 cm^{-1}; **HRMS** (NSI) calc. for $[C_{16}H_{19}O_2Cl_3Br]^+$ 426.96285 found 426.96325; **HPLC** (SSWhelk column, 0.5 mL/min, 0% iPrOH in hexanes, λ = 230 nm): t_R(major) = 23.8 min, t_R(minor) = 26.9 min, 92% ee.

5.2.16 Recycling of the immobilized Rh hollow fiber for the benzylic C–H insertion in a flow-to-flow Process

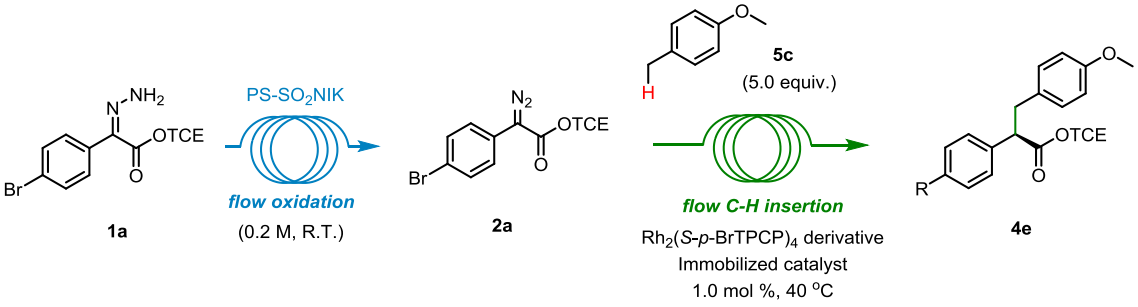

Scheme 5.13. Recyclability test of the sequential flow-flow reactor for benzylic C-H insertion

Run # 1

The first column was charged with PS-NIK resin (1.6 g) and the second column was filled first with anhydrous $Na_2S_2O_3$ (0.3 g) followed by activated drying agent (typically Acros <50 μm 4Å MS). Rh immobilized hollow fiber (30 cm, c.a. 1.0 mol%) was loaded into the PTFE tubing. A flame-dried 10 mL pear-shaped flask was charged with hydrazone (220 μmol, 1.1 equiv.), evacuated and backfilled with argon (3x), and charged with DCM (1.1 mL). This solution was injected into a 1.0 mL sample loop (effective starting material: 200 μmol, 1 equiv. 0.2 M) of the HPLC valve. 3 mL of DCM at a flow rate of 2.4 mL/h was used to push the hydrazone though the oxidizing and drying column. Another syringe pump was charged with 4-methoxytoluene (**5c**) in DCM (1 M, 5 mL). Before the intensely yellow/orange colored diazo-containing stream reached the t-connector (before the second column), the styrene solution was simultaneously fed together at a flow rate of 2.4 mL/h (overall flow 4.8 mL/h). When the mixture exited from the second column, the flow rates of two syringe pumps were reduced to 0.6 mL/h, each (overall flow rate: 1.2 mL/h). After completion of the addition, the collection vessel was marked as the first run.

Runs # 2 -10

The used PS-NIK column from the previous run was replaced with another column charged with fresh PS-NIK resin (1.6 g). Similarly, the used column for drying and scavenge agents was also replaced with another column charged with fresh agents. However, the Rh immobilized hollow fiber was not replaced and continuously used for the test of recyclability. The 0.2 M of hydrazone solution in DCM was injected into a 1.0 mL

sample loop of the HPLC valve. 3 mL of DCM at a flow rate of 2.4 mL/h was used to push the hydrazone though the oxidizing and drying column. Another syringe pump was charged with 4-methoxytoluene (**5c**) in DCM (1 M, 5 mL). Before the intensely yellow/orange colored diazo-containing stream reached the t-connector (before the second column), the styrene solution was simultaneously fed together at a flow rate of 2.4 mL/h (overall flow 4.8 mL/h). When the mixture exited from the second column, the flow rates of two syringe pumps were reduced to 0.6 mL/h, each (overall flow rate: 1.2 mL/h). After completion of the addition, the collection vessel was marked as 2-10 run.

The collected ten vessels were evaporated under reduced pressure, and trichloroethylene (typically 25–50 μL) was added as an internal standard (if needed $CDCl_3$ was added to obtain a fully homogeneous sample), and the crude yield determined by ^{1}H-NMR analysis. The NMR sample was added back to the remaining crude material, the combined sample evaporated under reduced pressure, and purified by automatic flash column chromatography (typically 12 g SiO_2, 1–3% Et_2O in hexanes over 20 CV). The ee of the material was determined by chiral HPLC analysis as indicated.

5.3 Results and discussions

Figure 5.1. describes the overall cascade reaction protocol in a flow system for selective C–H functionalization. The first column is filled with poly(styrene) supported NIK resin (PS-SO_2NIK), where relatively stable hydrazones are converted to diazo compounds. The PS-SO_2NIK resin was prepared by the procedure reported by S. M. Nicolle *et al*.[20] Byproducts from this step, including trace water and iodine leached from the first column, interacting with the dirhodium catalysts to give OH insertion product and carbene dimers,

respectively. To this end, the second column was filled with molecular sieves and sodium thiosulfate to remove these impurities.[28] The diazo compound stream from the first column and a coupling substrate stream are additionally dried and effectively mixed in the second column, after which the mixture flowed into a downstream polymeric hollow fiber flow reactor containing supported chiral dirhodium catalysts, where the C–H insertion products are generated and collected at the end of the fiber reactor. The backpressure regulator (40 psi) was installed at the end of the flow reactor to avoid solvent evaporation under certain reaction conditions (40 °C).

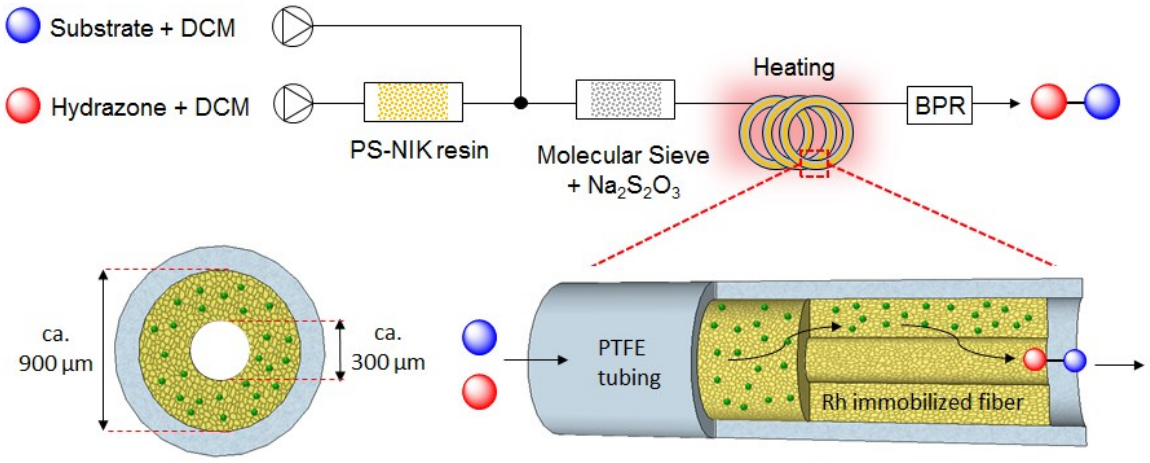

Figure 5.1. Schematic description of cascade reactions for scalable C–H functionalization in flow and Rh immobilized hollow fiber flow reactor.

The fiber reactor has small inner (ca. 300 µm) and outer diameters (ca. 900 µm) with a porous polymer wall. Embedded within the porous polymer matrix are commercial silica particles (Syloid, C803, surface area: 267 m^2/g, pore volume: 0.81cm^3/g), on which the dirhodium catalysts are grafted. The fiber is completely wrapped with non-permeable PTFE tubing, allowing the fiber to be used as an axial flow reactor. The SEM images of

cross section of silica embedded hollow fiber and PTFE wrapped fiber were shown in Figure 5.2.

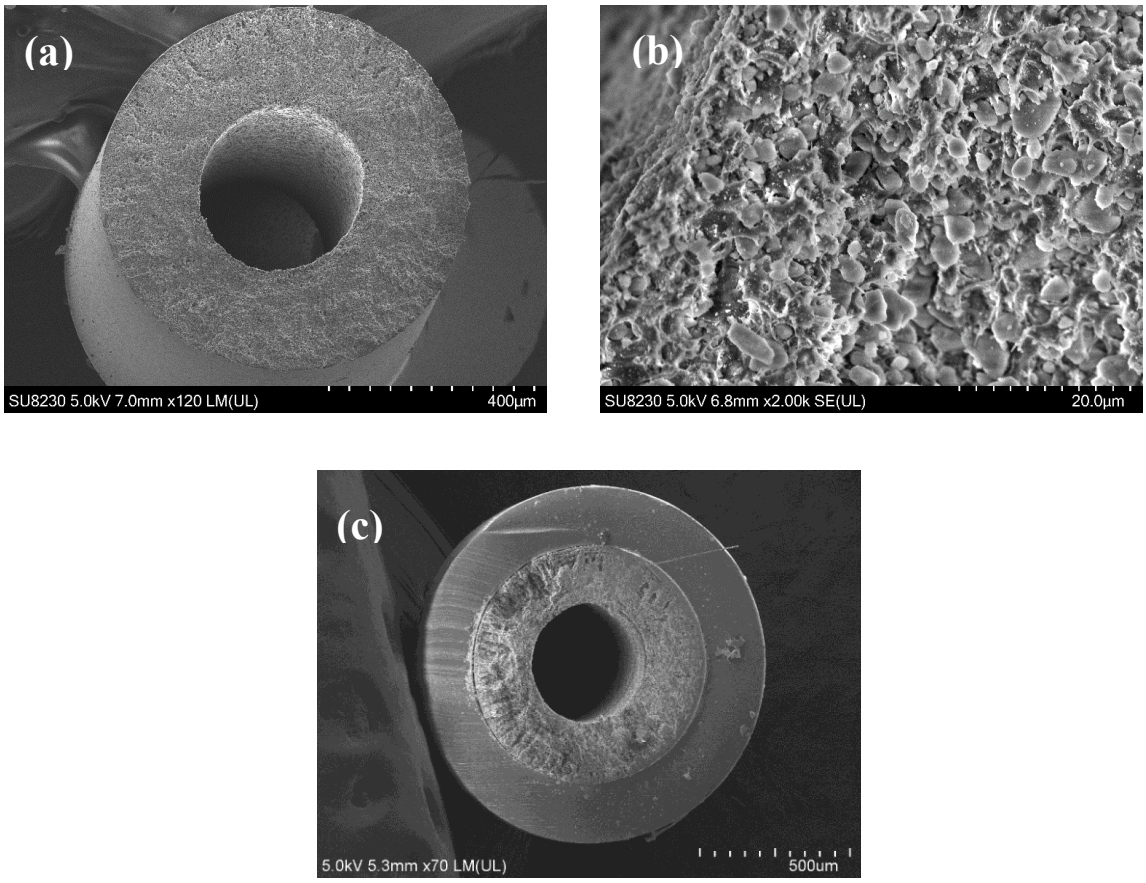

Figure 5.2. SEM images of (a) silica embedded bare hollow fiber (b) porous matrix of polymer and SiO_2 (c) wrapped silica embedded hollow fiber with PTFE tubing.

By comparison with the cellulose acetate fiber flow reactor that our group previously introduced to demonstrate the concept of a polymer fiber catalytic flow reactor,[32] this new fiber reactor has significantly improved performance in terms of solvent compatibility with the fiber material and solvent utilization in the flow system. The fiber is based on a commercially available poly(amide-imide)-based polymeric material

(Torlon®), which possesses strong solvent and chemical resistance. Importantly, the fiber does not dissolve in chlorinated solvents such as dichloromethane (DCM) that is commonly used in carbene based C–H functionalization reactions, which enables a broad utilization of this flow reactor for many variations of rhodium carbene based reactions. On the other hand, the cellulose acetate fiber previously used readily dissolves in DCM, and thus such fibers are not applicable in this flow reactor. As an alternative solvent, hexane was previously utilized but hexane can be functionalized by the many rhodium carbene catalysts[9], and the enantioselectivities of the products were generally lower than those under DCM solvent conditions.[11] Additionally, the axial direction of the microfluidic flow design in this study significantly reduced the utilization of solvent due to its small reactor volume. The previous design maintained a radial flow direction in the reactor, which required an excess sweeping solvent flow that generated additional waste and high operational cost.

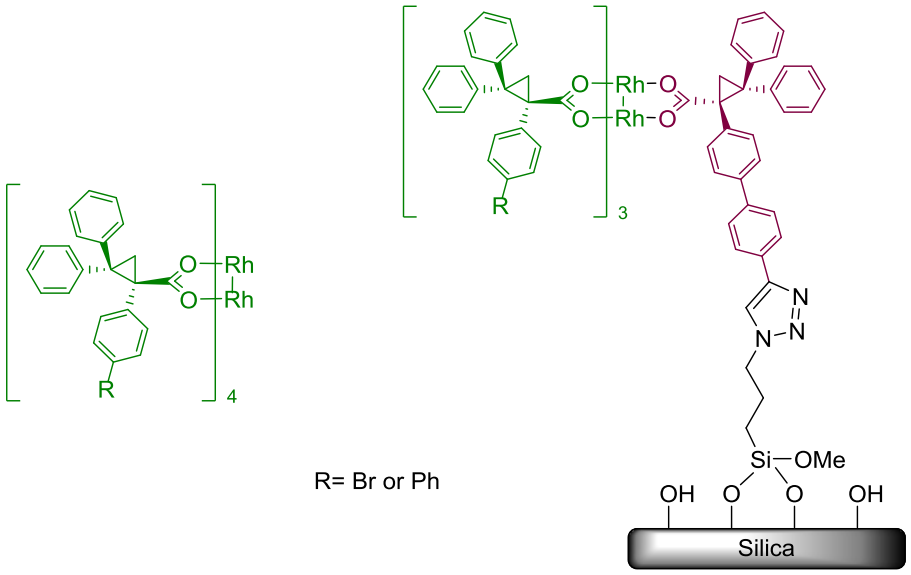

Figure 5.3. (left) Homogenous catalysts Rh_2(*S*-*p*-Br/Ph-TPCP)$_4$ and (right) immobilized Rh_2(*S*-*p*-Br/Ph-TPCP)$_3$(*S*-*p*-Ph-TPCP) catalysts on the silica embedded hollow fiber.

For the carbene reactions (cyclopropanation or C–H functionalizations) occurring in the downstream hollow fiber reactor, the benchmark homogeneous catalyst, Rh_2(*S*-*p*-Br/Ph-TPCP)$_4$, was modified and immobilized on the silica embedded hollow fiber (Figure 5.3.). One of the ligands of the homogeneous catalyst was exchanged with an analogous ligand containing a terminal alkyne, which was then clicked together with an azide functionalized silane on the silica support to yield a triazole linked catalyst.

Next, we applied the sequential flow reactors to the enantioselective synthesis of an array of cyclopropanes (Figure 5.4). The hydrazone starting materials were fully converted by excess PS-SO_2NIK resin, which avoids the deactivation of the dirhodium catalyst by unreacted hydrazone starting material.[28] The in-flow-synthesized aryldiazoacetate **2** was dried and mixed with styrene in the second column. This mixture was fed into the Rh immobilized fiber reactor to yield substituted cyclopropanes in a flow. Results from this flow-flow reactor were compared with a conventional batch or flow-batch systems. For the reactions in the batch system, pre-synthesized aryldiazoacetates were reacted with styrene in the presence of the homogenous dirhodium catalyst. In the case of the flow-batch system,[28] the aryldiazoacetates were synthesized in flow and directly consumed with styrene in the batch reactor. Cyclopropanes (**3a-3d**) from the flow-flow system were synthesized with high yields (85-92%) and enantioselectivities (91-99% ee), which are comparable to the batch or flow-batch systems (Figure 5.4).

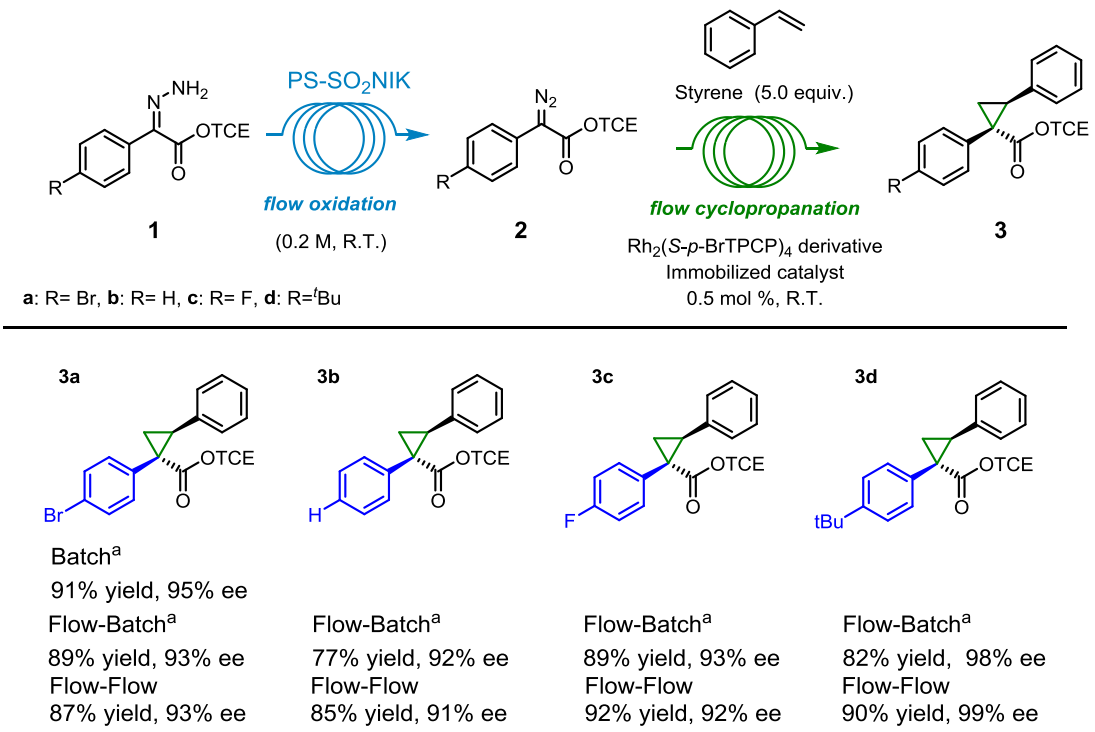

Figure 5.4. Cyclopropanations with aryldiazoacetates synthesized in flow. Data marked "a" are from ref [28].

Based on the successful demonstration of continuous synthesis of cyclopropanes directly from the stable hydrazone, benzylic C–H insertions in flow with 4-isopropyltoluene **5a**, 4-*n*-propyltoluene **5b** or 4-methoxytoluene **5c** (Figure 5.5), were demonstrated. These coupling substrates contain different types of C–H bonds such as primary, secondary or tertiary groups, which can react with carbenes to yield a mixture of various benzylic C–H inserted products. Depending on the ligand structure of the dirhodium catalyst, selectivity toward a specific type of C–H functionalization can be controlled. In particular, Rh_2(*S*-*p*-PhTPCP)$_4$ displays high selectivity toward primary C–H bond functionalization.[37] As in the cyclopropanation case, Rh_2(*S*-*p*-BrTPCP)$_4$ catalyzed the reaction with 4-isopropyltoluene **5a** in the batch or flow-batch to give high yield and

site selectivity (**4a** batch and flow-batch, 85% yield, >20:1 rr, 1°). Rh_2(*S*-*p*-BrTPCP)$_3$(*S*-*p*-PhTPCP) (Figure 5.3, right) catalyzed the reaction with *p*-bromophenyldiazoacetate **2a** and 4-isopropyltoluene **5a** in the flow-flow reactor, showing comparable results with the batch and flow-batch reactors in terms of yield (83 %), regioselectivity (>20:1) and enantioselectivity (96% ee) (**4a** flow-flow). When a different hydrazone was used as the starting material (phenylhydrazone **1b** or *p*-florophenylhydrazone **1c**) in the flow-flow reactor, slightly reduced yields (**4b** 76% and **4c** 73%, respectively) were obtained but excellent regioselectivities and enantioselectivities were still maintained (>20:1 rr for both and 98% and 96% ee, respectively). Other Rh_2(*S*-*p*-BrTPCP)$_3$(*S*-*p*-PhTPCP) catalyzed reactions (Figure 5.3, right) in the flow-flow reactor with 4-*n*-propyltoluene **5b** containing multiple C–H bonds (primary and secondary) also favor primary C–H bond (>20:1) functionalization over secondary C–H bonds with high enantioselectivity (97% ee) (**4d**). The 4-methoxytoluene **5c** was anticipated to be a more challenging substrate to functionalize due to competing primary C–H bonds at the methoxy and benzylic positions. Interestingly, primary C–H bond functionalization of the benzylic position was highly favored (>20:1 rr) with a moderately good yield (74%) and enantioselectivity (89%) (**4e**).

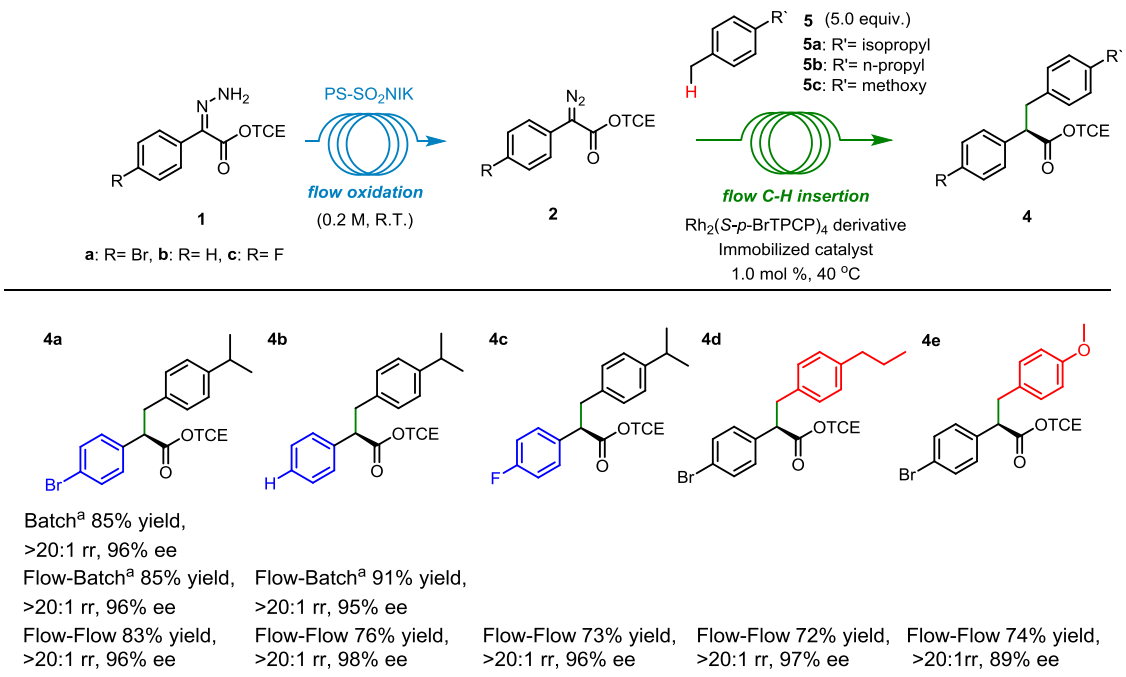

Figure 5.5. Benzylic C–H insertion in flow. Data marked "a" are from ref [28].

The scope of the immobilized dirhodium catalyzed C–H functionalization (Figure 5.3. right) using arylhydrazones, and methyl *tert*-butyl ether (MTBE) was then examined with the flow-flow reactor (Figure 5.6). The catalytic activity of the immobilized Rh_2(*S*-*p*-BrTPCP)$_4$ derivative catalyst (Cat A, Figure 5.6) for the reaction with *p*-bromophenyldiazoacetate **2a** and MTBE was similar to the homogeneous catalyst (Rh_2(*S*-*p*-BrTPCP)$_4$) in the batch and flow-batch reactors in terms of yield (69% and 70%, respectively) and enantioselectivity (66% and 63%, respectively).[28] However, the enantioselectivity of the ether C–H insertions (42-68% ee) with Cat A was relatively low compared to other C–H insertions because the ligand structure of the immobilized Rh_2(*S*-*p*-BrTPCP)$_4$ derivative catalyst (Cat A) does not effectively control the enantioselectivity for ether C–H insertion (**6a-6d** with Cat A). On the other hand, the immobilized Rh_2(*p*-PhTPCP)$_4$ derivative catalyst (Cat B, Figure 5.6) shows a dramatic increase in

enantioselectivity in ether C–H insertions. The ee for the Rh_2(S-p-PhTPCP)$_4$ derivative catalyzed ether C–H insertion with *p*-bromophenyldiazoacetate **2a** was improved from 63% ee to 91% ee (**6a** with Cat B, Figure 5.6), and the ether C–H insertion with phenyldiazoacetate **2b** or p-fluorodiazoacetate **2c** also gave increased ee (42→79% and 47→78%, respectively). Lastly, Cat B catalyzed the C–H insertion with *p-tert*-butyldiazoacetate **2d**, and MTBE shows an extremely high ee (99%, **6d** with Cat B), which was a significant improvement from the Cat A catalyzed reaction with same substrate **2d** (68% ee with Cat A). It should be noted that the use of a second immobilized catalyst in this unique flow reactor scheme shows the overall versatility of this approach.

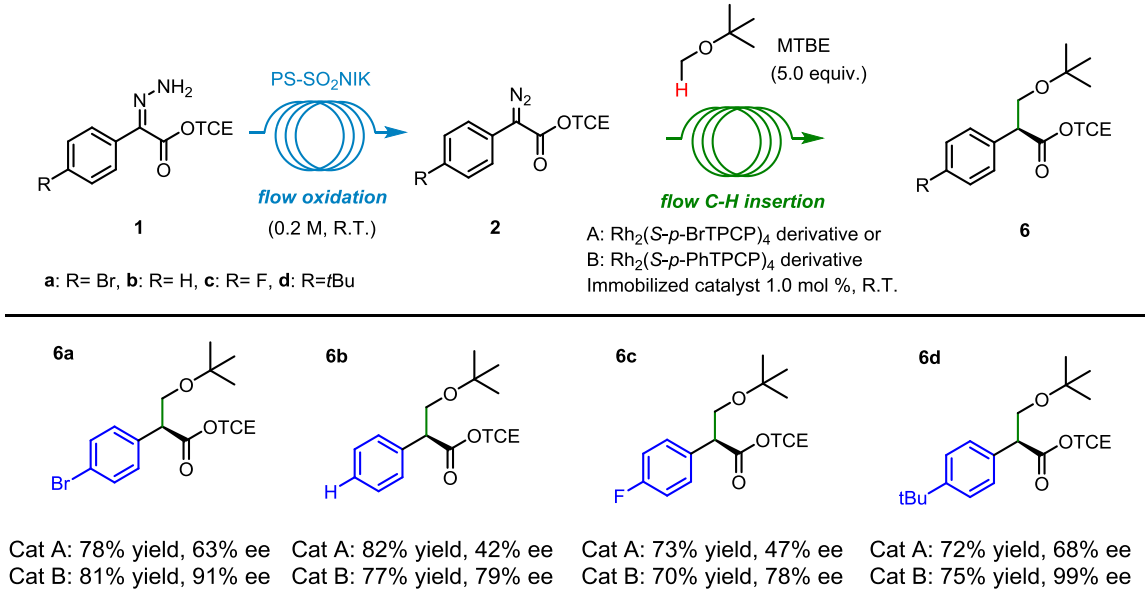

Figure 5.6. Ether C–H insertion in flow.

The application of a flow-flow reactor with the immobilized catalyst was further investigated for an allylic C–H insertion (Figure 5.7). The Rh_2(*S-p*-BrTPCP)$_4$ or Rh_2(*S-p*-

BrTPCP)$_3$(*S*-*p*-PhTPCP) (Figure 5.3 left and right) catalyzed reactions of *p*-bromophenyldiazoacetate **2a** and (E)-4-methylpent-2ene similarly favored primary C–H bond functionalization over tertiary C–H bonds (16:1, 1°) with high enantioselectivity (92% ee) (**7**). The isolated yields were similar in both the batch and flow-flow reactors.

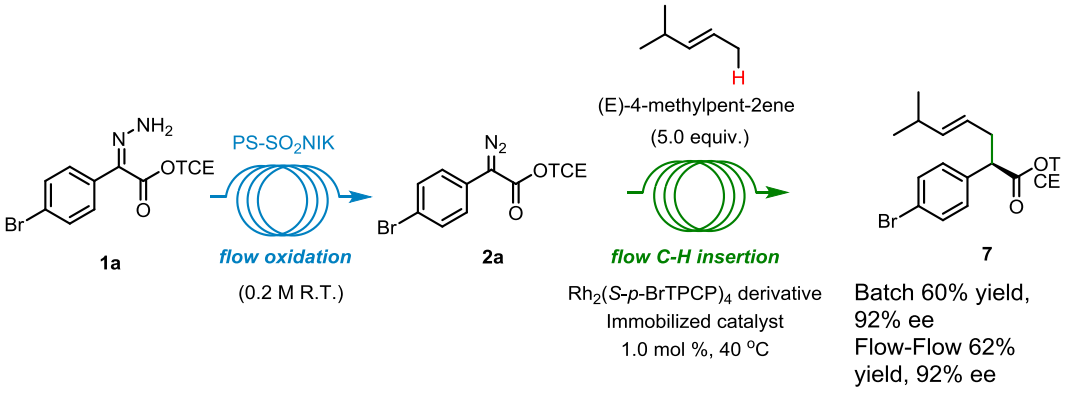

Figure 5.7. Allylic C–H insertion in flow.

As stated above, increasing the turnover number (TON) of the catalyst is an additional goal for this study. Immobilization of the catalyst could enable multiple recycling of the catalyst in the reactions using the same amount of catalyst, which can help significantly improve the TON of the catalyst. In figure 5.8, the evaluation of the recyclability of the flow-flow reactor was demonstrated through 0.2 mmol of hydrazone **1a** (0.4 M) and 1 mmol of 4-methoxytoluene **5c** (2.0 M, 5 eq) cycles in multiple runs. After each run, the PS-SO_2NIK resin, molecular sieves, and $Na_2S_2O_3$ were repacked in the first and second column for subsequent runs. Over 10 consecutive runs using the same immobilized catalyst, the isolated yields for **4e** were quite consistent, being only slightly reduced from 74% to 65%, with enantioselectivities remaining nearly stable from 89% ee. to 86 % ee. The Rh/Si content for the fresh (0.014) and 10 times cycled fiber (0.013) were measured from ICP analysis, and determined to be the same within error. This suggests

that the dirhodium did not significantly leach out of the fiber, and the slightly reduced yield in each cycle may be associated with a slow deactivation over time.

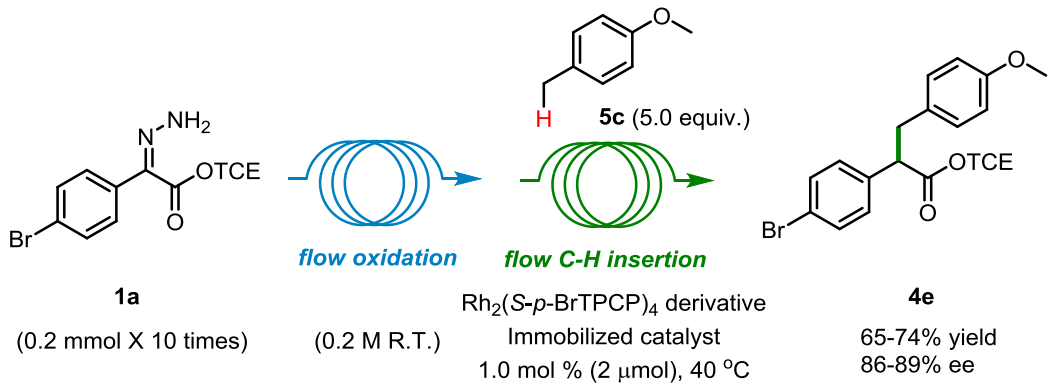

Recycle #	1	2	3	4	5	6	7	8	9	10
Yield (%)	74	72	67	70	71	71	68	65	65	65
e.e. (%)	89	89	88	87	87	87	87	87	86	86

Figure 5.8. Recyclability of Rh immobilized hollow fiber for benzylic C–H insertion.

5.4 Conclusions

In summary, we have demonstrated a potentially scalable and sustainable C–H functionalization by using a cascade reaction protocol, where relatively stable hydrazones were used as starting materials instead of highly energetic diazo compounds with a dirhodium catalyst that was immobilized in a microfluidic hollow fiber reactor. This approach significantly reduced the utilization of the solvent (DCM) over the only prior polymeric fiber flow reactor and improved the TON of the catalyst. A varied scope of challenging asymmetric C–H insertion reactions as well as cyclopropanations was explored, and the yield, site-selectivity and enantioselectivity of the products from the flow-flow reactor were similar with those from a conventional batch reactor or flow-batch

reactor. Considering the catalytic performance was also maintained over multiple recycles, and that different catalyst was effectively immobilized in the fibers, the process may be potentially scaled up by stacking multiple fibers in a reactor module. It is expected that this work will contribute to the future application of carbene based C–H functionalization at bulk scale.

5.5 References

(1) Davies, H. M. L.; Morton, D. Guiding Principles for Site Selective and Stereoselective Intermolecular C–H Functionalization by Donor/Acceptor Rhodium Carbenes. *Chem. Soc. Rev.* 2011, *40* (4), 1857–1869.

(2) Gutekunst, W. R.; Baran, P. S. C–H Functionalization Logic in Total Synthesis. *Chem. Soc. Rev.* **2011**, *40* (4), 1976–1991.

(3) Noisier, A. F. M.; Brimble, M. A. C–H Functionalization in the Synthesis of Amino Acids and Peptides. *Chem. Rev.* **2014**, *114* (18), 8775–8806.

(4) Yamaguchi, J.; Yamaguchi, A. D.; Itami, K. C–H Bond Functionalization: Emerging Synthetic Tools for Natural Products and Pharmaceuticals. *Angew. Chem. Int. Ed.* **2012**, *51* (36), 8960–9009.

(5) Sheldon, R. A. The E Factor: Fifteen Years On. *Green Chem.* **2007**, *9* (12), 1273.

(6) Jimenez-Gonzalez, C.; Ponder, C. S.; Broxterman, Q. B.; Manley, J. B. Using the Right Green Yardstick: Why Process Mass Intensity Is Used in the Pharmaceutical Industry to Drive More Sustainable Processes. *Org. Process Res. Dev.* **2011**, *15* (4), 912–917.

(7) Jiménez-González, C.; Constable, D. J. C.; Ponder, C. S. Evaluating the "Greenness" of Chemical Processes and Products in the Pharmaceutical Industry—a Green Metrics Primer. *Chem. Soc. Rev.* **2012**, *41* (4), 1485–1498.

(8) Qin, C.; Boyarskikh, V.; Hansen, J. H.; Hardcastle, K. I.; Musaev, D. G.; Davies, H. M. L. D2 -Symmetric Dirhodium Catalyst Derived from a 1,2,2-Triarylcyclo-Propanecarboxylate Ligand: Design, Synthesis and Application. *J. Am. Chem. Soc.* **2011**, *133*, 19198–19204.

(9) Liao, K.; Negretti, S.; Musaev, D. G.; Bacsa, J.; Davies, H. M. L. Site-Selective and Stereoselective Functionalization of Unactivated C–H Bonds. *Nature* **2016**, *533* (7602), 230–234.

(10) Guptill, D. M.; Davies, H. M. L. 2,2,2-Trichloroethyl Aryldiazoacetates as Robust Reagents for the Enantioselective C–H Functionalization of Methyl Ethers. *J. Am. Chem. Soc.* **2014**, *136* (51), 17718–17721.

(11) Negretti, S.; Cohen, C. M.; Chang, J. J.; Guptill, D. M.; Davies, H. M. L. Enantioselective Dirhodium(II)-Catalyzed Cyclopropanations with Trimethylsilylethyl and Trichloroethyl Aryldiazoacetates. *Tetrahedron* **2015**, *71* (39), 7415–7420.

(12) Liao, K.; Liu, W.; Niemeyer, Z. L.; Ren, Z.; Bacsa, J.; Musaev, D. G.; Sigman, M. S.; Davies, H. M. L. Site-Selective Carbene-Induced C–H Functionalization Catalyzed by Dirhodium Tetrakis(Triarylcyclopropanecarboxylate) Complexes. *ACS Catal.* **2018**, *8* (1), 678–682.

(13) Liao, K.; Pickel, T. C.; Boyarskikh, V.; Bacsa, J.; Musaev, D. G.; Davies, H. M. L. Site-Selective and Stereoselective Functionalization of Non-Activated Tertiary C–H Bonds. *Nature* **2017**, *551* (7682), 609–613.

(14) Goto, T.; Natori, Y.; Takeda, K.; Nambu, H.; Hashimoto, S. Catalytic Enantioselective C–H Functionalization of Indoles with α-Diazopropionates Using Chiral Dirhodium(II) Carboxylates: Asymmetric Synthesis of the (+)-α-Methyl-3-Indolylacetic Acid Fragment of Acremoauxin A. *Tetrahedron: Asymmetry* **2011**, *22* (8), 907–915.

(15) DeAngelis, A.; Shurtleff, V. W.; Dmitrenko, O.; Fox, J. M. Rhodium(II)-Catalyzed Enantioselective C−H Functionalization of Indoles. *J. Am. Chem. Soc.* **2011**, *133* (6), 1650–1653.

(16) Xu, X.; Deng, Y.; Yim, D. N.; Zavalij, P. Y.; Doyle, M. P. Enantioselective *Cis* -β-Lactam Synthesis by Intramolecular C–H Functionalization from Enoldiazoacetamides and Derivative Donor–acceptor Cyclopropenes. *Chem. Sci.* **2015**, *6* (4), 2196–2201.

(17) Müller, S. T. R.; Murat, A.; Maillos, D.; Lesimple, P.; Hellier, P.; Wirth, T. Rapid Generation and Safe Use of Carbenes Enabled by a Novel Flow Protocol with In-Line IR Spectroscopy. *Chem. Eur. J.* **2015**, *21* (19), 7016–7020.

(18) Roda, N. M.; Tran, D. N.; Battilocchio, C.; Labes, R.; Ingham, R. J.; Hawkins, J. M.; Ley, S. V. Cyclopropanation Using Flow-Generated Diazo Compounds. *Org. Biomol. Chem.* **2015**, *13* (9), 2550–2554.

(19) Hock, K. J.; Koenigs, R. M. The Generation of Diazo Compounds in Continuous Flow. *Chem. Eur. J.* **2018**, *24* (42) 10571-10583.

(20) Nicolle, S. M.; Hayes, C. J.; Moody, C. J. Alkyl Halide-Free Heteroatom Alkylation and Epoxidation Facilitated by a Recyclable Polymer-Supported Oxidant for the in-Flow Preparation of Diazo Compounds. *Chem. Eur. J.* **2015**, *21* (12), 4576–4579.

(21) Lévesque, É.; Laporte, S. T.; Charette, A. B. Continuous Flow Synthesis and Purification of Aryldiazomethanes through Hydrazone Fragmentation. *Angew. Chem. Int. Ed.* **2017**, *56* (3), 837–841.

(22) Audubert, C.; Marin, O. J. G.; Lebel, H. Batch and Continuous Flow One Pot Processes Using Amine Diazotization to Produce Silylated Diazo Reagents. *Angew. Chem. Int. Ed.* **2017**, *56* (22), 6294–6297.

(23) Lehmann, H. A Scalable and Safe Continuous Flow Procedure for In-Line Generation of Diazomethane and Its Precursor MNU. *Green Chem.* **2017**, *19* (6), 1449–1453.

(24) Mccaw, P. G.; Buckley, N. M.; Eccles, K. S.; Lawrence, S. E.; Maguire, A. R.; Collins, S. G. Synthesis of Cyclic α‐Diazo-β-Keto Sulfoxides in Batch and Continuous Flow. *J. Org. Chem.* **2017**, *82* (7), 3666–3679.

(25) Deadman, B. J.; O'Mahony, R. M.; Lynch, D.; Crowley, D. C.; Collins, S. G.; Maguire, A. R. Taming Tosyl Azide: The Development of a Scalable Continuous Diazo Transfer Process. *Org. Biomol. Chem.* **2016**, *14* (13), 3423–3431.

(26) Poh, J.-S.; Makai, S.; von Keutz, T.; Tran, D. N.; Battilocchio, C.; Pasau, P.; Ley, S. V. Rapid Asymmetric Synthesis of Disubstituted Allenes by Coupling of Flow-Generated Diazo Compounds and Propargylated Amines. *Angew. Chem. Int. Ed.* **2017**, *56* (7), 1864–1868.

(27) Yang, H.; Martin, B.; Schenkel, B. On-Demand Generation and Consumption of Diazomethane in Multistep Continuous Flow Systems. *Org. Process Res. Dev.* **2018**, *22* (4), 446-456.

(28) Rackl, D.; Yoo, C. J.; Jones, C. W.; Davies, H. M. L. Synthesis of Donor/Acceptor-Substituted Diazo Compounds in Flow and Their Application in Enantioselective Dirhodium-Catalyzed Cyclopropanation and C–H Functionalization. *Org. Lett.* **2017**, *19* (12), 3055–3058.

(29) Lévesque, É.; Laporte, S. T.; Charette, A. B. Continuous Flow Synthesis and Purification of Aryldiazomethanes through Hydrazone Fragmentation. *Angew. Chem. Int. Ed.* **2017**, *56* (3), 837–841.

(30) Takeda, K.; Oohara, T.; Anada, M.; Nambu, H.; Hashimoto, S. A Polymer-Supported Chiral Dirhodium(II) Complex: Highly Durable and Recyclable Catalyst for Asymmetric Intramolecular C-H Insertion Reactions. *Angew. Chem. Int. Ed.* **2010**, *49* (39), 6979–6983.

(31) Takeda, K.; Oohara, T.; Shimada, N.; Nambu, H.; Hashimoto, S. Continuous Flow System with a Polymer-Supported Dirhodium(II) Catalyst: Application to Enantioselective Carbonyl Ylide Cycloaddition Reactions. *Chem. Eur. J.* **2011**, *17* (50), 13992–13998.

(32) Moschetta, E. G.; Negretti, S.; Chepiga, K. M.; Brunelli, N. A.; Labreche, Y.; Feng, Y.; Rezaei, F.; Lively, R. P.; Koros, W. J.; Davies, H. M. L.; et al. Composite Polymer/Oxide Hollow Fiber Contactors: Versatile and Scalable Flow Reactors for Heterogeneous Catalytic Reactions in Organic Synthesis. *Angew. Chem. Int. Ed.* **2015**, *54* (22), 6470-6474.

(33) Davies, H. M. L.; Walji, A. M. Asymmetric Intermolecular C−H Activation, Using Immobilized Dirhodium Tetrakis((S)-N-(Dodecylbenzenesulfonyl)- Prolinate) as a Recoverable Catalyst. *Org. Lett.* **2003**, *5* (4), 479–482.

(34) Davies, H. M. L.; Walji, A. M. Universal Strategy for the Immobilization of Chiral Dirhodium Catalysts. *Org. Lett.* **2005**, *7* (14), 2941–2944.

(35) Godula, K.; Rabuka, D.; Nam, K. T.; Bertozzi, C. R. Synthesis and Microcontact Printing of Dual End Functionalized Mucin like Glycopolymers for Microarray Applications. *Angew. Chem. Int. Ed.* **2009**, *48* (27), 4973–4976.

(36) Bess, E. N.; Guptill, D. M.; Davies, H. M. L.; Sigman, M. S. Using IR Vibrations to Quantitatively Describe and Predict Site-Selectivity in Multivariate Rh-Catalyzed C–H Functionalization. *Chem. Sci.* **2015**, *6* (5), 3057–3062.

(37) Qin, C.; Davies, H. M. L. Role of Sterically Demanding Chiral Dirhodium Catalysts in Site-Selective C–H Functionalization of Activated Primary C–H Bonds. *J. Am. Chem. Soc.* **2014**, *136* (27), 9792–9796.

CHAPTER 6. SUMMARIES AND FUTURE WORKS

6.1 Summaries

6.1.1 Chapter 1

The general structure of organosilanes and their chemical properties relevant to immobilization on silica surfaces were explained. The use of organosilanes as CO_2 adsorbents (fundamental study) and linker agents for the immobilization of dirhodium catalysts (application focus), as well as an overview of CO_2 capture with solid supported amine adsorbents and dirhodium catalyzed C-H functionalization catalysis were introduced.

6.1.2 Chapter 2

In addition to the most common organosilane employed for CO_2 adsorption (aminopropysilane, APS), new, branched and linear aminosilanes having various amine moieties with ethyl or propyl spacers were synthesized and immobilized on an SBA-15 support. The adsorbents with branched silanes (B-ethyl, B-propyl) showed similar CO_2 uptakes with APS at similar active amine loadings, while the adsorbents with linear silane structures (L-ethyl, L-propyl) showed lower CO_2 capacities at a similar amine loading due to the lower amine efficiency of secondary amines over primary amines. From an oxidative degradation study, the order of oxidative stability of the prepared aminosilanes was: APS > L-propyl > B-propyl > B-ethyl > L-Ethyl. The strong oxidative resistance of the L-propyl adsorbent suggests that even though the amine molecules contain secondary amines, if the secondary amines and adjacent primary amines are separated with a propyl spacer, the

amine molecule has a relatively strong resistance against oxidative degradation compared with amine molecules with ethyl spacers. The IR peak wavelengths of the oxidized species on the linear aminosilanes were slightly different from those produced on branched aminosilanes. These peaks at wavelengths between 1600-1760 cm^{-1} were assigned to amide or imine species. The loss of H atoms resulting from the oxidation was verified by the normalized mol ratios of H/(C+N) of the fresh and oxidized adsorbents, where the oxidized adsorbents had lower H/(C+N) ratios compared with the fresh adsorbents. The decreasing trend of the H/(C+N) ratio for the adsorbents was qualitatively similar to the decreasing CO_2 uptake of the oxidized adsorbent.

6.1.3 Chapter 3

The high temperature (>80 °C) treatment on the dirhodium catalyst would lead to the catalyst restructuring or deactivation, which results in low enantioselective cyclopropanation. Thus, the dirhodium catalyst needs to be immobilized on support material at a lower temperature. The prepared catalysts with propyl, undecyl and phenyl linker showed similar catalytic activities. The linker structure between dirhodium catalyst and Si atom did not significantly affect the catalytic activity. The e.e. of the cyclopropanation with the immobilized Rh_2 catalysts were not maintained during the recycle runs via sequential filtration and drying of the catalyst. However, the same reaction with packed bed flow reactor provided stable yield and ee. The pore structure of the immobilized Rh_2 catalyst showed different reaction kinetics for cyclopropanation, whereby the Rh-propyl-SBA-15PLT catalyst having short pore length with large diameter showed faster kinetics than the Rh-Propyl-SBA-15 catalyst.

6.1.4 Chapter 4.

A tandem reaction system for rhodium-catalyzed cyclopropanation and C–H functionalization was developed based on a collaboration with the Davies group at Emory University. In this approach, aryldiazoacetates were generated from hydrazones in flow, followed by their immediate use with a dirhodium catalyst in subsequent carbenoid transformations in batch (flow to batch). For a clean carbene transformation with hydrazones, it was discovered that molecular sieve (drying agent) and sodium thiosulfate (iodine scavenger) were required. The generated aryldiazoacetates from hydrazones in flow performed equally well compared to the material generated under standard batch conditions. With this process, the need for bulk storage of potentially hazardous diazo compounds is eliminated, which provide a safer way to carry out rhodium-catalyzed reactions of diazo compounds.

6.1.5 Chapter 5.

A scalable and sustainable C–H functionalization was demonstrated by using a cascade reaction protocol, where relatively stable hydrazones were used as starting materials instead of diazo compounds, making diazonium compounds in a first flow reactor, followed by conversion with a dirhodium catalyst that was immobilized in a second, downstream microfluidic hollow fiber reactor. This approach significantly reduced the utilization of solvent (DCM) and improved the TON of the catalyst. A variety of C–H insertion reactions and cyclopropanations were explored. The yield, site-selectivity and enantioselectivity of the products from the flow-flow reactor were similar with those from a conventional batch reactor or flow-batch reactor. Considering that the catalytic

performance was also maintained over multiple recycles, and that different catalysts were effectively immobilized in the fibers, the process may be potentially scaled up by stacking multiple fibers in a reactor module, yielding a potentially safer approach to employment of dirhodium catalyzed coupling reactions on a large scale.

6.2 Future works

6.2.1 Design of new amine molecules based on the amine stability descriptors

With increasing interest in CO_2 adsorption with amine molecules, studies of the oxidative stability of various amine molecules have attracted researchers' attention because the stability of the amine molecules is directly connected to the lifetime of adsorbents for CO_2 adsorption processes. Long term stability if a critical criterion for potential commercialization of CO_2 capture facilities. Herein, a potential amine stability descriptor against oxidation is summarized.

From a prior study of the oxidative stability of amine molecules containing single amine moieties, primary amines (APS[1] and poly(allylamine) (PAA)[2]) and tertiary amines (DMAPS[1]) were identified as having higher oxidative stability than secondary amines (MAPS[1]). However, if the amine molecules contained multiple amine groups, the oxidative stability of the amine molecules differed from the stability trends of single amine moieties. More recently, these simple trends have been shown to not directly extend to multi-amine systems. For example, while aminosilanes containing secondary amines (DI[1], TRI[3]) and linear small amine molecules (TETA[4]) with ethyl spacers between adjacent amine groups showed poor oxidative stability, as expected, linear amine molecules (TPTA[4]) with propyl spacers between adjacent amine groups showed higher oxidative stability. Additionally,

dendritic branched amine molecules (EI-den, PI-den)[4] and branched aminosilanes (B-ethyl, B-propyl, Chapter 2) were observed to oxidize and lose their CO_2 capacities after oxidative treatments even though these molecules contain only primary and tertiary amines that do not readily oxidize when they exist as a single, isolated amine on a chain.

Based on these studies, it is suggested that the oxidative stability of amine molecules cannot be solely categorized by the amine types. Considering that amine molecules with propyl spacers between adjacent amine groups (e.g., TPTA, PI-den, L-propyl, B-propyl) show relatively higher oxidative stabilities compared to amine molecules with ethyl spacers (e.g.. TETA, EI-den, B-ethyl, L-ethyl), it appears that the molecular structure is a more important descriptor for the oxidative stability of the amine molecules. According to the findings in Chapter 2 and Pang et al.'s study[4], linear amine molecules with propyl spacers show higher oxidative stability than branched amine molecules with propyl spacers. Based on these observations, newly proposed linear poly(propylenimine) (PPI) showed excellent oxidative stability compared to linear PEI containing adsorbents.[5] However, these linear amine polymers mostly consist of secondary amines (only one primary amine group at the end of the polymer chain) so the amine efficiency for these linear polymers is typically lower than the branched amine molecules containing primary secondary and tertiary amines. W. Chaikittisilp *et al*.'s work[6] previously reported that the CO_2 capacities for flue gas capture (CO_2 concentration: 10-15%) with branched or linear PEI containing adsorbents were identical (2.5 mmol CO_2/g) at the similar amine loadings, but the CO_2 capacity for direct air capture (CO_2 concentration: 400 ppm) with linear PEI containing silica adsorbents (1.0 mmol CO_2/g) was lower than for branched PEI containing silica adsorbents (1.8 mmol CO_2/g) at similar amine loadings. This suggests that linear

PPI would be a promising amine polymer having good oxidative stability and CO_2 capacity (flue gas capture), but it is not an excellent adsorbent for direct air capture in terms of CO_2 capacity. Overall, to generate a promising CO_2 adsorbent with high amine efficiency and oxidative stability, amine molecules should have a high ratio of primary to the secondary amines and contain propyl (or potentially longer) spacers. However, a branched structure cannot be avoided if one seeks to increase the primary to secondary amine ratio. As shown in Chapter 2, however, if the amine molecule has a branched structure with a primary and tertiary amines, the amine molecules will also be oxidized no matter the two adjacent amines are separated by ethyl or propyl spacer. Thus the branched structure needs to be designed with different branching atoms (e.g., carbon) or species (phenyl group). The proposed design of new amine molecules having high amine efficiency and oxidative stability is shown in Figure 6.1.

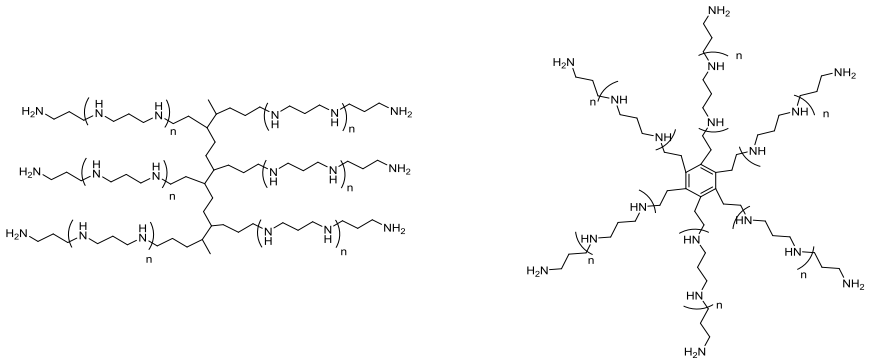

Figure 6.1. The proposed design of amine molecules having high amine efficiency and oxidative stability.

In principle, significant data now exists on the relative oxidative stability of different amine structures in the literature. These data may be semi-quantitatively correlated along with their related CO_2 capacities to hypothesize what the ideal amine

based sorbent may be from a CO_2 uptake and stability perspective. This is proposed as future work.

6.2.2 An intense kinetic study on the immobilized Rh_2 catalyst

In this dissertation, the immobilization of dirhodium catalysts on silica support materials both as powders and in polymeric composite fibers has been demonstrated. Reaction conditions for implementation of flow reactions were chosen from the batch reactions that had been already optimized for the homogeneous system. To further effectively facilitate the application of the flow-flow reactor, an additional kinetic study using the immobilized catalyst is needed to identify optimum reaction conditions for the heterogeneous system. To achieve this goal, a future study needs to be approached from more of a reaction engineering perspective. From an additional kinetic study in a batch reactor employing the react IR technique to monitor the reaction rate, the dominant factors (e.g., temperature, the concentration of reactants and substrates, the effect of impurities and products) on the reaction kinetics can be elucidated, which can then be utilized for optimizing the operation of the C-H functionalization in the flow reactor.

6.2.3 Immobilization of C_4 symmetry dirhodium catalyst

The immobilized dirhodium catalysts in chapters 3, 4 and 5 have a D_2 or C_2 symmetry structure. The accessible active sites of these catalysts are open to both rhodium atoms. However, C4 symmetry dirhodium catalysts such as the Rh2(2-Cl-TPCP)4 catalyst has only one single active site according to the simulated crystal structure, as shown in Figure 6.2.[7] Considering the previous immobilization location where the complex is

tethered to the support on D_2 or C_2 symmetry dirhodium catalysts, the C_4 symmetry dirhodium catalyst (Rh_2(2-Cl-TPCP)$_4$) will be immobilized through the A phenyl ring (Figure 6.2) using a similar approach, which might cause the blockage of the active site or lead to interference from the support surface. Thus, the immobilization of the C_4 symmetry catalysts through different ring positions such as the equatorial position B or the sterically blocked position C (Figure 6.2.) should be explored to determine how to effectively immobilize these powerful catalysts.

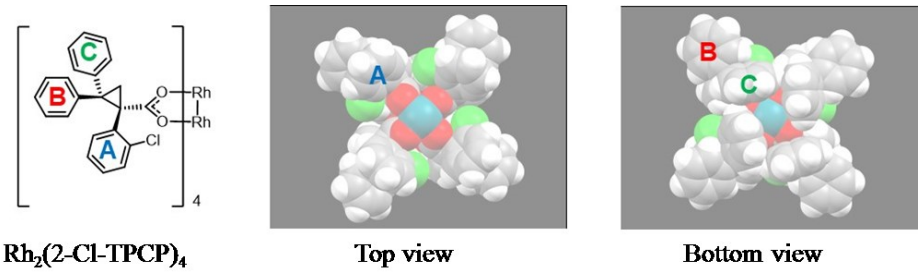

Rh_2(2-Cl-TPCP)$_4$ Top view Bottom view

Figure 6.2. The simulated crystal structure of C_4 symmetry Rh_2(2Cl-TPCP)$_4$ catalyst[7]

6.2.4 Developing an overall flow system for bulk C-H functionalization

In chapters 3-5, the continuous C-H functionalization in a flow reactor starting from relatively stable starting materials (hydrazone compounds) has been demonstrated. Even though the C-H functionalization in flow was successfully demonstrated in terms of yield and enantioselectivity compared with conventional batch reactions, the maximum scale used for the flow system was 2 mmol scale (general batch reaction lab scale: 0.1-0.4 mmol) with a single immobilized Rh hollow fiber. This is still far from the scale needed to confidently assert that this flow system is fully scalable for bulk scale (e.g., kg scale) C-H functionalization reactions.

To scale up this flow system, the oxidation column for diazo compound generation (PS-NIK column) and multiple stacking of hollow fibers in a single module would be essential points. Since the PS-NIK resin is a reactant for the synthesis of the diazo compound, the used packed resins need to be replaced periodically, which prevents the overall reactions from being processed continuously. However, the used PS-NIK resin can be easily generated by flowing aqueous KOH solution containing iodine through the column. For the continuous utilization of the PS-NIK resin column for the generation of diazo compounds, multiple PS-NIK resin columns need to be set up so that one of the new columns is used for the reaction while the previously used PS-NIK column is regenerated for the next run simultaneously. Thus a study on the consumption and regeneration rate of the PS-NIK resin is necessary to optimize the number of columns and flow conditions of the reactant (hydrazone) and KOH solution containing iodine, specifically regarding reagent flow rate and concentration.

The second part of the scale up plan entails staking multiple fibers in a single module for high throughput. With multiple fibers in parallel, the overall inlet flow needs to be evenly separated into each fiber to utilize all the fibers in a module. If a particular fiber in the module has relatively higher pressure drop than other fibers due to the slightly different dimension of the fiber, the flow rate of the fiber might be slower than through other fibers, or in the critical limit, the reactants may not flow into the fiber. To avoid this possible bypassing issue, the pressure drop of the hollow fibers need to be calculated and measured as a function of the inner diameter and length of the fiber. Based on the theoretical calculations and experimental flow tests with stacked fiber module, the length

and number of fibers in the module need to be optimized (e.g., 10 cm fiber x 5 ea vs. 5 cm fiber 10 ea).

In another option, utilization of narrow monolith fibers instead of hollow fiber would also be a practical approach. The wall thickness of the hollow fiber used in this dissertation was approximately 300 μm. Considering that the mass transport driving force in the radial direction is primarily diffusion in this axial flow reactor, the optimum dimension of the hollow fiber would be the narrow inner diameter and thin wall thickness to reduce the diffusion length. However, the narrow inner diameter of the hollow fiber would increase the pressure drop, which could cause an uneven distribution of the flow rate in each fiber, as stated above. In this context, if multiple monolith fibers (O.D. < 300 μm) are densely stacked in a module, the diffusion length of reactant would be decreased, which would improve the reaction kinetics (Figure 6.3).

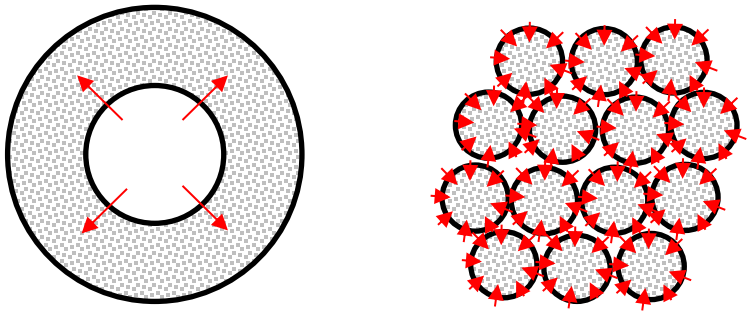

Hollow fiber Monolith

Figure 6.3. Conceptual comparison between hollow fiber and monolith fiber (red arrows indicate reactant diffusion direction)

6.2.5 Simulated moving bed (SMB) for separation of the product stream

The product stream from the flow reactor contains a mixture of desired products (e.g., cyclopropanation, C-H insertion), excess substrate, byproducts, and solvent.

Moreover, since the enantioselectivity of the synthesized products is not 100%, an additional chiral separation step will be required, as well as the regular separation step for the substrate and byproducts. To complete the overall C-H functionalization process in flow, a study of the separation processes to achieve the final pure product would be a promising project. For a continuous separation process, a simulated moving bed (SMB) process can be a potential choice. SMB is a highly engineered, cost-effective and environmentally friendly process for implementing chromatographic separations. An SMB process can separate multiple mixtures by simulated counter-current flow between the solid stationary phase and the liquid phase. Typically, a series of chromatography columns connected in a ring is continuously rotated while the feed and eluent solvent simultaneously flow into the columns for the separation, as shown in Figure 6.4.[8] If chiral stationary phase columns are used, the enantiomer separation is also possible. For this application, various solid stationary phase materials need to be screened to find an optimum retention time and axial dispersion of each product in the column, which may result in an effective separation of a single enantiomeric target product.

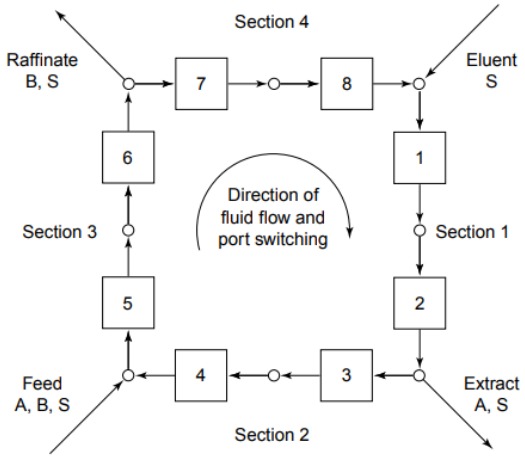

Figure 6.4. Scheme of Simulated moving bed (SMB)[8]

6.3 References

(1) Bollini, P.; Choi, S.; Drese, J. H.; Jones, C. W. Oxidative Degradation of Aminosilica Adsorbents Relevant to Postcombustion CO_2 Capture. *Energy Fuels* **2011**, *25* (5), 2416–2425.

(2) Bali, S.; Chen, T. T.; Chaikittisilp, W.; Jones, C. W. Oxidative Stability of Amino Polymer-Alumina Hybrid Adsorbents for Carbon Dioxide Capture. *Energy Fuels* **2013**, *27* (3), 1547–1554.

(3) Heydari-gorji, A.; Belmabkhout, Y.; Sayari, A. Degradation of Amine-Supported CO_2 Adsorbents in the Presence of Oxygen-Containing Gases. *Microporous Mesoporous Mater.* **2011**, *145* (1–3), 146–149.

(4) Pang, S. H.; Lee, L.-C.; Sakwa-Novak, M. A.; Lively, R. P.; Jones, C. W. Design of Aminopolymer Structure to Enhance Performance and Stability of CO_2 Sorbents: Poly(Propylenimine) vs. Poly(Ethylenimine). *J. Am. Chem. Soc.* **2017**, *139*, 3627–3630.

(5) Pang, S. H.; Lively, R. P.; Jones, C. W. Oxidatively-Stable Linear Poly(Propylenimine)-Containing Adsorbents for CO_2 Capture from Ultradilute Streams. *ChemSusChem* **2018**, *11* (15), 2628–2637.

(6) Chaikittisilp, W.; Khunsupat, R.; Chen, T. T.; Jones, C. W. Poly(Allylamine)-Mesoporous Silica Composite Materials for CO_2 Capture from Simulated Flue Gas or Ambient Air. *Ind. Eng. Chem. Res.* **2011**, *50* (24), 14203-14210.

(7) Liu, W.; Ren, Z.; Bosse, A. T.; Liao, K.; Goldstein, E. L.; Bacsa, J.; Musaev, D. G.; Stoltz, B. M.; Davies, H. M. L. Catalyst-Controlled Selective Functionalization

of Unactivated C-H Bonds in the Presence of Electronically Activated C-H Bonds. *J. Am. Chem. Soc.* **2018**, *140* (38), 12247–12255.

(8) Juza, M.; Mazzotti, M.; Morbidelli, M. Simulated Moving-Bed Chromatography and Its Application to Chirotechnology. *Trends Biotechnol.* **2000**, *18* (3), 108–118.